Universidade de Aveiro Departamento de Eletrónica, Telecomunicações e Informática
2015

Rui Manuel Dias Morais

Planeamento e Dimensionamento de Redes de Transporte Óticas Multicamada

Planning and Dimensioning of Multilayer Optical Transport Networks


Universidade de Aveiro Departamento de Eletrónica, Telecomunicações e
2015 Informática

Rui Manuel Dias Morais

Planeamento e Dimensionamento de Redes de Transporte Óticas Multicamada

Planning and Dimensioning of Multilayer Optical Transport Networks

Tese apresentada à Universidade de Aveiro para cumprimento dos requisitos necessários à obtenção do grau de Doutor em Engenharia Eletrotécnica, realizada sob a orientação científica do Doutor Armando Humberto Moreira Nolasco Pinto, Professor Associado do Departamento de Eletrónica, Telecomunicações e Informática da Universidade de Aveiro, coorientação científica do Doutor Paulo Miguel Nepomuceno Pereira Monteiro, Professor Associado do Departamento de Eletrónica, Telecomunicações e Informática da Universidade de Aveiro e coorientação empresarial do Doutor João Manuel Ferreira Pedro, Doutor em Engenharia Eletrotécnica e de Computadores pelo Instituto Superior Técnico e coordenador de atividades de investigação em otimização de redes na Coriant Portugal.

Apoio financeiro da Coriant Portugal Unipessoal, Lda. através do projecto NET-OPT e da Fundação para a Ciência e a Tecnologia através do projeto ONECI (PTDC/EEITEL/3303/2012).

Aos meus pais, António e Lídia

"'One cannot escape the feeling that these mathematical formulae have an independent existence and an intelligence of their own, that they are wiser than we are, wiser even than their discoverers, that we get more out of them than was originally put into them.'"

Heinrich Hertz

o júri / the jury

presidente / president

Doutor Fernando Joaquim Fernandes Tavares Rocha
Professor Catedrático da Universidade de Aveiro

vogais / examiners committee

Doutor Mário Marques Freire
Professor Catedrático da Faculdade de Engenharia da Universidade da Beira Interior

Doutora Maria do Carmo Raposo de Medeiros
Professora Associada da Faculdade de Ciências e Tecnologia da Universidade de Coimbra

Doutor João José de Oliveira Pires
Professor Auxiliar do Instituto Superior Técnico da Universidade de Lisboa

Doutor Amaro Fernandes de Sousa
Professor Auxiliar da Universidade de Aveiro

Doutor Armando Humberto Moreira Nolasco Pinto
Professor Associado da Universidade de Aveiro (orientador)

agradecimentos / acknowledgements

A orientação conjunta desta tese - concretizada num sólido mas independente apoio - prestada pelo Prof. Armando Nolasco Pinto, Prof. Paulo Monteiro e Dr. João Pedro foi uma mais valia para mim enquanto doutorando. Em primeiro lugar, quero agradecer ao Prof. Armando Nolasco Pinto pela introdução na investigação em redes óticas, assim como pelo excelente apoio científico, capacidade de incentivo e cuidado na revisão dos vários trabalhos submetidos. Seguidamente, quero deixar expresso o meu agradecimento ao Prof. Paulo Monteiro pela oportunidade concedida de fazer o meu doutoramento num ambiente empresarial multinacional e inovador como é a Coriant Portugal (à data Nokia Siemens Networks Portugal). Finalmente, deixo o meu agradecimento ao Dr. João Pedro pelo crucial e valioso apoio científico prestado, assim como por me ter proporcionado uma fácil e útil integração na Coriant Portugal.

Agradeço a todos os meus colegas e amigos do grupo de comunicações óticas do Instituto de Telecomunicações Aveiro e da Coriant Portugal. Tenho no entanto a destacar o João Ferreira, Filipe Ferreira, António Eira, João Santos, José Girão, Nélson Costa, Miguel Drummond e Bodhisattwa Gangopadhyay pelo bom ambiente sempre fomentado (especialmente na sala ex-RH), encorajamento, camaradagem e participação em disputadas e, por vezes, proveitosas discussões.

Saliento o meu agradecimento ao grande amigo José Pereira, pela incansável amizade, que tornou possível a minha presença em Aveiro sempre que foi necessária e, deste modo, a realização deste doutoramento entre Lisboa e Aveiro.

Um especial obrigado aos meus pais António e Lídia, ao meu irmão Ricardo, e ao meu afilhado Tomás, sem os quais nada faria sentido.

Para finalizar, um singular agradecimento à Vanessa Duarte cujo carinho, apoio e oferta de infinitos bons momentos trouxeram cor à etapa mais cinzenta deste sinuoso caminho.

A todos, que das mais inimagináveis e simples formas, contribuiram para que conseguisse ultrapassar este gigante desafio, um muito obrigado!

palavras-chave

redes de transporte multicamada, arquiteturas dos nós, desenho topológico, algoritmos genéticos, agregação, planeamento *greenfield* e multiperíodo, programação linear inteira, análise tecno-económica

resumo

Nesta tese é apresentado um estudo sobre o planeamento de redes de transporte óticas multicamada, considerando as diversas restrições de implementação. São propostos métodos de otimização para as várias etapas do planeamento da rede, nomeadamente desenho de topologias físicas, e dimensionamento de nós em ambiente *greenfield* e multiperíodo. Os métodos desenvolvidos baseiam-se em modelos de programação linear inteira (PLI), algoritmos heurísticos e métodos estatísticos.

Inicialmente, as principais tecnologias e as diferentes arquiteturas de nós usualmente utilizadas em redes de transporte óticas multicamada são apresentadas. Adicionalmente, são também abordados os principais esquemas de agregação e modos de transporte.

Assumindo que a localização dos nós é conhecida, a primeira etapa do processo de planeamento da rede é a implementação das ligações. Assim, é proposto um algoritmo genético para o desenho de topologias físicas sobreviventes com custo mínimo, bem como um modelo de dimensionamento para as ligações. Dentro do algoritmo heurístico vários operadores genéticos são avaliados, comparados e o seu erro calculado através de um modelo de PLI.

Posteriormente, os nós são planeados. Assim, são propostos modelos de otimização para o dimensionamento dos nós, adequados para cenários *greenfield*. Os modelos são baseados em PLI e calculam o número e tipo de módulos necessários para implementar arquiteturas fixas e flexíveis, tanto para a camada elétrica como ótica, tendo em consideração as restrições de implementação. Utilizando os modelos desenvolvidos, são realizadas análises comparativas técnico-económicas, com foco no CapEx, consumo energético e requisitos de espaço. Como resultado, e tendo por base um grande conjunto de simulações, é proposto um método de otimização baseado em regras simples para selecção da arquitetura do nó.

Finalmente, são apresentados métodos de otimização baseados em modelos PLI adequados para cenários multiperíodo. Os modelos consideram as várias arquiteturas para a camada elétrica e permitem um planeamento considerando reagregação sem interrupção de tráfego. Assim, é realizada uma análise comparativa técnico-económica e avaliados os benefícios alcançados através da exploração da reagregação sem interrupção de tráfego, destacando as condições onde estes são mais significativos.

keywords

multilayer transport networks, node architectures, topological design, genetic algorithms, grooming, greenfield and multi-period planning, integer linear programming, techno-economic analysis

abstract

This thesis presents a study on the planning of multilayer optical transport networks considering the various hardware implementation constraints. Optimization methods for the various stages of the network planning are proposed, namely physical topologies design, and greenfield and multi-period nodes dimensioning. The developed methods rely on integer linear programming models (ILP), heuristic algorithms and statistical methods.

Initially, the enabling technologies and the different node architectures usually employed in multilayer optical transport networks are presented. Additionally, the main grooming schemes and transport modes are also discussed.

Assuming that the node localization is known, the first stage of the overall network planning process is the deployment of the network links. Thus, a genetic algorithm for the design of survivable physical topologies with minimum cost is proposed, as well as a dimensioning model for links. Within the heuristic algorithm various genetic operators are evaluated, compared and benchmarked using an ILP model.

After, the nodes are planned. Therefore, optimization models for the nodes dimensioning to use in greenfield scenarios are proposed. The models are based on ILPs and calculate the number and type of modules required to implement fixed and flexible architectures, for both the electrical and the optical layer, taking into consideration the hardware implementation constraints. Using the developed models, comparative techno-economic analysis are performed focusing on the CapEx, power consumption, and footprint requirements. As a result, and based on the outcome of a large set of simulations, an optimization method based on simple rules for node architecture selection is proposed.

Finally, optimization methods based on ILPs to use in multi-period planning are presented. The models consider the various electrical layer architectures, and enable a planning considering hitless re-grooming. Then, a comparative techno-economic analysis is performed and the savings attained by exploiting hitless re-grooming evaluated, highlighting the conditions where such savings are more significant.

Table of contents

List of acronyms

ASE	amplified spontaneous emission
AWG	arrayed waveguide grating
CapEx	capital expenditures
C-band	conventional band
CFP	C form-factor pluggable
EDFA	erbium doped fiber amplifier
ESM	electrical switch module
EXC	electrical cross connect
GA	genetic algorithm
GFP	generic framing procedure
IETF	Internet engineering task force
ILP	integer linear programming
IP	Internet protocol
ITU-T	international telecommunication union - telecommunication standardization sector
LC	liquid crystal
LR	long-reach
MEMS	micro electro mechanical system
MPLS-TP	multi protocol label switching - transport profile
NP-hard	non deterministic polynomial time hard
NPS	network planning system

OAM	operation, administration and management
ODU	optical data unit
OEO	optical-electrical-optical
OpEx	operational expenditures
OSC	optical splitter or coupler
OSNR	optical signal-to-noise ratio
OTN	optical transport network
OTU	optical transport unit
RFA	Raman fiber amplifier
ROADM	reconfigurable optical add/drop multiplexer
SDH/SONET	synchronous digital hierarchy/synchronous optical networking
SR	short-reach
TCO	total cost of ownership
TDM	time division multiplexing
WDM	wavelength division multiplexing
WSC	wavelength splitter or coupler
WSS	wavelength selective switch
XFP	small form-factor plugabble

List of symbols

$\{i, j\}$	physical link between the nodes i and j
(o, d)	demand between the nodes o and d
α	cost factor
β	parameter of the Waxman probability
γ	parameter of the Waxman probability
$\delta(i)$	nodal degree of node i
$\delta^{max}(i)$	maximum nodal degree at node i
Δ	maximum distance in kilometers between any two nodes in the network
ϵ	grooming configuration
$\tau(i)$	add/drop ratio of node i for fixed frequency and directionless, and colorless and directionless architectures
$\tau^*(i)$	add/drop ratio of node i for colorless, directionless and contentionless ROADM
$\phi(i, j)$	probability of existing a link between the nodes i and j
a	module
$A(i)$	number of add/drop structures in the node i
A_C	set of modules
$B(o, s)$	variable indicating whether the shelf s is implemented in node o or not
b_u	cost of the solution obtained using the genetic algorithm
b_l	cost of the solution obtained using the ILP model
c	bit rate of the client signal

C	set of client bit rates
c^*	bit rate of the client signals requiring a two stage grooming for muxponders-based architectures
C^*	set of client bit rates requiring a two stage grooming for muxponders-based architectures
$CapEx_L$	total network CapEx for links
c_e	average cost per kWh over a year
c_f	cost of the optical fiber per kilometer
c_r	average rent cost of 1 m^2 per month over a year
c_o	cost related to enable the switching of an optical channel
c_{oa}	cost of a bidirectional optical amplifier
d	node that is destination of a demand
$D_c(o)$	number of client demands with bit rate c in node o
E_c	set of node pairs requesting at least one optical channel
E_p	set of physical links
$E_T(o)$	total power consumption required in the node o
G	graph
gap	difference between the upper and the lower bound
$H_c^{c^*,\epsilon}$	maximum number of client signals with bit rate c^* that can be groomed into a signal with bit rate c in configuration ϵ
$H_l^{c,\epsilon}$	maximum number of client signals with bit rate c that can be groomed into a signal with bit rate l in configuration ϵ
i	start node of a physical link
j	end node of a physical link
K	maximum number of optical channels supported by the transmission system
$K(i,j)$	maximum number of optical channels supported by the transmission system between the nodes i and j
l	bit rate of the line signal
L	set of line bit rates
$LL(i,j)$	link length in kilometers between the nodes i and j
$L(o,d)$	number of optical channels required between the nodes o and d
$[L(o,d)]$	matrix with the number of optical channels required between all node pairs
$L^{mb}(o,d)$	number of optical channels between the nodes o and d for muxponders-based architecture
$L^{nbe}(o,d)$	number of optical channels between the nodes o and d for non-blocking EXC architecture

$L^{pbe}(o,d)$	number of optical channels between the nodes o and d for partial non-blocking EXC architecture
m	bit of the genetic code
$M^{ads}_{amp}(i)$	number of in node amplification in the add/drop structure of node i
$M^{xc}_{amp}(i)$	number of pre/booster amplifiers in the cross connection structure of node i
$M_c(o)$	number of client modules with bit rate c in node o
$M_c(o,a)$	variable indicating whether the module a with bit rate c is used in node o or not
$M_c(o,s)$	number of client modules accepting signals with bit rate c in node o and shelf s
$M_c(o,a,s)$	variable indicating whether the module a with bit rate c is used in node o and shelf s or not
$M^{\epsilon}_c(o,d)$	number of muxponder modules with output bit rate c required for the demands between the nodes o and d and accepting traffic in the grooming configuration ϵ
$M^{\epsilon}_c(o,d,a)$	variable indicating whether the muxponder module a generating an output signal with bit rate c in the grooming configuration ϵ between the nodes o and d is used or not
$M^{\epsilon}_c(o)$	number of muxponder modules generating an output signal with bit rate c in the grooming configuration ϵ in the node o
$M^{mb}_{ctr}(o)$	number of control modules in node o for muxponders-based architectures
$M^{nbe}_{ctr}(o)$	number of control modules in node o for non-blocking EXC architectures
$M^{pbe}_{ctr}(o)$	number of control modules in node o for partial non-blocking EXCs architectures
$M^{CD}_{ctr}(i)$	number of control modules in node i for the colorless and directionless ROADM
$M^{CDC}_{ctr}(i)$	number of control modules in node i for the colorless, directionless, and contentionless ROADM
$M^{CF}_{ctr}(i)$	number of control modules in node i for colorless and fixed direction ROADM
$M^{FD}_{ctr}(i)$	number of control modules in node i for fixed frequency and directionless ROADM
$M^{FF}_{ctr}(i)$	number of control modules in node i for fixed frequency and fixed direction ROADM
$M^{nbe}_{esm}(o)$	number of ESMs in node o for non-blocking EXC architectures
$M^{pbe}_{esm}(o)$	number of ESMs in node o for partial non-blocking EXCs architectures
$M_l(o)$	number of line modules with bit rate l in node o
$M_l(o,s)$	number of line modules with with bit rate l in node o and shelf s
$M^{\epsilon}_l(o)$	number of muxponder modules generating an output signal with bit rate l in the grooming configuration ϵ in the node o
$M_l(o,a)$	variable indicating whether the module a with bit rate l is used in node o or not

$M_l(o,a,s)$	variable indicating whether the module a with bit rate l is used in node o and shelf s or not
$M_l^{\epsilon}(o,d,a)$	variable indicating whether the muxponder module a generating an output signal with bit rate l in the grooming configuration ϵ between the nodes o and d is used or not
$M_l^{\epsilon}(o,d)$	number of muxponder modules with output bit rate l required for the demands between the nodes o and d and accepting traffic in the grooming configuration ϵ
$M_l^{pbe}(o)$	number of line modules with bit rate l in the node o for partial non-blocking EXCs architectures
$M_{mwss}^{ads}(i)$	number of $P_i \times P_o$ WSSs required in the add/drop structure of node i
$M_{osc}^{ads}(i)$	number of OSC modules in the add/drop structure of node i
$M_{sf}^{CD}(i)$	number of shelves in node i for the colorless and directionless ROADM
$M_{sf}^{CDC}(i)$	number of shelves in node i for the colorless, directionless, and contentionless ROADM
$M_{sf}^{CF}(i)$	number of shelves in node i for colorless and fixed direction ROADM
$M_{sf}^{FD}(i)$	number of shelves in node i for fixed frequency and directionless ROADM
$M_{sf}^{FF}(i)$	number of shelves in node i for fixed frequency and fixed direction ROADM
$M_{sf}^{mb}(o)$	number of shelves in node o for muxponders-based architectures
$M_{sf}^{nbe}(o)$	number of shelves in node o for non-blocking EXC architectures
$M_{sf}^{pbe}(o)$	number of shelves in node o for partial non-blocking EXCs architectures
$M_{wsc}^{ads}(i)$	number of WSC modules in the add/drop structures of node i
$M_{wss}^{ads}(i)$	number of $1 \times P$ WSS modules in the add/drop structure of node i
$M_{wss}^{CF}(i,j)$	number of $1 \times P$ WSS modules in the add/drop structure of node i and direction j
$M_{wss}^{xc}(i)$	total number of $1 \times P$ WSSs in the cross connection structure of node i
N	number of nodes
$N(o)$	number of destination nodes of node o
o	node that is origin of a demand
$O_c(o,d,s)$	number of ports with bit rate c for the demands between the nodes o and d in node o and shelf s
$O_c(o,d,a)$	number of ports with bit rate c for the demands between the nodes o and d in module a
$\overline{O}_c(o,d,a)$	number of ports with bit rate c for the demands between the nodes o and d in module a already being used
$O_c(o,d,a,s)$	number of ports with bit rate c required for the demands between the nodes o and d in module a and shelf s
$\overline{O}_c(o,d,a,s)$	number of ports with bit rate c for the demands between the nodes o and d in module a and shelf s already being used

$O_c^{c^*,\epsilon}(o,d,a)$	number of input ports with bit rate c^* for the demands between the nodes o and d in the muxponder module a generating an output signal with bit rate c in the grooming configuration ϵ
$\overline{O}_c^{c^*,\epsilon}(o,d,a)$	number of input ports with bit rate c^* for the demands between the nodes o and d in the muxponder module a generating an output signal with bit rate c in the grooming configuration ϵ already being used
$O_l(o,d)$	number of ports with bit rate l for the demands between the nodes o and d
$O_l(o,d,a)$	number of ports with bit rate l for the demands between the nodes o and d in module a
$\overline{O}_l(o,d,a)$	number of ports with bit rate l for the demands between the nodes o and d in module a already being used
$O_l(o,d,s)$	number of ports with bit rate l for the demands between the nodes o and d in shelf s
$O_l(o,d,a,s)$	number of ports with bit rate l for the demands between the nodes o and d in module a and shelf s
$\overline{O}_l(o,d,a,s)$	number of ports with bit rate l for the demands between the nodes o and d in module a and shelf s already being used
$O_l^{c,\epsilon}(o,d,a)$	number of input ports with bit rate c for the demands between the nodes o and d in the muxponder module a generating an output signal with bit rate l in the grooming configuration ϵ
$\overline{O}_l^{c,\epsilon}(o,d,a)$	number of input ports with bit rate c for the demands between the nodes o and d in the muxponder module a generating an output signal with bit rate l in the grooming configuration ϵ already being used
$OpEx_N$	total network OpEx related to the power consumption and footprint requirements of the nodes
P	number of ports of the $1 \times P$ WSS module
P_c	number of ports of the client module accepting signals with bit rate c
$P_{ads}^{CD}(i,j)$	number of add/drop ports in the node i for the channels of direction j for the colorless and directionless ROADM
$P_{ads}^{CDC}(i,j)$	number of add/drop ports in the node i for the channels of direction j for the colorless, directionless and contentionless ROADM
$P_{ads}^{CF}(i,j)$	number of add/drop ports in the node i for the channels of direction j for the colorless and fixed direction ROADM
$P_{ads}^{FD}(i)$	number of add/drop ports needed in the add/drop structures of node i for the fixed frequency and directionless ROADM
P_i	number of input ports in the $P_i \times P_o$ WSS module
P_l	number of ports of the line module with bit rate l
P_o	number of output ports in the $P_i \times P_o$ WSS module
P_{osc}	number of ports of the OSC module
$R(i)$	number of signals requiring 3R regeneration in the node i
r_1, r_2	random numbers used in the tournament method of the genetic algorithm
$R_T(o)$	total number of racks in the node o

s	shelf
S	set of shelves
S_{amp}^{ads}	number of slots occupied by the amplifier in the add/drop structure of node i
S_{amp}^{xc}	number of slots occupied by the amplifier in the cross connection structure of node i
S_c	number of slots occupied by the client module with bit rate c
S_c^{ϵ}	number of slots occupied by the muxponders modules generating an output signal with bit rate c in the grooming configuration ϵ
S_{ctr}	number of slots occupied by the control modules for ROADM architectures
S_{ctr}^{mb}	number of slots occupied by the control modules for muxponders-based architectures
S_{ctr}^{pbe}	number of slots occupied by the control modules for partial non-blocking EXCs architectures
S_{esm}^{pbe}	number of slots occupied by the the ESMs for partial non-blocking EXCs architectures
S_l	number of slots occupied by the line module with bit rate l
S_l^{ϵ}	number of slots occupied by the muxponders modules generating an output signal with bit rate l in the grooming configuration ϵ
S_{mwss}^{ads}	number of slots occupied by the $P_i \times P_o$ WSS module in the add/drop structure
S_{osc}^{ads}	number of slots occupied by the OSC module in the add/drop structure
$span$	distance in kilometers between consecutive amplifiers
s_r	space occupied by one rack in m^2
S_{sf}	number of slots available in the shelf for ROADM architectures
S_{sf}^{mb}	number of slots available in the shelf for muxponders-based architectures
S_{sf}^{pbe}	number of slots available in the shelf for partial non-blocking EXCs architectures
$S_{tot}^{CD}(i)$	number of slots in node i for the colorless and directionless ROADM
$S_{tot}^{CDC}(i)$	number of slots in node i for the colorless, directionless and contentionless ROADM
$S_{tot}^{CF}(i)$	number of slots in node i for colorless and fixed direction ROADM
$S_{tot}^{FD}(i)$	number of slots in node i for fixed frequency and directionless ROADM
$S_{tot}^{FF}(i)$	number of slots in node i for fixed frequency and fixed direction ROADM
$S_{tot}^{mb}(o)$	number of slots in node o for muxponders-based architectures
$S_{tot}^{nbe}(o)$	number of slots in node o for non-blocking EXCs architectures
S_{wsc}^{ads}	number of slots occupied by the WSC modules used in cross connection structure
S_{wss}^{ads}	number of slots occupied by the $1 \times P$ WSS used in the add/drop structure
S_{wss}^{xc}	number of slots occupied by the $1 \times P$ WSS used in the cross connection structure

t	number of links added to the ring topology
$T(o)$	total traffic in node o in Gbit/s
$\overline{T}(o)$	weighted mean of the total traffic in node o
$t_c(o,d)$	number of client signals with bit rate c between the nodes o and d
$t_{c^*}(o,d)$	number of client signals with bit rate c^* between the nodes o and d
$t'_c(o,d)$	number of client signals with bit rate c between the nodes o and d in the second stage grooming for muxponders-based architectures
$[T_c]$	matrix with the number of client signals with bit rate c between all node pairs
$TP_c(o)$	percentage of total traffic with bit rate c in Gbit/s in node o
$T_S(i,j)$	costs depending on the number of transmission systems installed in the link between the nodes i and j
$T_O(i,j)$	costs depending on the number of optical channels that traverse the link between the nodes i and j
$Tsv_c^{mb}(o)$	number of short-reach transceivers with bit rate c in node o for muxponders-based architectures
$Tsv_{c^*}^{mb}(o)$	number of short-reach transceivers with bit rate c^* in the node o for muxponders-based architectures
$Tsv_c^{nbe}(o)$	number of short-reach transceivers with bit rate c in the node o for non-blocking EXC architectures
$Tsv_c^{pbe}(o)$	number of short-reach transceivers with bit rate c in the node o for partial non-blocking EXCs architecture
$Tsv_l^{mb}(o)$	number of long-reach transceivers with bit rate l in the node o for muxponders-based architectures
$Tsv_l^{nbe}(o)$	number of long-reach transceivers with bit rate l in the node o for non-blocking EXCs architectures
$Tsv_l^{pbe}(o)$	number of long-reach transceivers with bit rate l in the node o for partial non-blocking EXCs architectures
$U(i,j)$	number of transmission systems installed in the link between the nodes i and j
V	set of nodes
$W(i,j)$	number of optical channels that are routed through the link between the nodes i and j
X	set of muxponder modules used in the second stage grooming or in a single stage grooming for muxponders-based architectures
X^*	set of muxponder modules used in the first stage grooming for muxponders-based architectures
$Y(i,j)$	cost with right-of-way privileges and/or method used to deploy a transmission system between the nodes i and j

Z_{ij}^{od} variable indicating whether the optical channel between nodes o and d is routed through the link between the nodes i and j or not

List of figures

List of tables

CHAPTER 1

Introduction

Internet supports global telecommunications and has become a major driver of world economy and social interaction. However, the constant introduction of new services is pushing the bandwidth required in transport networks to its limits [1]. As a result, network operators demand costly network elements with more capacity, higher transmission rates and faster processing. On the other hand, operators also suffer an huge pressure to reduce the cost per bit transported due to the networks high deployment and maintenance costs [2]. Thus, operators need to be able to cope with the traffic growth while maintaining the offered quality of service in a cost efficient manner. In this context, an optimized network planning and dimensioning becomes critical.

Transport networks have evolved from point-to-point wavelength division multiplexing (WDM) systems towards multilayer flexible networks. Multilayer networks enable the interworking between electronic and optical technologies, allowing a more efficient groom, switch and transport of the traffic [5]. Additionally, flexible networks enable operators to setup connections and reconfigure established connections by remote action, thus making transport networks more responsive to the traffic changes [6, 7]. Nevertheless, these technological advances are increasing the complexity of the planning process. As a result, the manual and rule-of-thumb network planning strategies of the past are being replaced by sophisticated software tools. Usually, the planning tools aim to minimize the total cost of ownership (TCO) of the network. The network TCO can be divided into capital expenditures (CapEx) and operational expenditures (OpEx) [3, 4]. The CapEx is related to the costs with the setup of the infrastructure. This comprises the network physical infrastructure (i.e. network elements such as routers, switches, fibers) and software (for instance network management systems), as well as the building to host equipment and/or staff [3]. The OpEx is related to the costs to keep the network operating. This includes maintenance, power consumption, rents (such as buildings, equipment or fibers), service management, repairment, ongoing network planning

and marketing and pricing, among others [3].

The planning tool usually requires a set of input information that depends on the system vendor available equipment, and on the network operator requirements. Based on the processing of these input parameters, a cost efficient solution is obtained and a variety of outputs generated. Figure 1.1 illustrates the classical dimensioning process.

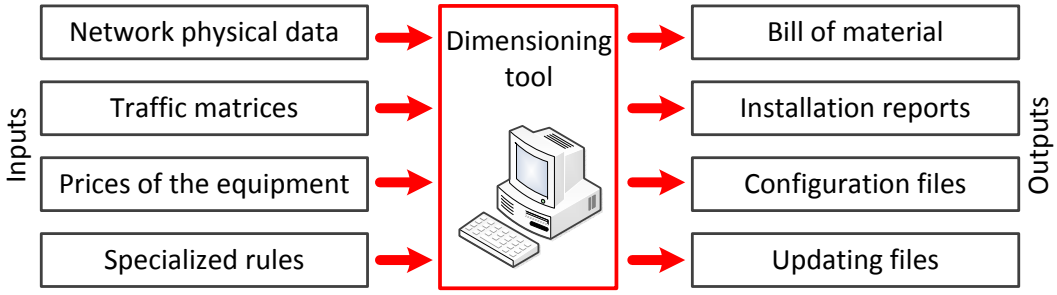

Figure 1.1: Classical dimensioning tools inputs and outputs [4].

As presented in Fig. 1.1, the input parameters can include the physical topology (or nodes location), client traffic matrices, prices for each component of the network elements, and specialized rules (for instance the survivability and grooming scheme or routing policy). The outputs generated generally includes the links and nodes equipment, installation reports, files for configurations and updates, reports with overall performance analysis and the network TCO.

1.1 Motivation and objectives

The network planning tool is important for both systems vendors and network operators and is used in the various stages of the telecommunications business. In the budgeting and implementation stages, a planning tool offering a cost-efficient solution to the network operator can be decisive to the system vendor, in a competing environment. After, in the operation stage, the planning tool can be used to re-optimize the available resources, bringing additional cost savings to network operators. Moreover, as new competing technologies are always being introduced, planning tools are also used to evaluate and compare the various alternatives before advancing to their manufacturing, market introduction and deployment. Thus, the planning tool directly affect the competitiveness of a vendor or an operator.

Nowadays, various planning tools for optical transport networks are commercially available, providing solutions in a non-vendor specific environment. Examples of such tools are AriaNetworks [8], WANDL [9], VPIsystems [10], SteelCentral (former OPNET SP Transport Planner) [11], and Detecon NetWorks [12]. Due to their commercial nature, these tools usually only provide support for mature, and with large market penetration, technologies. Even though, systems vendors and network operators desire to make prospective studies on competing technologies, take into account specialized implementation constraints or proprietary technology. Consequently, many operators and vendors make use of tailored in-house

developed software like Coriant TransNet [13] and 7196 [14], Alcatel-Lucent 1390 [15], Cisco network planning system (NPS) [16], Infinera NPS [17] or Ericsson optical networks planner [18]. However, due to their proprietary nature, these tools are not publicly available to perform comparative studies and evaluate the quality of the obtained solutions [19]. From the research point of view, the development of methodologies and optimization tools for transport networks planning is being intensively investigated [4, 20–33]. Most of the solutions rely on statistical methods [4, 20–24], heuristic algorithms [28, 30–33], or integer linear programming (ILP) models [25–30]. Statistical methods provide the fastest way to dimension a network, and are suitable for preliminary stages of the planning process, where information is not complete. However, they are very sensitive to changes in the assumptions used in their development, and the results can have a high level of uncertainty. Heuristic algorithms tend to be relatively fast, scalable, and suitable for large instances of the problem. However, optimal solutions are not guaranteed and changes to contain newly constraints can prove to be difficult. In opposition, with ILP models optimal solutions can be obtained, at least, for some instances of the problem. However, scalability limitations may arise depending on the computational resources available. Nevertheless, the type of solutions obtained and the models themselves can give an insight in key and structural aspects of the problem. Moreover, the ILP models also enable easy and quick changes. This is particularly relevant in an environment that new technologies are always being proposed and that requirements can differ substantially between operators.

Due to the challenges and importance of the planning and dimensioning of transport networks, for both academia and industry, this PhD was developed in collaboration between University of Aveiro, Instituto de Telecomunicações Aveiro, and Coriant Portugal. It has intended to contribute for the knowledge transfer between the academia and the industry, and has produced research in the area of planning multilayer optical networks, in its various stages. This thesis intended to achieve four main objectives:

1. Detailed study of the various implementation constraints, functionalities, and limitations, for the various multilayer transport nodes architectures. This includes the assembling of a realistic and consolidated database comprising the cost, number of slots and ports, and power consumption for all modules required by the architectures.

2. Development of tools for the optimized design of survivable physical topologies with minimum cost for links.

3. Development of optimization tools for multilayer nodes dimensioning that takes into consideration the hardware implementation constraints, suitable for greenfield and multi-period scenarios.

4. Perform accurate techno-economic comparisons between the different architectures.

1.2 Thesis outline

This thesis is organized in seven chapters. Chapter 2 consists of a state-of-art review about multilayer optical transport networks. The chapter introduces and explains the main concepts and notions used throughout the thesis. It starts by describing the main functions performed by the links and the nodes in a transport network, then the relation between the network transport mode and the grooming scheme that can be employed is presented. Thereafter the links architecture is presented in detail, followed by the general nodes implementation. The remaining of the chapter is devoted to the detailed description of the various fixed and flexible architectures used to implement the electrical and the optical layer of a node.

The first stage of the overall network design process is the deployment of the network links. Therefore, Chapter 3 presents a genetic algorithm for the design of survivable physical topologies with minimum CapEx for links. As the convergence of the genetic algorithms depends on the used genetic operators, we analyze their impact on the quality of the obtained solutions. The performance of different initial population generators, selection methods, crossover operators and population sizes are compared and benchmarked using an ILP model and a set of node locations of real-world transport networks.

After the deployment of the network links, the nodes must be planned. Thus, dimensioning models for nodes are proposed in Chapter 4. The models calculate the number and type of modules required to implement fixed and flexible architectures, for both the electrical and the optical layer. Regarding the electrical layer, the developed model is based on ILP formulations and intend to optimize the grooming of the client signals. For the optical layer, an analytical model is proposed, allowing the calculation of the number of modules required to implement reconfigurable optical add/drop multiplexers (ROADM) with different levels of flexibility. All the proposed models take into consideration the hardware implementation constraints. Nevertheless, the developed models are sufficiently generic in a way that they are not vendor or technology specific.

In Chapter 5, a comparative techno-economic analysis for greenfield scenarios is presented, using the models presented in Chapter 4. The analysis focus on the CapEx, power consumption, and footprint requirements. The followed methodology assumes a single node, varying the factors that have an impact on the node performance. For the comparative analysis of the electrical layer architectures, different traffic loads and client traffic patterns are considered. Regarding the optical layer architectures, different number of add/drop channels and nodal degrees are taken into consideration. By focusing the analysis on a single node, it is possible to generate a meaningful set of simulations not biased by network-wide design decisions (e.g., routing), thus gaining insight on key factors affecting the performance of the various node architectures. As a result of the comparative techno-economic study, an optimization method based on node architecture selection is proposed. The optimization method is based on statistical and simple rules, identifying the scenarios where a determined architecture (electrical and optical) brings advantages. Then, when considering the network and using the developed rules, the total network OpEx can be minimized by selecting the architecture of each node

accordingly.

The last stage of the overall network design process is the multi-period (or brownfield) planning. At this stage, capacity is already deployed in the network and the goal is to accommodate the new client signals in an optimized manner. In Chapter 6, detailed dimensioning models to use in multi-period planning are proposed, and a comparative techno-economic analysis presented. This chapter focused on the electrical layer architectures. Importantly, the potential savings attained by exploiting hitless re-grooming are also assessed, highlighting the traffic conditions where such savings are more significant. Once again, and due to the same reasons pointed out before, the analysis assumes a single node, different client traffic patterns and levels of traffic variability. Finally, the main conclusions and suggestions for future research directions are presented in Chapter 7.

1.3 Main contributions

This thesis proposes optimization methods and methodologies for the various planning stages of multilayer transport networks. Furthermore, various comparative techno-economic analysis are performed, for both greenfield and multi-period scenarios. In the author's opinion, the most important results of thesis are the following:

1. Study of the main characteristics of transport network topologies and proposal of a genetic algorithm that can be used to determine the least cost network topology [J1, J2, J3, B1, C1, C2, C9].

2. Development of optimization models to calculate the quantities and costs of network elements for fixed and flexible multilayer node architectures in greenfield scenarios. Performance of various techno-economic studies for the CapEx, power consumption and footprint requirements for single nodes and networks [J4, C3, C4, C5, C6, C7, C8, C11, C12, C13].

3. Proposal of an optimization method based on statistical and simple rules for total network OpEx minimization. The method enables node architecture selection by site, depending on its specific properties and requirements [J4].

4. Development of optimization models to calculate the quantities and costs of network elements for fixed and flexible electrical node architectures in multi-period scenarios. Performance of various techno-economic studies for the CapEx, power consumption and footprint requirements for single nodes [J5, C10, C14].

5. Identification of the scenarios and traffic conditions where hitless re-grooming can bring cost benefits [J5, C14].

1.4 List of publications

The major achievements obtained during this work were submitted to the scientific international community through the following listed publications.

Book chapter

[B1] R. M. Morais and A. N. Pinto, "Chapter 7, Topological design using genetic algorithms", *Intelligent Systems for Optical Networks Design: Advancing Techniques*, pp. 153-173, IGI Global, USA, 2013.

Papers in journals

[J5] R. M. Morais, J. Pedro, P. Monteiro, A. N. Pinto, "Benefits of node architecture flexibility and hitless re-grooming in transport networks", *IEEE/OSA Journal of Optical Communications and Networking*, 2015 *(submitted)*.

[J4] R. M. Morais, J. Pedro, P. Monteiro, A. N. Pinto, "Impact of node architecture in the power consumption and footprint requirements of optical transport networks", *IEEE/OSA Journal of Optical Communications and Networking*, Vol. 5, No. 5, pp. 421 - 436, May 2013.

[J3] R. M. Morais, C. Pavan, A. N. Pinto, C. Agra, "Genetic algorithm for the topological design of survivable optical transport networks", *IEEE/OSA Journal of Optical Communications and Networking*, Vol. 3, No. 1, pp. 17 - 26, January 2011.

[J2] S. Routray, R. M. Morais, J. F. Rocha, A. N. Pinto, "Statistical model for link lengths in optical transport networks", *IEEE/OSA Journal of Optical Communications and Networking*, Vol. 5, No. 7, pp. 762 - 773, July 2013.

[J1] C. Pavan, R. M. Morais, J. F. Rocha, A. N. Pinto, "Generating realistic optical transport network topologies", *IEEE/OSA Journal of Optical Communications and Networking*, Vol. 2, No. 1, pp. 80 - 90, January 2010.

Papers in conference proceedings

[C14] R. M. Morais, J. Pedro, P. Monteiro, A. N. Pinto, "Impact of grooming architecture of transport nodes in line interface count for multi-period planning", *Proc Optical Fiber Communications Conference And Exhibition - OFC*, Los Angeles, USA, pp. Th1I.5, May 2015 *(to be published)*.

[C13] R. M. Morais, J. Pedro, P. Monteiro, A. N. Pinto, "On the impact of client to line port blocking in the line interface count and footprint of transport networks", *Proc International Conf. on Transparent Optical Networks - ICTON*, Graz, Austria, pp. Tu.A4.6, July 2014.

[C12] R. M. Morais, J. Pedro, P. Monteiro, A. N. Pinto, "The cost dependence between the node architecture, the grooming scheme and the traffic pattern in optical networks", *Proc International Conf. on Transparent Optical Networks - ICTON*, Cartagena, Spain, pp. Tu.C4.4, June 2013.

[C11] A. N. Pinto, R. M. Morais, J. Pedro, P. Monteiro, "Total cost of ownership comparison between single and mixed line rate networks", *Proc International Conf. on Transparent Optical Networks - ICTON*, Cartagena, Spain, pp. Tu.C4.3, June 2013.

[C10] C. Pavan, R. M. Morais, A. N. Pinto, "Evaluation of ongoing capacity provisioning methods in optical networks", *Proc Conf. on Telecommunications - ConfTele*, Castelo Branco, Portugal, pp. 337 - 340, May 2013.

[C9] R. M. Morais, P. Monteiro, A. N. Pinto, "Generating near-optimal survivable topologies", *Proc International Conf. on Transparent Networks - ICTON*, pp. We.B3.2, Coventry, United Kingdom, July 2012.

[C8] A. N. Pinto, R. M. Morais, J. Pedro, P. Monteiro, "Cost evaluation in optical networks: Node architecture and energy consumption", *Proc International Conf. on Transparent Networks - ICTON*, pp. Tu.D2.4, Coventry, United Kingdom, July 2012.

[C7] R. M. Morais, C. Pavan, J. F. Rocha, A. N. Pinto, "Estimating extra capacity for dedicated protection in mesh optical transport networks", *Proc European Conf. on Networks and Optical Communications and Conf. on Optical Cabling and Infrastructure - NOC/OC*, pp. OCG - 8, Newcastle, United Kingdom, July 2011.

[C6] R. M. Morais, C. Pavan, A. N. Pinto, "Estimating the energy consumption in survivable optical transport networks", *Proc International Conference on Computer as a Tool - EUROCON*, Lisbon, Portugal, April 2011.

[C5] R. M. Morais, C. Pavan, A. N. Pinto, "Equipment and energy related costs in survivable optical networks", *Proc European Conf. on Networks and Optical Communications - NOC*, Faro, Portugal, pp. 99 - 104, June 2010.

[C4] A. N. Pinto, C. Pavan, R. M. Morais, "Dimensioning optical networks: A practical approach", *Proc International Conf. on Transparent Networks - ICTON*, Munich, Germany, pp. Mo.C4.5, June 2010.

[C3] C. Pavan, R. M. Morais, A. N. Pinto, "Estimation of CapEx in survivable optical transport networks", *Proc European Conf. on Networks and Optical Communications - NOC*, Faro, Portugal, pp. 263 - 268, June 2010.

[C2] R. M. Morais, C. Pavan, A. N. Pinto, C. Agra, "Genetic algorithm for the design of survivable optical transport networks: Operators comparison", *Proc Congresso da APDIO*, Lisboa, Portugal, pp. 123 - 130, September 2009.

[C1] R. M. Morais, C. Pavan, C. Agra, A. N. Pinto, "Design of survivable optical networks with minimum CapEx", *Proc Conf. on Telecommunications - ConfTele*, Santa Maria da Feira, Portugal, pp. 307 - 310, May 2009.

References

[1] Cisco (2014). "Cisco visual networking index: Forecast and methodology, 2013-018 (2014)," Tech. Rep. [Online]. Available: http://www.cisco.com/c/en/us/solutions/collateral/service-provider/ip-ngn-ip-next-generation-network/white_paper_c11-481360.pdf

[2] Alcatel-Lucent (2009). "The new economics of telecom networks - bringing value back to the network," Tech. Rep. [Online]. Available: http://images.tmcnet.com/online-communities/ngc/pdfs/application-enablement/whitepapers/The-New-Economics-of-Telecom-Networks.pdf

[3] S. Verbrugge, D. Colle, M. Pickavet, P. Demeester, S. Pasqualini, A. Iselt, A. Kirstädter, R. Hülsermann, F.-J. Westphal, and M. Jäger, "Methodology and input availability parameters for calculating OpEx and CapEx costs for realistic network scenarios," *Journal of Optical Networking*, vol. 5, no. 6, pp. 509–520, June 2006.

[4] C. Pavan, "Dimensioning of Multilayer Optical Networks," Ph.D. thesis, University of Aveiro, 2011.

[5] T. Lehman, X. Yang, N. Ghani, F. Gu, C. Guok, I. Monga, and B. Tierney, "Multilayer networks: An architecture framework," *IEEE Communications Magazine*, vol. 49, no. 5, pp. 122–130, May 2011.

[6] P. Serna, I. S. Barla, S. Duhovnikov, C. M. Machuca, and D. Schupke, "Evaluation of transponder and regenerator pre-provisioning," in *Proc Conference of Telecommunication, Media and Internet Techno-Economics - CTTE*, 2012.

[7] S. Frisken, S. Poole, and G. Baxter, "Wavelength-selective reconfiguration in transparent agile optical networks," *Proceedings of the IEEE*, vol. 100, no. 5, pp. 1056–1064, May 2012.

[8] Arianetworks (2014). [Online]. Available: http://www.aria-networks.com/

[9] Wandl - wide area network design laboratory (2014). [Online]. Available: http://www.wandl.com/html/index.php

[10] Vpisystems - multi-layer trasnport optimization and planning (2014). [Online]. Available: http://www.vpisystems.com/solutions/multi-layer-transport-planning---optimization/

[11] Steelcentral (2014). [Online]. Available: http://www.riverbed.com/products/performance-management-control/

[12] Networks - Detecon (2014). [Online]. Available: https://www.networks.detecon.com/drupal/en/startseite

[13] Transnet/transconnect design and planning tools (2014). [Online]. Available: http://www.coriant.com/products/transnet_transconnect.asp

[14] 7196 optical planning tool (2014). [Online]. Available: http://www.coriant.com/products/7196.asp

[15] Alcatel-lucent 1390 network planning tool (2014). [Online]. Available: http://www.alcatel-lucent.com/products/1390-network-planning-tool

[16] Cisco network planning and design (2014). [Online]. Available: http://www.cisco.com/c/en/us/products/cloud-systems-management/network-planning-solution/index.html

[17] Infinera (2013). "Infinera network planning system (NPS)," Tech. Rep. [Online]. Available: http://www.infinera.com/pdfs/mgmt/infn_nps_DS-IMS-01-002-0409-00.pdf

[18] Ericsson (2009). "Ericsson optical networks planner," Tech. Rep. [Online]. Available: http://archive.ericsson.net/service/internet/picov/get?DocNo=28701-FGC1010524&Lang=EN&rev=C

[19] P. Pavon-Marino and J.-L. Izquierdo-Zaragoza, "On the role of open-source optical network planning," in *Proc Optical Fiber Communication Conference and Exposition and the National Fiber Optic Engineers Conference - OFC/NFOEC*, pp. Th1E.1, March 2014.

[20] S. K. Korotky, "Network global expectation model: A statistical formalism for quickly quantifying network needs and costs," *IEEE/OSA Journal of Lightwave Technology*, vol. 22, no. 3, pp. 703–722, March 2004.

[21] J.-F. Labourdette, E. Bouillet, R. Ramamurthy, and A. Akyamac, "Fast approximate dimensioning and performance analysis of mesh optical networks," *IEEE/ACM Transactions on Networking*, vol. 13, no. 4, pp. 906–917, August 2005.

[22] C. Pavan, R. M. Morais, and A. N. Pinto, "Quantifying the restoration capacity in optical mesh networks," in *Proc. Next Generation Internet Networks - NGI*, pp. 1–5, July 2009.

[23] C. Pavan, R. M. Morais, A. R. Correia, and A. N. Pinto, "Dimensioning of optical networks with incomplete information," in *Proc. Fourth Advanced International Conference Telecommunications - AICT*, pp. 261–264, June 2008.

[24] S. Routray, R. M. Morais, J. da Rocha, and A. N. Pinto, "Statistical model for link lengths in optical transport networks," *IEEE/OSA Journal of Optical Communications and Networking*, vol. 5, no. 7, pp. 762–773, July 2013.

[25] K. Zhu and B. Mukherjee, "Traffic grooming in an optical WDM mesh network," *IEEE Journal on Selected Areas in Communications*, vol. 20, no. 1, pp. 122–133, January 2002.

[26] R. Dutta and G. N. Rouskas, "A survey of virtual topology design algorithms for wavelength routed optical networks," *Optical Networks*, vol. 1, pp. 73–89, September 2000.

[27] D. Cieslik, *Network Design Problems*, Wiley, 2009.

[28] X. Dong, T. El-Gorashi, and J. Elmirghani, "IP over WDM networks employing renewable energy sources," *IEEE/OSA Journal of Lightwave Technology*, vol. 29, no. 1, pp. 3 –14, January 2011.

[29] I. Katib and D. Medhi, "IP/MPLS-over-OTN-over-DWDM multilayer networks: An integrated three-layer capacity optimization model, a heuristic, and a study," *IEEE Transactions on Network and Service Management*, vol. 9, no. 3, pp. 240–253, September 2012.

[30] G. Shen, L. Peng, Y. Shen, and H. Sardesai, "Optimal node hardware module planning for layer-one optical transport networks," *IEEE/OSA Journal of Optical Communications and Networking*, vol. 3, no. 12, pp. 937–946, December 2011.

[31] H. Zhu, H. Zang, K. Zhu, and B. Mukherjee, "A novel generic graph model for traffic grooming in heterogeneous WDM mesh networks," *IEEE/ACM Transactions on Networking*, vol. 11, no. 2, pp. 285–299, April 2003.

[32] E. Bouillet, G. Ellinas, J.-F. Labourdette, and R. Ramamurthy, *Path Routing in Mesh Optical Networks*, John Wiley & Sons, 2007.

[33] A. Tzanakaki, K. Katrinis, T. Politi, A. Stavdas, M. Pickavet, P. Van Daele, D. Simeonidou, M. O'Mahony, S. Aleksić and, L. Wosinska, and P. Monti, "Dimensioning the future pan-european optical network with energy efficiency considerations," *IEEE/OSA Journal of Optical Communications and Networking,* , vol. 3, no. 4, pp. 272 –280, April 2011.

CHAPTER 2

Transport modes, links and nodes architectures

Internet traffic can be highly variable and uncertain [1–4]. Traffic variability and uncertainty may arise from different causes such as the growth of content sharing, the widespread use of cloud computing, large social events, or network failures. This traffic variability can be observed in granularity, geographic and temporal distribution [1–4]. Thus, network operators need to be able to cope with the traffic changes while maintaining the offered quality of service. In the past, they have relied in overprovisioning (and underutilizing) the network resources [4]. Currently, operators are under pressure to lower the cost per bit transported. In order to achieve that, the deployment of flexible transport networks is being pursued [5–9].

Optical transport networks comprise a set of network elements, connected by optical fiber links, and have the function of providing transport, routing, supervision, and survivability to the client signals [10, 11]. To optimize the available resources, the low-speed client signals need to be efficiently groomed into high-speed optical channels. Nowadays, the grooming is realized by electronic devices, thus multilayer nodes are implemented where an electrical and an optical layer processes the signal [8, 12–14]. However, optical-electrical-optical (OEO) conversions and electronic processing are costly operations [9, 15, 16]. Depending on the placement of OEO conversion elements, optical transport networks can operate in opaque, transparent or translucent mode [15]. Currently, multi-layer nodes can be implemented using a variety of architectures with different levels of flexibility [5, 8, 9, 17, 18]. In this chapter the network modes of operation, the links, and the nodes architectures are discussed.

The chapter is organized in six sections. The node functions, the network modes of operation and their respective grooming schemes are presented in Section 2.1. Section 2.2 is devoted to the links architecture, and Section 2.3 to the general nodes architecture. The detailed description of the nodes electrical layer is presented in Section 2.4. Regarding the node optical layer, the considered architectures are presented in Section 2.5. Finally, in Section 2.6 the chapter is summarized.

2.1 Transport modes and grooming schemes

An optical transport network can be seen as set of bidirectional links connecting nodes. Optical links have the function of provisioning connection of an optical signal between two adjacent nodes [15, 19]. Nodes can perform six main functions: encapsulation; electrical switching; deterministic or statistical multiplexing (grooming); wavelength assignment; optical switching; and optical multiplexing [15, 19]. The client signals, regardless of the native protocol, are received by the node and encapsulated using a standard/protocol that meets transport networks requirements (Optical Transport Network (OTN) is the common choice in optical transport networks, nowadays). The encapsulation process attaches controlling information to the client signal [15, 19]. The encapsulated client signals can then be electrically switched, groomed, routed, and forwarded toward their final destination, allowing the rearrangement and interconnection of lower data rate signals to, or between, higher bit rate signals. To efficiently fill these high bit rate signals, time division multiplexing (TDM) or statistical multiplexing can be deployed [15, 19]. Afterward, the optical layer is responsible for the wavelength assignment, optical switching and multiplexing. We are assuming that the wavelengths are assigned following the International Telecommunication Union - Telecommunication Standardization Sector (ITU-T) grid [20]. After, optical switching enables one or more wavelengths to be switched in the optical domain between different ports. Finally, to take advantage of the spectrum range provisioned by a single fiber, optical multiplexing is performed. Wavelength division multiplexing (WDM) is a technology in which several wavelengths are combined and transmitted over a single fiber [15, 19].

As aforementioned, an optical transport network can operate in opaque, transparent or translucent mode [15]. A transport mode is identified in function of its utilization of OEO conversions, and is closely related to the ability of the node to perform electrical and/or optical switching. A network configured in opaque transport mode performs OEO conversion of the signals at the end of each transmission system, i.e., at every node [15]. A network operating in a transparent mode keeps the signal of a source destination connection in the optical domain at every intermediate nodes, i.e., except in the end nodes the signal does not undergo OEO conversion [15]. In translucent networks the signals travel through the network in the optical domain, however in some intermediate nodes it goes to OEO conversion [15]. In the context of node functions, the encapsulation, electrical switching, grooming, wavelength assignment, and WDM multiplexing are required under all the transport modes. Additionally, transparent and translucent networks require optical switching. Table 2.1 summarizes the node required functions for the three transport modes considered.

In the following, we briefly describe the main characteristics of the three transport modes and relate them with the grooming scheme. The description is illustrated by a 4-nodes network example. In all the transport modes illustration (see Figs. 2.1, 2.2 and 2.3) ports used to send/receive client signals are represented as gray squares and ports used to send/receive wavelengths are represented as colored squares. Equipment of the electrical layer is presented with gray background whereas equipment of the optical layer is presented with white

Table 2.1: Relation between the network mode of operation, the grooming scheme, and the end and intermediate node functions. Functions that are not present in all nodes are in italic.

Transport mode	**Opaque**	**Transparent**	**Translucent**
Grooming scheme	• Link-by-link	• Single-hop	• Multi-hop
End nodes	• Encapsulation • Electrical switching • Grooming • Wavelength assignment • WDM multiplexing	• Encapsulation • Electrical switching • Grooming • Wavelength assignment • WDM multiplexing	• Encapsulation • Electrical switching • Grooming • Wavelength assignment • WDM multiplexing
Intermediate nodes	• Electrical switching • Grooming • Wavelength assignment • WDM multiplexing	• Optical switching • WDM multiplexing	• *Electrical switching* • *Grooming* • *Wavelength assignment* • Optical switching • WDM multiplexing

background.

2.1.1 Opaque transport mode

A network configured in opaque transport mode performs OEO conversion of the signals at the end of each transmission system [15]. In this kind of networks the signals are regenerated at every node since they have to be converted to the electronic domain. An advantage of this mode is that it eliminates accumulation of physical impairments and allows full flexibility in client signals switching and grooming [15]. Thus, it can improve capacity utilization of optical channels by providing traffic grooming at every node. Moreover, wavelength continuity is not a requirement as the signal goes to the electrical domain at every intermediate node. However, this solution typically increases the CapEx and the power consumption of the network because every node needs to carry out OEO conversion for each single wavelength [9, 15, 16, 21].

Figure 2.1 presents the 4-nodes network example operating in opaque mode. To take advantage of the OEO conversion at every intermediate node, a link-by-link grooming scheme is used [13, 22]. In the link-by-link grooming scheme every client signal can be groomed with any other client signal that share the same link [13, 22]. As can be observed in Fig. 2.1, the client signal between the nodes one and four is groomed with the client signal between the nodes one and two and two and three in the link between the nodes one and two. After, in the transmission system between the nodes two and four, the same client signal is groomed with the one between the nodes two and four.

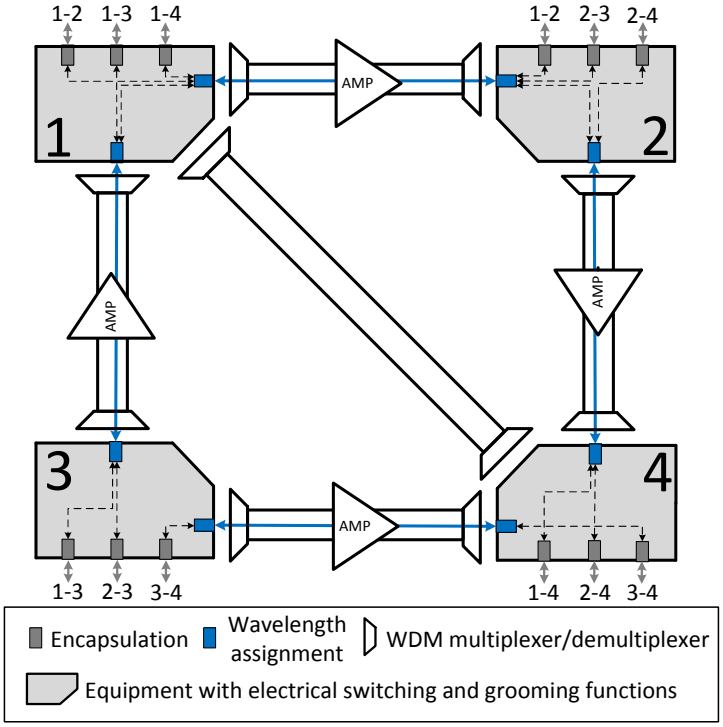

Figure 2.1: Opaque mode of operation with a link-by-link grooming scheme. As OEO conversion is performed at every node, the clients can be groomed independently of their source and destination, provided that they share a common transmission system in the path. Each node requires electrical switching, grooming, wavelength assignment, and WDM multiplexing functions.

2.1.2 Transparent transport mode

A network operating in transparent mode keeps the signal in the optical domain at every intermediate nodes of the path between the source and the destination [15]. Electrical regeneration is not present, thus the quality of the optical signals degrade as they traverse the optical components along the route limiting the maximum transmission length of the optical path [15, 19]. As this type of network only performs OEO conversion at the end nodes of the path, capacity utilization of the wavelength channels is restricted to client signals with the same end points. Moreover, wavelength continuity must be guaranteed.

Figure 2.2 presents the 4-nodes network example operating in transparent mode thus, employing a single-hop grooming scheme [13, 22]. In the single-hop grooming scheme only client signals with the same source and destination can be groomed into the same wavelength. At each node, add and drop wavelengths are sent to the electrical layer, whereas through wavelengths are switched in the optical domain. In the example presented in Fig. 2.2, each pair of nodes have a dedicated wavelength that remains in the optical layer in each intermediate node. Note that only client signals with the same end-points share the same wavelength.

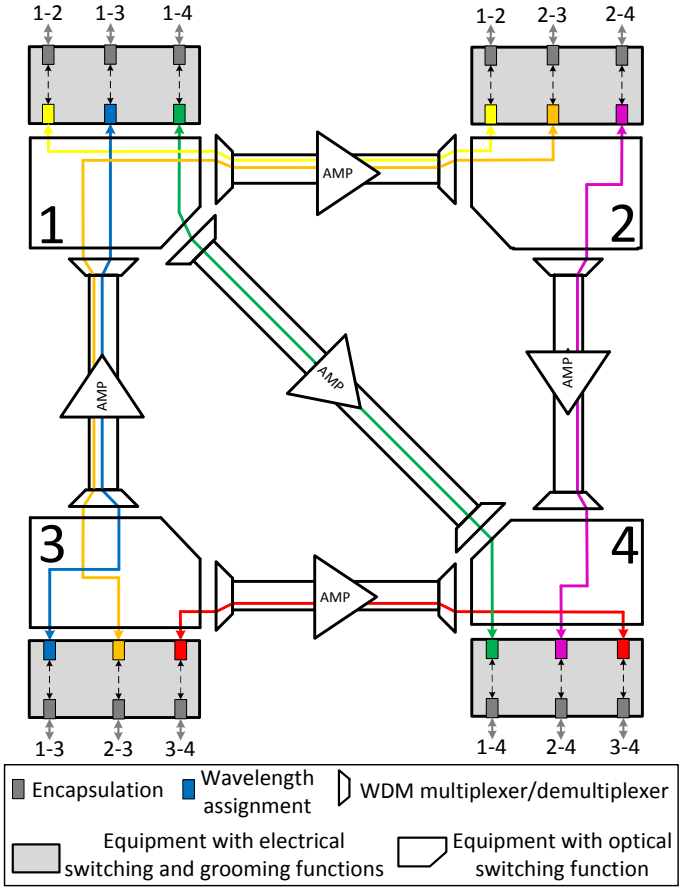

Figure 2.2: Transparent mode of operation with a single-hop grooming scheme. As OEO conversion is only performed at the end-nodes, grooming of client signals is restricted to services with the same end-points. Each node requires WDM multiplexing and optical switching functions.

2.1.3 Translucent transport mode

In order to take the advantages of the two above mentioned types of networks, an alternative to opaque and transparent networks are translucent networks [15]. In translucent networks, the signal suffer OEO conversion in selected intermediate locations before it reaches its destination. The signals are converted to the electronic domain to improve signal quality, or when sub-wavelength switching and grooming needs to be performed. Therefore, capacity utilization of wavelengths can be better optimized in translucent networks.

Figure 2.3 presents the 4-nodes network example operating in translucent mode thus, employing a multi-hop grooming scheme [13, 22]. In the multi-hop grooming scheme client signals with different source and destination nodes can share the same lightpath up to some common intermediate node. Client signals can use more than one lightpath to travel from the source to the destination node. At each node, lightpaths carrying local traffic or carrying client traffic that needs to be switched to a different lightpath are sent to the electrical layer whereas lightpaths carrying through traffic are kept in the optical layer. In the example presented in Fig. 2.3, the client signal between the nodes one and four is groomed with the client signals between the nodes one and two and one and three from node one to node three.

At the node three the signals are sent to the electrical domain and switched. The client signal between the nodes one and four is switched to the lightpath between the nodes three and four. Note that the client signals between the nodes two and four and three and four are also switched to that lightpath and groomed with the one between the nodes one and four.

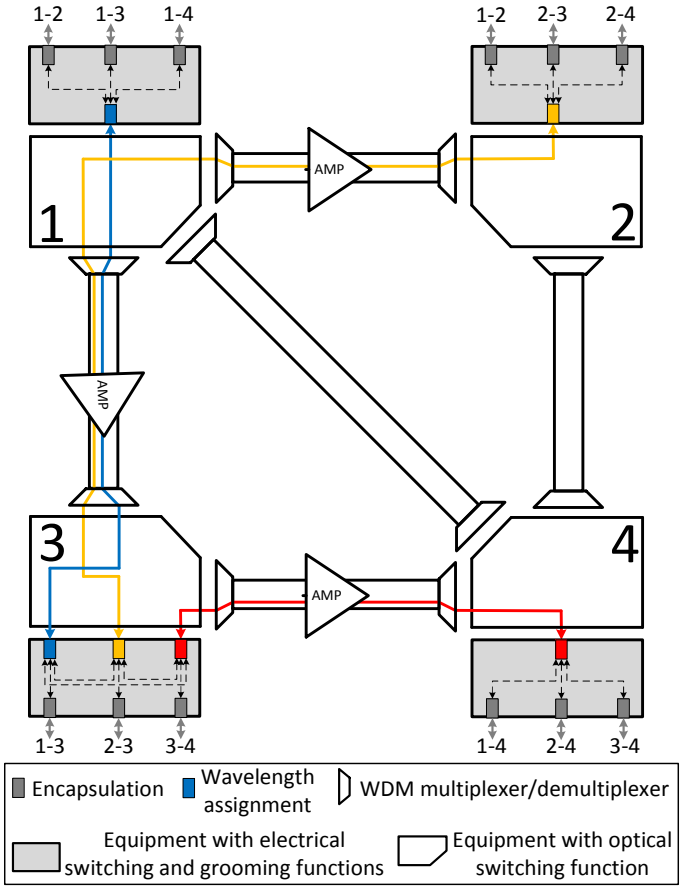

Figure 2.3: Translucent mode of operation with a multi-hop grooming scheme. As OEO conversion is performed at selected nodes, a client signal can use more than one lightpath to reach its destination. Each node requires WDM multiplexing and optical switching functions and may require electrical switching, grooming and wavelength assignment.

2.2 Links architecture

Links can be composed by one or more transmission systems. The transmission system starts and ends in the node and has the function of transport a WDM signal between directly connected nodes [15, 19]. To perform this function, the transmission system comprises a pair of optical fibers and amplifiers, see Fig. 2.4.

The optical fiber is the medium where the optical signal is transmitted and is capable of transporting data on wavelengths [19]. As the WDM signal propagates into the fiber it suffers different linear and nonlinear impairments [23]. One of the limiting effect is fiber attenuation. To counteracts fiber attenuation the optical signal needs to be amplified or became too weak for a correct detection. Therefore, inline optical amplifiers are incorporated

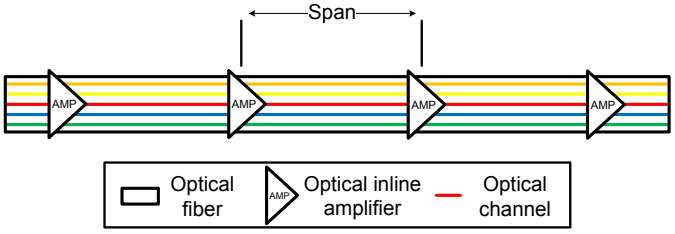

Figure 2.4: Bidirectional transmission system architecture: optical fiber and inline optical amplifiers.

in the transmission system. The separation between consecutive amplification stages is called the span [15, 19]. Typically, an amplifier acts over the complete spectral range at once (e.g., the conventional band, i.e. the C-band, from 1531 nm to 1570 nm [20]), so all the wavelengths are amplified at the same time. Moreover, optical amplifiers are transparent to protocol, modulation and bit rate thus, they can be changed without replacing the amplifier. Currently, erbium doped fiber amplifiers (EDFA) [24] and Raman fiber amplifiers (RFA) [25] are available for transport applications. Note that optical amplifiers do not perform the reshaping and retiming of the signal, thus the signal may still need to be regenerated periodically. Besides increasing the signal strength, the optical amplifier also degrades the optical signal-to-noise ratio (OSNR) due to the addition of amplified spontaneous emission (ASE) noise [24].

In commercial systems, transmission systems are installed within conduits [26]. The general purpose of the conduit is to provide a protected pathway for the transmission system. Conduits can be buried on the ground or submersed in the water, and usually follow major railways, roads, rivers, or oceans [26]. Typically, inline optical amplifiers are modules installed into small cabinets located along the conduit.

2.3 Nodes architecture

Nowadays, high-capacity multilayer transport nodes are customizable systems assembled with multiple types of modules [16, 18, 27, 28]. As depicted in Fig. 2.5, multilayer nodes consist of three main building blocks: modules with different functions and number of ports, shelves to provide a common infrastructure to the modules, and the rack to support and provide power to the shelves [16, 18, 27, 28]. Both the electrical and the optical layer equipment are implemented in a similar way, however requiring different types of modules and shelves.

A module (also named card or blade) is an independent device with well-defined functionalities (e.g., encapsulation, grooming, wavelength assignment) [16, 18, 28]. Modules enclose the electrical (e.g. chips, processors) and the optical (e.g. lasers, photodiodes) components necessary to perform the given function(s). Usually, modules have connections through the front panel and the backplane. Front panel interworking is typically made via optical connectors whereas backplane communication uses electrical pin connectors [16, 28]. In the remaining, front panel connections will be simply referred as ports. Ports are equipped with transceivers (e.g., small form-factor plugabble (XFP) or C form-factor pluggable (CFP)) and are used

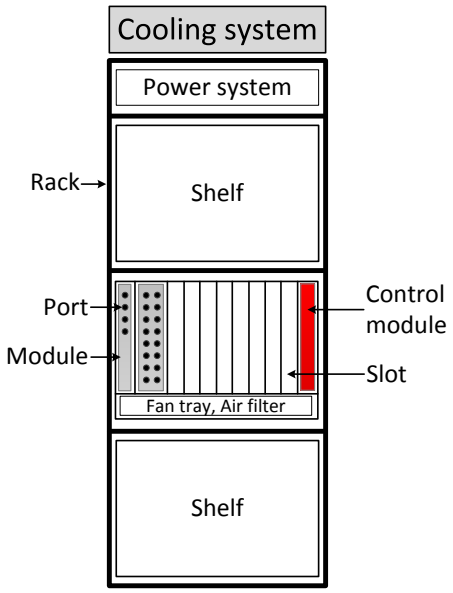

Figure 2.5: Node schematic: port, module, slot, shelf and rack. High-performance nodes are sets of modules each one with particular functionalities. Each module has a specific number of ports and occupies a pre-determined number of slots in a shelf. The shelf is then attached into a rack that provides power and cooling to the system.

to interconnect two different modules through optical fibers. In the remainder of this work we always assume bidirectional connections. A transceiver implements the physical media adaptation functions to transmit and receive the optical signals over the defined reach [29]. Depending on the travel distance, short-reach or long-reach transceivers must be used [29]. Usually, short-reach transceivers are gray, i.e. are wavelength independent and long-reach transceivers are colored, i.e. are wavelength dependent. Additionally, data information can also be exchanged between modules using the backplane. Note that modules connected to different backplanes generally cannot communicate with each other except when there is an external link (such as a short-reach fiber link) connecting them [16, 18, 28]. We are going to assume single-shelf backplanes [28]. The space offered by the shelf is usually divided into units of space called slots. Each type of module can occupy one or more slots in the shelf. Moreover, some predetermined slots are reserved for the control modules that are required for operation, administration and management (OAM) of the system [28]. Shelves are attached into racks. The rack provides mechanics for mounting multiple shelves and provides power and cooling to the system. Figure 2.5 presents the schematic of a rack that can support up to three shelves, a power and a cooling system. The shelf in the middle has 12 slots and it is equipped with three modules. One module with four ports occupying one slot, another module with sixteen ports occupying two slots and the control module.

In the following a detailed overview of the modules required to implement fixed and flexible architectures in the electrical and the optical layer of the node is presented. Fixed node architectures, requires technicians to visit the node site for reconfiguration whereas flexible node architectures enable operators to remotely reconfigure their networks through the

management system software [18].

2.4 Electrical layer

The client signals originated, typically, from IP routers, Ethernet or SDH/SONET switches are encapsulated, switched, and groomed into line signals. In transport networks, currently encapsulation, electrical switching and electrical grooming is usually realized using OTN technology [12, 30]. OTN is a circuit switch technology defined in ITU-T Standard G.709 and provides an unified transport platform that supports various types of client services [10]. To widely support the different services, the client traffic is encapsulated into optical data units (ODU), regardless of the original protocol. The ODU is the basic payload that is electronically switched and groomed [10, 30]. One drawback of circuit switching is that it is a technology with constant bit rate. As the network is becoming more packet dominated (e.g., layer-2 Ethernet, layer-3 IP), technologies with constant bit rate can introduce inefficiencies in bandwidth utilization [12, 31]. Therefore, electrical switching and grooming in transport networks are evolving to handle either packets (typically $<$ 1 Gbit/s) or circuits (typically $\geq$ 1 Gbit/s). The current technology of choice for packet switching transport networks is the multi protocol label switching - transport profile (MPLS-TP) [19, 32]. MPLS-TP is a customization of MPLS that is being defined by the Internet Engineering Task Force (IETF) and align the efficiency of packet networking with the reliability required in transport networks operation. This technology labels the units of data and provides switching and grooming by manipulating these labels [32]. In transport networks MPLS-TP is usually implemented with generic framing procedure (GFP) over OTN optical transport units (OTU) [10, 30, 33].

The physical implementation of the electrical layer can have a fixed or a flexible architecture. A fixed architecture supports manual circuit switching and a flexible architecture can support automatic circuit or packet switching. Fixed architectures are assumed to be realized via muxponders or cascades of muxponders whereas flexible architectures demand electrical cross connects (EXC), that are assumed to allow remote reconfiguration [18]. In the following, a detailed description of the architectures considered is presented.

2.4.1 Muxponders-based architecture

This section presents the fixed architecture based on muxponders [18, 34, 35]. A muxponder is a module that can groom multiple low data rate client signals into an high data rate signal, providing a combination of encapsulation and grooming functionalities [16, 18, 34, 35]. Muxponders with line ports also provide wavelength assignment. A muxponder module has input ports to receive the smaller bit rate signals and output ports to send the groomed higher bit rate signals. This type of architecture is referred as fixed because reconfiguration requires a technician visit to the site, and the mixture of client signals (grooming configuration) provided by each muxponder is defined by the module itself [16, 18, 34, 35]. If a different grooming configuration is required a new type of module needs to be used. This architecture

also introduces constraints in the interconnection of the client signals to the muxponder module. Particularly, all client signals that are to be groomed into the same high data rate signal must be connected to the same module. Moreover, access to specific client signals involves the full demultiplexing of all client signals and re-multiplexing of the remaining ones. We assume that all input muxponder ports are client ports and the output muxponder ports can be used to cascade muxponders or as line ports. The muxponder output port can support a pluggable transceiver, thus acting as a short or long reach module.

An example of a fixed architecture is presented in Fig. 2.6. Each solid close box represents a required module that needs to be inserted into a shelf, see Figs. 2.5 and 2.6. Gray circles are client ports and color circles represent line ports. Additionally, gray arrows depict client signals and color arrows depict line signals. Fig. 2.6 presents an example where three muxponders and one transponder are required. The transponder is used when the client signal bit rate is the same than the line signal bit rate, thus not performing grooming. Typically, muxponder modules provide TDM between two or more constant bit rates. For example, 2.5 Gbit/s signals into 10 Gbit/s or a mixture of 10 Gbit/s and 40 Gbit/s into a 100 Gbit/s line signal. In some cases, muxponder modules with the required client and line bit rates are not accessible. In this case a two stage grooming is necessary. For instance, let us assume two types of muxponders (4×2.5 Gbit/s to 10 Gbit/s and 10×10 Gbit/s to 100 Gbit/s) and a line signal at 100 Gbit/s. In this case, grooming a 2.5 Gbit/s client signal into a 100 Gbit/s line signal requires a two stage grooming. The first muxponder generates a 10 Gbit/s signal and the second one grooms the signal along with others and transmits a 100 Gbit/s wavelength, see Fig. 2.6. Moreover, client signals switching between different line signals can only be performed by external interconnection and involves the full signal demultiplexing, as can be observed in Fig. 2.6. In this architecture the backplane only provides monitoring of the modules.

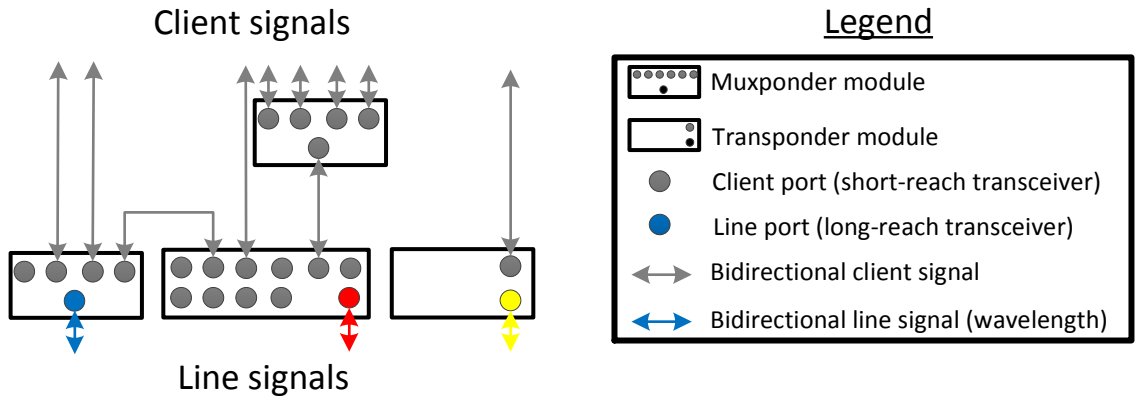

Figure 2.6: Muxponder-based architecture example. The fixed architecture requires muxponders or cascades of muxponders and transponders. The figure presents three types of muxponders, two of them in a two stage architecture.

2.4.2 Electrical cross connects based architectures

This section presents the flexible architecture based on EXCs. EXCs are equipments that allow circuit switching or packet switching of client signals through backplane communication [8, 14, 16, 18, 28, 34, 36, 37]. EXCs comprise client modules to receive the client signals and to perform encapsulation, electrical switching modules, and line modules to perform grooming and wavelength assignment. The ports of the client modules are equipped with short-reach transceivers whereas the ports of the line modules are equipped with long-reach transceivers. Usually, the modules port density depends on the port bit rate and slot capacity of the equipment. In general, EXCs can perform non blocking switching [27, 28, 37]. Thus, client signals can be connected to any module that is configured to accept them as the EXC can be remotely controlled through the electrical switch module (ESM) [16, 18, 27, 28]. The ESM is then responsible to switch the client signals via backplane to the line modules or between line modules.

An example of a general EXC is presented in Fig. 2.7. Each solid close box represents a required module. Gray circles are client ports and color circles represent line ports. Additionally, gray arrows depict client signals and color arrows depict line signals. Solid lines represent connections via fibers and dashed lines represent connections via backplane and controlled by the ESM module. It can be observed three types of client modules that can accept three different client bit rates (one module for each bit rate), three line modules, and one ESM. Independently of the wavelength in which the client signal will be transported, it can be connected to any module that is able to accept it. The ESM module receives the signals from the different client modules and switch them into the line modules and between line modules.

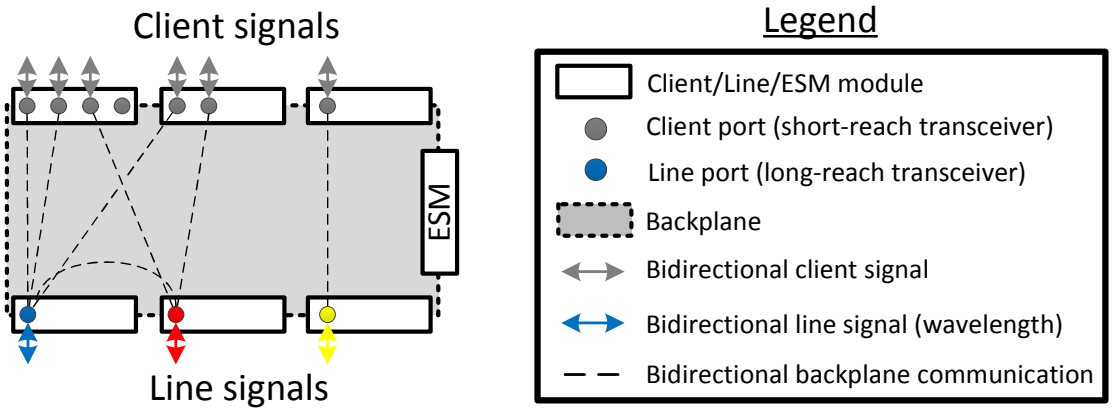

Figure 2.7: Electrical cross connect example. The flexible architecture requires a shelf enabling backplane switching, one type of client module per client service, line modules and an electrical switch module (ESM). The figure presents three types of client modules, three line modules, and one ESM.

When discussing in which layer the electrical switching should be performed, three principal node architectures can be distinguished: parallel, layered and hybrid [14, 16, 36, 37]. In the parallel architecture (see Fig. 2.8(a)), independent ODU and MPLS switches exist for the circuit and packet traffic, respectively [36]. Note that the use of either only ODU

or only MPLS switch is also an alternative. As in this option the switches are independent devices, the same wavelength cannot be shared for circuit and packet traffic. Thereby creating possible network inefficiencies. In the layered architecture (see Fig. 2.8(b)), the packet traffic is not directly encapsulated onto a wavelength but passes through the ODU switch first [36]. Packet traffic is encapsulated into ODUs that are then switched and groomed along with circuit traffic in the ODU switch. This solution offers an alternative approach for better bandwidth exploitation as it allows the coexistence of circuit and packet traffic within the same wavelength. However, at the cost of doubling the number of equipments. In the hybrid architecture (see Fig. 2.8(c)), an integrated switch matrix is used for processing both the circuit and the packet traffic [16, 36, 38–40]. This can lead to cost savings, as the common parts (e.g., power supply, OAM communication, racks, fans) are shared, and the communication devices between layers (e.g., short-reach transceivers) reduced. Moreover, circuit and packet traffic can share the same wavelength.

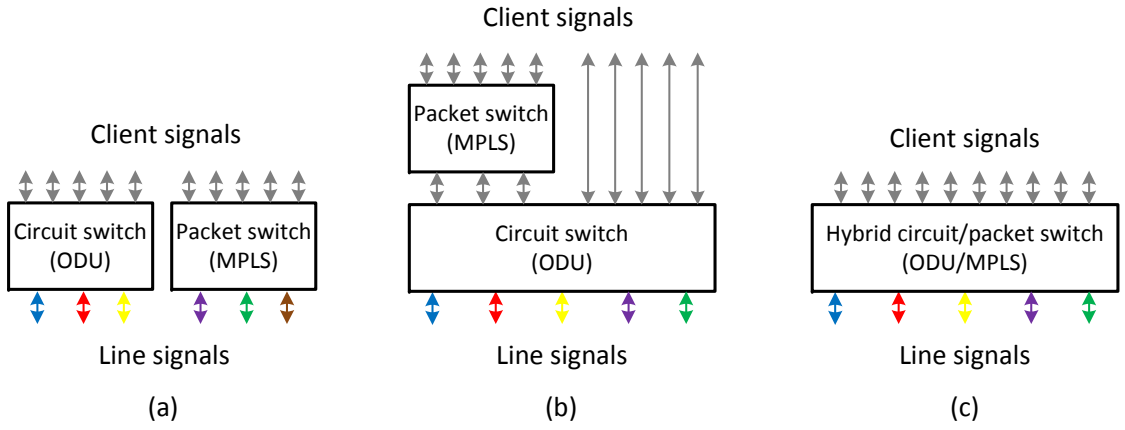

Figure 2.8: Flexible node architectures: (a) parallel, (b) layered, (c) hybrid. In parallel nodes separate ODU and MPLS switches exist for the circuit and packet traffic. The layered nodes do not encapsulate the packet traffic directly onto a wavelength but always passes through the ODU switch first. In the hybrid nodes, the switch matrix is used for processing both the circuit and the packet traffic. Regardless the node deployed, the line signal is an OTU.

2.5 Optical layer

In opaque networks, the node optical layer is only responsible to perform WDM multiplexing. In transparent and translucent networks optical switching is also performed in the optical layer. In these transport modes, when a wavelength reached a node, it could either be switched to the electrical layer to stop at the node (add/drop channels) or switched between different optical links to pass through the node (through channels). The key enabler for the switching of wavelength channels is the ROADM [1, 5, 41–45]. ROADMs can have different implementations with various degrees of flexibility. Flexibility in the context of the optical layer refers to the ability of providing remote reconfiguration for the switching, central frequency and direction of a wavelength [1, 5, 18, 44].

2.5.1 Building blocks

Several basic modules are currently available for the deployment of the optical layer of the node [5, 19, 44, 45]. The diagrams of the modules used as building blocks are shown in Fig. 2.9. The figures emphasized the function performed by the module rather than the technology used for its implementation. Note that each module is bidirectional and needs to be inserted into a shelf that provides monitoring and controlling, see Fig. 2.5.

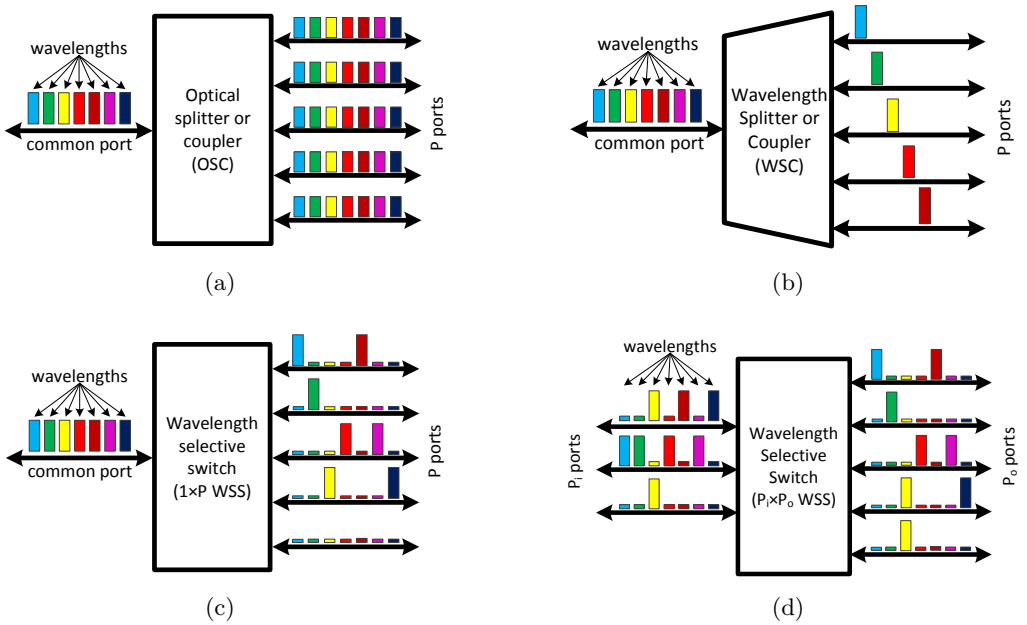

Figure 2.9: Common building blocks for the nodes optical layer: (a) Optical splitter or coupler (OSC), (b) wavelength splitter or coupler (WSC), (c) $1 \times P$ wavelength selective switch (WSS), and (d) $P_i \times P_o$ wavelength selective switch (WSS).

The module presented in Fig. 2.9(a) is the optical splitter or coupler (OSC) [5, 44]. An optical splitter distributes the optical power from the input port (on the left) to all the output ports (on the right). Generally this type of module operates over all the frequency range of the transmission system [5, 44]. In the opposite direction the optical power is coupled. As can be seen in Fig. 2.9(a) the full WDM signal is present in all the ports.

In Fig. 2.9(b) a wavelength splitter or coupler (also referred to as a WDM multiplexer/ demultiplexer) is presented. The wavelength splitter or coupler (WSC) is a module to multiplex and demultiplex optical channels in different wavelengths [5, 44]. A WSC is usually implemented by an arrayed waveguide grating (AWG) [5, 44]. In this type of module the wavelength or wavelengths assigned to each port are fixed. As can be observed in Fig. 2.9(b), the WDM signal in the left port is demultiplexed to the right ports. However, each port is associated with a specific wavelength and cannot operate in a different one. In the opposite direction it acts as a multiplexer.

The wavelength selective switches (WSS) presented in Figs. 2.9(c) and 2.9(d) are active devices, thus enabling wavelength reconfiguration under software command [5, 44, 45]. WSSs

can dynamically switch individual or a set of wavelengths into any port [5, 44, 45]. WSSs are currently being deployed using liquid crystal (LC) and micro electro mechanical systems (MEMS) [5, 44, 45]. A $1 \times P$ WSS is a module that is able to switch a selected wavelength or wavelengths from a single common optical port to any one of the P output ports. As shown in Fig. 2.9(c), the WDM signal presented in the left port is demultiplexed and switched to the right ports. The wavelengths that are present in the right ports can be remotely changed without restrictions. In the opposite direction it multiplex the wavelength or wavelengths to the common port.

The $P_i \times P_o$ WSS presented in Fig. 2.9(d) is a generalization of a $1 \times P$ WSS [5, 44, 45]. This module is able to switch individual or a set of wavelengths from any input port to any output port, as long as there are no multiple copies of the same wavelength in a single port. As shown in Fig. 2.9(d) the wavelengths received by the input ports (on the left) can be dynamically switched to any of the output ports (on the right), and vice-versa.

Opaque networks only demand a WSC module at both ends of the transmission systems. In transparent and translucent networks the ROADM is responsible to multiplex and switch the wavelength channels. ROADMs comprise one or more modules presented in Fig. 2.9, and are composed by a cross connection structure and an add/drop structure [5, 18]. The cross connection structure is responsible to switch the wavelength signals between different transmission systems that reach the node, and between the transmission systems and the add/drop structure. The add/drop structure provides the interface between the electrical layer and the cross connection structure. All ROADM architectures allow full flexibility in the cross connection structure. However, some implementations have two major limitations in the add/drop structure: they can only operate in a fixed wavelength, and the channel operated by each port can only be sent to/received from one transmission system [1, 5, 18, 44]. In the following, a detailed overview of ROADM architectures with different degrees of flexibility is presented.

2.5.2 Cross connection structure

The cross connection structure is responsible to switch the wavelengths to the appropriate transmission system to continue their paths, or to the add/drop structure to terminate at the node. We assume that the cross connection structure is implemented in the same way in all considered ROADM architectures and it is composed of one $1 \times P$ WSS module and a pre/booster amplifier per transmission system, i.e. per direction, see Fig. 2.10 [1, 5, 18]. Alternative solutions for cross connection structures are also possible. For instance, broadcast and select architectures are implemented with a OSC in the incoming direction of a transmission system and a WSS in the outcoming direction, enabling multicast communication [5, 44]. However, they are out of the scope of this work. Further details can be found in [1, 5, 41–44, 46–49]. The P ports of the WSS module are connected to all the remaining directions and to the add/drop structure(s), selecting the wavelengths to route between the different directions and between the directions and the add/drop structure. Considering the

West fiber in Fig. 2.10 it can be observed that two wavelengths (red and blue) are switched to the add/drop structure to terminate their paths whereas the remaining two (green and orange) are switched to the others directions. The green optical channel is switched to the East transmission system and the orange to the South.

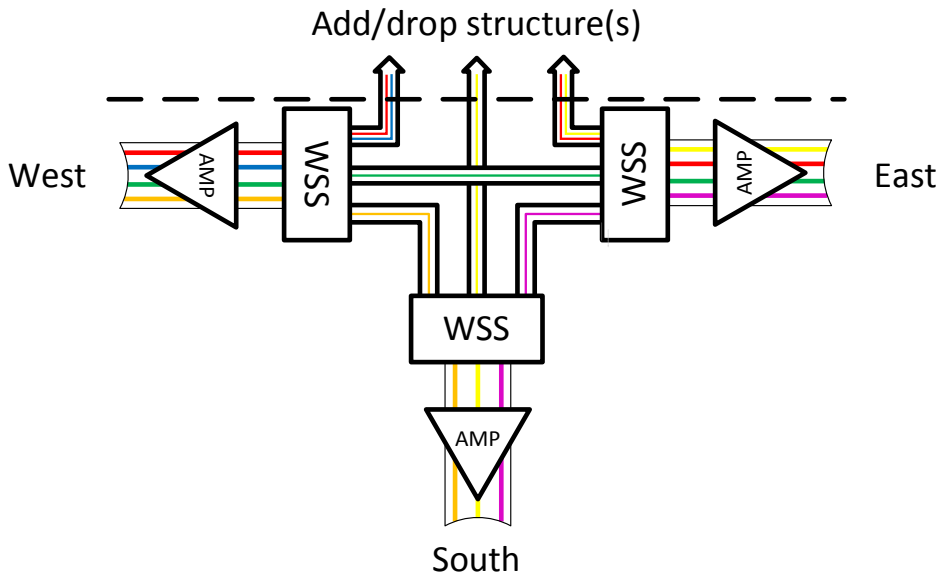

Figure 2.10: Cross connection structure of a ROADM. The cross connection structure is composed by one $1 \times P$ bidirectional WSS per transmission system and is responsible to switch the wavelength signals between the different transmission systems that reach the node and between the transmission systems and the add/drop structure.

Each WSS must be directly connected to all the other WSSs and to the add/drop structure to enable full flexibility. Thus, the maximum number of transmission systems that can converge to the node, i. e. nodal degree, is limited by the port density in the WSS and by the number of add/drop structures deployed.

2.5.3 Add/drop structure: fixed frequency and fixed direction

The add/drop structure defines the node flexibility. The node architecture shown in Fig. 2.11 is the fixed frequency and fixed direction ROADM [5, 18, 44]. In this architecture the wavelength and the direction of the add/drop channel is fixed, and reconfiguration always requires the technician intervention on the site. The fixed frequency and fixed direction add/drop structure requires a dedicated WSC module per transmission system. Therefore signals can only be sent to one direction and on the fixed wavelength defined by the WSC port. As can be observed in Fig. 2.11, the wavelengths represented as red need to be plugged into a specific port of the WSC module. To reconfigure a service wavelength, the transceiver must be moved to the WSC port operating in the corresponding wavelength. Moreover, since the add/drop structure is unique for each transmission system, moving a wavelength to another direction requires physically moving the transceiver to the WSC module of the desired direction. As can be observed in Fig. 2.11, the WSC attached to the West direction

can only sent/receive signals in that specific direction.

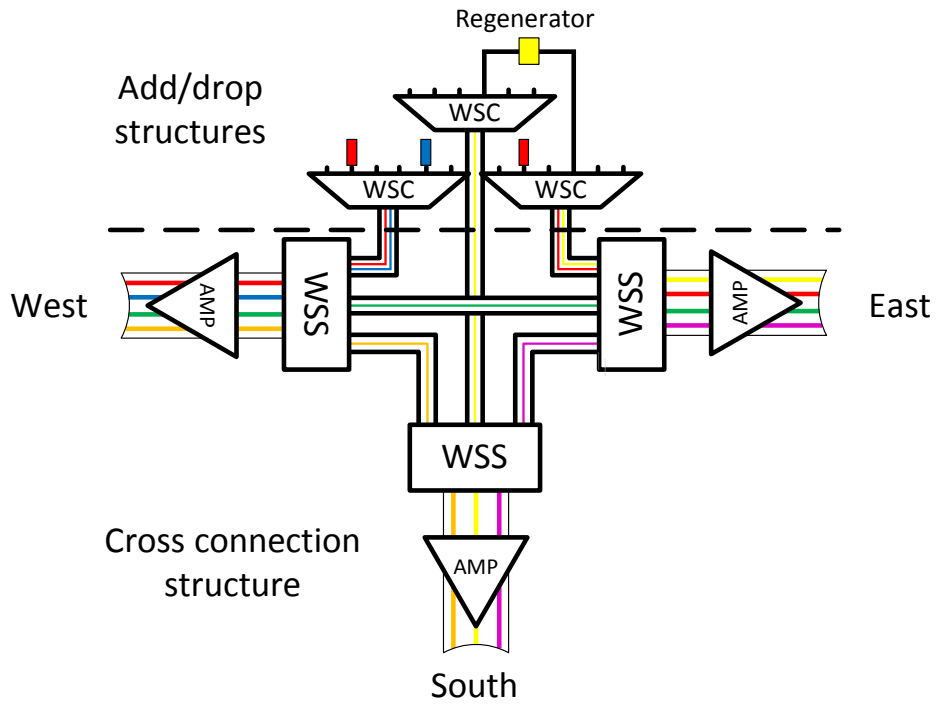

Figure 2.11: ROADM architecture with fixed frequency and fixed direction add/drop structure. One WSC module is dedicated per transmission system. This architecture requires WSC, WSS and amplifier modules. Changes in the wavelength or in the direction of a specific add/drop channel requires manual intervention on the site.

2.5.4 Add/drop structure: colorless and fixed direction

In a colorless architecture the wavelength assigned to any add/drop port can be change remotely [5, 18, 44]. In the previous architecture the WSC module restrict each add/drop port to only one particular wavelength. To eliminate this constraint a WSS module can be used to replace the WSC module and provide the colorless functionality [5, 44]. Alternative colorless ROADM architectures can be implemented with an OSC module instead of a WSS module [5]. However, this type of architecture is not considered in this work. Note that the colorless functionality demands wavelength tunable transmitters and receivers [5]. A colorless and fixed direction add/drop ROADM is presented in Fig. 2.12. The implementation is similar to the fixed frequency and fixed direction architecture presented in Fig. 2.11 but replacing the WSC by WSS modules. Moreover, as the WSS module can be remotely reconfigured, changes in the wavelength that a specific port is operating can be performed without the need of physically changing the port. However, this ROADM architecture still has a dedicated add/drop structure per transmission system. As the WSS module have a limited number of ports that is usually smaller than the maximum number of wavelengths that can be multiplexed into a single transmission system, a cascade of WSS modules can be used to increase the add/drop port count.

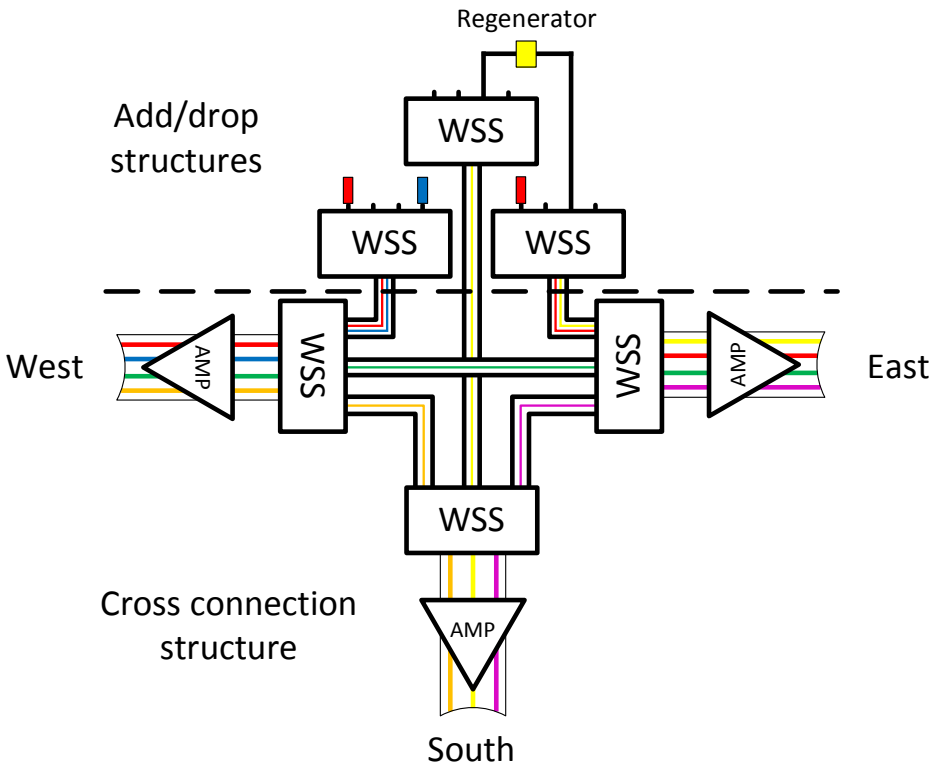

Figure 2.12: ROADM architecture with colorless and fixed direction add/drop structure. WSS modules are dedicated per transmission system. Changes in the wavelength can be made remotely whereas changes in the direction of a specific add/drop channel requires manual intervention on the site.

2.5.5 Add/drop structure: fixed frequency and directionless

In a directionless ROADM any add/drop channel can be remotely redirected to any transmission system that converges to the node [5, 18, 44]. Directionless architectures are implemented by sharing the same add/drop structure between all transmission systems starting/ending on the ROADM. The fixed frequency and directionless add/drop structure shown in Fig. 2.13 requires one WSC and one WSS module per add/drop structure. The add/drop channels are connected to a WSC module, thus not enabling the colorless functionality. After, a WSS module that is connected to all the node directions switch the wavelengths to the appropriate transmission system. Changes in the direction of an add/drop channel can be performed remotely. In spite of a WSC module is usually able to multiplex/demultiplex all the channels that a single transmission system can support, as the add/drop structure is shared, the maximum number of add/drop channels is limited by the number of add/drop structures implemented.

2.5.6 Add/drop structure: colorless and directionless

The colorless and directionless ROADM is presented in Fig. 2.14 [5, 18, 44]. This architecture enables that both the wavelength and/or the direction of a specific add/drop channel can be remotely changed. The add/drop channels feed the $P \times 1$ WSS module, where all

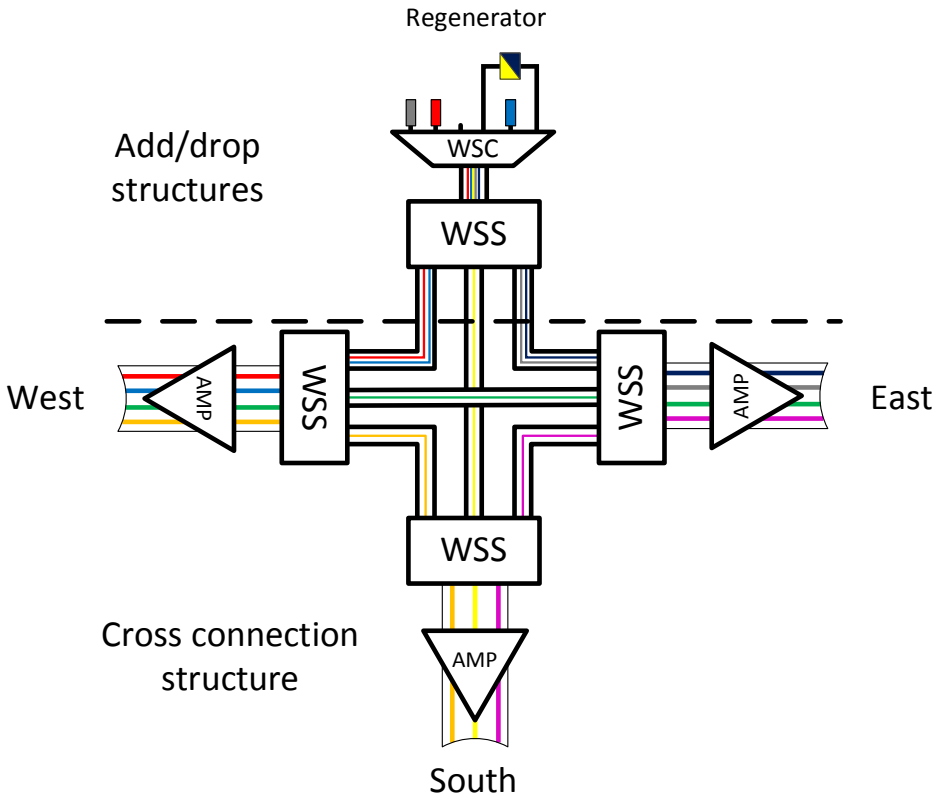

Figure 2.13: ROADM architecture with fixed frequency and directionless add/drop structure. The add/drop structure is shared between all the transmission systems. One WSC and one WSS module are required per add/drop structure. Changes in the wavelength requires manual intervention on the site whereas changes in the direction can be made remotely.

the signals are multiplexed. This WSS module is connected to another $1 \times P$ WSS that is connected to all the node directions, see Fig 2.14(a). In this way, both the wavelength and the direction are dynamically reconfigurable. However, multiples copies of the same wavelength cannot be transmitted along the same add/drop structure even if directed to different transmission systems. This is referred as the contention problem [5]. As an example, consider the wavelength represented as yellow and coming from the South direction in Fig. 2.14(a). Even if the yellow wavelength is available in the East transmission system, a wavelength conversion needs to be performed in the regenerator, otherwise the two wavelengths are blocked in the WSS common port of the add/drop structure, see Fig. 2.14(a).

As previously discussed, the maximum number of add/drop channels per add/drop structure is restricted by the number of ports in the WSS. However, in this architecture a cascade of WSSs is avoided due to the losses imposed to the signal [42, 48, 50]. To increase the maximum number of add/drop channels, the number of add/drop structures can be increased, at the cost of a reducing the maximum nodal degree allowed. An alternative extended colorless and directionless add/drop structure is the architecture presented in Fig. 2.14(b) [18, 42, 48]. The add/drop channels feed the $P \times 1$ WSS before going through an OSC module. The OSC module aggregates all WDM signals that arrive from the different WSSs in the add/drop

structure. An amplifier is usually required at the output/input of the OSC module in order to compensate the losses imposed by the WSSs and OSC modules [42]. Finally, the combined signal is transmitted to another $1 \times P$ WSS module that is connected to all directions, and routes the wavelengths to their intended destinations.

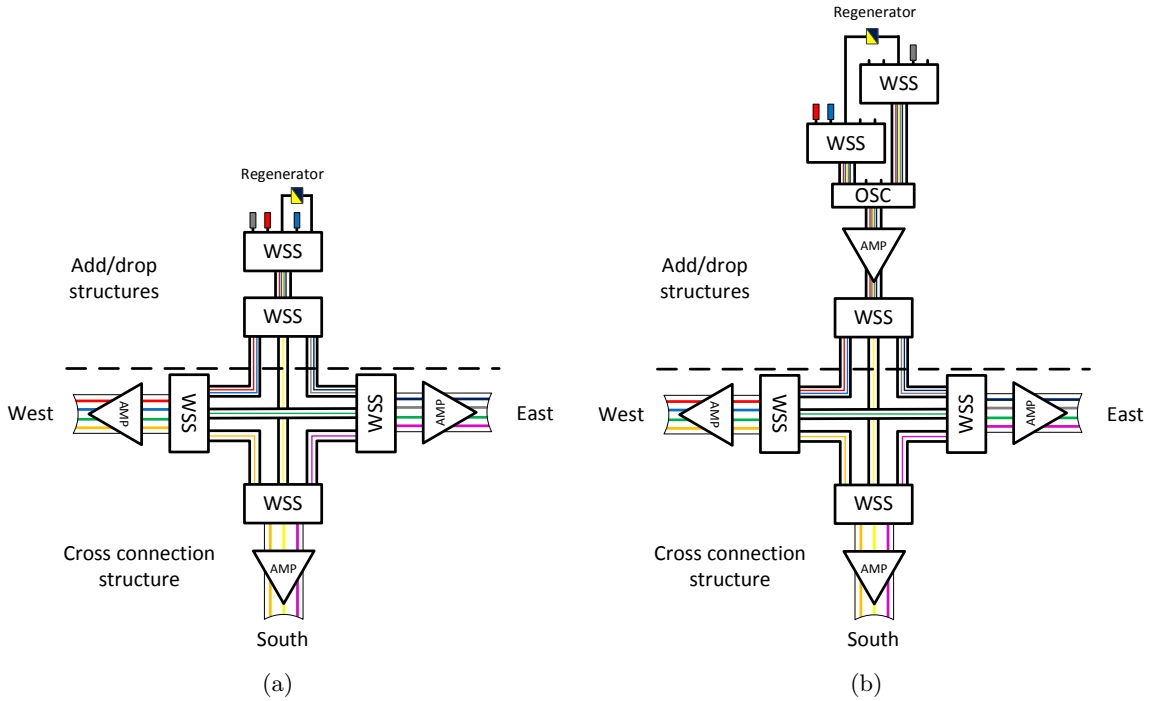

Figure 2.14: ROADM architecture with colorless and directionless add/drop structure. This architecture requires WSS, OSC, and amplifier modules. Changes in the wavelength or in the direction of a specific add/drop channel can be made remotely. The architecture presented in (b) is an extended version to increase the maximum number of add/drop channels.

2.5.7 Add/drop structure: colorless, directionless and contentionless

In a contentionless ROADM, a transmitter/receiver can be assigned to any wavelength as long as that wavelength is not already in use on the output port [5, 18, 44, 46]. The colorless, directionless and contentionless ROADM is presented in Fig. 2.15. The add/drop structure is equipped with $P_i \times P_o$ WSS. As aforementioned, the $P_i \times P_o$ WSS can switch any wavelength from any input port to any output port. The P_i ports receive the add/drop channels that are switched to any of the P_o directions of the node. As can be seen if Fig. 2.15 as long as the signals represented as red follow different paths they can be connected to the same add/drop structure without blocking. A $P_i \times P_o$ WSS module may not provide sufficient add/drop ports. An extended architecture to increase the add/drop ratio is the implementation of more than one add/drop structure, thus decreasing the maximum nodal degree. Note that a cascade of $1 \times P$ WSS cannot be deployed as removes the contentionless capability.

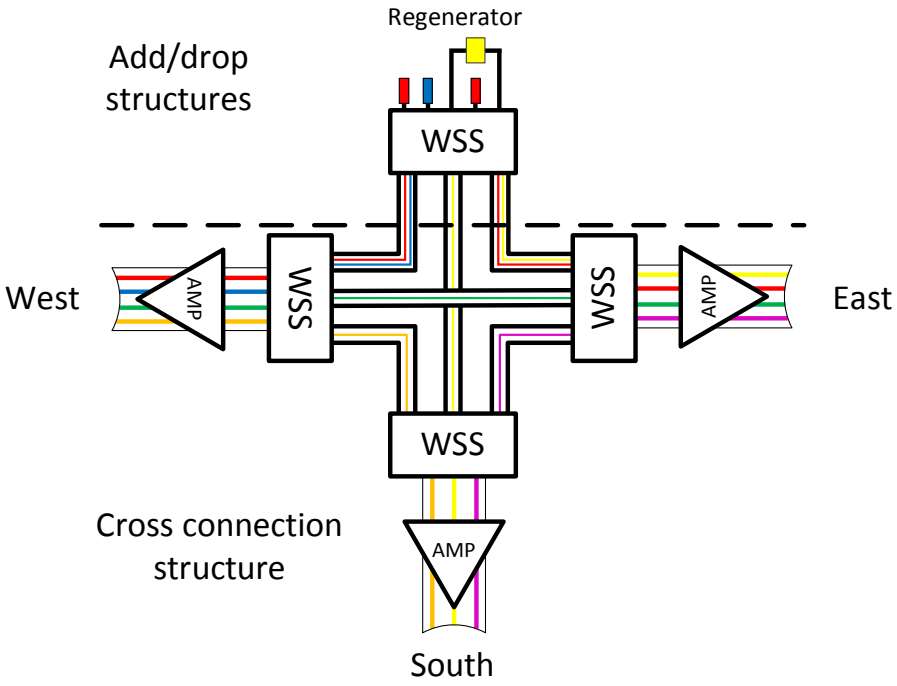

Figure 2.15: ROADM architecture with colorless, directionless and contentionless add/drop structure. This architecture only requires $P_i \times P_o$ WSS modules. Multiples copies of the same wavelength can be used within the same add/drop structure provided that they follow different directions.

2.6 Chapter summary

This chapter overview the transport modes of operation and the architectures to implement the transmission system, the electrical and the optical layer of the node. The chapter starts by presenting the opaque, transparent and translucent transport modes of operation and relating them with the grooming schemes. The link-by-link grooming scheme is used in opaque networks, and the single-hop grooming scheme is used in transparent ones. Regarding translucent networks, as OEO conversion can be performed in selected nodes, a multi-hop grooming scheme can be employed. The transmission system architecture is then overviewed. Later, the building blocks used in a general node architecture are presented. Considering the architectures to implement the electrical layer of the node, a fixed architecture based on muxponders, and a flexible architecture based on EXCs are presented in detail. Regarding the optical layer, the building blocks used in the various ROADM architectures are explained. Finally, ROADMs with fixed frequency, fixed direction, colorless, directionless and contentionless capabilities are described.

References

[1] N. Amaya, G. Zervas, and D. Simeonidou, "Introducing node architecture flexibility for elastic optical networks," *IEEE/OSA Journal of Optical Communications and Networking*, vol. 5, no. 6, pp. 593–608, June 2013.

[2] O. Klopfenstein, "Access network dimensioning with uncertain traffic forecasts," in *Proc International Telecommunications Network Strategy and Planning Symposium - NETWORKS*, pp. 1–52, October 2008.

[3] A. Feldmann, A. Greenberg, C. Lund, N. Reingold, J. Rexford, and F. True, "Deriving traffic demands for operational IP networks: Methodology and experience," *IEEE/ACM Transactions on Networking*, vol. 9, no. 3, pp. 265–279, June 2001.

[4] S. Yang and F. Kuipers, "Traffic uncertainty models in network planning," *IEEE Communications Magazine*, vol. 52, no. 2, pp. 172–177, February 2014.

[5] S. Gringeri, B. Basch, V. Shukla, R. Egorov, and T. Xia, "Flexible architectures for optical transport nodes and networks," *IEEE Communications Magazine*, vol. 48, no. 7, pp. 40 –50, July 2010.

[6] N. Sambo, P. Castoldi, F. Cugini, G. Bottari, and P. Iovanna, "Toward high-rate and flexible optical networks," *IEEE Communications Magazine*, vol. 50, no. 5, pp. 66–72, May 2012.

[7] S. Gringeri, N. Bitar, and T. Xia, "Extending software defined network principles to include optical transport," *IEEE Communications Magazine*, vol. 51, no. 3, pp. 32–40, March 2013.

[8] S. Roy, A. Malik, A. Deore, S. Ahuja, O. Turkcu, S. Hand, and S. Melle, "Evaluating efficiency of multi-layer switching in future optical transport networks," in *Proc Optical Fiber Communication Conference and Exposition and the National Fiber Optic Engineers Conference - OFC/NFOEC*, pp. NTh4J.2, March 2013.

[9] T. Engel, A. Autenrieth, and S. Voll, "Quantitative analysis of network architectures for future national optic transport networks (OTN)," in *Symposium on Photonic Networks - ITG*, pp. 1–7, May 2010.

[10] *ITU-T Recommendation G.709/Y.1331, Interfaces for the optical transport network (OTN)*, International Telecommunication Union Std., 2009.

[11] *ITU-T Recommendation G.872, Interfaces for the optical transport network*, International Telecommunication Union Std., 2012.

[12] S. Zhang, M. Tornatore, G. Shen, and B. Mukherjee, "Evolution of traffic grooming from SDH/SONET to flexible grid," in *Proc European Conference and Exhibition on Optical Communication - ECOC*, pp. We.1.E.1, September 2013.

[13] S. De Maesschalck, M. Pickavet, D. Colle, and P. Demeester, "Multi-layer traffic grooming in networks with an IP/MPLS layer on top of a meshed optical layer," in *Proc IEEE Global Telecommunications Conference - GLOBECOM*, vol. 5, pp. 2750 – 2754, December 2003.

[14] O. Gerstel, "Simple analytical estimation of router bypass effectiveness," in *Proc European Conference and Exhibition on Optical Communication - ECOC*, pp. Th.10.F.3, September 2010.

[15] E. Bouillet, G. Ellinas, J.-F. Labourdette, and R. Ramamurthy, *Path Routing in Mesh Optical Networks*, John Wiley & Sons, 2007.

[16] F. Rambach, B. Konrad, L. Dembeck, U. Gebhard, M. Gunkel, M. Quagliotti, L. Serra, and V. Lopez, "A multilayer cost model for metro/core networks," *IEEE/OSA Journal of Optical Communications and Networking*, vol. 5, no. 3, pp. 210–225, March 2013.

[17] V. Eramo, M. Listanti, R. Sabella, and F. Testa, "Definition and performance evaluation of a low-cost/high-capacity scalable integrated OTN/WDM switch," *IEEE/OSA Journal of Optical Communications and Networking*, vol. 4, no. 12, pp. 1033–1045, December 2012.

[18] R. M. Morais, J. Pedro, P. Monteiro, and A. N. Pinto, "Impact of node architecture in the power consumption and footprint requirements of optical transport networks," *IEEE/OSA Journal of Optical Communications and Networking*, vol. 5, no. 5, pp. 421–436, May 2013.

[19] R. Ramaswami, K. N. Sivarajan, and G. H. Sasaki, *Optical Networks: A Practical Perspective*, Morgan Kaufmann, 2010.

[20] *ITU-T Recommendation G.694.1, Spectral grids for WDM applications: DWDM frequency grid*, International Telecommunication Union Std., 2012.

[21] B. Ramamurthy, H. Feng, D. Datta, J. Heritage, and B. Mukherjee, "Transparent vs. opaque vs. translucent wavelength-routed optical networks," *Proc Optical Fiber Communication Conference and the International Conference on Integrated Optics and Optical Fiber Communication - OFC/IOOC*, vol. 1, pp. 59–61 vol.1, February 1999.

[22] K. Zhu, H. Zhu, and B. Mukherjee, *Traffic Grooming in an Optical WDM Mesh Network*, Springer, 2002.

[23] G. Agrawal, *Fiber-Optic Communication Systems*, Wiley, 1997.

[24] E. Desurvire, *Erbium-Doped Fiber Amplifiers: Principles and Applications*, Wiley-Interscience, 2002.

[25] C. Headley and G. Agrawal, *Raman Amplification in Fiber Optical Communication Systems*, Elsevier Science, 2005.

[26] The Plastics Pipe Institute, *Handbook of Polyethylene Pipe*, The Free Library, 2007.

[27] L. Wang, R. Lu, Q. Li, X. Zheng, and H. Zhang, "Energy efficient design for multi-shelf IP over WDM networks," in *Proc IEEE Conference on Computer Communications Workshops - INFOCOM WKSHPS*, pp. 349–354, April 2011.

[28] G. Shen, L. Peng, Y. Shen, and H. Sardesai, "Optimal node hardware module planning for layer-one optical transport networks," *IEEE/OSA Journal of Optical Communications and Networking*, vol. 3, no. 12, pp. 937–946, December 2011.

[29] J. M. Simmons, "On determining the optimal optical reach for a long-haul network," *IEEE/OSA Journal of Lightwave Technology*, vol. 23, no. 3, pp. 1039–1048, March 2005.

[30] M. Carroll, J. Roese, and T. Ohara, "The operator's view of OTN evolution," *IEEE Communications Magazine*, vol. 48, pp. 46–52, September 2010.

[31] Y. Koike, "MPLS-TP: Overview and status," in *Proc Optical Fiber Communication Conference and Exposition and the National Fiber Optic Engineers Conference - OFC/NFOEC*, pp. 1–45, March 2013.

[32] A. Kasim, *Delivering Carrier Ethernet: Extending Ethernet beyond the LAN*, McGraw-Hill, 2008.

[33] *ITU-T Recommendation G.7044/Y.1347, Hitless adjustment of ODUflex (GFP)*, International Telecommunication Union Std., 2011.

[34] A. Deore, O. Turkcu, S. Ahuja, S. Hand, and S. Melle, "Total cost of ownership of WDM and switching architectures for next-generation 100 Gb/s networks," *IEEE Communications Magazine*, vol. 50, no. 11, pp. 179 –187, November 2012.

[35] M. Scheffel, R. Prinz, C. Gruber, A. Autenrieth, and D. Schupke, "Optimal routing and grooming for multilayer networks with transponders and muxponders," in *Proc IEEE Global Telecommunications Conference - GLOBECOM*, pp. 1–6, December 2006.

[36] A. Autenrieth, J. P. Elbers, H. Schmidtke, M. Macchi, and G. Rosenzweig, "Benefits of integrated packet/circuit/wavelength switches in next-generation optical core networks," in *Proc Optical Fiber Communication Conference and Exposition and the National Fiber Optic Engineers Conference - OFC/NFOEC*, pp. NMC4, March 2011.

[37] I. Katib and D. Medhi, "IP/MPLS-over-OTN-over-DWDM multilayer networks: An integrated three-layer capacity optimization model, a heuristic, and a study," *IEEE Transactions on Network and Service Management*, vol. 9, no. 3, pp. 240–253, September 2012.

[38] V. Eramo, M. Listanti, R. Sabella, and F. Testa, "Integrated OTN/WDM switching architecture equipped with the minimum number of OTN switches," *IEEE/OSA Journal of Optical Communications and Networking*, vol. 6, no. 2, pp. 138–151, February 2014.

[39] W. Sun, Q. Li, H. He, and W. Hu, "Design of a hybrid packet and circuit switching network node," in *International Conference on Photonics in Switching - PS*, pp. 1–4, September 2012.

[40] D. Brunina, D. Liu, and K. Bergman, "An energy-efficient optically connected memory module for hybrid packet- and circuit-switched optical networks," *IEEE Journal of Selected Topics in Quantum Electronics*, vol. 19, no. 2, pp. 3 700 407–3 700 407, March 2013.

[41] S. Thiagarajan, L. Blair, and J. Berthold, "Direction-independent add/drop access for multi-degree ROADMs," in *Proc Optical Fiber Communication Conference and Exposition and the National Fiber Optic Engineers Conference - OFC/NFOEC*, pp. OThA7, February 2008.

[42] A. Devarajan, K. Sandesha, R. Gowrishankar, B. Kishore, G. Prasanna, R. Johnson, and P. Voruganti, "Colorless, directionless and contentionless multi-degree ROADM architecture for mesh optical networks," in *International Conference on Communication Systems and Networks - COMSNETS*, pp. 1 –10, January 2010.

[43] P. Ji and Y. Aono, "Colorless and directionless multi-degree reconfigurable optical add/drop multiplexers," in *Wireless and Optical Communications Conference - WOCC*, pp. 1 –5, May 2010.

[44] P. Pavon-Marino and M. Bueno-Delgado, "Dimensioning the add/drop contention factor of directionless ROADMs," *IEEE/OSA Journal of Lightwave Technology*, vol. 29, no. 21, pp. 3265 –3274, November 2011.

[45] J. Homa and K. Bala, "ROADM architectures and their enabling WSS technology," *IEEE Communications Magazine*, vol. 46, no. 7, pp. 150 –154, July 2008.

[46] R. Jensen, "Optical switch architectures for emerging colorless/directionless/contentionless ROADM networks," in *Proc Optical Fiber Communication Conference and Exposition and the National Fiber Optic Engineers Conference - OFC/NFOEC*, pp. OThR3, March 2011.

[47] P. Roorda and B. Collings, "Evolution to colorless and directionless ROADM architectures," in *Proc Optical Fiber Communication Conference and Exposition and the National Fiber Optic Engineers Conference - OFC/NFOEC*, pp. NWE2, February 2008.

[48] G. Prasanna, B. Kishore, G. Omprasad, K. Raju, R. Gowrishankar, K. Venkataramaniah, R. Johnson, and P. Voruganti, "Versatility of a colorless and directionless WSS based ROADM architecture," in *Proc International Communication Systems and Networks and Workshops - COMSNETS*, pp. 1–8, January 2009.

[49] T. Zami, "Optical cross-connect with adaptive intra-node contention," in *Proc European Conference and Exhibition on Optical Communication - ECOC*, pp. Th.2.E.5, September 2013.

[50] S. Tibuleac and M. Filer, "Transmission impairments in DWDM networks with reconfigurable optical add-drop multiplexers," *IEEE/OSA Journal of Lightwave Technology*, vol. 28, no. 4, pp. 557–598, February 2010.

CHAPTER 3

Survivable topological design and links dimensioning

The proliferation of Internet access and the appearance of new telecommunications services are originating a demand for resilient networks with extremely high capacity [1]. With such huge amount of traffic traversing a single optical fiber a link failure may lead to catastrophic consequences affecting critical applications from governmental agencies, banks or health services. These traffic interruptions have also associated big economical losses for operators due to the downtime costs [2]. Therefore, design a network topology with the required characteristics to recover connections in case of failure is of paramount importance in optical transport networks.

The nodes location is one of the first pieces of information that the network designer has, corresponding to the location of the central offices where the traffic is added and dropped. Thus, the first stage of the overall network design process is the topological design. At this stage the connections between the nodes are established, i.e. the conduits are deployed. The network topological design should guarantee a reliable network, and this depends on which links are going to be implemented [3, 4]. An optimized solution depends on the traffic requirements. However, the traffic to be transported by the network is hard to forecast and is continuously changing [5, 6]. In practice, several probable traffic scenarios are defined and evaluated, then the lowest cost network that will remain feasible for the majority of the scenarios is implemented [5]. Therefore, the development of methods to quickly design physical topologies at minimum cost is crucial. In this chapter, the problem of jointly design the physical topology, ensure survivability, and minimize the network CapEx related to the links is addressed. In order to deal with this problem a genetic algorithm is developed, and the impact of the genetic operators on the quality of the obtained solutions analyzed.

The chapter is organized in six sections. In Section 3.1 an introduction to the survivable topological design problem is given, and the mathematical formulation of the dimensioning problem is presented in Section 3.2. After, Section 3.3 is devoted to the detailed explanation

of the two initial population generators, the two selection methods, and the two crossover operators considered within the genetic algorithm. Section 3.4 presents the ILP used to benchmark the obtained solutions. In Section 3.5 the impact of the genetic operators on the quality of the solutions is analyzed. Finally, Section 3.6 summarizes the chapter.

3.1 Survivable topological design problem

The most cost effective way to connect a set of nodes is known to be the minimum spanning tree [7]. The minimum spanning tree ensures that between any pair of nodes exists, at least, one path, thus exists connectivity. However, survivability is not guaranteed. To ensure the network survivability, a pre-specified number of disjoint paths between any pair of nodes is required. The disjoint paths can be disjoint by links or by nodes, depending on the type of failures in analysis. In optical networks, the failure of multiple fibers at the same time is extremely rare [8]. The majority of failures regard single-link failures. Thus, we aim to design a network topology survivable against any single link failure. A survivable topology against single link failures requires two link disjoint paths between each pair of nodes [9]. To ensure survivability a protection scheme have also to be implemented. We focus on path dedicated protection, where a link disjoint backup path is used to protect each optical channel [8]. In this scheme the backup path has dedicated resources that cannot be shared with others working and backup paths. When a working path link fails all the affected demands are switched to their respective dedicated backup path. The survivable topological design problem, not allowing the use of parallel edges, is strongly NP-hard [3, 10]; thus ILP models only lead to optimal solutions, within reasonable time and computational effort, for small networks. Consequently, heuristics are commonly used to search for near-optimal solutions.

The topological design problem has attracted the attention of many researchers [3, 11–27]. Commonly, two main methodologies are used for designing a topology with certain requirements: statistical modeling and optimization methods. In the first approach, statistical properties of real networks are obtained through collection and interpretation of topology related characteristics [11–15]. After, the topologies are designed to resemble the statistical properties observed [11, 12]. In the second approach, an objective function to be either maximized or minimized is developed, and an optimization method (ILP or heuristic) is used to find the most suitable topology that maximize/minimize that objective function [3, 4, 16–27]. The objective function usually aims to minimize the CapEx, the power consumption, or the number of fibers in the network. For instance, in [16–19] the optimization focus in minimizing the cost associated with the optical fibers and in [20], the authors attempt to minimize cost through the trade-off between the fiber length and number of wavelengths. None of these works consider the network survivability. Optimization methods for the topological design of survivable networks can be found in [4, 21–27]. In [21–23] ILP models and heuristics are analyzed to minimize the total number of links, and in [24, 25] the 2-connected graph concept is used for the topological design. Authors in [26] presents an heuristic method for the joint minimization of the CapEx and the power consumption with survivability requirements. A

state of art in ILP models and decomposition methods for the survivable design problem can be found in [3, 27]. Regarding genetic algorithms in the design of telecommunication networks, the works [28, 29] uses it. In [28], a genetic algorithm is presented to route and dimension dynamic optical networks, without considering the network survivability, and in [29] a genetic algorithm to minimize the CapEx of an all-optical network considering physical impairments is proposed.

For a better understanding of the problem under study, an example is presented. The nodes location and the traffic matrix are the inputs of the problem. In the example, presented in Fig. 3.1, the distance between nodes one and two, one and three, two and four, and three and four, is of 500 km and the distance between nodes one and four, and two and three is of 707 km. The used traffic is an uniform and unitary matrix, i.e., two demands exist between all pairs of nodes, the working and the backup.

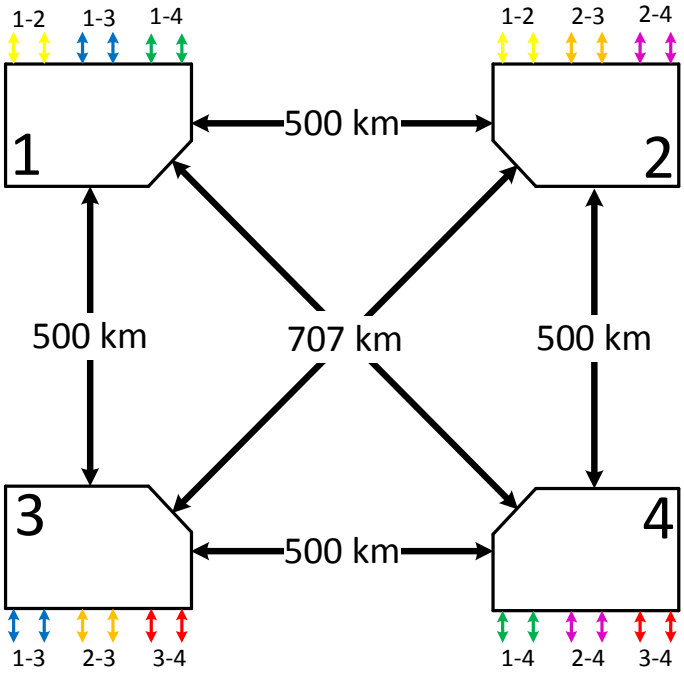

Figure 3.1: Inputs of the survivable topological design problem. Given the nodes location and the traffic model the goal is the connect all the nodes ensuring the survivability of all demands against single link failures at minimum CapEx for links.

One feasible solution of the problem is the topology and routing presented in Fig. 3.2. The solid lines represent the working path of each demand and the dashed lines represent the corresponding backup path. The routing scheme is the shortest path in number of hops for the working path and the second shortest path in number of hops for the dedicated backup path. The required spacing between amplifiers is assumed to be of 80 km. As each link only has one transmission system, a total of 32 optical amplifiers are required.

As an example, consider the demand between the nodes one and three (shown in blue) and the demand between the nodes two and three (shown in orange) in Fig. 3.2. Since there is a direct connection between the nodes one and three, the demand will be sent directly through this link. Note that the same connection also transports the demand between the nodes two

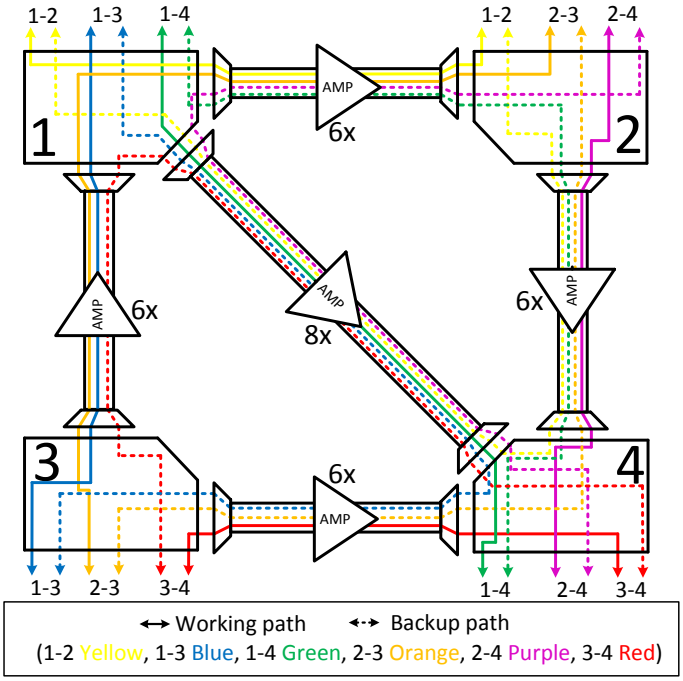

Figure 3.2: Dimensioned network using a dedicated protection scheme, corresponding to a feasible solution for the survivable topological design problem. Working paths are represented as solid lines and backup paths as dashed lines. The shortest path in number of hops was considered for both paths.

and three and belongs to the backup path of the demand between the nodes three and four. If the link between the nodes one and three fails, the demands between the nodes one and three and two and three will be affected, requiring a backup path that not go through that failed link. The demand between one and three is re-routed by the links between nodes one and four, and later in the link between the nodes four and three. The other affected demand which was formerly carried by the links between the nodes two and one, and one and three is carried by the links between the nodes two and four and later by the link between the nodes four and three, see Fig. 3.2.

3.2 Links dimensioning

Links are sets of transmission systems comprising the optical fiber and optical amplifiers, see Fig. 2.4. The set of links deployed must guarantee the connectivity between all pairs of nodes regardless the transport mode used in the network. Thus, in this chapter we assume a general node that can operate in opaque, transparent or translucent mode.

A network topology is generally represented as a graph $G(V, E_p)$, where $V = \{1, \ldots, N\}$, is the set of nodes, where N is the number of nodes, and $E_p = \{\{i, j\} : i, j \in V, i < j\}$, is the set of links. In this chapter, E_p represents all bidirectional links that can be deployed, and the goal is to find a subset of E_p that corresponds to the survivable topology at minimum CapEx for links. The nodes location defines the distance between them, i. e., the links length. The link length in kilometers between the node i and j will be denoted by $LL(i, j)$.

The network has to support a given traffic, corresponding to a set of demands between nodes. A demand can be seen as a flow between the origin node, o, and the destination node, d. The set of node pairs requesting at least one optical channel defines the logical topology, and is denoted by $E_c = \{(o,d) : o,d \in V, o \neq d\}$. Each demand can be supported by one or more optical channels. The required capacity between the network nodes can be represented as a matrix, $[L(o,d)]$, in which the elements $L(o,d)$ hold the number of optical channels required between the origin node o to the destination node d. We consider that currently deployed optical transport networks contain bidirectional transmission systems and symmetric traffic. Hence, all demands are bidirectional and $L(o,d) = L(d,o)$.

The CapEx regarding links is composed by a cost depending on the number of transmission systems installed, and a cost depending on the number of optical channels that traverses each transmission system. The costs depending on the number of transmission systems installed in the link $\{i,j\}$, $T_S(i,j)$, are the costs with its deployment plus the cost with the optical fibers, and optical amplifiers. The cost with the optical fiber is proportional to the length $LL(i,j)$ between the nodes. The number of optical amplifiers depends on $LL(i,j)$ and on the *span*. Therefore, $T_S(i,j)$ can be assumed to be given by

$$T_S(i,j) = \left(Y(i,j) + LL(i,j)c_f + \left\lceil \frac{LL(i,j)}{span} - 1 \right\rceil c_{oa} \right) U(i,j), \quad \forall \{i,j\} \in E_p, \tag{3.1}$$

where $Y(i,j)$ is the cost with right-of-way privileges and/or method used to deploy a transmission system between the nodes i and j, c_f is the cost of the optical fiber per kilometer, $\lceil (LL(i,j)/span) - 1 \rceil$ is the number of optical amplifiers, and c_{oa} is the cost of a bidirectional optical amplifier. As one or more transmission systems can be required, the integer non-negative variable $U(i,j)$ indicates the number of transmission systems installed in the link between the nodes i and j.

The number of transmission systems installed, $U(i,j)$, is dependent on the maximum number of optical channels that a transmission system can support and on the number of optical channels that are routed through the link $\{i,j\}$, $W(i,j)$. The value of $W(i,j)$ is calculated by adding the number of optical channels, $L(o,d)$, for all demands that traverse the link $\{i,j\}$. Thus,

$$W(i,j) = \sum_{(o,d) \in E_c} L(o,d)(Z_{ij}^{od} + Z_{ji}^{od}), \quad \forall \{i,j\} \in E_p, \tag{3.2}$$

where Z_{ij}^{od} and Z_{ji}^{od} are binary variables that indicate whether the optical channel between nodes o and d is routed through the link $\{i,j\}$ or not. As the links can be traversed in both ways, the variables Z_{ij}^{od} indicate if the demand (o,d) traverse the link in the direction from nodes i to j whereas the variables Z_{ji}^{od} are related to the direction from j to i. The number of transmission systems installed, $U(i,j)$, is then obtained using $W(i,j)$ by

$$U(i,j) = \left\lceil \frac{W(i,j)}{K(i,j)} \right\rceil, \quad \forall \{i,j\} \in E_p, \tag{3.3}$$

where $K(i,j)$ is the capacity of a particular transmission system in number of optical channels.

The costs depending on the number of optical channels that traverse the link between the nodes i and j, $T_O(i,j)$, are related to the costs associated to transport and switch one optical channel. For instance, a pair of long-reach transceivers in opaque networks, or the cost related to enable the switching of an optical channel in transparent and translucent networks. Given that c_o is that cost, $T_O(i,j)$ can be calculated by

$$T_O(i,j) = c_o W(i,j), \quad \forall \{i,j\} \in E_p. \tag{3.4}$$

Therefore, the CapEx for links, $CapEx_L$, is given by the sum of the cost $T_S(i,j)$ plus $T_O(i,j)$ for all links,

$$CapEx_L = \sum_{\{i,j\} \in E_p} T_S(i,j) + T_O(i,j). \tag{3.5}$$

The topological design problem is characterized by being hard in complexity, time consumption, and memory requirements. Consequently, exact solutions within reasonable time can only be obtained for small networks. As optical transport networks can have more than 100 nodes [15, 30], ILP models are prohibitive for larger networks. In the following, a heuristic approach and an ILP model to obtain solutions that minimize $CapEx_L$ with survivability requirements are presented. The ILP model is used to evaluate the quality of the solutions obtained using the genetic algorithm in terms of accuracy and time consumption, for small networks. The topology and the paths between the nodes are obtained by the values of the variables $U(i,j)$, Z_{ij}^{od} and Z_{ji}^{od}, respectively.

3.3 Genetic algorithm

Genetic algorithms are search algorithms based on the mechanics of natural selection [31]. In every generation (iteration), a new set of artificial individuals (solutions) is created, using pieces of the previous generation. The new population is expected to be globally fittest than their progenitors. A genetic algorithm has the following steps: generation of an initial population, encoding, evaluation, selection, crossover, mutation, and decoding [31, 32]. Figure 3.3 presents a flowchart of a generic genetic algorithm.

A set of initial feasible solutions for the problem (individuals) is generated, forming the initial population. Every solution is represented by an individual in the population. In order to uniquely identify each one, they are codified into a genetic code. The genetic code needs to preserve all the information regarding the solution as well as guarantees that the information can be transferred to the offsprings. After, the genetic algorithm modifies this population repeatedly. All the individuals of the population are evaluated, i.e., the cost of the solutions is calculated. Then, pairs of individuals are chosen under selection rules, usually based on the evaluation of each individual. After, the selected pairs of individuals

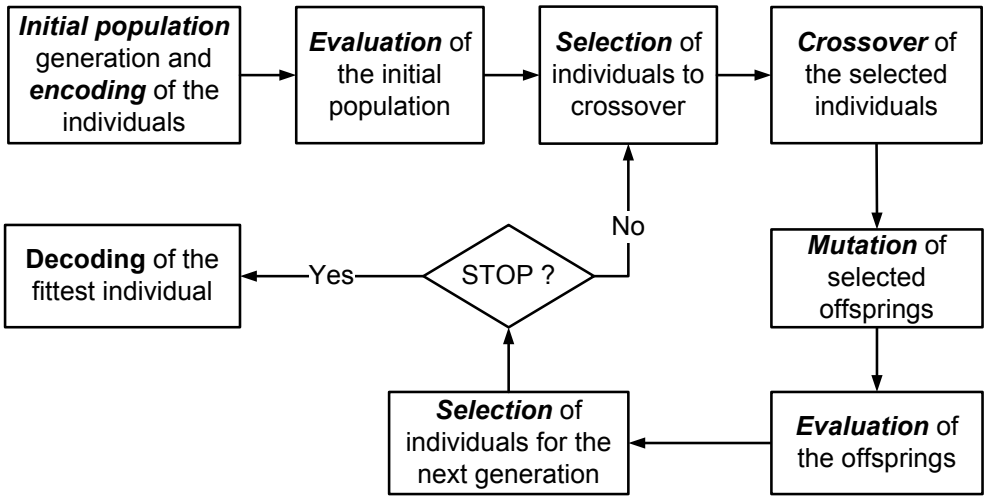

Figure 3.3: Flowchart of a generic genetic algorithm.

are combined under crossover rules, giving rise to others pairs of individuals (offsprings). To increase the population diversity, mutations can also be applied at this stage. The offsprings are then also evaluated and a new population is selected from individuals belonging to both generations. This procedure is repeated until the halting criteria is reached. At this point, the fittest individual is decoded corresponding to the best solution achieved.

The convergence of a genetic algorithm is dependent on the used operators. In the following, two initial population generators, two selection methods, and two crossover operators are presented within the genetic algorithm.

3.3.1 Initial population

A feasible solution for the problem is a network topology with at least two link-disjoint paths between any pair of nodes. We use two topology generators to create the initial population set. One generates completely random topologies, based on [33]. The other generates topologies that preserve the main characteristics of real telecommunication networks, based on [30].

The random topology generator starts by designing a ring topology connecting all nodes of the network, thus guaranteeing that all initial solutions are feasible [33]. The ring topology is randomly generated for each individual. After, t links are added to the ring topology, connecting t pairs of randomly selected nodes. The number t of additional links is randomly generated and ranges from 0 to $N(N-3)/2$, i.e., from a ring to a full mesh network. Figure 3.4 presents some possible topologies generated using this method for a 4-nodes network. The links of the ring topology are displayed as solid black lines. Additional links are presented as dashed grey lines.

The topology generator presented in [30] models a survivable transport network as a set of interconnected smaller sub-networks and introduces constraints to guarantee the characteristics showed by real ones, see Fig. 3.5. The topology generator is based on the Waxman approach, where the probability of a pair of nodes being directly connected depends on the

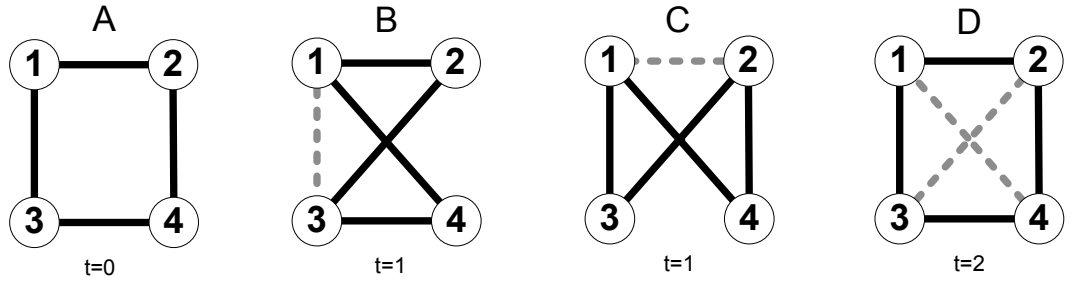

Figure 3.4: Generation of initial population solutions using the random topology generator presented in [33]. The algorithm starts by designing a ring topology (black solid lines). Afterwards a random number, t, is generated corresponding to the number of additional links to be added to the ring (grey dashed lines). The end nodes of each individual link are randomly selected.

Euclidian distance between them [34]. The method starts by partitioning the plane where the network will be implemented into regions of equal size. The nodes are then placed into the regions, see Fig. 3.5(a). Note that the node location is an input of the problem. After the above procedure, we may have regions without nodes, with one, two, or more than two nodes. If a region has two or more nodes an additional procedure is required, that is, if there are two nodes they are directly connected; if there are more than two nodes they are connected as a closed cycle, see Fig. 3.5(b). For regions with more than three nodes, the way the nodes are directly connected follows the Waxman link probability [30, 34]. The probability, $\phi(i,j)$, of existing a link between the node i and the node j is given by [34]

$$\phi(i,j) = \beta \exp \frac{-LL(i,j)}{\gamma\Delta}, \quad \forall\{i,j\} \in E_p, \tag{3.6}$$

where $LL(i,j)$ is the distance, in kilometers, between the node i and j; Δ is the maximum distance between any two nodes in the network; and following [30], γ and β are both assumed to be 0.4.

Once the nodes inside each region are interconnected, new links should be added to interconnect the regions, guaranteeing the network survivability. This process also follows the Waxman link probability, however, each node of the selected pair belongs to different regions. In order to guarantee that the generated topology will be survivable, some precautions should be taken into account: if a region has only one node, this node must be connected to at least two nodes of neighbor regions; if the region has only two nodes, each one must be connected to a node in neighbor regions; if a region has more than two nodes, at least two nodes must be connected to nodes of neighbor regions, see Fig. 3.5(c). Two nodes of a region can be connected to the same destination node in a neighbor region only if node-disjoint paths are not required. At this phase we have a connected and survivable network topology (at least against single link failures). Afterwards, a random number of additional links are added to the network, see Fig. 3.5(d).

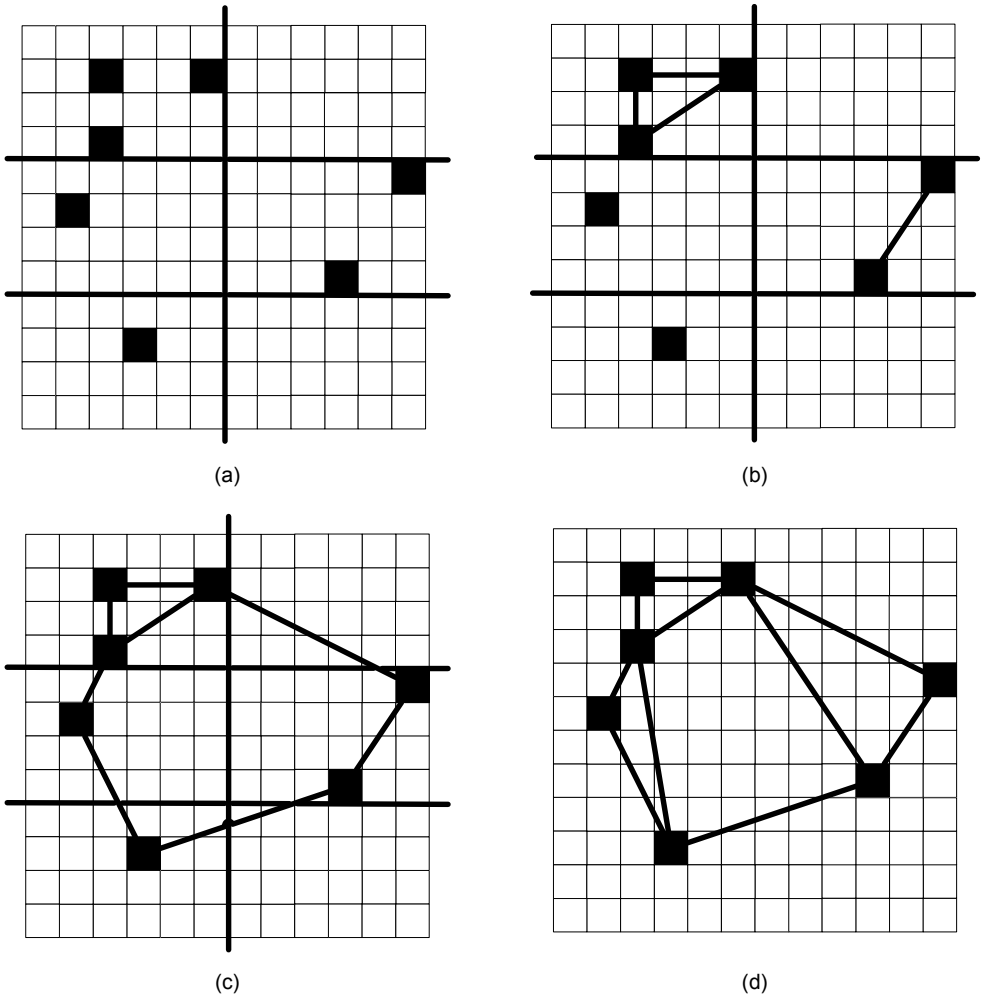

Figure 3.5: Generation of initial population solutions using the topology generator that resembles the properties of real world networks [30]: (a) The plane and the nodes placed into regions. (b) Intra-region survivability. (c) Region interconnection. (d) A possible network topology over a six-region plane.

3.3.2 Encoding and decoding

The encoding corresponds to the creation of a genetic code that uniquely represents a solution. To encode the solutions, we used the concatenation of the rows of the upper triangular matrix of the adjacency matrix. The adjacency matrix is an $N \times N$ matrix in which an element in position i, j is 1 if node i is directly connected to node j, and 0 otherwise. As the network links are bidirectional, the adjacency matrix is symmetric. As an example, consider the four node network topology presented in Fig. 3.2. The adjacency matrix of the network is

$$[g] = \begin{bmatrix} 0 & \mathbf{1} & \mathbf{1} & \mathbf{1} \\ 1 & 0 & \mathbf{0} & \mathbf{1} \\ 1 & 0 & 0 & \mathbf{1} \\ 1 & 1 & 1 & 0 \end{bmatrix}, \tag{3.7}$$

and the respective genetic code is,

$$1\ 1\ 1 \mid 0\ 1 \mid 1.$$

Given the genetic code of the solutions, the decoding is the inverse operation. Note that the decoding operation is only performed at the end and for the best solution achieved.

3.3.3 Evaluation

The evaluation consists of determining the CapEx for links, $CapEx_L$, of each topology. To calculate $CapEx_L$ we determine two paths for each demand (a working and a backup path) and use them to calculate the number of optical channels needed in each link, thus $W(i,j)$. We assume that the working path is the shortest path (in number of hops) and the backup path is the second-shortest path. The working path is determined using the Dijkstra algorithm. To obtain a second link disjoint shortest path, the links in the working path are overweighted, and the backup path is determined using the Dijkstra algorithm a second time. If two or more shortest paths exist, we use the first path encountered. Note that the feasibility of the solutions can only be guaranteed at the initial population. Later on, if the two disjoint paths cannot be obtained, the solution is removed from the population. The two link-disjoint paths determined using the Dijkstra algorithm will be used to give values to the variables Z_{ij}^{od} and Z_{ji}^{od}. After all the demands have been routed, $W(i,j)$ is obtained using Eq. (3.2) and $U(i,j)$ using Eq. (3.3). With the values for the variables $W(i,j)$ and $U(i,j)$ determined, the cost $T_S(i,j)$ is obtained using Eq. (3.1) and the cost $T_O(i,j)$ is calculated using Eq. (3.4). Finally, $CapEx_L$ is calculated using expression (3.5).

The use of the shortest paths in number of hops is an approximation used in the proposed genetic algorithm. This approximation is assessed in the following, using the ILP model.

3.3.4 Selection

In the selection phase, pairs of individuals are chosen for crossover. Usually, individuals are selected based on their fitness, i.e., the cost of the respective solution. The selection method usually emphasizes the fitter individuals expecting that their offspring will have higher fitness too. However, a strong selection can reduce the diversity of the population, leading to suboptimal solutions; contrariwise a weak selection can result in slow evolution [31, 32]. Two different selection methods that differ in the selection pressure are used: the roulette wheel and the tournament method [31].

In the roulette wheel method, solutions are chosen based on their fitness. The lower cost solutions have higher probability to be chosen for crossover than solutions with higher cost. After all solutions are evaluated, the total generation cost is determined by adding all the solution costs. The next step is the calculation of the solution fitness. The fitness of each solution is the difference between the total generation cost and the cost of the solution. In this way, the solutions with lower cost will have higher fitness than the solutions with higher cost. Finally, the selection probability is calculated by the ratio between the solution fitness

and the sum of the fitness among all individuals. Therefore, solutions with lower cost have greater probability of being selected for crossover. Table 3.1 shows an example of the crossover probability calculation using the roulette wheel method for the solutions presented in Fig. 3.4. As can be seen solution A has the smaller cost and therefore the highest probability to be chosen. The opposite happens in solution D where its higher cost leads to the smallest probability.

Table 3.1: Example of the crossover probability determination using the roulette wheel selection method.

Individual	**Genetic code**	**Cost**	**Fitness**	**Probability**
A	110011	20	100	0.28
B	111101	30	90	0.25
C	111110	30	90	0.25
D	111111	40	80	0.22
TOTAL	———	120	360	1

In the tournament method, the fitness of each solution has a smaller impact in the selection of individuals for crossover. The selection is done randomly. Four individuals are randomly selected from the population and grouped two by two. Afterwards, two numbers, r_1 and r_2, ranging between 0 and 1 are randomly generated. If $r_1 < 0.75$, the solution with the smaller cost from the first group is selected for crossover; otherwise the less-fit individual is selected. The same occurs for the second group.

3.3.5 Crossover and mutation

In the crossover operation, pairs of individuals previously selected are combined, giving rise to another pair of new individuals. Usually the crossover operators respect the following properties [31, 32]:

- The crossover of two equal individuals will lead to a new pair of individuals like the previous ones,
- The crossover of two individuals that are in the nearby of the search space will generate individuals next to them.

There is no guarantee that the crossover of two individuals with good fitness will generate a high quality individual as well. A crossover is called lethal when produce individuals with low fitness and this comes from two highly adapted individuals [31]. To assess the impact of the crossover operator in the quality of the obtained solutions two crossover operators are analyzed: the single point crossover and the uniform crossover [31, 32].

In the single point crossover, a border between two elements of the genetic code is randomly selected. The two left sides of progenitor 1 and progenitor 2 are copied to offspring 1 and

offspring 2, respectively. The right sides of each code shall be exchanged, i.e., the right side of progenitor 1 is copied to offspring 2 and the right side of progenitor 2 is copied to offspring 1. An example is displayed in Table 3.2. In this example, the border is placed between the fourth and the fifth element of the genetic code for the two progenitors.

Table 3.2: Example of the single point crossover.

Individual	**Genetic code**					
Progenitor 1	1	1	1	1	**0**	**1**
Progenitor 2	1	0	1	1	**1**	**1**
Offspring 1	1	1	1	1	**1**	**1**
Offspring 2	1	0	1	1	**0**	**1**

In the uniform crossover, a mask is randomly generated. If the crossover mask bit m is 1, the offspring 1 receives the bit m from progenitor 1 and offspring 2 receives the bit m from progenitor 2. If the mask bit m is 0, offspring 1 inherits the bit m from progenitor 2 and offspring 2 inherits it from progenitor 1. The example in Table 3.3 illustrates this process.

Table 3.3: Example of the uniform crossover.

Individual	**Genetic code**					
Progenitor 1	1	**1**	1	1	**0**	1
Progenitor 2	1	**0**	1	1	**1**	1
Mask	0	**1**	1	0	**0**	1
Offspring 1	1	**1**	1	1	**1**	1
Offspring 2	1	**0**	1	1	**0**	1

The mutation operation consists of a simple exchange of 0's to 1's, or vice versa (add or remove links), at random locations of the genetic code, for a randomly selected number of individuals. This operation has the goal of increasing the diversity of the population.

After the individuals are evaluated, selected, and reproduced, the next generation is created. The selection of the individuals to form the next generation is made from the present generation and the generated offspring. We consider that a maximum of 20% of individuals are selected from the present generation, the remaining 80% are offsprings, to make available for crossover the maximum number of different links as possible.

3.4 Integer linear programming model

The ILP model is used to benchmark the solutions obtained using the genetic algorithm. The ILP model is the following [21–23, 27]:

$$minimize \quad CapEx_L = \sum_{\{i,j\} \in E_p} T_S(i,j) + T_O(i,j) \tag{3.5}$$

subject to

$$\sum_{j \in V \setminus \{o\}} Z_{ij}^{od} - \sum_{j \in V \setminus \{d\}} Z_{ji}^{od} = \begin{cases} 2, & i = o \\ 0, & i \neq o, d \\ -2, & i = d \end{cases}, \quad \forall (o,d) \in E_c, \forall i \in V \tag{3.8}$$

$$\sum_{(o,d) \in E_c} L(o,d)(Z_{ij}^{od} + Z_{ji}^{od}) \leq K(i,j)U(i,j), \quad \forall \{i,j\} \in E_p \tag{3.9}$$

$$U(i,j) \in \mathbb{N}_0, \quad \forall \{i,j\} \in E_p \tag{3.10}$$

$$Z_{ij}^{od}, Z_{ji}^{od} \in \{0,1\}, \quad \forall (o,d) \in E_c, \forall \{i,j\} \in E_p \tag{3.11}$$

The objective function, to be minimized, is the expression (3.5). Constraints (3.8) are the usual flow conservation constraints and ensure that, for each (o,d) pair, we route two units of flow from node o to node d. Figure 3.6 shows an example of two units flow from the origin node o to the destination node d. The source node sends two units of flow and the destination node has to receive those two units of flow. In the remaining nodes, being neither origin nor destination, the receive flow have to be send, constraints (3.8).

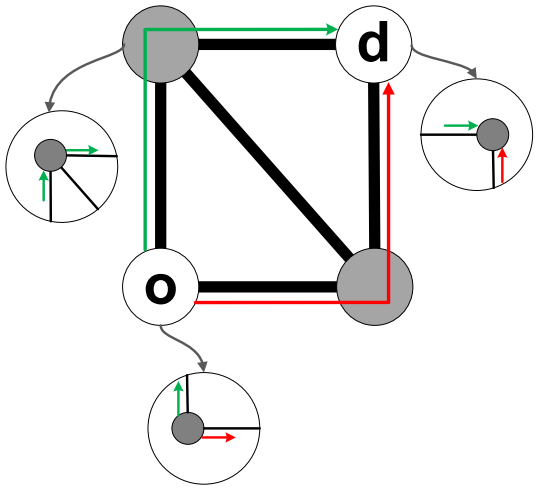

Figure 3.6: Example of two flows in a network. The origin node, o, sends two flows that are received by the destination node, d. In the intermediary nodes the received flows need to be sent. The two flows are sent through disjoint links.

Constraints (3.8) together with (3.9) guarantee the connectivity between all pairs of nodes. Constraints set (3.9) connects the sets of variables, guaranteeing that the total number of optical channels that crosses the link $\{i,j\}$, in both directions, does not exceeds the maximum capacity, $K(i,j)$, of the number of installed transmission systems, $U(i,j)$. Constraints set (3.10) defines the variables $U(i,j)$ as non negative integer variables, allowing the installation of more than one transmission system in each link. The disjointness of the two flows, to ensure

survivability, is enforced by constraints (3.11). As the variables Z_{ij}^{od} and Z_{ji}^{od} are binary, the two flows cannot traverse the same links, even if using different transmission systems. Hence, the existence of two link-disjoint paths for each origin destination pair is guaranteed.

3.5 Impact of genetic algorithm operators

As aforementioned, the convergence of the genetic algorithm depends on the used operators. Hence, this section reports the computational results obtained using the genetic algorithm and the ILP model. The genetic algorithm is implemented in C++. Using the genetic algorithm feasible solutions, corresponding to upper bounds for the optimal value, are obtained. The ILP model is used to obtain lower bounds and is solved using the branch and bound method from the commercial optimization software Xpress IVE 1.18 [35]. The results are obtained using a PC Intel Core 2 at 1.83 GHz and 1 GB RAM. The halting criteria used for the ILP model is the obtention of the optimal solution or 10 hours of processing time. In the genetic algorithm we performed 100 iterations, which required less than four minutes for the largest network. We observed marginal improvements in the solutions obtained when increasing this number of iterations.

To evaluate the quality of the obtained solutions the *gap* between the upper, b_u, and the lower, b_l, bound is calculated as follows

$$gap = \frac{100(b_u - b_l)}{b_u}, \tag{3.12}$$

where b_u is the cost of the solution obtained using the genetic algorithm and b_l the cost of the solution obtained using the ILP model.

The computational results are obtained for the node location of nine real telecommunications networks. We assume that all links can be implemented. As the cost of deploy a link is hard to obtain, and for a matter of simplicity we consider $Y(i,j) = 0,\ \forall\{i,j\} \in E_p$. The maximum number of optical channels supported by each transmission system is 80, i.e., $K(i,j) = 80,\ \forall\{i,j\} \in E_p$. We also consider that the maximum distance between optical amplifiers is 80 km, i.e., $span = 80$. The cost with the required equipments in normalized monetary units (m.u) is presented in Table 3.4 [36].

Table 3.4: Costs with the transmission system [36].

Equipment	**Notation**	**Cost (m.u.)**	**Quantity**
Optical fiber	c_f	0.80	per km
Optical amplifier	c_{oa}	1.92	per fiber and per span
Switch of an optical channel	c_o	0.66	per fiber per channel

To assess the impact of the initial population, selection method, crossover operator and number of individuals in the population, we perform five runs for each of the following combinations of operators:

- 100 individuals, roulette wheel selection, single point crossover;
- 100 individuals, tournament selection, single point crossover;
- 100 individuals, roulette wheel selection, uniform crossover;
- 100 individuals, tournament selection, uniform crossover;
- 500 individuals, roulette wheel selection, single point crossover;
- 500 individuals, tournament selection, single point crossover;
- 500 individuals, roulette wheel selection, uniform crossover;
- 500 individuals, tournament selection, uniform crossover.

3.5.1 The impact of the initial population

We start by assessing and comparing the quality of the obtained solutions when using different initial population generators. The presented results are obtained using uniform traffic. The initial populations are randomly generated [33] or following [30], as described in subsection 3.3.1. The number of nodes, the number of regions and the number of nodes placed in each region are presented in Table 3.5, for all considered networks.

Table 3.5: Real world reference networks [30].

Network	**Nodes**	**Regions**	**Nodes per region**
VIA	9	2	5 - 4
RNP	10	4	0 - 8 - 1 - 1
vBNS	12	3	3 - 4 - 5
CESNET	12	3	4 - 7 - 1
ITALY	14	2	12 - 2
NFSNET	14	2	7 - 7
AUSTRIA	15	3	3 - 4 - 8
GERMANY	17	4	8 - 2 - 5 - 2
SPAIN	17	4	8 - 2 - 7 - 0

Figure 3.7 shows the evolution of the *gap* for the best solution obtained, among all combinations, for initial populations generated using the random topology generator (Fig. 3.7(a)) and using the topology generator presented in [30] (Fig. 3.7(b)).

As can be seen, for initial populations generated using the random topology generator, the optimal solution is obtained for the three smallest networks. With the increase in the number of nodes the *gap* also increases reaching almost 15%, see Fig. 3.7(a). For initial populations generated using the topology generator presented in [30], see Fig. 3.7(b), the genetic algorithm also obtains the optimal solution for networks with less than 12 nodes. The

exception is the CESNET network in which the best solution obtained has a *gap* of 4.1%. Increasing the number of nodes the *gap* also increases. However, the solutions obtained within 100 iterations have *gaps* always smaller than 10%, see Fig. 3.7(b).

Considering the best solution obtained for all networks and combinations, only for the networks in which the optimal solution is obtained, an initial population randomly generated obtains a solution as good as the one obtained using [30]. In all the other networks the solutions obtained using the topology generator presented in [30] have smaller cost. The improvements range between 1% and 10%. One reason for this is that in the random topology generator all the links have the same probability to be chosen. Contrariwise, in the topology generator presented in [30] longer links have smaller probability than shorter ones. We also used a ring-based random topology generator in which the ring topology is equal for all initial individuals. However, in this case the links that belong to this ring are maintained at the crossover operation being changed only in the mutation operation, which penalize the obtained results.

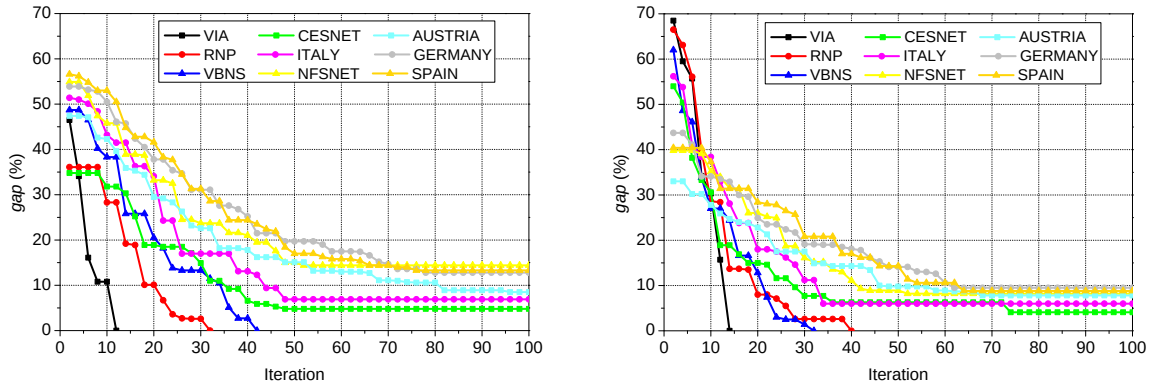

Figure 3.7: Evolution of the gap for the best solution obtained for the nine reference networks in each iteration for initial populations generated with the: (a) random topology generator [33] and (b) topology generator presented in [30].

3.5.2 The impact of the combinations

In this section, the eight operators combinations are compared and analyzed. The presented results are obtained using an initial population generated using [30] and uniform traffic. Figure 3.8 presents the best solution obtained in each iteration by the genetic algorithm, for each combination. Results for the vBNS network, a network with 12 nodes, are presented in Fig. 3.8(a). In Fig. 3.8(b) are presented the results for the SPAIN network, a network with 17 nodes. The lower bound obtained using the ILP model is also presented as a solid line.

As can be seen in Fig. 3.8(a), for the 12 nodes network, the convergence to a solution is fast for all combinations. The difference between the best solution obtained for each combination is not significant. As the number of nodes increases, the convergence to a solution is slower. As can be seen in Fig. 3.8(b), the convergence to a solution is only visible after the 60^{th}

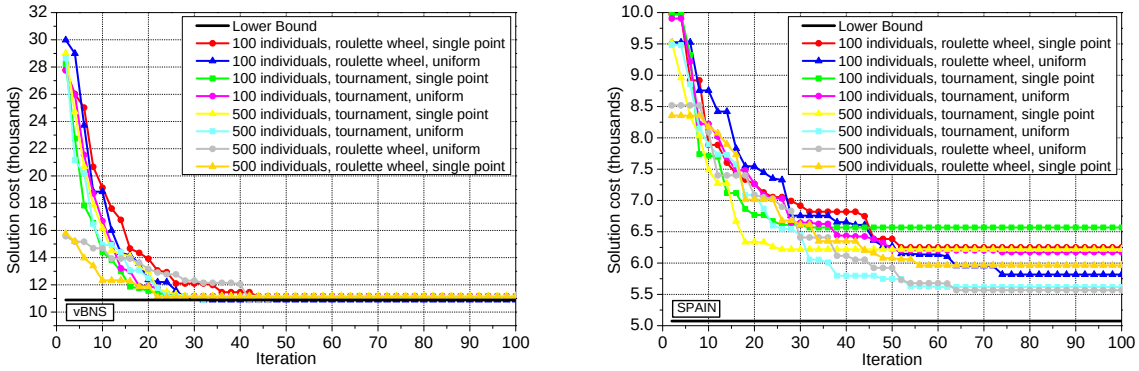

(a) (b)

Figure 3.8: Evolution of the best solution obtained in each iteration using the topology generator presented in [30] for the eight considered combinations and lower bound obtained using the ILP model (solid black line) for: (a) vBNS network (12 nodes) and (b) SPAIN network (17 nodes).

iteration. The difference between the quality of the obtained solutions increases as well.

To compare the eight combinations the gap of the best solution obtained for each method, among the five runs, is presented in Table 3.6. The best solution obtained is bold marked. The genetic algorithm with a population of 500 individuals, roulette wheel selection and uniform crossover obtains the best solution for eight networks, see Table 3.6. Moreover, a population of 500 individuals, tournament selection and uniform crossover equals the best solution obtained in six networks. The second best solution is also always obtained by one of these combinations. The difference between the solutions obtained by each combination ranges between 0% and 14%, tending to increase with the raise of the number of nodes.

Table 3.6: Gap of the best solution obtained with each of the eight considered combinations for initial populations generated using [30].

	100 individuals				**500 individuals**			
	Single point		**Uniform**		**Single point**		**Uniform**	
Network	**R. wheel**	**Tourn.**	**R. wheel**	**Tourn.**	**R. wheel**	**Tourn.**	**R. wheel**	**Tourn.**
VIA	**0.0 %**	**0.0 %**	**0.0 %**	**0.0 %**	**0.0 %**	**0.0 %**	**0.0 %**	**0.0 %**
RNP	2.6 %	7.9 %	3.5 %	2.7 %	1.9 %	1.9 %	**0.0 %**	**0.0 %**
vBNS	1.9 %	2.5 %	0.0 %	2.7 %	2.1 %	2.7 %	**0.0 %**	**0.0 %**
CESNET	6.0 %	8.9 %	4.1 %	6.0 %	7.0 %	7.3 %	4.8 %	**4.1 %**
ITALY	15.6 %	16.3 %	8.5 %	10.1 %	21.1 %	10.4 %	**6.0 %**	**6.0 %**
NFSNET	13.2 %	22.2 %	9.7 %	11.3 %	10.5 %	13.1 %	**8.2 %**	8.7 %
AUSTRIA	17.6 %	14.8 %	9.8 %	11.3 %	13.9 %	13.7 %	**7.8 %**	8.4 %
GERMANY	19.6 %	22.4 %	13.9 %	13.9 %	16.8 %	14.9 %	**9.5 %**	**9.5 %**
SPAIN	18.8 %	22.7 %	12.8 %	17.8 %	14.9 %	18.4 %	**8.8 %**	9.7 %

Making a comparison among the combinations, the uniform crossover obtains better solutions than the single point crossover, independently of the number of individuals and selection

method, see Table 3.6. The uniform crossover does not preserve large blocks of the progenitors genetic code to the offsprings, therefore it increases the population diversity and allows the genetic algorithm to obtain better solutions. On the other hand, fixing the crossover operator, the solutions obtained using the roulette wheel selection method are quite similar to the ones obtained using the tournament method. Improvements are observed when using the roulette wheel selection method. Comparing the results obtained with the different sizes of population, fixing the selection method and crossover operator, large populations (500 individuals) obtain better solutions than smaller ones (100 individuals). However, runs were also performed with populations of 1000 individuals and only residual improvements were obtained, with relation to solutions obtained with 500 individuals.

In spite of the individuals generation and the crossover operators being random, the difference between the solutions obtained by each run, among the five, is not significant. Moreover, as the size of the network increases such difference decreases.

3.5.3 The impact of the traffic pattern

Finally, the impact of the traffic model in the obtained solutions is analyzed. The non-uniform traffic is randomly generated with $0 \geq L(o,d) \geq 5$. The *gap* and the processing time for the solutions obtained using the ILP model and the genetic algorithm (GA) are presented in Table 3.7.

Table 3.7: Computational results using the ILP model and the genetic algorithm for uniform and non-uniform demand matrices.

		Uniform traffic				**Non-uniform traffic**			
		ILP		**GA**		**ILP**		**GA**	
Network	**Nodes**	**Time**	**gap**	**Time**	**gap**	**Time**	**gap**	**Time**	**gap**
VIA	9	1 s	0.0 %	8 s	0.0 %	4 s	0.0 %	8 s	0.0 %
RNP	10	42 s	0.0 %	27 s	0.0 %	24 m	0.0 %	27 s	3.2 %
vBNS	12	2 m	0.0 %	32 s	0.0 %	10 h	1.8 %	32 s	4.6 %
CESNET	12	7 h	0.0 %	01 m	4.1 %	10 h	0.3 %	01 m	5.7 %
ITALY	14	10 h	4.4 %	02 m	6.0 %	10 h	3.2 %	02 m	9.3 %
NFSNET	14	10 h	3.0 %	02 m	8.2 %	10 h	5.7 %	02 m	9.6 %
AUSTRIA	15	10 h	4.4 %	02 m	7.7 %	10 h	8.0 %	02 m	10.8 %
GERMANY	17	10 h	6.7 %	04 m	9.5 %	8 h$^{(*)}$	8.6 %	04 m	12.2 %
SPAIN	17	10 h	8.3 %	04 m	8.8 %	10 h	8.4 %	04 m	13.0 %

$^{(*)}$ Overloaded memory

For uniform traffic, the ILP model obtained the optimal solution for networks with less than 12 nodes. However, it is worth to note that the vBNS and CESNET networks required substantially different processing time, in spite of having the same number of nodes, see

Table 3.7. A reason for this may be found in the difference of the geographical area where the networks are implemented. The vBNS network, with 12 nodes, is in the USA and the CESNET network, also with 12 nodes, is in the Czech Republic. Due to the larger area that the vBNS network has to cover, the majority of its links are fixed since the beginning due to the distance. For networks with more than 12 nodes the ILP model obtains a solution with a gap smaller than 8.3% within 10 hours. With the exception of the GERMANY and SPAIN networks, the ILP model obtains a solution with a *gap* smaller than 10% in less than 3 hours.

The genetic algorithm is much faster than the ILP model and obtains near optimal solutions. For networks with less than 12 nodes the genetic algorithm obtains either the optimal solution or a solution with a gap of 4% within 1 minute. For networks with more than 12 nodes the genetic algorithm obtains solutions with *gaps* smaller than 10% within 4 minutes. A solution was obtained in approximately 45 minutes for a network with 100 nodes. In this case, the gap was not calculated as this problem cannot be addressed using the ILP model within a reasonable time and computational effort.

The topology obtained using the ILP model and the genetic algorithm for the GERMANY network with uniform traffic can be observed in Fig. 3.9(a). The dashed links are the ones that differ in both solutions. The black dashed lines represent the links of the topology obtained using the genetic algorithm. The grey dashed lines represent the links of the topology obtained using the ILP model. The black solid lines represent the common links to both solutions. None of the topologies obtained are optimal, see Table 3.7. However, the majority of the optimal links are already present in both solutions.

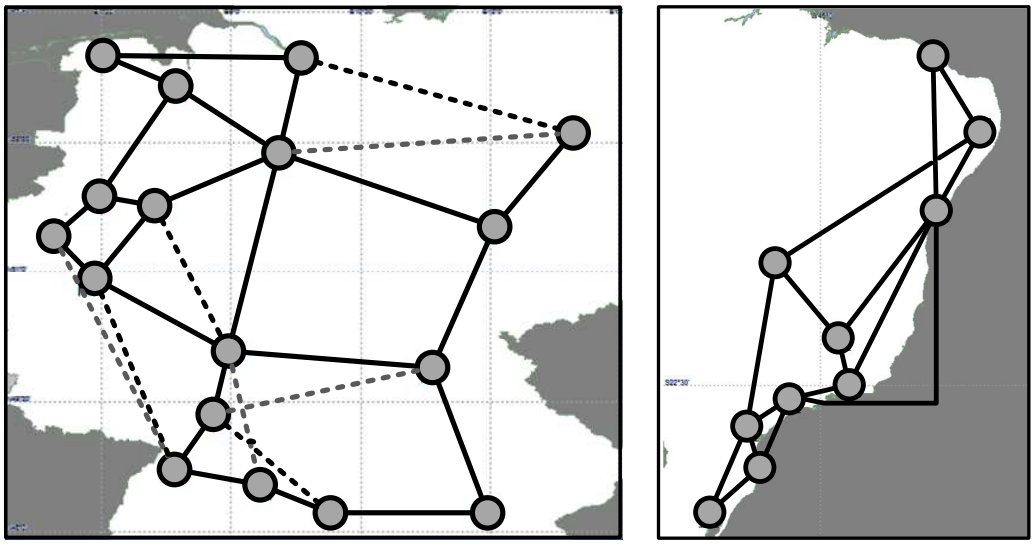

(a) (b)

Figure 3.9: Topologies obtained using the ILP model and the genetic algorithm for the node location of (a) GERMANY network with uniform traffic and (b) RNP network with non-uniform traffic. The dashed links differ in both solutions and the solid links are common.

Considering non-uniform traffic, the complexity of the problem increases. In this case the ILP model only obtained the optimal solution, within the time limit, for networks with less

than 10 nodes. However, solutions with a *gap* smaller than 8.6% can still be obtained in 10 hours. We also observe that the ILP model obtains solutions with *gaps* smaller than 10% within 3 hours of processing time. For the GERMANY network, the computer runs out of memory before the end of the 10 hours of processing time.

The genetic algorithm maintains the processing time, although the results obtained suffered an increase in the *gap*. We observed that the responsibility of such increase is due to the routing algorithm. The optimal routing is not always the shortest path, sometimes longer routes can optimize the network available resources. Fig. 3.9(b) depicts the best result obtained with the node location of the RNP network, using the ILP model and the genetic algorithm with a non-uniform traffic. As can be seen in Table 3.7, the genetic algorithm obtained a solution with a gap of 3.2%. Nevertheless, the physical topology obtained is the optimal, see Fig. 3.9(b). The gap is only due to suboptimal routing.

3.6 Chapter summary

This chapter describes the work developed in order to design survivable topologies at minimum CapEx for links. The chapter starts by presenting an introduction to the survivable topological design problem and the dimensioning model for links. Later a genetic algorithm is showed. Two initial population generators, two selection methods, two crossover operators, and two sizes of populations are reported and compared within the genetic algorithm. Additionally, an integer linear programming model is also presented to evaluate the quality of the genetic algorithm solutions. Computational results obtained using the node location of real telecommunication networks showed that initial populations generated using a method that preserves the main characteristics of real optical networks improves the quality of the obtained solutions. Moreover, crossover operators that do not preserve large blocks of the genetic code increase the diversity of the population and the probability of finding better solutions. The results accuracy and the saved processing time encourage the use of this kind of heuristic within the survivable topological design problem in optical transport networks.

References

[1] A. Gladisch, R.-P. Braun, D. Breuer, A. Ehrhardt, H.-M. Foisel, M. Jaeger, R. Leppla, M. Schneiders, S. Vorbeck, W. Weiershausen, and F. Westphal, "Evolution of terrestrial optical system and core network architecture," *Proceedings of the IEEE*, vol. 94, no. 5, pp. 869–891, June 2006.

[2] P. Babarczi, "Survivable Optical Network Design with Unambiguous Shared Risk Link Group Failure Localization," Ph.D. thesis, Budapest University of Technology and Economics, 2011.

[3] H. Kerivin and A. R. Mahjoub, "Design of survivable networks: A survey," *Networks*, vol. 46, pp. 1–21, August 2005.

[4] R. M. Morais, "Desenho Topológico de Redes Ópticas," Master's thesis, University of Aveiro, Aveiro, Portugal, 2008.

[5] O. Klopfenstein, "Access network dimensioning with uncertain traffic forecasts," in *Proc International Telecommunications Network Strategy and Planning Symposium - NETWORKS*, pp. 1–52, October 2008.

[6] S. Yang and F. Kuipers, "Traffic uncertainty models in network planning," *IEEE Communications Magazine*, vol. 52, no. 2, pp. 172–177, February 2014.

[7] D. Cieslik, *Network Design Problems*, Wiley, 2009.

[8] S. Ramamurthy, L. Sahasrabuddhe, and B. Mukherjee, "Survivable WDM mesh networks," *IEEE/OSA Journal of Lightwave Technology*, vol. 21, no. 4, pp. 870–883, April 2003.

[9] D. Jungnickel, *Graphs, Networks and Algorithms*, Springer Publishing Company, 2007.

[10] M. R. Garey and D. S. Johnson, *Computers and Intractability: A Guide to the Theory of NP-Completeness*, W. H. Freeman & Co., 1990.

[11] S. Hyung Yook, H. Jeong, and A. László Barabási, "Modeling the Internet's large-scale topology," *Proc. National Academy of Science - PNAS*, vol. 99, no. 21, pp. 13382–13386, October 2002.

[12] C. Palmer and J. Steffan, "Generating network topologies that obey power laws," in *Proc IEEE Global Telecommunications Conference - GLOBECOM*, vol. 1, pp. 434–438, December 2000.

[13] M. Faloutsos, P. Faloutsos, and C. Faloutsos, "On power-law relationships of the Internet topology," in *Proceedings of the Conference on Applications, Technologies, Architectures, and Protocols for Computer Communication - SIGCOMM*, pp. 251–262, September 1999.

[14] A. Barabási and E. Bonabeau, "Scale-free networks," *Scientific American*, May 2003.

[15] S. Routray, R. M. Morais, J. da Rocha, and A. N. Pinto, "Statistical model for link lengths in optical transport networks," *IEEE/OSA Journal of Optical Communications and Networking*, vol. 5, no. 7, pp. 762–773, July 2013.

[16] Y. Xin, G. Rouskas, and H. Perros, "On the physical and logical topology design of large-scale optical networks," *IEEE/OSA Journal of Lightwave Technology*, vol. 21, no. 4, pp. 904–915, April 2003.

[17] C. Guan and V. Chan, "Efficient physical topologies for regular WDM networks," in *Proc Optical Fiber Communication Conference and Exposition and the National Fiber Optic Engineers Conference - OFC/NFOEC*, pp. TuH1, February 2004.

[18] H. V. Nguyen and D. L. Truong, "Survivable physical topology design for all-optical metro core networks," in *Proc International Conference on Computing, Management and Telecommunications - ComManTel*, pp. 38–42, January 2013.

[19] G. Xiao, Y.-W. Leung, and K.-W. Hung, "Two-stage cut saturation algorithm for designing all-optical networks," *IEEE Transactions on Communications*, vol. 49, no. 6, pp. 1102–1115, June 2001.

[20] H. Liu and F. Tobagi, "Physical topology design for all-optical networks," in *Proc International Conference on Broadband Communications, Networks and Systems - BROADNETS*, pp. 1–10, October 2006.

[21] S. Soni and H. Pirkul, "Design of survivable networks with connectivity requirements," *Telecommunication Systems*, vol. 20, no. 1-2, pp. 133–149, May 2002.

[22] A. Balakrishnan, T. L. Magnanti, and P. Mirchandani, "Connectivity-splitting models for survivable network design," *Networks*, vol. 43, no. 1, pp. 10–27, January 2004.

[23] A. Balakrishnan, P. Mirchandani, and H. P. Natarajan, "Connectivity upgrade models for survivable network design," *Operations Research*, vol. 57, no. 1, pp. 170–186, February 2009.

[24] D. Habibi, H. Nguyen, Q. Phung, and K. meng Lo, "Establishing physical survivability of large networks using properties of two-connected graphs," in *TENCON 2005 IEEE Region 10*, pp. 1–5, November 2005.

[25] X. Ma, S. Kim, and K. Harfoush, "Towards realistic physical topology models for Internet backbone networks," in *Proc International Symposium on High-Capacity Optical Networks and Enabling Technologies - HONET*, pp. 36–42, December 2009.

[26] N. Dharmaweera, R. Parthiban, and Y. Sekercioglu, "Multi-constraint physical topology design for all optical networks," in *Proc International Conference on Telecommunications - ICT*, pp. 463–469, May 2011.

[27] S. Soni, R. Gupta, and H. Pirkul, "Survivable network design: The state of the art," *Information Systems Frontiers*, vol. 1, no. 3, pp. 303–315, October 1999.

[28] I. De Miguel, R. Vallejos, A. Beghelli, and R. J. Durán, "Genetic algorithm for joint routing and dimensioning of dynamic WDM networks," *IEEE/OSA Journal of Optical Communications and Networking*, vol. 1, no. 7, pp. 608–621, November 2009.

[29] D. A. R. Chaves, C. J. A. Bastos-Filho, and J. Martins-Filho, "Multiobjective physical topology design of all-optical networks considering QoS and CapEx," in *Proc Optical Fiber Communication Conference and Exposition and the National Fiber Optic Engineers Conference - OFC/NFOEC*, pp. JThA45, March 2010.

[30] C. Pavan, R. M. Morais, J. da Rocha, and A. N. Pinto, "Generating realistic optical transport network topologies," *IEEE/OSA Journal of Optical Communications and Networking*, vol. 2, no. 1, pp. 80–90, January 2010.

[31] D. E. Goldberg, *Genetic Algorithms in Search, Optimization and Machine Learning*, Addison-Wesley Longman Publishing Co., 1989.

[32] J. Dreo, A. Pétrowski, P. Siarry, and E. Taillard, *Metaheuristics for Hard Optimization: Methods and Case Studies*, Springer, 2005.

[33] J.-F. Labourdette, E. Bouillet, R. Ramamurthy, and A. Akyamac, "Fast approximate dimensioning and performance analysis of mesh optical networks," *IEEE/ACM Transactions on Networking*, vol. 13, no. 4, pp. 906–917, August 2005.

[34] B. Waxman, "Routing of multipoint connections," *IEEE Journal on Selected Areas in Communications*, vol. 6, no. 9, pp. 1617–1622, December 1988.

[35] Fico Xpress optimization suite (2010). [Online]. Available: http://www.fico.com/en/products/fico-xpress-optimization-suite/

[36] R. Huelsermann, M. Gunkel, C. Meusburger, and D. A. Schupke, "Cost modeling and evaluation of capital expenditures in optical multilayer networks," *Journal of Optical Networking*, vol. 7, pp. 814–833, September 2008.

CHAPTER 4

Nodes dimensioning

Transmission systems are often deployed in large number and are shared by a large number of wavelengths, therefore nodes are generally considered the most expensive part of an optical transport network. Moreover, nodes play a key role as they are responsible to aggregate the client traffic into wavelengths and switch that wavelengths between transmission systems. As the gap between the capacity offered by a single wavelength and the bandwidth required by a typical service request is increasing, network planners need to carefully select which mixture of client signals should be aggregated as well as in which locations the grooming operation should be performed. Thus, the development of optimization methods for the accurate dimensioning of multilayer nodes is a capital concern in transport networks.

Usually, nodes dimensioning models have been neglecting the constraints imposed by the hardware implementation such as the types of available modules, the size of the backplane, the number of ports per module, or the extra modules for OAM and switching control [1–3]. However, optimal module planning is an important problem in network dimensioning and deployment. An optimized module planning can minimize the total number of modules, shelves and racks resulting in cost reduction joint with power consumption and footprint requirements savings. Moreover, it allows an alignment between the planned solution and the deployed one. Thus, it is important to optimally plan and organize the modules. In this chapter a dimensioning model that calculates the number and type of modules at each node providing that the traffic requirements are fully supported is presented. The model considers all the architectures for the electrical and optical layer presented in Chapter 2, and focuses on greenfield planning, i.e. no pre-deployed capacity exists.

The chapter is organized in five sections. The inputs and assumptions of the dimensioning model for the different node architectures are presented in Section 4.1. In Section 4.2, the dimensioning model for the muxponders-based architecture is presented, and Section 4.3 is devoted to the model considering EXCs based architectures. The dimensioning model for the

optical layer can be found in Section 4.4. At the end, Section 4.5 summarizes the chapter.

4.1 Dimensioning model

The development of dimensioning models is an active research field in the literature. Dimensioning models are closely related to the grooming operation as it determines the number of ports and wavelengths required. Traffic grooming was first studied to aggregate SDH/SONET traffic in order to minimize the number of wavelengths used in ring topologies [4]. Later such studies were extended to mesh topologies [5, 6]. Previous works include minimization of network blocking [6–8], or total network cost [9]. These works rely on ILP models or heuristics, which require complete information about the network topology and traffic requirements. In a preliminary network evaluation, network planners can desire to have an estimation of the network resources without having complete information. In this context, semi-empirical formulations to dimensioning optical transport networks with limited inputs are described in [10–12]. The aim is to quickly estimate the amount of traffic that can be carried over a given network, or, conversely, given the traffic to be supported, to assess the characteristics of the topology required. In later years, traffic grooming considering the physical-layer impairments [13–15], intended to minimize the power consumption [16–18], or in multilayer networks [18–21] is also receiving increasing interest. The optimization of multilayer networks has been focused on the two layer IP-over-WDM [18, 19], or the three layer IP-over-OTN-over-WDM [20, 21] architectures. Regarding the optical layer, the majority of the works investigate the feasibility and scalability of different ROADM architectures in terms of cost [22–25], power consumption [25–27], optical impairments [28–30], or blocking probability [31–34]. In all the previous works, the nodes are assumed to be only port count. Moreover, the dimensioning of the client side as well as the required control modules are not taken into consideration. In [1–3] the modules planning problem is addressed. The works [1, 2] focus on the link-by-link grooming scheme, and in [3] in the minimization of the power consumption in multi-shelf nodes.

A multilayer network is represented as a graph $G(V, E_c, E_p)$ where $V = \{1, \ldots, N\}$, is the set of nodes, $E_c = \{(o, d) : o, d \in V\}$ is the set of node pairs exchanging traffic, defining the logical topology, and $E_p = \{\{i, j\} : i, j \in V\}$, is the set of links defining the physical topology. Network nodes exchange traffic from a origin node, o, to a destination node, d. Henceforward, we focus on the OTN technology defined in ITU-T recommendation G.709 [35], however the approaches and models are extendable to support other technologies such as SDH/SONET or Ethernet. The client traffic to be supported by the network can be represented in $N \times N$ matrices $[T_c]$, where c is the bit rate of the client signals. The set of all client bit rates is denoted by $C = \{c : c \in \{1.25, 2.5, 10, 40, 100\}\}$. The elements $t_c(o, d)$ of the $[T_c]$ matrix, hold the demands with bit rate c in units of transmission (e.g., ODU2), between the nodes o and d. As an example the matrix $[T_{10}]$ represents all 10 Gbit/s (ODU2) client signals between all pairs of nodes. These lower bit rate client signals are then groomed to form a higher bit rate line signal, l. The set of line bit rates will be denoted

by $L = \{l : l \in \{2.5, 10, 40, 100\}\}$, corresponding to an OTU1, OTU2, OTU3 and OTU4, respectively. The ITU-T recommendation G.709 specifies that it is possible to mix various lower bit rate signals, with different bit rates, into a single higher bit rate signal. The OTN grooming configurations are presented in Fig. 4.1. An OTN grooming configurations, ϵ, is defined as the maximum number of lower bit rate signals that can be groomed. For instance 4×2.5 Gbit/s to 10 Gbit/s and 2×40 Gbit/s + 2×10 Gbit/s to 100 Gbit/s are two possible grooming configurations.

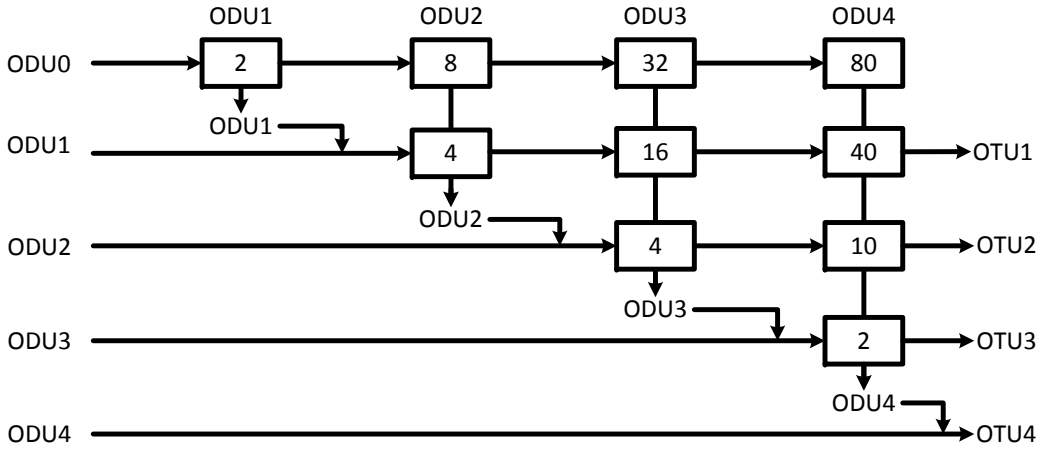

Figure 4.1: OTN grooming configurations, ϵ. The presented values are the maximum number of lower bit rate signals that can be groomed into the next higher bit rate signal. Various lower bit rate signals, with different bit rates can be groomed into a single higher bit rate signal.

To implement the architectures for the electrical and optical layer of the node, various equipments can be used. Figure 4.2 presents examples of the assumptions regarding the implementation of the node architectures presented in Chapter 2. Figure 4.2(a) is related to the muxponders-based and ROADM architectures, Fig. 4.2(b) to the non-blocking EXC architecture, and Fig. 4.2(c) to the partial non-blocking EXCs architecture. In the displayed example, the rack can accommodate either three shelves occupying one row each (see Fig. 4.2(a) and (c)) or one shelf with three rows (see Fig. 4.2(b)). The muxponders-based and ROADM architectures do not require a shelf enabling the switching of client signals by backplane. In these architectures the backplane only provides communication of OAM data between the modules and the control module (red module). The interconnection between modules (if needed) is done by external links thus, any module can be plugged into any available slot in the shelf (see Fig. 4.2(a)). In EXCs-based architectures the backplane (gray areas) provides communication of OAM data to the control module, however it also allows data signal communication between different modules. As aforementioned in Section 2.4.2, EXCs-based architectures require an additional control module, the ESM (blue modules). In the non-blocking EXC architecture, a common backplane is shared between all the modules deployed in the rack, for instance the three row shelf presented in Fig. 4.2(b). Thus, the modules can be inserted in any slot as the backplane is common to all. The ESM is responsible to switch the client signals via backplane to the line modules or between line modules.

Note that this is an example, and in order to behave as a non-blocking EXC architecture the shelf size needs to be large enough to accommodate all the required modules. Alternatively, in the partial non-blocking EXCs architecture, shelves of smaller size can be deployed in the rack, offering a more scalable solution, for instance up to three shelves per rack (see Fig. 4.2(c)). In this solution only modules inserted in the same shelf can communicate through the backplane. Thereby restricting switching and grooming to modules sharing the same shelf. Therefore, in both planning and operation phase, the interconnection between client and line modules connected to different shelves should be prevented.

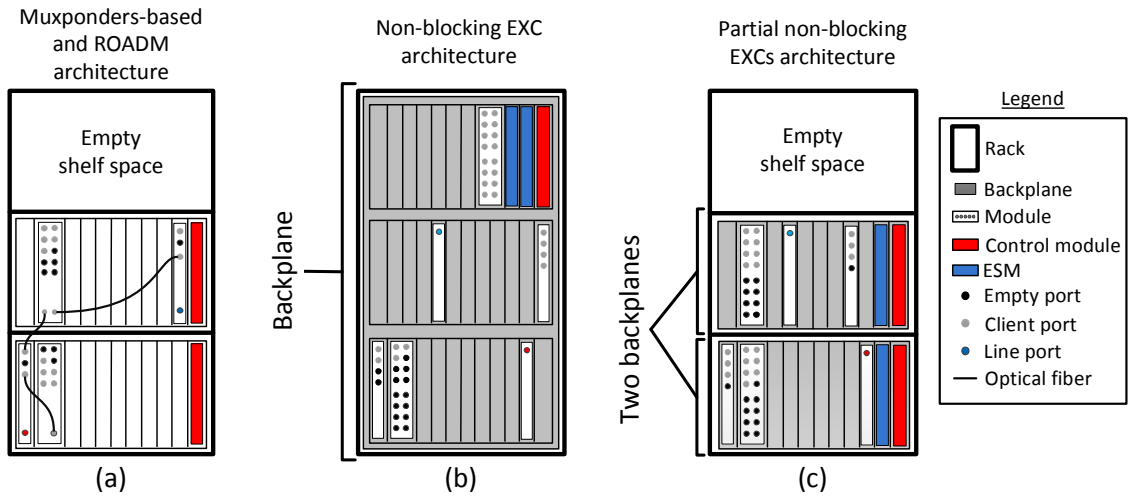

Figure 4.2: Node architectures implementation: (a) muxponders-based and ROADM architectures; (b) non-blocking EXC architecture, (b) partial non-blocking EXCs architecture.

Select which grooming configuration should be used in order to minimize the number of required modules is a typical combinatorial optimization problem. This problem was modeled as a bin-packing problem (or Knapsack problem) [36] with the architectures related constraints taken into account. We focus on the single-hop grooming scheme in this chapter. In this way, we can decouple the grooming process from the physical topology and routing algorithm. In order to deal with this problem ILPs models are used.

4.2 Muxponders-based architecture

The muxponders-based architecture, i.e. fixed grooming, requires various types of muxponders, and transponder modules, see Fig. 2.6. A muxponder module has various input ports to receive client signals and one output port to generate a higher or equal bit rate signal. The transponder module will be treated as a muxponder in which the bit rate of the input client signal is equal to the bit rate of the line signal. The availability of muxponders of certain type depends on the system vendor. If a muxponder receiving client signals with bit rate c and generating a target output signal with bit rate l is not available, a cascade of muxponders is required. We assume a maximum of two stage grooming in this thesis. However, the extension for more grooming stages can be straightforward achieved. Hereafter,

$c^* \in C$ will denote a client bit rate requiring a two stage grooming. The subset of client bit rates requiring a two stage grooming will be denoted by $C^* \subset C$. Note that the client bit rates $c^* \in C^*$ need to be groomed into a bit rate $c \in C \setminus C^*$, i.e. a client bit rate for which exists a muxponder accepting it and generating a signal with bit rate l. We assume that one cascade of muxponders is always available: $c^* \rightarrow c \rightarrow l$. As aforementioned a muxponder module defines one or a few grooming configurations, ϵ. The set of muxponder modules used in the first stage grooming will be denoted by $X^* = \{\epsilon\}$, i.e. muxponders accepting signals with bit rate c^* and generating signals with bit rate $c \neq l$. The set of muxponder modules used in the second stage grooming, or in a single stage grooming, will be denoted by $X = \{\epsilon\}$, i.e. muxponders accepting signals with bit rate c and generating signals with bit rate l.

As an example let us consider that c can be a client signal at 1.25 Gbit/s, 2.5 Gbit/s, 10 Gbit/s, or 40 Gbit/s and l a signal at 40 Gbit/s or 100 Gbit/s. Moreover, consider that the unique muxponder types accepting signals at 1.25 Gbit/s and 2.5 Gbit/s are the ones corresponding to configurations 1 and 2 presented in Table 4.1. A muxponder accepting client signals operating at 1.25 Gbit/s or 2.5 Gbit/s and generating an output signal at 40 Gbit/s or 100 Gbit/s is not available. Thus, these inputs define $C^* = \{1.25, 2.5\}$, $C \setminus C^* = \{10, 40\}$, $X^* = \{1, 2\}$, and $X = \{3, 4, 5, 6\}$.

Table 4.1: Example of available muxponders.

Input signals bit rate				**Output signal bit rate**	**Grooming configuration (ϵ)**
1.25 Gbit/s	2.5 Gbit/s	10 Gbit/s	40 Gbit/s		
4	2	0	0	10 Gbit/s	1
6	1	0	0	10 Gbit/s	2
0	0	4	0	40 Gbit/s	3
0	0	0	1	40 Gbit/s	4
0	0	10	0	100 Gbit/s	5
0	0	2	2	100 Gbit/s	6

In the first stage grooming, client signals with bit rate c^* are groomed into client signals with bit rate c through a given grooming configuration $\epsilon \in X^*$. The input and output ports of muxponders used in the first stage grooming are equipped with short reach transceivers, see Fig. 2.6. The total number of short-reach transceivers with bit rate c^* in the node o for muxponders-based architectures, $Tsv_{c^*}^{mb}(o)$, only depends on the number of client signals with the given bit rate, $t_{c^*}(o, d)$. Thus, is given by

$$Tsv_{c^*}^{mb}(o) = \sum_{d \in V} t_{c^*}(o, d), \quad \forall c^* \in C^*, \forall o \in V. \tag{4.1}$$

The number of muxponder modules with output bit rate c required for the demands

between the nodes o and d and accepting traffic in the grooming configuration $\epsilon \in X^*$, $M_c^\epsilon(o,d)$, depends on the type of muxponder modules available and on $t_{c^*}(o,d)$. A grooming operation is performed at this stage, to aggregate client signals with bit rate c^* into client signals with bit rate c. Thus, the following ILP is used to minimize $M_c^\epsilon(o,d)$,

$$minimize \quad \sum_{c \in C \setminus C^*} \sum_{\epsilon \in X^*} \sum_{(o,d) \in E_c} M_c^\epsilon(o,d) \tag{4.2}$$

subject to

$$t_{c^*}(o,d) \leq \sum_{\epsilon \in X^*} H_c^{c^*,\epsilon} M_c^\epsilon(o,d), \qquad \forall (o,d) \in E_c, \forall c^* \in C^* \tag{4.3}$$

$$\sum_{c^* \in C^*} c^* t_{c^*}(o,d) \leq \sum_{\epsilon \in X^*} c M_c^\epsilon(o,d), \qquad \forall (o,d) \in E_c \tag{4.4}$$

$$M_c^\epsilon(o,d) \in \mathbb{N}_0, \qquad \forall (o,d) \in E_c, \forall \epsilon \in X^* \tag{4.5}$$

Objective function (4.2) is a generic cost function of the total number of muxponder modules of all types. Constraint (4.3) indicates that the $t_{c^*}(o,d)$ client signals with bit rate c^* need to be groomed into muxponder modules with output bit rate c in one grooming configuration ϵ, $M_c^\epsilon(o,d)$, considering that a maximum of $H_c^{c^*,\epsilon}$ input signals with bit rate c^* can be accepted in that configuration (for instance the values in Table 4.1). Constraint (4.4) ensures that the total bandwidth required between nodes o to d for all client signals with bit rate c^* is smaller or equal to the bandwidth of all output signals with bit rate c in all muxponders. Finally, constraints (4.5) define the variables $M_c^\epsilon(o,d)$ as non negative integer variables allowing the use of more than one muxponder module between the same node pairs.

The total number of muxponder modules with grooming configuration $\epsilon \in X^*$ required to groom the client signals with bit rate c^* into a signal with bit rate c in the node o, $M_c^\epsilon(o)$, is given by

$$M_c^\epsilon(o) = \sum_{d \in V} M_c^\epsilon(o,d), \quad \forall \epsilon \in X^*, \forall o \in V. \tag{4.6}$$

As the signals generated in the first stage grooming are input signals of the muxponders used in the second stage, $t_c(o,d)$ needs to be updated to $t'_c(o,d)$ by

$$t'_c(o,d) = t_c(o,d) + \sum_{\epsilon \in X^*} M_c^\epsilon(o,d), \quad \forall c \in C \setminus C^*, \forall (o,d) \in E_c. \tag{4.7}$$

Thus, the total number of short-reach transceivers with bit rate c in node o, $Tsv_c^{mb}(o)$, is given by

$$Tsv_c^{mb}(o) = \sum_{d \in V} t'_c(o,d), \quad \forall c \in C \setminus C^*, \forall o \in V. \tag{4.8}$$

Note that each output signal of $M_c^\epsilon(o,d)$ requires two short reach transceivers, one at the

output port of the first stage grooming muxponder and another at the input port of the second stage grooming muxponder, see Fig. 2.6.

The muxponders used in the second stage (or in a single stage grooming) receive input signals with bit rate c and generate output line signals with bit rate l. The number of muxponder modules with output bit rate l required for the demands between the nodes o and d and accepting traffic in the grooming configuration $\epsilon \in X$, $M_l^\epsilon(o,d)$ is also calculated using an ILP. The ILP is similar to the one used for the first stage grooming but replacing $M_c^\epsilon(o,d)$ by $M_l^\epsilon(o,d)$, and $t_{c^*}(o,d)$ by $t'_c(o,d)$,

$$minimize \quad \sum_{l\in L}\sum_{\epsilon\in X}\sum_{(o,d)\in E_c} M_l^\epsilon(o,d) \tag{4.9}$$

subject to

$$t'_c(o,d) \leq \sum_{\epsilon\in X} H_l^{c,\epsilon} M_l^\epsilon(o,d), \qquad \forall (o,d)\in E_c, \forall c \in C \setminus C^* \tag{4.10}$$

$$\sum_{c\in C\setminus C^*} ct_c(o,d) \leq \sum_{\epsilon\in X} l M_l^\epsilon(o,d), \qquad \forall (o,d)\in E_c \tag{4.11}$$

$$M_l^\epsilon(o,d) \in \mathbb{N}_0, \qquad \forall (o,d)\in E_c, \forall \epsilon \in X \tag{4.12}$$

Objective (4.9) is the usual generic cost function. Constraints (4.10) and (4.11) guarantees that all client signals are aggregated in one grooming configuration, ϵ, and that the total bandwidth provided by line signals is higher or equal than all client signals bandwidth. Finally, constraints (4.12) define $M_l^\epsilon(o,d)$ as non negative integer variables.

As in the first stage grooming, $M_l^\epsilon(o)$, is given by

$$M_l^\epsilon(o) = \sum_{d\in V} M_l^\epsilon(o,d), \quad \forall \epsilon \in X, \forall o \in V. \tag{4.13}$$

The muxponders M_l^ϵ are equipped with long-reach transceivers. Thus, as we assume single output ports, the total number of long-reach transceivers with bit rate l in the node o, $Tsv_l^{mb}(o)$, is given by

$$Tsv_l^{mb}(o) = M_l^\epsilon(o), \quad \forall l \in L, \forall o \in V. \tag{4.14}$$

All the modules need to be connected into a shelf, and each type of module occupies a given number of slots. The total number of slots at node o in muxponders-based architectures, $S_{tot}^{mb}(o)$, is achieved by multiplying the total number of modules by its respective size in number of slots,

$$S_{tot}^{mb}(o) = \sum_{\epsilon\in X^*} M_c^\epsilon(o) S_c^\epsilon + \sum_{\epsilon\in X} M_l^\epsilon(o) S_l^\epsilon, \quad \forall o \in V, \tag{4.15}$$

where S_c^ϵ and S_l^ϵ are the number of slots required by the muxponders with output c and l, in configuration ϵ, respectively. To accommodate the $S_{tot}^{mb}(o)$ required slots, one or more shelves

are necessary. Each shelf can support a given number of slots, S_{sf}^{mb}, being some reserved for the mandatory control modules. We assume that each shelf requires one control module. Thus, the number of control modules in node o, $M_{ctr}^{mb}(o)$, equals the number of shelves, $M_{sf}^{mb}(o)$. Considering that S_{ctr}^{mb} is the number of slots reserved for the control module, we have $S_{sf}^{mb} - S_{ctr}^{mb}$ available slots per shelf. In this type of architecture any module can be connected to any shelf, see Fig. 4.2(a). Therefore, the number of shelves in node o for muxponders-based architectures, $M_{sf}^{mb}(o)$, equals the number of control modules and is given by

$$M_{sf}^{mb}(o) = M_{ctr}^{mb}(o) = \left\lceil \frac{S_{tot}^{mb}(o)}{S_{sf}^{mb} - S_{ctr}^{mb}} \right\rceil, \quad \forall o \in V. \tag{4.16}$$

Note that more than one control module can be present in each shelf for protection purposes. In this case, S_{ctr}^{mb} should account for the various control modules required.

4.3 Electrical cross connects based architectures

The EXC-based architecture, presented in Fig. 2.7, requires client modules for each c type of traffic, line modules, and an ESM per shelf. In this case any demand can be plugged into any client port of any client module, independently of the destination node, provided that they share a common backplane. Moreover, all possible grooming configurations are allowed. In the following the models for non-blocking EXC and partial blocking EXCs architectures are presented.

4.3.1 Non-blocking electrical cross connect

The client signals are received by client modules equipped with short-reach transceivers. The total number of short-reach transceivers with bit rate c required in the node o for non-blocking EXCs architectures, $Tsv_c^{nbe}(o)$, is given by

$$Tsv_c^{nbe}(o) = \sum_{d \in V} t_c(o,d), \quad \forall\ c \in C, \forall\ o \in V. \tag{4.17}$$

Client modules can have one or more ports. Thus, the number of client modules accepting signals with bit rate c, required in the node o, $M_c(o)$, is given by

$$M_c(o) = \left\lceil \frac{\sum_{d \in V} t_c(o,d)}{P_c} \right\rceil, \quad \forall\ c \in C, \forall\ o \in V, \tag{4.18}$$

where P_c is the number of ports of the client module accepting signals with bit rate c.

The client signals are groomed to form line signals. The ILP to minimize the number of line modules with bit rate l in node o, $M_l(o)$, used in non-blocking EXC architectures is as follows,

$$minimize \quad \sum_{l \in L} \sum_{o \in V} M_l(o) \tag{4.19}$$

subject to

$$\sum_{c \in C} ct_c(o,d) \leq \sum_{l \in L} lO_l(o,d), \quad \forall (o,d) \in E_c \tag{4.20}$$

$$M_l(o) \geq \frac{\sum_{d \in V} O_l(o,d)}{P_l}, \quad \forall l \in L, \forall o \in V \tag{4.21}$$

$$O_l(o,d) \in \mathbb{N}_0, \quad \forall l \in L, \forall (o,d) \in E_c \tag{4.22}$$

$$M_l(o) \in \mathbb{N}_0, \quad \forall l \in L, \forall o \in V \tag{4.23}$$

Objective (4.19) is the generic cost function and intends to minimize the number of line modules in the network. Constraints (4.20) ensures that the bandwidth provided by all the line signals between the nodes o and d, $O_l(o,d)$, is higher or equal than the bandwidth requested by all client signals between the same node pairs. Constraint (4.21) ensures that the number of line modules with bit rate l is higher or equal to the relation between the number of required line signals with bit rate l for all destination nodes, and the number of output ports that the line module can support P_l. Finally, constraints (4.22) and (4.23) define the variables $O_l(o,d)$ and $M_l(o)$ as non negative integer variables. It is worth to note that this ILP is similar to the one used for muxponders-based architectures. However, constraint (4.10) related to the grooming configuration restrictions is replaced by constraint (4.21) regarding the number of ports in each line module.

Line modules ports are equipped with long-reach transceivers. The number of long-reach transceivers with bit rate l in the node o, $Tsv_l^{nbe}(o)$, is given by

$$Tsv_l^{nbe}(o) = \sum_{d \in V} O_l(o,d), \quad \forall l \in L, \forall\ o \in V. \tag{4.24}$$

The total number of slots for client and line modules at node o in non-blocking EXCs architectures, $S_{tot}^{nbe}(o)$, is then achieved by

$$S_{tot}^{nbe}(o) = \sum_{c \in C} M_c(o) S_c + \sum_{l \in L} M_l(o) S_l, \quad \forall o \in V, \tag{4.25}$$

where S_c is the number of slots occupied by the client module with bit rate c and S_l is the number of slots occupied by the line module with bit rate l. As in the muxponders-based architectures, we assume that each shelf requires one control module and that each module can be plugged into any available slot in the shelf, see Fig. 4.2(b). However, in this case an additional ESM module is needed. Hence, as only one shelf, $M_{sf}^{nbe}(o)$, is used in this type of architecture, only one control module, $M_{ctr}^{nbe}(o)$, and one ESM, $M_{esm}^{nbe}(o)$, is required in node o for non-blocking EXC architecture. Thus,

$$M_{sf}^{nbe}(o) = M_{ctr}^{nbe}(o) = M_{esm}^{nbe}(o) = 1, \quad \forall o \in V. \tag{4.26}$$

4.3.2 Partial non-blocking electrical cross connects

In partial non-blocking EXCs architecture the interconnection between client and line modules connected to different backplanes needs to be prevented. We assume that the client and line modules used in this type of architecture are the same as the ones used in the non-blocking EXC architecture. The total number of short-reach transceivers with bit rate c required in the node o for partial non-blocking EXCs architecture, $Tsv_c^{pbe}(o)$, is the same as for non-blocking grooming. Thus, is given by Eq. (4.17).

In this case, the grooming operation needs to take into consideration the shelf in which the client and the line modules are connected. Therefore, both the number of client and line modules are optimized using an ILP. In order to formulate the ILP, the binary variable $B(o,s)$ is introduced. The variable $B(o,s)$ is 1 if shelf s is implemented in node o, otherwise takes the value 0. The set of shelves will be denoted by $S = \{s\}$. Thus, the number of client modules accepting signals with bit rate c, in node o and shelf s, $M_c(o,s)$, and the number of line modules with with bit rate l, in node o and shelf s, $M_l(o,s)$, are minimized by

$$\begin{aligned} \textit{minimize} \quad & \sum_{o\in V}\sum_{s\in S}\left(\sum_{c\in C} M_c(o,s) + \sum_{l\in L} M_l(o,s) \right. \\ & \left. + B(o,s)\right) \end{aligned} \tag{4.27}$$

subject to

$$t_c(o,d) \leq \sum_{s\in S} O_c(o,d,s), \qquad \forall (o,d) \in E_c, \forall c \in C \tag{4.28}$$

$$M_c(o,s) \geq \frac{\sum_{d\in V} O_c(o,d,s)}{P_c}, \qquad \forall c \in C, \forall s \in S \tag{4.29}$$

$$\sum_{c\in C} ct_c(o,d) \leq \sum_{l\in L}\sum_{s\in S} lO_l(o,d,s), \qquad \forall (o,d) \in E_c \tag{4.30}$$

$$M_l(o,s) \geq \frac{\sum_{d\in V} O_l(o,d,s)}{P_l}, \qquad \forall l \in L, \forall s \in S \tag{4.31}$$

$$\begin{aligned} & \sum_{c\in C} M_c(o,s)S_c + \sum_{l\in L} M_l(o,s)S_l \\ & \qquad \leq (S_{sf}^{pbe} - (S_{ctr}^{pbe} + S_{esm}^{pbe}))B(o,s), \qquad \forall o \in V, \forall s \in S \end{aligned} \tag{4.32}$$

$$O_c(o,d,s) \in \mathbb{N}_0, \qquad \forall c \in C, \forall (o,d) \in E_c, \forall s \in S \tag{4.33}$$

$$O_l(o,d,s) \in \mathbb{N}_0, \qquad \forall l \in L, \forall (o,d) \in E_c, \forall s \in S \tag{4.34}$$

$$M_c(o,s) \in \mathbb{N}_0, \qquad \forall c \in C, \forall o \in V, \forall s \in S \tag{4.35}$$

$$M_l(o,s) \in \mathbb{N}_0, \qquad \forall l \in L, \forall o \in V, \forall s \in S \tag{4.36}$$

$$B(o,s) \in \{0,1\}, \qquad \forall o \in V, \forall s \in S \tag{4.37}$$

Objective (4.27) is the generic cost function intended to minimize the total number of modules and shelves of the network. Constraint (4.28) ensures that all $t_c(o,d)$ client signals with bit rate c have a client port in one of the shelves s, in each of the nodes o and d, $O_c(o,d,s)$. Constraint (4.29) guarantees that the total number of client ports with bit rate c in the node o, and shelf s, $O_c(o,d,s)$, is smaller or equal than the number of client modules installed in that particular shelf, $M_c(o,s)$, assuming that each client module has P_c available ports. Constraint (4.30) ensures that the bandwidth provided by all the line ports in all the shelves, $O_l(o,d,s)$, is higher or equal than the bandwidth requested by all client signals. Constraint (4.31) is similar to constraint (4.29), however considering line modules in all the shelves, $M_l(o,s)$. Finally, constraints (4.32) guarantees that in each node o, the number of slots required for client and line modules in the same shelf, $B(o,s)$, does not exceeds it maximum number of slots. Note that each shelf requires one control module occupying S_{ctr}^{pbe} slots, and an additional ESM module occupying S_{esm}^{pbe} slots, thus $S_{sf}^{pbe} - (S_{ctr}^{pbe} + S_{esm}^{pbe})$ slots are available for client and line modules in each shelf. Constraints (4.34)-(4.36) define the variables $O_c(o,d,s)$, $O_l(o,d,s)$, $M_c(o,s)$ and $M_l(o,s)$ as non negative integer variables. At last, constraint (4.37) defines the variable $B(o,s)$ as binary.

The total number of line modules with bit rate l in the node o, $M_l^{pbe}(o)$, is given by

$$M_l^{pbe}(o) = \sum_{s \in S} M_l(o,s), \quad \forall l \in L, \forall o \in V. \tag{4.38}$$

Line modules ports are equipped with long-reach transceivers. Thus, the number of long-reach transceivers with bit rate l in the node o, $Tsv_l^{pbe}(o)$, is given by

$$Tsv_l^{nbe}(o) = \sum_{d \in V} \sum_{s \in S} O_l(o,d,s), \quad \forall l \in L, \forall o \in V. \tag{4.39}$$

In this architecture the number of shelves required at each node is minimized using the ILP. Therefore, the number of control modules in node o, $M_{ctr}^{pbe}(o)$, equals the number of ESMs, $M_{esm}^{pbe}(o)$, and the number of shelves, $M_{sf}^{pbe}(o)$, and is given by

$$M_{sf}^{pbe}(o) = M_{ctr}^{pbe}(o) = M_{esm}^{pbe}(o) = \sum_{s \in S} B(o,s), \quad \forall o \in V. \tag{4.40}$$

4.4 Reconfigurable optical add/drop multiplexer architectures

This section presents the dimensioning model for the optical layer, thus for the ROADM architectures. The ROADMs are responsible to multiplex and switch the wavelength signals. A wavelength can traverse one or more ROADMs between the origin node o to the destination node d. The number of wavelengths that need to be routed through the network depends on the electrical layer architecture. For the muxponders-based architecture the number of wavelengths required between the nodes o and d, $L^{mb}(o,d)$, is given by the sum among all line muxponders modules,

$$L^{mb}(o,d) = \sum_{\epsilon \in X} M_l^{\epsilon}(o,d), \quad \forall (o,d) \in E_c. \tag{4.41}$$

Regarding non-blocking EXC architecture, $L^{nbe}(o,d)$, is given by

$$L^{nbe}(o,d) = \sum_{l \in L} O_l(o,d), \quad \forall (o,d) \in E_c, \tag{4.42}$$

and for partial non-blocking EXCs architecture, $L^{pbe}(o,d)$, by

$$L^{pbe}(o,d) = \sum_{l \in L} \sum_{s \in S} O_l(o,d,s), \quad \forall (o,d) \in E_c. \tag{4.43}$$

In the following, this variable will be referred independently of the electrical layer architecture thus, it will be named simply as $L(o,d)$.

As referred above, the wavelength channels are routed through the physical links $\{i,j\}$. Therefore, we will used the indexes i and j in this section as the ROADMs are related to the physical topology. The physical topology, E_p, and the number of transmission systems installed, $U(i,j)$, are inputs of the model. For instance, E_p and $U(i,j)$ can be obtained using the methods presented in Chapter 3. The number of transmission systems defines the nodal degree, $\delta(i)$, which can be calculated by

$$\delta(i) = \sum_{j \in V} U(i,j), \quad \forall i \in V. \tag{4.44}$$

The maximum nodal degree per node is limited by the number of output ports in the 1 $\times$ P WSS used in the cross connection structure, and by the number of required add/drop structures, see Section 2.5.2. Thus, the maximum nodal degree at node i, $\delta^{max}(i)$, is given by

$$\delta^{max}(i) = P + 1 - A(i), \quad \forall i \in V, \tag{4.45}$$

where $A(i)$ is the number of add/drop structures in the node i.

The cross connection structure is implemented in the same way in all the considered ROADM architectures, see Section 2.5. One 1 $\times$ P WSS module and one pre/booster amplifier module are required per transmission system. Therefore, the total number of 1 $\times$ P WSSs, $M_{wss}^{xc}(i)$, and pre/booster amplifiers, $M_{amp}^{xc}(i)$, used in the cross connection structure of node i is calculated by

$$M_{wss}^{xc} = M_{amp}^{xc} = \delta(i), \quad \forall i \in V. \tag{4.46}$$

It is worth to note that modules used in ROADM architectures can be connected in any available slot. The space occupied by the modules used in the cross connection structure will be calculated with the ones used in the add/drop structure as they can share the same shelf.

4.4.1 Fixed frequency and fixed direction

The fixed frequency and fixed direction add/drop structure, see Fig. 2.11, only requires one WSC module per transmission system. We assume that the WSC is capable of multiplex/demultiplex all the wavelengths supported by the transmission system, K. Thus, the number of WSC modules in the add/drop structure of the node i, $M_{wsc}^{ads}(i)$, equals the nodal degree,

$$M_{wsc}^{ads}(i) = \delta(i), \quad \forall i \in V. \tag{4.47}$$

The total number of slots required at node i in fixed frequency and fixed direction ROADM, $S_{tot}^{FF}(i)$, is calculated by multiplying the total number of modules required in the add/drop and cross connection structures by its respective size in number of slots. Thus, it is given by

$$S_{tot}^{FF}(i) = M_{wss}^{xc}(i)S_{wss}^{xc} + M_{amp}^{xc}(i)S_{amp}^{xc} + M_{wsc}^{ads}(i)S_{wsc}^{ads}, \quad \forall i \in V, \tag{4.48}$$

where $S_{wss}^{xc}, S_{amp}^{xc}$ and S_{wsc}^{ads} are the number of slots occupied by the $1 \times P$ WSS, amplifier, and WSC modules, respectively. As in the electrical layer, we assume that each shelf requires a control module. Thus, the number of control modules in node i for fixed frequency and fixed direction ROADM, $M_{ctr}^{FF}(i)$, equals the number of shelves, $M_{sf}^{FF}(i)$, and is given by

$$M_{sf}^{FF}(i) = M_{ctr}^{FF}(i) = \left\lceil \frac{S_{tot}^{FF}(i)}{S_{sf} - S_{ctr}} \right\rceil, \quad \forall i \in V. \tag{4.49}$$

4.4.2 Colorless and fixed direction

The colorless and fixed direction add/drop structure, see Fig. 2.12, still has a dedicated add/drop structure per transmission system. However, in this case the number of $1 \times P$ WSS modules depends on the number of add/drop channels per direction. The maximum number of channels that can be added/dropped per structure is limited by the number of ports in the $1 \times P$ WSS module. Let $P_{ads}^{CF}(i,j)$ be the number of add/drop ports needed in the node i for the channels of direction j. Thus, if $P_{ads}^{CF}(i,j) > P$ a cascade of $1 \times P$ WSS is required. The number of $1 \times P$ WSS modules required in the add/drop structure of node i and direction j, $M_{wss}^{CF}(i,j)$, is then given by

$$M_{wss}^{CF}(i,j) = \begin{cases} 1, & \text{if} \quad P_{ads}^{CF}(i,j) \leq P \\ \left\lceil \frac{P_{ads}^{CF}(i,j)}{P} \right\rceil + 1, & \text{if} \quad P_{ads}^{CF}(i,j) > P \end{cases}, \quad \forall (i,j) \in E_p. \tag{4.50}$$

The total number of $1 \times P$ WSS modules required in the add/drop structure in node i, $M_{wss}^{ads}(i)$, is then calculated as

$$M_{wss}^{ads}(i) = \sum_{j \in V} M_{wss}^{CF}(i,j), \quad \forall i \in V. \tag{4.51}$$

The total number of slots required at node i in colorless and fixed direction ROADM, $S_{tot}^{CF}(i)$, is calculated as

$$S_{tot}^{CF}(i) = M_{wss}^{xc}(i)S_{wss}^{xc} + M_{amp}^{xc}(i)S_{amp}^{xc} + M_{wss}^{ads}(i)S_{wss}^{ads}, \quad \forall i \in V, \tag{4.52}$$

where S_{wss}^{ads} is the number of slots occupied by the $1 \times P$ WSSs used in the add/drop structure. Once again, the number of control modules in node i for colorless and fixed direction ROADM, $M_{ctr}^{CF}(i)$, equals the number of shelves, $M_{sf}^{CF}(i)$ and is given by

$$M_{sf}^{CF}(i) = M_{ctr}^{CF}(i) = \left\lceil \frac{S_{tot}^{CF}(i)}{S_{sf} - S_{ctr}} \right\rceil, \quad \forall i \in V. \tag{4.53}$$

4.4.3 Fixed frequency and directionless

The fixed frequency and directionless add/drop structure, see Fig. 2.13, share the add/drop structure between all the transmission systems. One WSS and one WSC module is required per add/drop structure. The number of add/drop structures required in a given node depends on the number of add/drop channels. The total number of add/drop ports needed in the add/drop structures of node i, $P_{ads}^{FD}(i)$, is given by

$$P_{ads}^{FD}(i) = \sum_{d \in V} L(o,d) + 2R(i), \quad \forall i \in V : i = o, \tag{4.54}$$

where $R(i)$ is the number of signals requiring regeneration in the node i. Note that each regenerated signal requires two ports in the add/drop structure. The number of WSC modules, $M_{wsc}^{ads}(i)$, and $1 \times P$ WSS modules, $M_{wss}^{ads}(i)$, required in node i, to cope with the $P_{ads}^{FD}(i)$ signals, equals the number of add/drop structures, $A(i)$. Thus, is given by

$$A(i) = M_{wsc}^{ads}(i) = M_{wss}^{ads}(i) = \left\lceil \frac{P_{ads}(i)}{K} \right\rceil, \quad \forall i \in V, \tag{4.55}$$

where K is the capacity of the transmission system in number of channels. By equation (4.45) it can be seen that each additional add/drop structure reduces the maximum nodal degree of the node.

The total number of slots required at node i in fixed frequency and directionless ROADM, $S_{tot}^{FD}(i)$, is calculated as

$$S_{tot}^{FD}(i) = M_{wss}^{xc}(i)S_{wss}^{xc} + M_{amp}^{xc}(i)S_{amp}^{xc} + M_{wsc}^{ads}(i)S_{wsc}^{ads} + M_{wss}^{ads}(i)S_{wss}^{ads}, \quad \forall i \in V, \tag{4.56}$$

and the number of control modules in node i, $M_{ctr}^{FD}(i)$, equals the number of shelves, $M_{sf}^{FD}(i)$ and is given by

$$M_{sf}^{FD}(i) = M_{ctr}^{FD}(i) = \left\lceil \frac{S_{tot}^{FD}(i)}{S_{sf} - S_{ctr}} \right\rceil, \quad \forall i \in V. \tag{4.57}$$

4.4.4 Colorless and directionless

Regarding the modules necessary to implement the colorless and directionless add/drop structure, see Fig. 2.14, $1 \times P$ WSS, OSC, and amplifier modules can be required per add/drop structure. As in the fixed frequency and directionless ROADM, the add/drop structure is shared between all the node directions. The total number of add/drop ports needed in the add/drop structures of node i, $P_{ads}^{CD}(i)$, is calculated using (4.54). To cope with the $P_{ads}^{CD}(i)$ signals, one or more add/drop structures can be required. However, in the cases that $\delta^{max}(i)$ is reached, the extended architecture presented in Fig. 2.14(b) is used. The number of add/drop structures required in node i is given by

$$A(i) = \begin{cases} \left\lceil \frac{P_{ads}^{CD}(i)}{P} \right\rceil, & \text{if} \quad P_{ads}^{CD}(i) \leq P(P - \delta(i) + 1) \\ \\ \left\lceil \frac{P_{ads}^{CD}(i)}{P.P_{osc}} \right\rceil, & \text{if} \qquad P_{ads}^{CD}(i) > P(P - \delta(i) + 1) \end{cases}, \quad \forall i \in V, \tag{4.58}$$

where P_{osc} is the number of ports in the OSC module.

The number of $1 \times P$ WSS modules depends on the number of add/drop structures and on $P_{ads}^{CD}(i)$. If $P_{ads}^{CD}(i) \leq P(P-\delta(i)+1)$ only two $1 \times P$ WSS modules are required per add/drop structure, see Fig. 2.14(a), whereas if $P_{ads}^{CD}(i) > P(P - \delta(i) + 1)$ more modules are needed, see Fig. 2.14(b). One $1 \times P$ WSS is required per add/drop structure for the connection to the different transmission systems, and further $1 \times P$ WSS modules are necessary to support the $P_{ads}^{CD}(i)$ signals. Thus, the number of $1 \times P$ WSS modules required in the add/drop structures of node i, $M_{wss}^{ads}(i)$, is given by

$$M_{wss}^{ads}(i) = \begin{cases} 2A(i), & \text{if} \quad P_{ads}^{CD}(i) \leq P(P - \delta(i) + 1) \\ \\ A(i) + \left\lceil \frac{P_{ads}^{CD}(i)}{P} \right\rceil, & \text{if} \qquad P_{ads}^{CD}(i) > P(P - \delta(i) + 1) \end{cases}, \quad \forall i \in V. \tag{4.59}$$

For the case that $P_{ads}^{CD}(i) > P(P - \delta(i) + 1)$, OSC and amplifier modules are required to implement the extended architecture. The number of OSC modules, $M_{osc}^{ads}(i)$, and in node amplification, $M_{amp}^{ads}(i)$, required in node i, equals the number of add/drop structures, $A(i)$, and is given by

$$M_{osc}^{ads}(i) = M_{amp}^{ads}(i) = \begin{cases} 0, & \text{if} \quad P_{ads}^{CD}(i) \leq P(P - \delta(i) + 1) \\ \\ A(i), & \text{if} \qquad P_{ads}^{CD}(i) > P(P - \delta(i) + 1) \end{cases}, \quad \forall i \in V. \tag{4.60}$$

The total number of slots required at node i in the colorless and directionless add/drop structure, $S_{tot}^{CD}(i)$, is calculated as

$$S_{tot}^{CD}(i) = M_{wss}^{xc}(i)S_{wss}^{xc} + M_{amp}^{xc}(i)S_{amp}^{xc} + M_{wss}^{ads}(i)S_{wss}^{ads} + M_{amp}^{ads}(i)S_{amp}^{ads} + M_{osc}^{ads}(i)S_{osc}^{ads}, \quad \forall i \in V, \tag{4.61}$$

where S_{osc}^{ads} is the number of slots required by the OSC module in the add/drop structure. Once again we assume one control module per shelf. Thus, the number of shelves, $M_{sf}^{CD}(i)$, and of control modules, $M_{ctr}^{CD}(i)$, required in node i for the colorless and directionless ROADM is given by

$$M_{sf}^{CD}(i) = M_{ctr}^{CD}(i) = \left\lceil \frac{S_{tot}^{CD}(i)}{S_{sf} - S_{ctr}} \right\rceil, \quad \forall i \in V. \tag{4.62}$$

4.4.5 Colorless, directionless and contentionless

The colorless, directionless and contentionless add/drop structure, see Fig. 2.15, only requires one $P_i \times P_o$ WSS per add/drop structure. The total number of add/drop ports needed in the add/drop structures of node i, $P_{ads}^{CDC}(i)$, is calculated using (4.54). To accommodate the $P_{ads}^{CDC}(i)$ channels one or more add/drop structures can be required. In this case a cascade of $1 \times P$ WSS modules is avoided as it removes the contentionless functionality. The total number of $P_i \times P_o$ WSS required at node i, $M_{mwss}^{ads}(i)$, equals the number of add/drop structures and is given by

$$A(i) = M_{mwss}^{ads}(i) = \left\lceil \frac{P_{ads}^{CDC}(i)}{P_i} \right\rceil, \quad \text{if} \quad P_{ads}^{CDC}(i) \leq P_i(P_o - \delta(i) + 1), \quad \forall i \in V. \tag{4.63}$$

The total number of slots required at node i in the colorless, directionless and contentionless ROADM, $S_{tot}^{CDC}(i)$, is calculated as

$$S_{tot}^{CDC}(i) = M_{wss}^{xc}(i)S_{wss}^{xc} + M_{amp}^{xc}(i)S_{amp}^{xc} + M_{mwss}^{ads}(i)S_{mwss}^{ads}, \quad \forall i \in V, \tag{4.64}$$

where S_{mwss}^{ads} is the number of slots required by the $P_i \times P_o$ WSS module in the add/drop structure. The number of shelves, $M_{sf}^{CDC}(i)$, and of control modules, $M_{ctr}^{CDC}(i)$, required in node i for the colorless, directionless and contentionless ROADM is calculated as

$$M_{sf}^{CDC}(i) = M_{ctr}^{CDC}(i) = \left\lceil \frac{S_{tot}^{CDC}(i)}{S_{sf} - S_{ctr}} \right\rceil, \quad \forall i \in V. \tag{4.65}$$

4.5 Chapter summary

This chapter describes the developed nodes dimensioning models for each of the electrical and optical layer architectures considered. The models consider the imposed implementation restrictions and determine the required building blocks, given the traffic requirements and the network topology. The chapter starts by presenting the assumed nodes implementation, followed by the inputs of the model for the grooming function. After, models based on

ILPs for the muxponders-based and EXCs based architectures are reported. Regarding EXC based architectures, either non-blocking and partial non-blocking EXCs architectures are considered. At the end, a dimensioning model for each of the ROADM architectures presented is also developed.

References

[1] G. Shen, L. Peng, Y. Shen, and H. Sardesai, "Optimal node hardware module planning for layer-one optical transport networks," *IEEE/OSA Journal of Optical Communications and Networking*, vol. 3, no. 12, pp. 937–946, December 2011.

[2] G. Shen, Y. Shen, and H. Sardesai, "Optimal hardware module planning and switch backplane configuration for layer-one traffic grooming," in *Proc Optical Fiber Communication Conference and Exposition and the National Fiber Optic Engineers Conference - OFC/NFOEC*, pp. NMD3, March 2010.

[3] L. Wang, R. Lu, Q. Li, X. Zheng, and H. Zhang, "Energy efficient design for multi-shelf IP over WDM networks," in *Proc IEEE Conference on Computer Communications Workshops - INFOCOM WKSHPS*, pp. 349–354, April 2011.

[4] O. Gerstel, P. Lin, and G. Sasaki, "Combined WDM and SONET network design," in *Proc IEEE Conference on Computer Communications - INFOCOM*, vol. 2, pp. 734–743, March 1999.

[5] H. Zhu, H. Zang, K. Zhu, and B. Mukherjee, "A novel generic graph model for traffic grooming in heterogeneous WDM mesh networks," *IEEE/ACM Transactions on Networking*, vol. 11, no. 2, pp. 285–299, April 2003.

[6] K. Zhu and B. Mukherjee, "Traffic grooming in an optical WDM mesh network," *IEEE Journal on Selected Areas in Communications*, vol. 20, no. 1, pp. 122–133, January 2002.

[7] R. Dutta and G. N. Rouskas, "A survey of virtual topology design algorithms for wavelength routed optical networks," *Optical Networks*, vol. 1, pp. 73–89, 2000.

[8] I. Chlamtac, A. Ganz, and G. Karmi, "Lightpath communications: An approach to high bandwidth optical WAN's," *IEEE Transactions on Communications*, vol. 40, no. 7, pp. 1171–1182, July 1992.

[9] B. T. Doshi, S. Dravida, P. Harshavardhana, O. Hauser, and Y. Wang, "Optical network design and restoration," *Bell Labs Technical Journal*, vol. 4, no. 1, pp. 58–84, January 1999.

[10] S. K. Korotky, "Network global expectation model: A statistical formalism for quickly quantifying network needs and costs," *IEEE/OSA Journal of Lightwave Technology*, vol. 22, no. 3, pp. 703–722, April 2004.

[11] J.-F. Labourdette, E. Bouillet, R. Ramamurthy, and A. Akyamac, "Fast approximate dimensioning and performance analysis of mesh optical networks," *IEEE/ACM Transactions on Networking*, vol. 13, no. 4, pp. 906–917, August 2005.

[12] C. Pavan, "Dimensioning of Multilayer Optical Networks," PhD thesis, Department of Electronic, Telecommunications and Informatics, University of Aveiro, 2011.

[13] G. Shen and R. Tucker, "Sparse traffic grooming in translucent optical networks," *IEEE/OSA Journal of Lightwave Technology*, vol. 27, no. 20, pp. 4471–4479, October 2009.

[14] M. Batayneh, D. Schupke, M. Hoffmann, A. Kirstadter, and B. Mukherjee, "Optical network design for a multiline-rate carrier-grade Ethernet under transmission-range constraints," *IEEE/OSA Journal of Lightwave Technology*, vol. 26, no. 1, pp. 121–130, January 2008.

[15] G. Shen, Y. Shen, and H. Sardesai, "Cross-layer traffic grooming for optical networks with hybrid layer-one and layer-zero signal regeneration," in *Proc Optical Fiber Communication Conference and Exposition and the National Fiber Optic Engineers Conference - OFC/NFOEC*, pp. NThA6, March 2010.

[16] M. M. Hasan, F. Farahmand, A. N. Patel, and J. P. Jue, "Traffic grooming in green optical networks," in *Proc. IEEE International Conference on Communications - ICC*, pp. 1–5, May 2010.

[17] X. Dong, T. El-Gorashi, and J. Elmirghani, "IP over WDN networks employing renewable energy sources," *IEEE/OSA Journal of Lightwave Technology*, vol. 29, no. 1, pp. 3–14, January 2011.

[18] G. Shen and R. S. Tucker, "Energy-minimized design for IP over WDM networks," *IEEE/OSA Journal of Optical Communications and Networking*, vol. 1, no. 1, pp. 176–186, June 2009.

[19] G. Huiban, S. Perennes, and M. Syska, "Traffic grooming in WDM networks with multilayer switches," in *Proc. IEEE International Conference on Communications - ICC*, vol. 5, pp. 2896–2901, May 2002.

[20] I. Katib and D. Medhi, "IP/MPLS-over-OTN-over-DWDM multilayer networks: An integrated three-layer capacity optimization model, a heuristic, and a study," *IEEE Transactions on Network and Service Management*, vol. 9, no. 3, pp. 240–253, September 2012.

[21] S. De Maesschalck, M. Pickavet, D. Colle, and P. Demeester, "Multi-layer traffic grooming in networks with an IP/MPLS layer on top of a meshed optical layer," in *Proc IEEE Global Telecommunications Conference - GLOBECOM*, vol. 5, pp. 2750 – 2754, December 2003.

[22] F. Naruse, Y. Yamada, H. Hasegawa, and K. Sato, "Evaluations of OXC hardware scale and network resource requirements of different optical path add/drop ratio restriction schemes," *IEEE/OSA Journal of Optical Communications and Networking*, vol. 4, no. 11, pp. B26–B34, November 2012.

[23] P. Ji and Y. Aono, "Colorless and directionless multi-degree reconfigurable optical add/drop multiplexers," in *Proc Wireless and Optical Communications Conference - WOCC*, pp. 1–5, May 2010.

[24] S. Thiagarajan, L. Blair, and J. Berthold, "Direction-independent add/drop access for multi-degree ROADMs," in *Proc Optical Fiber Communication Conference and Exposition and the National Fiber Optic Engineers Conference - OFC/NFOEC*, pp. OThA7, February 2008.

[25] M. De Groote, K. Manousakis, P. Kokkinos, D. Colle, M. Pickavet, K. Christodoulopoulos, E. Varvarigos, and P. Demeester, "Cost comparison of different translucent optical network architectures," in *Proc Conference on Telecommunications Internet and Media Techno Economics - CTTE*, pp. 1–8, June 2010.

[26] V. Eramo, A. Germoni, A. Cianfrani, M. Listanti, and C. Raffaelli, "Evaluation of power consumption in low spatial complexity optical switching fabrics," *IEEE Journal of Selected Topics in Quantum Electronics*, vol. 17, no. 2, pp. 396–405, April 2010.

[27] N. Akar, V. Eramo, and C. Raffaelli, "Comparative analysis of power consumption in asynchronous wavelength modular optical switching fabrics," *Optical Switching and Networking*, vol. 8, no. 3, pp. 139–148, July 2011.

[28] N. Amaya, G. Zervas, and D. Simeonidou, "Introducing node architecture flexibility for elastic optical networks," *IEEE/OSA Journal of Optical Communications and Networking*, vol. 5, no. 6, pp. 593–608, June 2013.

[29] R. Jensen, "Optical switch architectures for emerging colorless / directionless / contentionless ROADM networks," in *Proc Optical Fiber Communication Conference and Exposition and the National Fiber Optic Engineers Conference - OFC/NFOEC*, pp. OThR3, March 2011.

[30] S. Tibuleac and M. Filer, "Transmission impairments in DWDM networks with reconfigurable optical add-drop multiplexers," *IEEE/OSA Journal of Lightwave Technology*, vol. 28, no. 4, pp. 557–598, February 2010.

[31] S. Thiagarajan and S. Asselin, "Nodal contention in colorless, directionless ROADMs using traffic growth models," in *Proc Optical Fiber Communication Conference and Exposition and the National Fiber Optic Engineers Conference - OFC/NFOEC*, pp. NW3F.2, March 2012.

[32] J. Pedro and S. Pato, "Impact of add/drop port utilization flexibility in DWDM networks," *IEEE/OSA Journal of Optical Communications and Networking*, vol. 4, no. 11, pp. B142–B150, November 2012.

[33] P. Pavon-Marino and M. Bueno-Delgado, "Dimensioning the add/drop contention factor of directionless ROADMs," *IEEE/OSA Journal of Lightwave Technology*, vol. 29, no. 21, pp. 3265–3274, November 2011.

[34] M. Feuer, S. Woodward, P. Palacharla, X. Wang, I. Kim, and D. Bihon, "Intra-node contention in dynamic photonic networks," *IEEE/OSA Journal of Lightwave Technology*, vol. 29, no. 4, pp. 529–535, February 2011.

[35] *ITU-T Recommendation G.709/Y.1331, Interfaces for the optical transport network (OTN)*, International Telecommunication Union Std., 2009.

[36] E. Coffman Jr., J. Csirik, G. Galambos, S. Martello, and D. Vigo, "Bin packing approximation algorithms: Survey and classification," in *Handbook of Combinatorial Optimization*, Springer New York, pp. 455–531, 2013.

CHAPTER 5

Greenfield planning

Given the broad variety of solutions and technologies available, it is not straightforward to evaluate which one should be implemented in order to reduce the cost. At the electrical layer, select whether muxponders architectures remain efficient or an EXC should be implemented is a key cost aspect. Regarding the optical layer, the decision is which level of flexibility the ROADM should have to support and switch the wavelengths in a cost efficient way. Thus, techno-economic studies are decisive to identify the most profitable deployment solution and assess the influence of the various cost contributions.

Usually, techno-economic analysis are performed considering all nodes equipped equally and uniform traffic. However, in real scenarios, the nodes can have different requirements and should be equipped accordingly. Moreover, while the focus of the existing studies was mainly on the CapEx, nowadays, OpEx related costs such as the cost with the power consumption, the footprint requirements, or the upgrade capabilities are important factors that should be taken into consideration. In this chapter, an analysis and comparison between the various node architectures presented in Chapter 2 using the models presented in Chapter 4 is reported. The analysis focuses on the CapEx, power consumption and footprint requirements. As the nodes dimensioning model assumes an end-to-end grooming scheme, the impact of the grooming process can be decoupled from the routing algorithm. Therefore, we analyze a single node, varying the factors that have an impact on the node performance. For the electrical layer we analyze one single node under different traffic loads, traffic patterns, and exchanging traffic with a different number of destination nodes. Regarding the optical layer we analyze one single node increasing the nodal degree and number of add/drop channels. Based on the outcome of a meaningful set of simulations, an optimization method based on node architecture selection is proposed. We identify simple rules and scenarios where a determined architecture (electrical and optical) brings advantage. Then, when considering the network and after routing the demands, we can quickly optimize the total network cost

by selecting the architecture of each node accordingly.

The chapter is organized in five sections. In Section 5.1, an analysis to the CapEx, power consumption and footprint requirements of the architectures for the electrical layer is presented, and in Section 5.2 a similar analysis for the optical layer architectures is reported. To evaluate the relative influence of the modules in the total network cost, Section 5.3 is devoted to a sensitivity analysis. After, in Section 5.4 the optimization method based on node architecture selection is presented, and its applicability demonstrated. At the end, in Section 5.5 the chapter is summarized.

5.1 Electrical layer

The results obtained using the dimensioning model for the electrical layer presented in Sections 4.2 and 4.3 are reported in this section. As aforementioned, we analyze one network node using different traffic loads, traffic patterns and number of destination nodes. The number of destination nodes is the number of other nodes to/from which the node has at least a demand. We consider four client bit rates (1.25 Gbit/s, 2.5 Gbit/s, 10 Gbit/s, and 40 Gbit/s) and a single line bit rate of 100 Gbit/s, defining $C = \{c : c \in \{1.25, 2.5, 10, 40\}\}$ and $L = \{l : l \in \{100\}\}$. The type of available modules, the number of ports, the number of required slots, the power consumption in Watts (W), and the price in monetary units (m.u.) are presented in Table 5.1 [1–3].

The transceivers are assumed to be the same for all the architectures. Thus, 1.25 Gbit/s, 2.5 Gbit/s, 10 Gbit/s, and 40 Gbit/s short-reach (SR) transceivers and a 100 Gbit/s long-reach (LR) transceiver are required, given the bit rates in C and L. Three muxponders are available, one generating a 10 Gbit/s signal and two generating a 100 Gbit/s signal, see Table 5.1. The 10 Gbit/s muxponder can accept all mixtures of 1.25 Gbit/s and 2.5 Gbit/s signals and generates a 10 Gbit/s signal. Thus, it can have five grooming configurations corresponding to the five alternatives to groom 1.25 Gbit/s and 2.5 Gbit/s signals into a 10 Gbit/s signal. Additionally two 100 Gbit/s muxponders are available, one accepting 2 $\times$ 10 Gbit/s + 2 $\times$ 40 Gbit/s signals and another accepting 10 $\times$ 10 Gbit/s signals, defining two more grooming configurations. Thus, the muxponders modules available define $C^* = \{1.25, 2.5\}$, $X^* = \{1, \ldots, 5\}$, $C \backslash C^* = \{10, 40\}$, and $X = \{6, 7\}$. For EXCs-based architectures one module per bit rate is available. Regarding the non-blocking EXC architecture, the shelf, the respective control module and the ESM are selected from the list in order to accommodate all the required modules with the smaller size EXC possible. For partial non-blocking EXCs architectures, the 16 slots shelf is always deployed. Regarding the power consumption of the modules, we assume that each module always consumes its typical power, presented in Table 5.1, even if not all available ports are in use. The power consumption of each shelf, the corresponding control module, and the ESM (in EXC architectures) is accounted since its deployment, as it is a fixed component.

In the framework of this study, we assume that the total traffic of node o, $T(o)$, is distributed over the four client bit rates, defining a traffic pattern. The considered total traffic

Table 5.1: Modules specifications for the electrical layer [1–3].

Module type	Variable	Ports	Parameter	Slots	Parameter	Power consumption (W)	Price (m.u.)
Transceivers							
1.25 Gbit/s (SR)	$Tsv_{1.25}$	-	-	-	-	1	0.02
2.5 Gbit/s (SR)	$Tsv_{2.5}$	-	-	-	-	1	0.05
10 Gbit/s (SR)	Tsv_{10}	-	-	-	-	3.5	0.1
40 Gbit/s (SR)	Tsv_{40}	-	-	-	-	8	0.4
100 Gbit/s (LR)	Tsv_{100}	-	-	-	-	15	14
Muxponder modules							
10 Gbit/s[(1)]	$M_{10}^{1...5}$	1	-	1	$S_{10}^{1...5}$	50	1.2
100 Gbit/s[(2)]	M_{100}^{6}	1	-	2	S_{100}^{6}	150	16
100 Gbit/s[(3)]	M_{100}^{7}	1	-	2	S_{100}^{7}	150	13
Shelf	M_{sf}^{mb}	-	S_{sf}^{mb}	16[(4)]	-	[(5)]	[(5)]
Control	M_{ctr}^{mb}	-	-	1	S_{ctr}^{mb}	300	5.3
Electrical cross connect modules							
1.25 Gbit/s	$M_{1.25}$	32	$P_{1.25}$	1	$S_{1.25}$	224	3.8
2.5 Gbit/s	$M_{2.5}$	24	$P_{2.5}$	1	$S_{2.5}$	360	4.5
10 Gbit/s	M_{10}	10	P_{10}	1	S_{10}	340	5
40 Gbit/s	M_{40}	2	P_{40}	1	S_{40}	320	6.4
100 Gbit/s	M_{100}	1	P_{100}	1	S_{100}	360	12
Shelf	M_{sf}^{pbe}	-	S_{sf}^{pbe}	16[(4)]	-	[(5)]	[(5)]
Control	M_{ctr}^{pbe}	-	-	1	S_{ctr}^{pbe}	400	8.3
ESM	M_{esm}^{pbe}	-	-	1	S_{esm}^{pbe}	200	3
Shelf	M_{sf}^{nbe}	-	S_{sf}^{nbe}	32[(4)]	-	[(5)]	[(5)]
Control	M_{ctr}^{nbe}	-	-	1	S_{ctr}^{nbe}	600	13
ESM	M_{esm}^{nbe}	-	-	1	S_{esm}^{nbe}	225	3.5
Shelf	M_{sf}^{nbe}	-	S_{sf}^{nbe}	64[(4)]	-	[(5)]	[(5)]
Control	M_{ctr}^{nbe}	-	-	1	S_{ctr}^{nbe}	900	31
ESM	M_{esm}^{nbe}	-	-	2	S_{esm}^{nbe}	300	6
Shelf	M_{sf}^{nbe}	-	S_{sf}^{nbe}	128[(4)]	-	[(5)]	[(5)]
Control	M_{ctr}^{nbe}	-	-	1	S_{ctr}^{nbe}	1200	76
ESM	M_{esm}^{nbe}	-	-	3	S_{esm}^{nbe}	500	10

[(1)] All mixture of 1.25 Gbit/s and 2.5 Gbit/s to 10 Gbit/s (5 grooming configurations)
[(2)] 2 × 10 Gbit/s + 2 × 40 Gbit/s to 100 Gbit/s
[(3)] 10 × 10 Gbit/s to 100 Gbit/s
[(4)] Number of available slots
[(5)] Included in the control modules

is of 200 Gbit/s, 400 Gbit/s, 600 Gbit/s and 800 Gbit/s. Moreover, to evaluate the dependence of the node architecture with the traffic pattern we consider the four traffic patterns presented in Table 5.2. We denote by $\overline{T}(o)$ the traffic weighted mean in node o.

The number of client demands with bit rate c in node o, $D_c(o)$, is then calculated as

$$D_c(o) = \left\lceil \frac{TP_c(o)}{c} \right\rceil, \tag{5.1}$$

where $TP_c(o)$ is the percentage of $T(o)$ with bit rate c in Gbit/s. Note that $T(o)$ equals the sum of $TP_c(o)$ over all c. The $D_c(o)$ demands are then randomly distributed, each demand

Table 5.2: Client traffic patterns.

Pattern Id	1.25 Gbit/s	2.5 Gbit/s	10 Gbit/s	40 Gbit/s	Weighted mean ($\overline{T}(o)$)
1	60%	30%	10%	0%	2.5 Gbit/s
2	10%	20%	50%	20%	13.6 Gbit/s
3	5%	10%	50%	35%	19.3 Gbit/s
4	0%	5%	30%	65%	29.1 Gbit/s

at a time, by the destination nodes, d, using an uniform distribution thus, defining the values of $t_c(1, d)$, with $d \in \{1, \ldots, N\}$. Five and ten destination nodes are considered. The above procedure is repeated 100 times for each combination of total traffic, traffic pattern, and number of destination nodes, in order to generate a meaningful data set.

In the following sections, the obtained results are analyzed. Figures 5.1, 5.2 and 5.3 display the average values calculated using the 100 realizations for the CapEx, the power consumption and the footprint requirements, respectively. Additionally, the error bars present the minimum and maximum value obtained. In all the cases, the results for muxponders-based architectures are presented in bars with solid fill, for non-blocking EXC in bars filled with diagonal lines, and for partial non-blocking EXCs in bars filled with vertical lines. Moreover, to evaluate the relative influence of the modules, the results are grouped by client, line and control modules. Client modules are modules equipped with short-reach transceivers, and line modules the ones equipped with long-reach transceivers. Thus, the muxponders used in the first stage grooming and the modules to receive the client signals in EXC-based architectures belong to the client modules. The muxponders used in the second stage grooming and the modules used to form the line signals in EXC-based architectures belong to the line modules. The control modules are the shelf, the control module and, in EXC-based architectures, the ESM. The results regarding the client modules are represented in blue, the line modules in gray, and the control modules in red, see Figs. 5.1, 5.2 and 5.3.

5.1.1 Capital expenditures

An analysis to the CapEx of the different electrical layer architectures is reported in this section. Figure 5.1(a) is related to the CapEx in scenarios where the traffic is distributed according to pattern 1, Fig. 5.1(b) to pattern 2, Fig. 5.1(c) to pattern 3, and Fig. 5.1(d) to pattern 4. The left side presents the results for five destination nodes and the rigth side for ten destination nodes.

As can be seen in Fig. 5.1, only minor differences between the total CapEx obtained for the different traffic patterns can be seen, fixing the total traffic. A slight increase in the CapEx is observed from 5 to 10 destination nodes. Comparing the architectures, the muxponders-based architecture always presents lower CapEx than the EXC-based solutions. The saves can reach 50%, however it is worth to note that this difference can be decreased in the OpEx

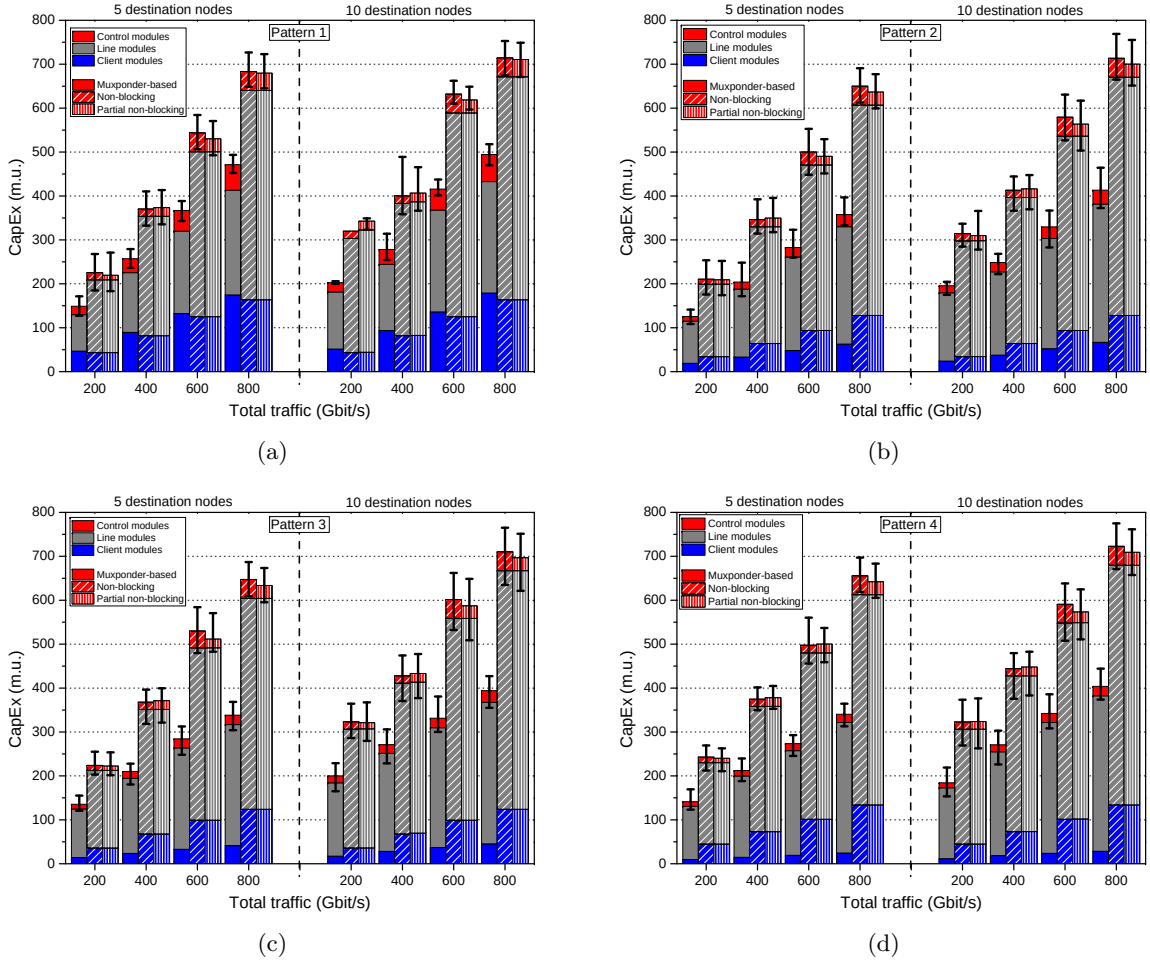

Figure 5.1: CapEx for muxponders-based, non-blocking EXC, and partial non-blocking EXCs architectures considering 5 and 10 destination nodes with total traffic distributed according to: (a) pattern 1, (b) pattern 2, (c) pattern 3, and (d) pattern 4.

related to the technicians. Considering the EXC-based architectures it can be seen that the CapEx related to the client and line modules is the same for both the non-blocking EXC and partial non-blocking EXCs architectures. The differences between the two approaches reside in the control modules. For low traffic loads (for instance 200 Gbit/s and 400 Gbit/s), non-blocking EXC tends to present lower CapEx than partial non-blocking EXCs. In these cases a slightly larger shelf can bring some benefits in terms of number of ESMs and control modules required. With the increase of the total traffic the requirements in terms of shelf size increases as well (for instance 600 Gbit/s and 800 Gbit/s). In this case the use of various smaller shelves can bring cost benefits, see Fig. 5.1.

Analyzing the contribution of the types of modules, it can be seen that the line modules dominate the total CapEx. This behavior was expected as the line modules are the most expensive ones, see Table 5.1. The percentage of CapEx regarding line modules ranges between 50% and 87% in muxponders-based architectures, and between 70% and 85% in EXC-based architectures. The CapEx related with the client modules correspond to a percentage

ranging between 7% and 34% in muxponders-based architectures, and between 13% and 24% in the EXC-based solutions. The bigger amplitude showed by the percentages in the muxponders-based architecture, reflects their higher dependence on the traffic pattern. For instance, patterns where only single stage grooming is needed for the majority of the traffic (for instance pattern 4) requires only a few client modules. Regarding control modules, they have a residual impact on the CapEx, contributing with a percentage ranging between 5% and 12% in muxponders-based architectures and between 4% and 7% in EXC-based architectures. The higher values presented in the muxponders solution regards the patterns where a two stage grooming is required for the majority of the traffic (for instance pattern 1). In this case, the huge number of modules required increases the number of shelves and control modules. Considering the amplitude of the results, muxponders-based architectures tend to present lower amplitude than EXC-based architectures. However, the amplitude obtained represent a variability of the total CapEx between 2% and 32% in muxponders-based architectures and between 1% and 37% in EXCs-based solutions.

5.1.2 Power consumption

A similar analysis but regarding the power consumption is presented in this section. Figure 5.2(a) is related to traffic distributed according to pattern 1, Fig. 5.2(b) to pattern 2, Fig. 5.2(c) to pattern 3, and Fig. 5.2(d) to to pattern 4. The left side regards five destination nodes and right side ten destination nodes.

As depicted in Fig. 5.2, muxponders-based architectures present lower power consumption than EXCs-based solutions. The differences range between 35% and 227%. Moreover, the power consumed by the client and line modules in the non-blocking EXC and in the partial non-blocking EXCs architectures is the same, and the differences between both architectures are only observed in the control modules, as in the CapEx analysis. However, in this case, the partial non-blocking EXCs architecture only outperforms non-blocking EXC architectures for 200 Gbit/s total traffic. To higher traffic loads the power required by the control modules of the various shelves required penalize the power consumption of the node.

Regarding the power consumption of the different types of modules, it can be seen that the line modules power consumption is of the same order of magnitude than the one of the client modules. The percentage of the total power consumption for client and line modules ranges between 15% and 50% in muxponders architectures. For EXCs-based architectures the percentage of power consumed by client modules ranges between 30% and 50% and the line modules between 38% and 57%. The control modules in muxponders architectures have a percentage ranging between 21% and 27% whereas in EXCs-based architectures ranges between 6% and 13%. Therefore, this result suggests that the control modules have an higher impact on the total power consumption of the node than in the total CapEx. The amplitude presented by the results is smaller than the one observed in the CapEx. For muxponders-based architectures the amplitude of the results correspond to a percentage ranging between 5% and 26%, and for EXCs architectures between 0% and 29%.

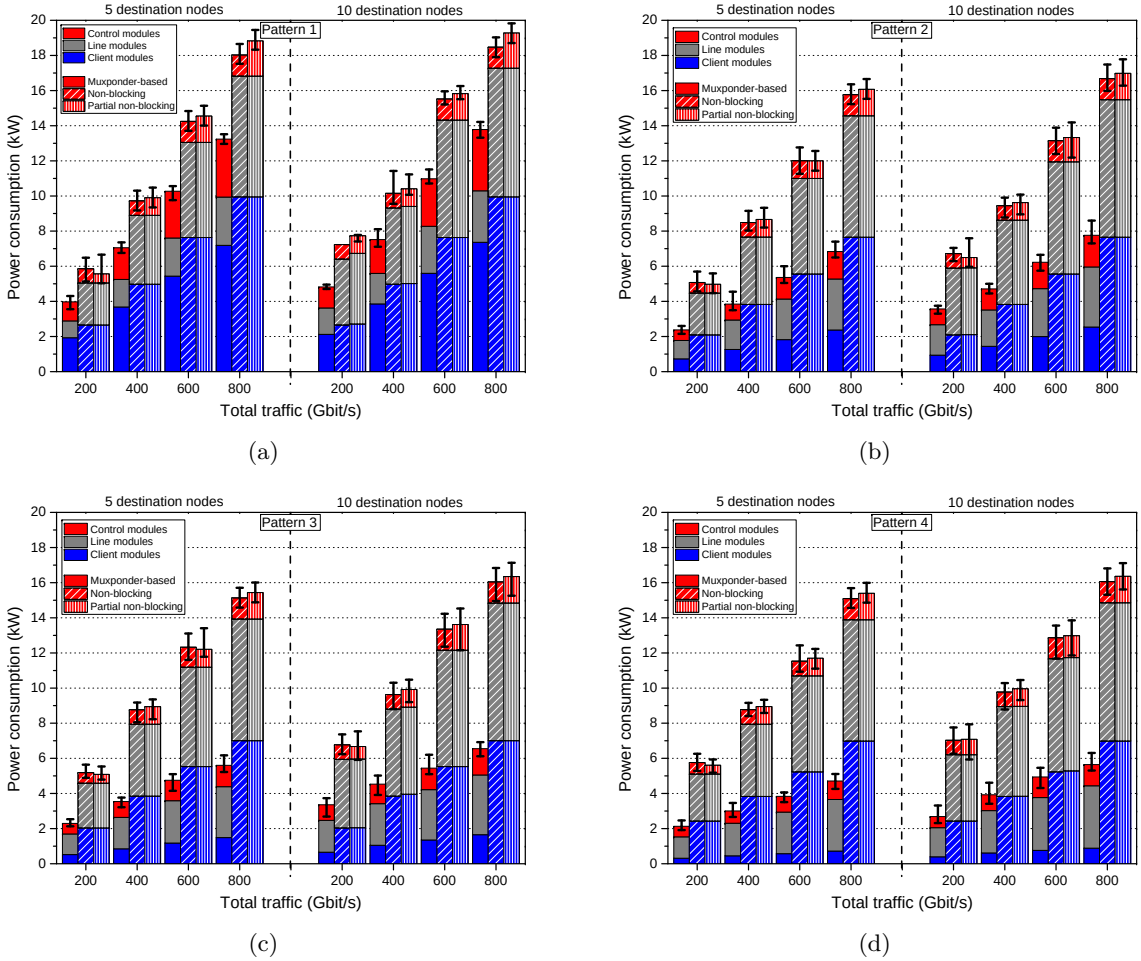

Figure 5.2: Power consumption for muxponders-based, non-blocking EXC, and partial non-blocking EXCs architectures considering 5 and 10 destination nodes with total traffic distributed according to: (a) pattern 1, (b) pattern 2, (c) pattern 3, and (d) pattern 4.

5.1.3 Footprint requirements

In the following, an analysis to the footprint requirements is presented. To better understand the differences between the architectures, the results are presented in number of slots. Figure 5.3(a) is related to traffic distributed according to pattern 1, Fig. 5.3(b) to pattern 2, Fig. 5.3(c) to pattern 3, and Fig. 5.3(d) to to pattern 4. The black solid lines mark the number of slots that can be accommodated into a single rack, assuming that each rack can support up to three shelves with 16 slots each, i.e. 42 slots. Note that in the non-blocking EXC architecture one rack is always deployed.

As depicted in Fig. 5.3, the muxponders-based architecture is the one requiring more number of slots. Moreover, in traffic patterns where a two stage grooming is required for a high percentage of the traffic these differences can reach 187%, for instance see Fig. 5.3(a). Although a single muxponder module provides a combination of encapsulation and grooming functions, they tend to occupy a larger number of slots, see Table 5.1. Moreover, the difference between the number of slots required by the muxponders and by the EXCs-based architectures

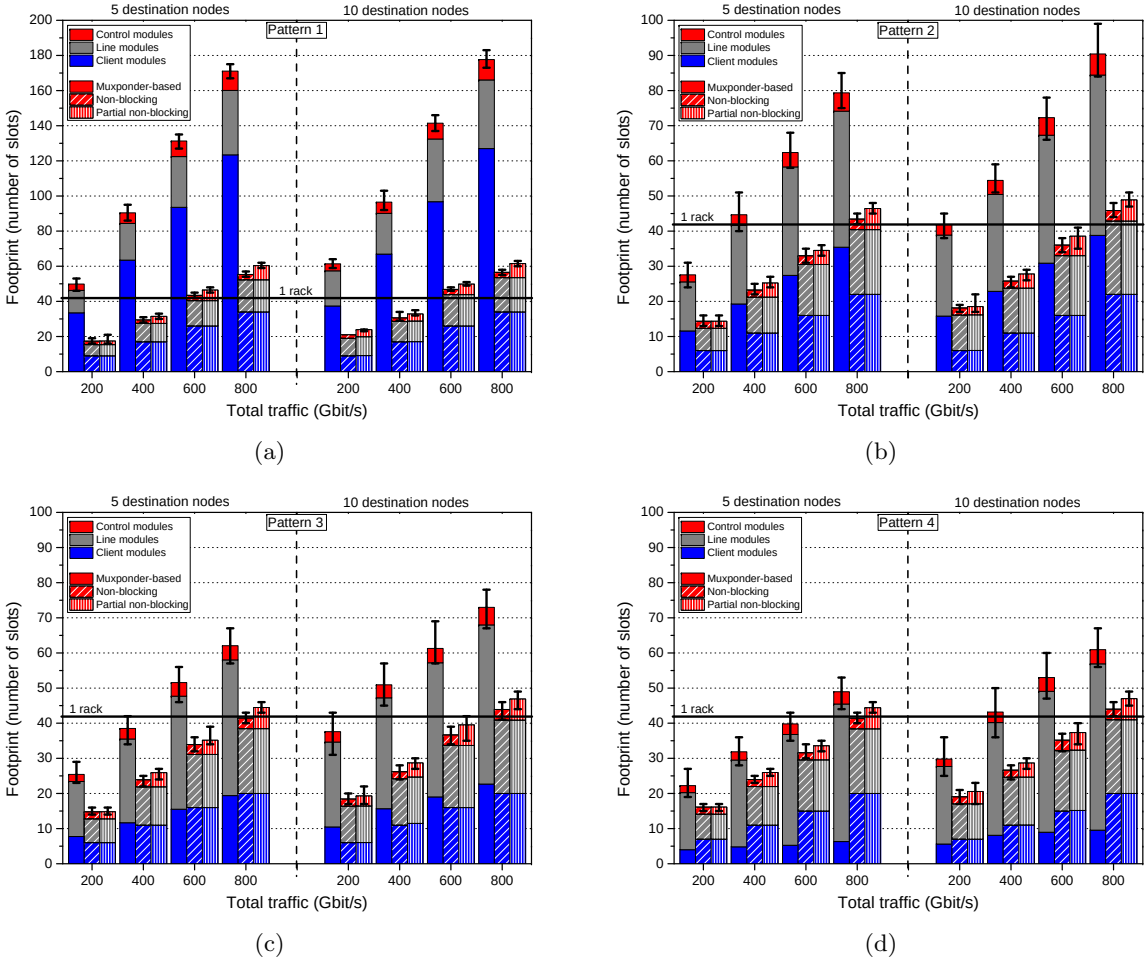

Figure 5.3: Footprint requirements in number of slots for muxponders-based, non-blocking EXC, and partial non-blocking EXC considering 5 and 10 destination nodes with total traffic in: (a) pattern 1, (b) pattern 2, (c) pattern 3, and (d) pattern 4.

tend to increase with the increase of the number of destination nodes. This can be explained by the fact that only client signals to be groomed can be connected to the same muxponder module, thus with the increase of the number of destination nodes the chances of having the modules completely filled decrease, impacting the node footprint. Architectures employing an EXC tend to require less number of slots. However, in spite of the number of slots required for client and line modules being the same for both non-blocking EXC and partial non-blocking EXCs architectures, the number of slots required for control modules in partial non-blocking EXCs architectures tend to be higher. In the partial non-blocking EXCs architectures each shelf requires an ESM and a control module, with the increase in the number of required shelves, the number of slots required for control modules increases as well. In opposition, in the non-blocking EXC architecture the control modules are shared between all client and line modules. It is worth to note that one rack is almost always sufficient to accommodate all the shelves in partial non-blocking EXCs. Considering the muxponders-based architecture, only for low traffic loads one rack can accommodate all the required modules.

In muxponders-based architectures, client modules represent a percentage ranging between 15% and 72% and line modules a percentage ranging between 22% and 77%. As in the CapEx and power consumption cases the traffic pattern is responsible by those variations. The control modules in muxponders-based architectures account only to a percentage ranging between 6% and 9% of the total node footprint. Regarding the EXC-based architectures, the client modules represent a percentage ranging between 32% and 60% and the line modules a percentage ranging between 33% and 57%. The control modules contribute with a percentage ranging between 5% and 14%. The amplitude obtained for the footprint is comparable to the one obtained for the power consumption. For muxponders-based architectures it represents a variability ranging between 5% and 35% whereas for EXC-based architectures represents a variability between 0% and 21%.

5.2 Optical layer

The results obtained using the dimensioning model for the optical layer presented in Section 4.4 are presented in this section. We analyze one network node with different nodal degrees and different number of add/drop channels. For the ROADM architectures with dedicated add/drop structure, we assume an equal number of add/drop channels per direction. Thus, in this case the total number of add/drop channels is divided by the nodal degree. A node with degree two, four, six, and eight is considered with a number of add/drop channels ranging from 2 to 80. The available modules specifications are presented in Table 5.3, which was created considering the values available in [1–3]. The same shelf and control module are assumed in all the ROADM architectures.

Table 5.3: Modules specifications for the optical layer [1–3].

Module type	**Variable**	**Ports**	**Parameter**	**Slots**	**Parameter**	**Power consumption (W)**	**Price (m.u.)**
WSC	M_{wsc}	80	K	3	S_{wsc}	40	2.3
$1 \times P$ WSS	M_{wss}	9	P	2	S_{wss}	40	4
$1 \times P$ WSS	M_{wss}	20	P	2	S_{wss}	45	6
OSC	M_{osc}	9	P_{osc}	1	S_{osc}	5	0.08
$P_i \times P_o$ WSS	M_{mwss}	9×9	$P_i \times P_o$	2	S_{mwss}	55	48
Shelf	M_{sf}	-	S_{sf}	16(1)	-	(2)	(2)
Control	M_{ctr}	-	-	1	S_{ctr}	300	5.3

(1) Number of available slots
(2) Included in the control modules

5.2.1 Add/drop ratio analysis

Some ROADM architectures offer a maximum number of add/drop ports that can be smaller than the maximum number of channels that can reach the node. The add/drop ratio of a node is then defined as the relation between the maximum number of add/drop channels

that the add/drop structures can support, and the maximum number of add/drop channels of all directions. The architectures with a dedicated add/drop structure per direction, for instance the fixed frequency and fixed direction and the colorless and fixed direction architectures, always have an add/drop ratio of one. This is, all the channels of all the directions can be added/dropped at a node. Considering the ROADM architectures in which the add/drop structure is shared among all the node directions, for instance the fixed frequency and directionless, the colorless and directionless, and the colorless, directionless and contentionless architectures, the add/drop ratio depends on the nodal degree and on the number of add/drop structures required to accommodate all the add/drop channels.

Considering the fixed frequency and directionless, and the colorless and directionless architectures, the add/drop ratio only depends on the number of ports in the $1 \times P$ WSS module used in the cross connection structure. As can be seen in Table 5.3, the number of ports available allows each add/drop structure to support all the K channels of the fiber. For instance, the WSC module can multiplex/demultiplex all the K channels, moreover 1×9, and 1×20 WSSs are currently available. As typical values for K are 80 or 96 channels, a cascade of WSSs can reach that value per add/drop structure. As an example, the use of one 1×9 WSS connected to five 1×20 WSS can reach 100 add/drop ports per add/drop structure. Note that even if the number of add/drop ports available is higher than K, each add/drop structure can only be use to K add/drop channels because of the connection via fiber between the different modules. Therefore, the add/drop ratio of node i, $\tau(i)$, for fixed frequency and directionless, and colorless and directionless architectures is calculated as the relation between the maximum number of add/drop structures allowed, given by Eq. (4.45), and the nodal degree of the node

$$\tau(i) = \frac{(P - \delta(i) + 1)K}{\delta(i)K}, \quad \text{if } \delta(i) \leq \delta^{max}(i). \tag{5.2}$$

Regarding the colorless, directionless and contentionless ROADM architecture, each add/drop structure cannot accommodate all the K channels. As can be seen in Table 5.3, only 9×9 WSS modules are available. Moreover, a cascade of WSSs cannot be deployed in this type of architecture. Thus, the add/drop ratio of node i for colorless, directionless and contentionless ROADM, $\tau^*(i)$, is calculated as

$$\tau^*(i) = \frac{(P_o - \delta(i) + 1)P_i}{\delta(i)K}, \quad \text{if } \delta(i) \leq \delta^{max}(i). \tag{5.3}$$

Figure 5.4 presents the add/drop ratio calculated using Eqs. (5.2) and (5.3), for cross connection structures using 1×9 WSS (red circles), and 1×20 WSS (red squares), and for colorless, directionless and contentionless architecture using 9×9 WSS (blue triangles). Note that for cross connection structures using 1×9 WSS and for the colorless, directionless and contentionless architecture using 9×9 WSS the maximum nodal degree is of nine. Considering cross connection structures using 1×20 WSS a maximum nodal degree of 20 can be achieved. As can be seen in Fig. 5.4, the add/drop ratio decreases with the increase of the

nodal degree. However, excluding the colorless, directionless and contentionless architecture, add/drop ratios higher than 0.5 are observed for the majority of the nodal degrees. Regarding the colorless, directionless and contentionless architecture an add/drop ratio of 0.5 is never achieved. In this case, $\tau^*(i)$ ranges from 0.45 to 0.01.

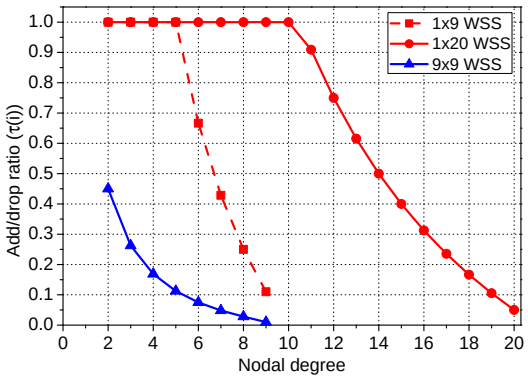

Figure 5.4: Add/drop ratio analysis for cross connection structures using 1×9 WSS, and 1×20 WSS and for colorless, directionless and contentionless architecture using 9×9 WSS. With the increase of the nodal degree the add/drop ratio decreases.

In the following an analysis to the results obtained for the CapEx, power consumption and footprint requirements is presented. As the maximum nodal degree considered is eight, the cross connection structure is assumed to be deployed using 1×9 WSSs in all the ROADM architectures.

5.2.2 Capital expenditures

An analysis of the CapEx for the ROADM architectures is presented in this section. Figure 5.5 presents the obtained results for the fixed frequency and fixed direction (black line), fixed frequency and directionless (black dashed line), colorless and fixed direction (gray line), and colorless and directionless using 1×9 WSS (red line), and 1×20 WSS (red dashed line). Figure 5.5(a) is related to nodes with degree two, Fig. 5.5(b) to nodal degree four, Fig. 5.5(c) to nodal degree six, and Fig. 5.5(d) to nodal degree eight. To guarantee the detail in the analysis, the results for colorless, directionless and contentionless add/drop structures are presented in Fig. 5.6.

As can be seen in Fig. 5.5, the fixed frequency and fixed direction (black line), and the fixed frequency and directionless architectures (black dashed line) have the same CapEx, independently of the number of add/drop channels. The fixed frequency and fixed direction ROADM has an add/drop ratio of one, thus it can accommodate all the channels. Moreover, as the add/drop structure is dedicated per direction the maximum capacity is installed since its deployment. Considering the fixed frequency and directionless architecture, the uniform behavior is related to the maximum number of add/drop channels considered. If more add/drop channels were used a step in the channel 81 should be observed, corresponding to the deployment of another add/drop structure. In this case, the increase in the CapEx is of 6.3 m.u., corresponding to the addition of a WSC and a WSS module. In these types of

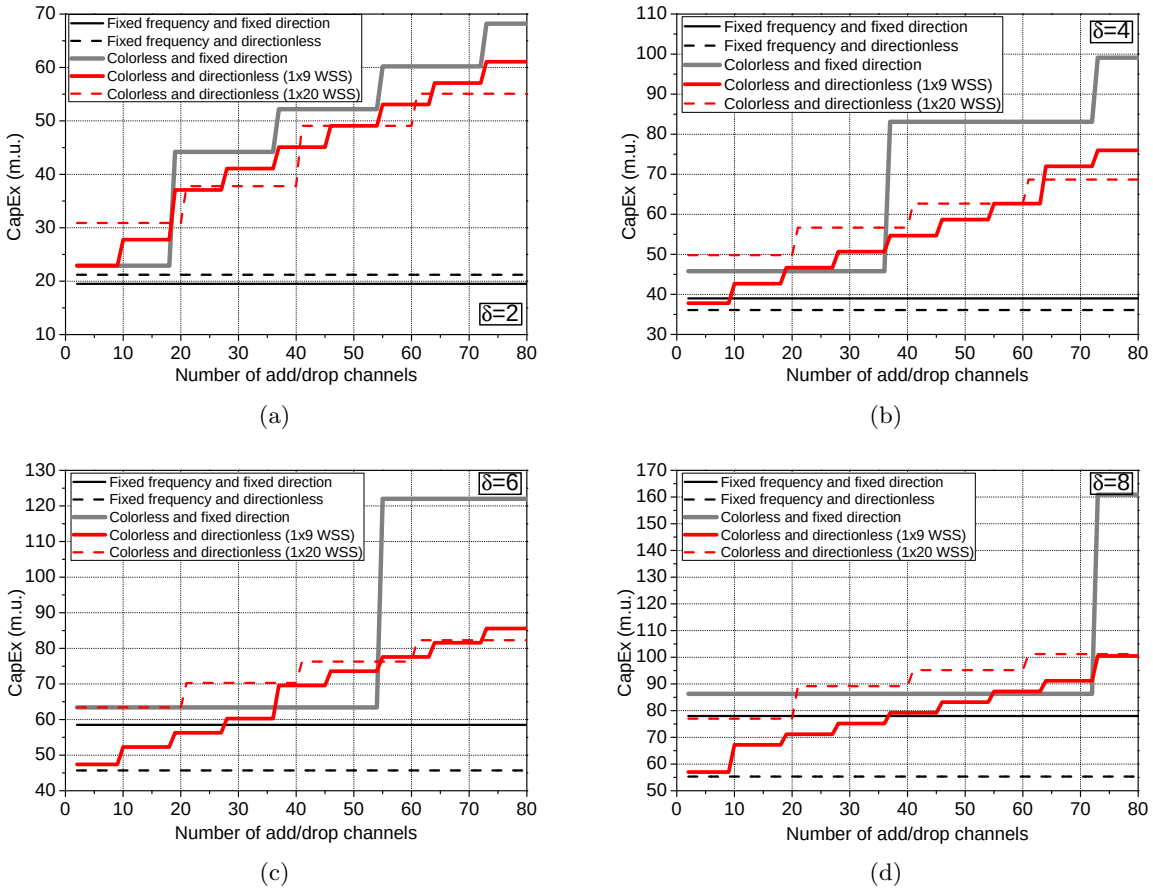

Figure 5.5: Evolution of the CapEx with the increase of the number of add/drop channels for fixed frequency and fixed direction, fixed frequency and directionless, colorless and fixed direction, and colorless and directionless using 1×9 WSS, and 1×20 WSS ROADMS with: (a) degree two, (b) degree four, (c) degree six, and (d) degree eight.

ROADMs, the CapEx only increases with the increase of the nodal degree. The colorless and fixed direction (gray line), and the colorless and directionless (red line) architectures presents a stepwise behavior, due to their modular characteristics. For the colorless and fixed direction (gray line) architecture two steps can be observed. The first, and bigger, step is related to the deployment of a cascade of WSS (between 18 and 19 add/drop channels in Fig. 5.5(a), between 36 and 37 add/drop channels in Fig. 5.5(b), between 52 and 53 add/drop channels in Fig. 5.5(c), and between 72 and 73 add/drop channels in Fig. 5.5(d)). Up to that point a single $1 \times P$ WSS is required per transmission system, after that a cascade of WSSs is required. Note that with the increase of the nodal degree this step starts happening in higher number of add/drop channels as the channels are splitted by more directions, see Fig. 5.5. The second step is related to the addition of new WSSs modules, after the deployment of the cascade of WSSs. For instance, between the 36 and 37 add/drop channel in Fig. 5.5(a). Note that, this type of step is only observed in Figs. 5.5(a) and 5.5(b). Considering the colorless and directionless ROADM (red lines), two types of steps can also be observed: the first for each additional $P = 9$ or $P = 20$ channels which is related to the addition of another WSS

module to the add/drop structure, and the second step for each $P.P_{osc}$ channels, related to the addition of another add/drop structure. As each additional add/drop structure requires an OSC, an amplifier, and at least two WSSs, the impact of adding an add/drop structure is greater than of the addition of another WSS. For instance in the colorless and directionless ROADM using 1×9 WSSs, consider the steps between 18 and 19 add/drop channels in Fig. 5.5(a), between 62 and 63 add/drop channels in Fig. 5.5(b), between 36 and 37 add/drop channels in Fig. 5.5(c), and between 9 and 10; and 72 and 73 add/drop channels in Fig. 5.5(d).

The CapEx for colorless, directionless and contentionless ROADMs is presented Fig. 5.6. The blue line refers to node with degree two, the black line to degree four, the red line to degree six, and the green line to degree eight. As can be observed, the CapEx for colorless, directionless and contentionless ROADMs also presents a stepwise behavior. In this case only one step is observed, corresponding to the addition of another add/drop structure, i.e. a $P_i \times P_o$ WSS. Note that with the increase of the nodal degree, and as presented in Section 5.2.1, the maximum number of add/drop channels that the ROADM can accommodate decreases substantially. For degree two (blue line), up to 72 add/drop channels can be supported, however for degree eight (green line) the maximum number of add/drop channels is of 18.

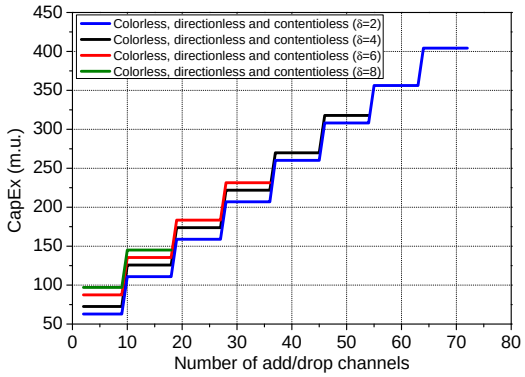

Figure 5.6: Evolution of the CapEx with the increase of the number of add/drop channels for colorless, directionless and contentionless ROADMs with degree two, four, six, and eight.

As expected, the CapEx increases with the nodal degree, for all the architectures. Even if the number of add/drop channels is the same, the increase of the nodal degree implies an increase in the number of WSSs used in the cross connection structure. Comparing the CapEx between the various architectures, it can be seen that the colorless, directionless and contentionless ROADM is much more expensive than all the others architectures. This is mainly due to the cost of the 9×9 WSS which is much more costly than all other modules, see Table 5.3. Considering the remaining architectures, the most cost-efficient architecture depends on the scenario in which the node is operating. Excluding nodes with degree two, the fixed frequency and directionless architecture is the one with lower CapEx, see Fig. 5.5. In degree two nodes, the fixed frequency and fixed direction offers a CapEx efficient solution as the nodal degree is low, see Fig. 5.5(a). With the increase of the nodal degree, and as the add/drop structure is dedicated per direction, this type of ROADM starts having higher

CapEx because a WSS and a WSC module is required per additional pair of fibers. The colorless and fixed direction ROADM (gray lines) presents low CapEx for low number of add/drop channels. After, when a cascade of WSSs is required the CapEx suffers an huge increase. For high number of add/drop channels, the CapEx of this type of ROADM can be greater than the colorless and directionless ROADM, however offering less flexibility. Finally, the colorless and directionless ROADMs (red lines) are the architectures that offer a pay as you growth solution. Comparing the solutions employing 1×9 WSS to the one employing 1×20 WSS in the add/drop structure, it can be seen that for low nodal degrees and low number of add/drop channels the use of 1×9 WSS offers a more efficient solution. With the increase of the number of add/drop channels, the availability of more ports in the 1×20 WSS reduces the number of required modules. It is worth to note that with the increase of the nodal degree the boundary point where an architecture employing 1×20 WSS presents lower CapEx than an architecture using 1×9 WSS appears at higher number of add/drop channels. As an example, between the channel 19 and 20 in Fig. 5.5(a), between the 64 and 65 add/drop channel in Fig. 5.5(b), and between the 74 and 75 channel in Fig. 5.5(c). For degree eight, see Fig. 5.5(d), the architecture using 1×9 WSS presents lower CapEx up to 80 add/drop channels.

5.2.3 Power consumption

This section presents the analysis to the power consumption. Figure 5.7 presents the obtained results for the fixed frequency and fixed direction (black line), fixed frequency and directionless (black dashed line), colorless and fixed direction (gray line), colorless and directionless using 1×9 WSS (red line), and 1×20 WSS (red dashed line), and colorless, directionless and contentionless (blue line) architectures. Figure 5.7(a) is related to nodes with nodal degree two, Fig. 5.7(b) to nodal degree four, Fig. 5.7(c) to nodal degree six, and Fig. 5.7(d) to nodal degree eight.

The same behavior as the described in the previous section can be observed. However, in this case the impact of starting a cascade of WSSs or adding another add/drop structure is much higher, see Figs. 5.5 and 5.7. Comparing the power consumption required by the architectures, it can be seen that for low number of add/drop channels a colorless, directionless and contentionless architecture (blue line) consumes less power than all the remaining architectures, for all nodal degrees. With the increase of the number of add/drop channels this architecture starts consuming more power, and for $\delta(i) = 2$ it can be the one requiring more power for high number of add/drop channels, see Fig. 5.7(a). In opposition, the fixed frequency and directionless ROADM (black dashed line) has low power consumption for high number of add/drop channels, being the most power efficient architecture in the majority of the scenarios, see Fig. 5.7. The fixed frequency and fixed direction ROADM (black line) provides a power-efficient solution for high number of add/drop channels and low nodal degree, see Figs. 5.7(a) and 5.7(b). However, with the increase of the nodal degree the power required by this architecture suffers an huge increase, turning it into one of the architectures

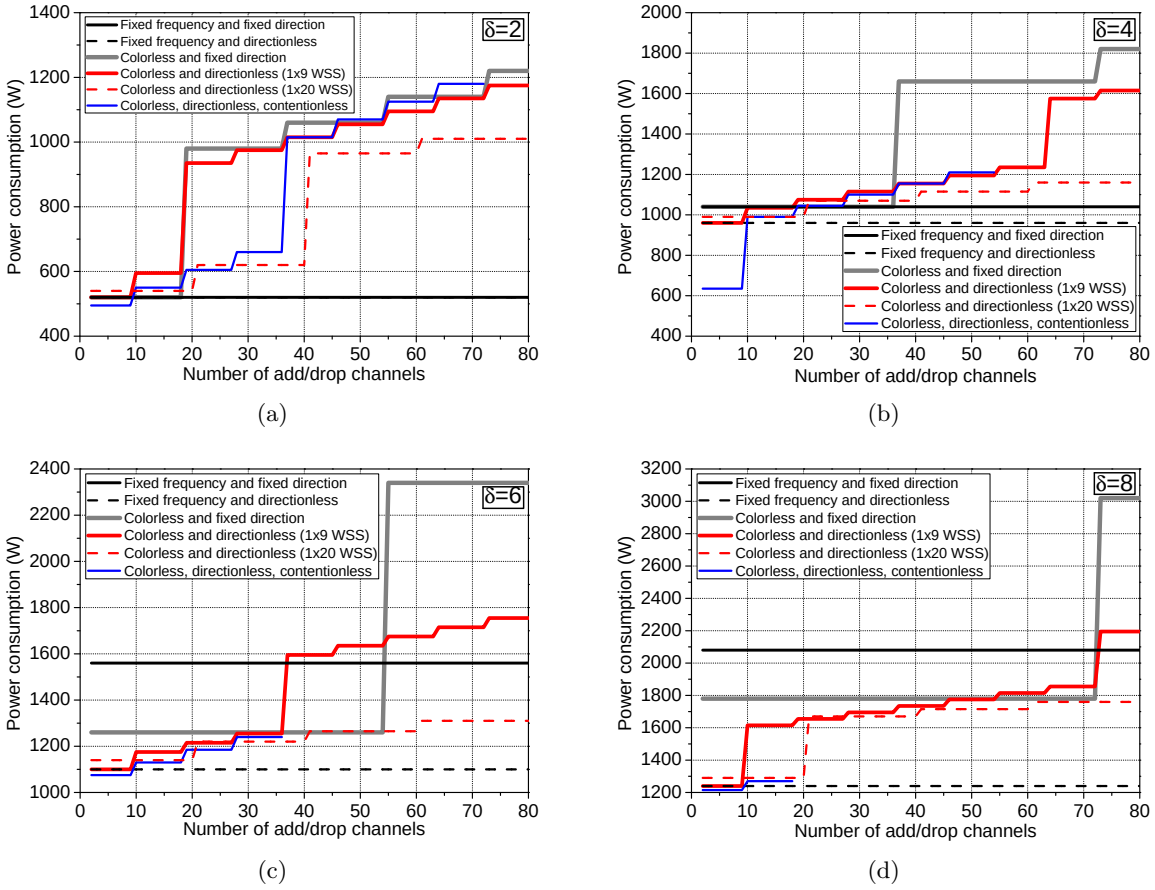

Figure 5.7: Evolution of the power consumption with the increase of the number of add/drop channels for fixed frequency and fixed direction, fixed frequency and directionless, colorless and fixed direction, colorless and directionless using 1×9 WSS, and 1×20 WSS, and colorless, directionless and contentionless ROADMS with: (a) degree two, (b) degree four, (c) degree six, and (d) degree eight.

consuming more power for $\delta(i) = 8$, see Fig. 5.7(d). As in the CapEx, the colorless and fixed direction ROADM (gray line) consumes low power as long as a cascade of WSSs is avoided, and the nodal degree is low, see Figs. 5.7(a) and 5.7(b). After, the power consumption suffers an huge increase making that architecture the one that consumes more power for high number of add/drop channels, independently of the nodal degree. Contrariwise of what happens in the CapEx, the colorless and directionless architecture employing 1×20 WSS (red dashed line) almost always consume less power than the colorless and directionless architecture using 1×9 WSS (red line). Only for very few number of add/drop channels the architecture using 1×9 WSS consumes less power. This behavior is due to the differences in terms of power consumption between both modules being smaller than the difference in terms of price. Thus, as architectures using 1×20 WSS require less number of modules, they tend to consume less power.

5.2.4 Footprint requirements

After the analysis to the CapEx and power consumption required by the various ROADM architectures, this section presents a similar analysis regarding the footprint requirements in number of slots. Figure 5.8 presents the obtained results for the fixed frequency and fixed direction (black line), fixed frequency and directionless (black dashed line), colorless and fixed direction (gray line), colorless and directionless using 1×9 (red line), and 1×20 WSS (red dashed line), and colorless, directionless and contentionless (blue line) architectures. As in the previous sections, Fig. 5.8(a) is related to nodes with nodal degree two, Fig. 5.8(b) to nodal degree four, Fig. 5.8(c) to nodal degree six, and Fig. 5.8(d) to nodal degree eight.

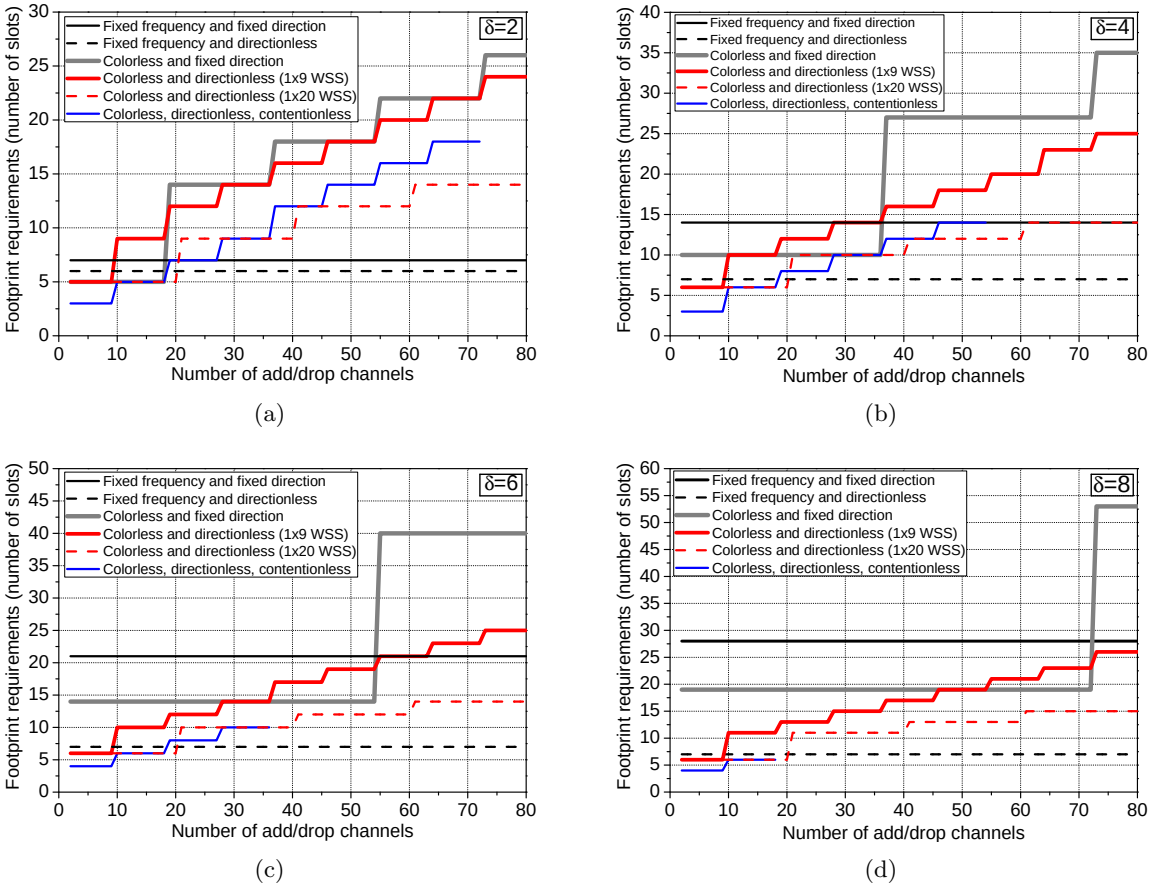

Figure 5.8: Evolution of the footprint requirements, in number of slots, with the increase of the number of add/drop channels for fixed frequency and fixed direction, fixed frequency and directionless, colorless and fixed direction, colorless and directionless using 1×9 WSS, and 1×20 WSS, and colorless, directionless and contentionless ROADMS with: (a) degree two, (b) degree four, (c) degree six, and (d) degree eight.

The same behavior as the one observed in the previous sections is obtained for the node footprint, i.e. the fixed frequency and fixed direction, and the fixed frequency and directionless ROADMs only scale with the nodal degree, whereas the colorless and fixed direction, the colorless and directionless, and the colorless, directionless and contentionless architectures presents a stepwise function, see Fig. 5.8. As can be observed, the number of required slots is

almost always below 32, thus only two shelves are required for the majority of the scenarios. The unique exception is the colorless and fixed direction ROADM (gray line) for nodes with degrees four, six and eight, and high number of add/drop channels, see Figs. 5.8(b), 5.8(c) and 5.8(d). In this case three or even four shelves can be required.

Comparing the number of slots required by each architecture, it can be observed that for low number of add/drop channels the colorless, directionless and contentionless architecture (blue line) tend to require less space that all the remaining ROADM architectures. With the increase of the number of channels the footprint of this type ROADM increases. As in the previous cost factors, fixed frequency and directionless architectures (black dashed line) tend to be more efficient with the increase of the number of add/drop channels. The fixed frequency and fixed direction ROADM (black line) suffers an huge increase in the footprint requirements with the increase of the nodal degree, turning the architecture one of the ROADMs requiring more slots. The colorless and fixed direction ROADM (gray line) only provides a good solution for $\delta(i) = 2$ and low number of add/drop channels. Considering the colorless and directionless architecture, the solution employing 1×20 WSS (red dashed line) always requires the same or less number of slots than the one using 1×9 WSS (red line).

As pointed out in the presented analysis, depending on the scenario where the node is operating and the cost factor in analysis, the most cost-efficient architecture varies. For high number of number of add/drop channels and small nodal degree, the simpler structure of the architectures with dedicated add/drop structure presents some benefits. However, for small number of add/drop channels and high nodal degree, ROADMs that share the add/drop structure tend to be more cost-efficient.

5.3 Sensitivity analysis

To evaluate the relative influence of the modules price and power consumption in the total network CapEx and total network power consumption, and understand the sensitivity of the results, this section presents a sensitivity analysis [7]. A sensitivity analysis to the footprint is not performed as variations in the number of ports of the modules would require new simulations. The price and power consumption of the modules presented in Tables 5.1 and 5.3 were varied in a pre-determined range, one class at a time, and then the total CapEx and total power consumption compared. The considered class of modules are: client, line, control and ROADM. The assumed ranges of the price and power consumption for each type of module are $\pm 15\%$ and $\pm 50\%$. To avoid the comparison between all combinations of electrical and optical layer architectures, a colorless and directionless ROADM using a 1×9 WSS is considered in the optical layer for the electrical layer architectures comparison. Morevoer, the muxponders-based and the partial non-blocking EXCs architectures are assumed in the electrical layer when comparing the ROADM architectures. We considered a backbone network in Italy, with 31 nodes and 51 links [5]. We also assume that each fiber can support up to 80 wavelengths, $K = 80$, and that the maximum transparent length of an optical channel is 2000 km [6]. Inline amplification is not considered, and the total traffic is of 30 Tbit/s randomly distributed over

the 31 nodes. For each node, the traffic pattern is randomly generated. The $D_c(o)$ client demands are then attributed to random pairs of nodes and routed using the shortest path in number of physical hops.

The obtained results for the CapEx are presented in Fig. 5.9. Figure 5.9(a) displays the results considering variations in the electrical layer modules. Gray bars are related to the muxponders-based architecture, red bars to the non-blocking EXC, and blue bars to the partial non-blocking EXCs architecture. The left side presents the results obtained by varying the price of the client modules, the center regards line modules, and the right side control modules. Figure 5.9(b) presents the results considering variations in the ROADM modules. Black bars are related to the fixed frequency and fixed direction ROADM, light gray bars to fixed frequency and directionless, purple bars to the colorless and fixed direction, green bars to the colorless and directionless using 1×9 WSS, orange bars to the colorless and directionless using 1×20 WSS, and yellow bars to the colorless, directionless and contentionless ROADM architecture. The left side presents the results considering the electrical layer deployed with the muxponders-based architecture, and the right side to the partial non-blocking EXCs architecture.

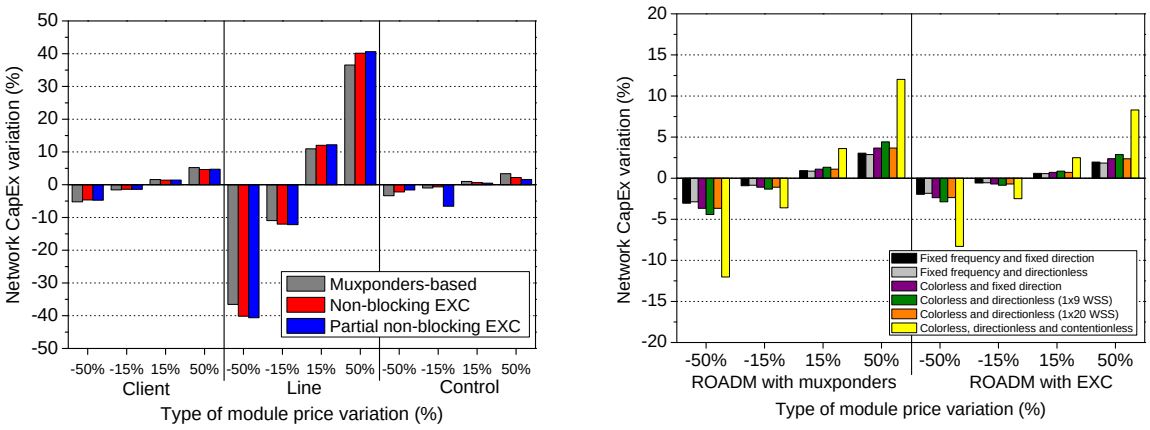

Figure 5.9: Network CapEx variation by type of module price variation: (a) for the electrical layer, and (b) ROADMs. The line modules have the highest impact in the network CapEx. In the ROADMs, the colorless, directionless and contentionless architecture has the higher impact. Variations in the price of the client, control modules and ROADMs have residual impact.

As shown in Fig. 5.9 the line modules are the most influential parameter in the analysis, followed by the colorless, directionless and contentionless ROADM. Variations in the price of the client, control modules, and modules used in the remaining ROADM architectures have a residual impact on the total network CapEx. The variations in the price of the line modules implies a variation of almost that percentage in the total network CapEx. As can be observed in Fig. 5.9(a), a variation of $\pm 15\%$ and $\pm 50\%$ results in a total network variation of $\pm 12\%$ and $\pm 40\%$, respectively. In the opposite are client, control modules, and modules used in the remaining ROADM architectures, where a variation of $\pm 50\%$ in the modules price results in a variation of less than 5% in the total network CapEx. The lower CapEx presented by

the muxponders-based architecture increases the impact of the ROADMs price in the total network CapEx, see Fig. 5.9(b).

Figure 5.10 presents the results obtained considering the power consumption. Figure 5.10(a) is related to the electrical layer architectures and Fig. 5.10(b) to the ROADM architectures. The bars colors are the same as described in Fig. 5.9.

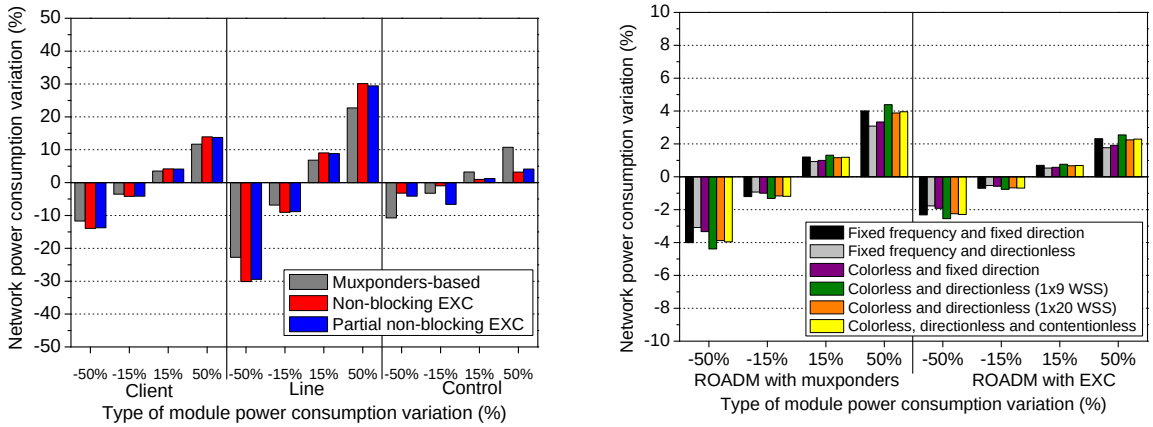

Figure 5.10: Network power consumption variation by type of module power consumption variation: (a) for the electrical layer, and (b) ROADMs. The line modules and the ROADMs have the highest impact in the network power consumption. Variations in the power consumption of the control modules have residual impact.

As can be observed in Fig. 5.10, the line modules are again the most influential module in the total power consumption. However, the impact of the client and control modules increases. The total network variations obtained by varying the line modules continues being more than half of the enforced variation. A variation of ±15% and ±50% in the line modules power consumption results in a total network variation of ±9% and ±30%, respectively. The client modules have less impact in the total network power consumption, presenting variations of ±4% and ±13% when varying the modules power consumption in ±15% and ±50%, respectively. Regarding ROADMs, a variation of ±15% and ±50% results in a total network variation of ±1% and ±4%, respectively. It is worth to note that the number of required slots has an impact on the power consumption. Muxponder-based architectures tend to require more slots, which is reflected in the higher power requirements of the control modules, see Fig. 5.3. Due to this, variations in the control modules power consumption has an impact in the total network power consumption in muxponder-based architectures, see gray bars in Fig. 5.10(a). In this case, a variation of ±15% and ±50% in the power consumption of the control modules implies a variation of ±3% and ±12% in the total network power consumption.

5.4 Optimization method

The analysis performed in Sections 5.1 and 5.2 suggests that an heterogeneous network, i.e. a network where each node is equipped with a different architecture, can present lower cost than an homogeneous network, i.e. a network where all the network nodes are equipped equally. As pointed out before a given architecture do not presents the lower CapEx, power consumption and footprint requirements, it depends on the scenario where the node is operating and cost factor in analysis. In this section, we propose an optimization method based on node architecture selection for the OpEx related to the power consumption and footprint requirements. The optimization method consists of simple rules identifying the scenarios where each architecture consumes less power and requires less number of slots. Then, and depending on the relation between the cost with the power consumption and the cost with the footprint requirements, the most cost efficient architecture is selected. The method focus on the power consumption and footprint requirements, however the same methodology can be applied to others costs such as the maintenance, reparation related costs or the CapEx.

The OpEx related to the power consumption and footprint requirements, $OpEx_N$, is assumed to be the accumulated cost during one year. Let $E_T(o)$ and $R_T(o)$ be the total power consumption and the total number of racks required in the node o. Note that $E_T(o)$ is calculated as the product between the number of required modules of each type and its respective power consumption, and $R_T(o)$, is the smallest integer not less than the ratio between the number of shelves required in the node o and the maximum number of shelves per rack. Thus, $OpEx_N$ is calculated as

$$OpEx_N = \sum_{o \in V} E_T(o) 8760 c_e + R_T(o) s_r 12 c_r, \tag{5.4}$$

where 8760 is the number of hours of one year, c_e is the average cost per kWh over a year, s_r is the space occupied by one rack in m^2, 12 is the number of months of one year, and c_r is the average rent cost of 1 m^2 per month over a year. In order to simplify the analysis, and because realistic values for c_e and c_r are difficult to obtain, we consider the cost factor α given by,

$$\alpha = \frac{s_r 12 c_r}{8760 c_e}. \tag{5.5}$$

Considering (5.4) and (5.5) we obtain,

$$OpEx_N = \pi \sum_{o \in V} E_T(o) + \alpha R_T(o), \tag{5.6}$$

where $\pi = 8760 c_e$. Note that according to [4], nowadays α is of the order of 10. To minimize $OpEx_N$ we propose a set of simple rules to select the architecture for each node. Considering the electrical layer, the rules are based on estimations using linear regressions of the results. Considering the ROADMs, and in order to facilitate the analysis, we assume two sets of ROADMs: low flexibility and high flexibility. The low flexibility ROADMs are assumed to be

the fixed frequency and fixed direction, the fixed frequency and directionless, and the colorless and fixed direction. The high flexibility ROADMs are the colorless and directionless using 1×9 WSS, and 1×20 WSSs, and the colorless, directionless and contentionless architectures. In the optical layer, the rules were empirically defined based on the results analysis.

As presented in Section 5.1, the power consumption and the number of slots required by the electrical layer architectures depends on the total traffic, $T(o)$, on the weighted mean defined by the traffic pattern, $\overline{T}(o)$, and on the number of destination nodes, $N(o)$, on node o. Moreover, as muxponders-based architectures tend to consume less power but require more number of slots than EXC-based architectures, the most efficient architecture will depend on the value of α. Therefore, to avoid time consuming simulations in order to select the most efficient architecture, we developed an expression per architecture that estimates $E_T(o)$ and $R_T(o)$, given $T(o)$, $\overline{T}(o)$, and $N(o)$. To obtain one single expression three kinds of linear regressions were performed. Firstly, we obtain one expression per traffic pattern and number of destination nodes for $E_T(o)$ (and $R_T(o)$), i.e. one linear regression of the total values presented in Fig. 5.2 (and Fig. 5.3) per architecture. The independent variable of this type of equations is $T(o)$ whereas the dependent variable is $E_T(o)$ in kW (and $R_T(o)$ in number of slots). This methodology led to eight expressions per electrical layer architecture (four per number of destination nodes), dependent on $T(o)$. The type of expression is linear,

$$E_T(o) = a_0 T(o) + b_0, \tag{5.7}$$

in which a_0 and b_0 depend on $T(o)$. Similar equations are obtained for $R_T(o)$. At this stage, new sets for regression were considered. Two sets with the four a_0 and other two with the four b_0, one entry per considered traffic pattern. Each set corresponds to a given number of destination nodes. Using the same methodology, regressions were performed over the four sets using $\overline{T}(o)$ as independent variable and a_0 and b_0 as dependent. After this step, two equations dependent on $T(o)$ and $\overline{T}(o)$ per architecture are obtained. One regarding five destination nodes and another regarding ten destination nodes. The equations are of the type

$$E_T(o) = (a_{0,0}\overline{T}(o) + a_{0,1})T(o) + (b_{0,0}\overline{T}(o) + b_{0,1}). \tag{5.8}$$

At this stage, four sets per number of destination nodes are considered. One with the two $a_{0,0}$, another with the two $a_{0,1}$, and two more with the $b_{0,0}$ and $b_{0,1}$. Linear regressions in which $N(o)$ is the independent variable and $a_{0,0}$, $a_{0,1}$, $b_{0,0}$, and $b_{0,1}$ the dependent variables are performed at this stage. This leads to equations of the type

$$E_T(o) = (a_{0,0,0}N(o)+a_{0,0,1})\overline{T}(o)+(a_{0,1,0}N(o)+a_{0,1,1}))T+((b_{0,0,0}N(o)+b_{0,0,1})\overline{T}(o)+(b_{0,1,0}N(o)+b_{0,1,1})). \tag{5.9}$$

At this phase, we achieve one single expression per architecture depending on $T(o)$, $\overline{T}(o)$ and $N(o)$ to estimate $E_T(o)$ and $R_T(o)$. Table 5.4 presents the obtained expressions for $E_T(o)$ and $R_T(o)$ per architecture.

Table 5.4: Electrical layer estimations.

Architecture	Estimation
Muxponders-based	$E_T(o) = 0.016T(o) + ((-0.002N(o) + 0.026)\overline{T}(o) + (0.210N(o) - 0.252))$ $R_T(o) = \left\lceil \frac{(-0.006\overline{T}(o)+(-0.002N(o)+0.204))T(o)+\left((0.003N(o)+0.003)\overline{T}(o)+(2.718N(o)-4.654)\right)}{46} \right\rceil$
Non-blocking EXC	$E_T(o) = 0.022T(o) + \left((-0.001N(o) + 0.039)\overline{T}(o) + (0.304N(o) - 0.154)\right)$ $R_T(o) = \left\lceil \frac{(-0.001\overline{T}(o)+(-0.001N(o)+0.066))T(o)+((-0.005N(o)+0.142)\overline{T}(o)+(0.775N(o)-0.258))}{46} \right\rceil$
Partial non-blocking EXCs	$E_T(o) = 0.024T(o) + \left((-0.005N(o) + 0.075)\overline{T}(o) + (0.423N(o) - 1.274)\right)$ $R_T(o) = \left\lceil \frac{(-0.001\overline{T}(o)+(-0.001N(o)+0.076))T(o)+((-0.014N(o)+0.225)\overline{T}(o)+(1.228N(o)-3.817))}{46} \right\rceil$

Regarding the optical layer, a similar methodology is not necessary. First of all, the footprint required by the most efficient ROADM is always smaller than one rack, see Fig. 5.8. Thus, in this case, the selection rules only depends on the power consumption of the architecture. By simple inspection of the results, it can be seen that for low flexibility ROADMs (see black and gray lines in Fig. 5.7), the fixed frequency and directionless architecture always offer the most power efficient solution. However, for $\delta(i) = 2$ and $P_{ads}(i) \leq 18$ all the architectures present the same level of power efficiency. Considering high flexibility ROADM architectures (see red and blue lines in Fig. 5.7), it can be observed that the colorless, directionless and contentionless architecture is the most efficient if $P_{ads}(i) \leq 10$ or $21 \leq P_{ads}(i) \leq 28$, and $\delta(i) < 8$. Moreover, it is also the most power efficient ROADM if $\delta(i) = 8$ and $P_{ads}(i) \leq 18$. In the remaining scenarios the colorless and directionless ROADM using 1×20 WSS outperforms the previous ROADM, i.e. if $11 \leq P_{ads}(i) \leq 20$ or $P_{ads}(i) \geq 29$, and $\delta(i) < 8$, or if $\delta(i) = 8$ and $P_{ads}(i) \geq 19$. In summary, Table 5.5 presents the proposed rules. These rules can be used to quickly optimize the overall network cost, depending on the estimated requirements of each individual node. For instance, this simple optimization method can be used as a first approach to estimate the most suitable electrical and optical layer architecture for a given node. However, tools to perform the routing and wavelength assignment and the regeneration placement optimization are still required for a more detailed planning.

As an example of the applicability of this method, we considered a backbone network in Italy, with 31 nodes and 51 links with the same assumptions presented in the Section 5.3. In the following, we compare implementations where all the network nodes have the same architecture (homogeneous network architecture) with the optimized solution, where the architecture of each node is selected according to the optimized rules presented in Table 5.5 (optimized network architecture). Note that the rules are used to select the most efficient architecture. Then, the planning is performed using the models presented in Chapter 4.

Figure 5.11 presents the relation between the obtained OpEx savings provided by using the optimized method and the cost factor, α. Figure 5.11(a) presents the savings provided by the optimized method in homogeneous networks with the electrical layer architectures (black lines), low flexibility ROADMs (red lines), and high flexibility ROADMs (blue lines).

Table 5.5: Node architecture selection rules.

Architecture	Selection rules
Electrical layer	Select the architecture with minimum $E_T(o) + \alpha R_T(o)$ (estimated using the equations presented in Table 5.4).
Low flexibility ROADM	Any if $\delta(i) = 2$ and $P_{ads}(i) \leq 18$. Fixed frequency and directionless in the remaining scenarios.
High flexibility ROADM	Colorless, directionless and contentionless if $P_{ads}(i) \leq 10$ or $21 \leq P_{ads}(i) \leq 28$, and $\delta(i) < 8$. Or if $P_{ads}(i) \leq 18$ and $\delta(i) = 8$. Colorless and directionless (1×20 WSS) if $11 \leq P_{ads}(i) \leq 20$ or $P_{ads}(i) \geq 29$, and $\delta(i) < 8$. Or if $P_{ads}(i) \geq 19$ and $\delta(i) = 8$.

Figure 5.11(b) presents the minimum and the maximum total savings. Minimum savings are calculated as the difference between the least expensive electrical layer architecture together with the least expensive ROADM architecture, and the optimized solution. Maximum savings are calculated using the most expensive electrical layer and ROADM architecture.

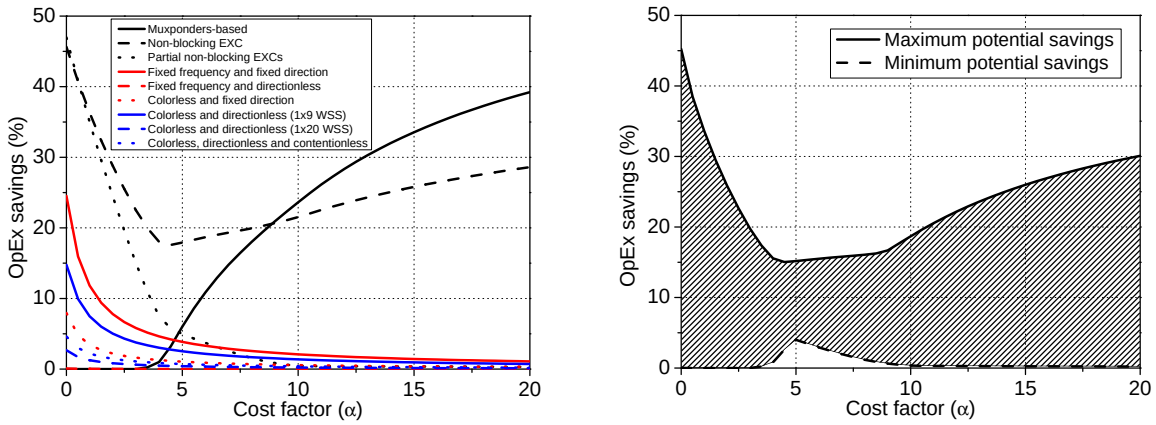

(a) (b)

Figure 5.11: Percentage of OpEx savings provided by using the optimized method in spite of a homogeneous network architecture: (a) for the electrical layer and ROADM architectures alone and, (b) for the minimum and maximum total network savings. The minimum and the maximum total savings are calculated between the optimized solution and the most and least expensive homogeneous network architecture, respectively. The optimized method achieve savings under all the considered scenarios.

Considering only the electrical layer architectures (black lines), the optimized solution can bring savings up to 47% of the OpEx related to the power consumption and floor space per year. Regarding low flexibility ROADMs (red lines), the savings are smaller because only the power consumption is taken into account. In this case, the optimized solution presents savings between 0% and 25%. The fixed frequency and directionless architecture always

presents the lower power consumption, therefore an homogeneous architecture employing this type of ROADM achieves the same solution as an optimized one. Considering high flexibility ROADMs (blue lines) the savings span between 0.1% and 15%. Note that the savings depend on the homogeneous architecture used and on α. Considering each part alone, only for muxponders-based architectures and $\alpha < 3.5$, and for the fixed frequency and directionless architecture the optimized solution does not achieve any savings. For all the remaining scenarios the heterogeneous network architecture presents lower OpEx. Considering the total OpEx (electrical + optical), it can be observed that the minimum savings span between 0.1% and 4% and that the maximum savings span between 15% and 45%. Hence, in all the scenarios the proposed optimization method achieves OpEx savings, which is a significant result supporting the relevance of this type of analysis. It is worth to note that the presented results depend on the distribution of the client traffic, network topology and routing algorithm.

5.5 Chapter summary

Using the developed dimensioning model and considering different factors that affect the nodes performance we have evaluated and compared the CapEx, the power consumption and the footprint requirements of the different node architectures. For the electrical layer, we compare fixed grooming based on muxponder modules, with flexible grooming using non-blocking EXC and partial non-blocking EXCs. Results show that the CapEx and the power consumption are, in most cases, smaller for the muxponders-based architectures. Regarding footprint requirements, EXC-based architectures tend to be more efficient. From the optical layer point of view fixed frequency and fixed direction, fixed frequency and directionless, colorless and fixed direction, and colorless and directionless using 1×9 WSS, and 1×20 WSS, and colorless, directionless and contentionless architectures are analyzed. In this type of structure the most efficient architecture depends on a relation between the nodal degree and the number of add/drop channels. A sensitivity analysis of the modules was also performed. Results show that the line modules are the most influential parameter in the total network CapEx and total network power consumption. Variations in the modules used in the ROADM, in the client modules, and in the control modules have a smaller impact. Using the performed analysis, we proposed an optimization method based on node architecture selection. Results show that to optimize the network OpEx related to the power consumption and footprint requirements, the architecture of each node should be selected depending on the amount and pattern of the traffic, and on the number of pairs of fibers convergent to the node.

References

[1] F. Rambach, B. Konrad, L. Dembeck, U. Gebhard, M. Gunkel, M. Quagliotti, L. Serra, and V. Lopez, "A multilayer cost model for metro/core networks," *IEEE/OSA Journal of Optical Communications and Networking*, vol. 5, no. 3, pp. 210–225, March 2013.

[2] W. Van Heddeghem, F. Idzikowski, W. Vereecken, D. Colle, M. Pickavet, and

P. Demeester, "Power consumption modeling in optical multilayer networks," *Photonic Network Communications*, vol. 24, no. 2, pp. 86–102, January 2012.

[3] R. M. Morais, J. Pedro, P. Monteiro, and A. N. Pinto, "Impact of node architecture in the power consumption and footprint requirements of optical transport networks," *IEEE/OSA Journal of Optical Communications and Networking*, vol. 5, no. 5, pp. 421–436, May 2013.

[4] Infinera. (2012) "Network efficiency quotient," Tech. Rep. [Online]. Available: http://www.infinera.com/pdfs/whitepapers/Infinera-WP-Network_Efficiency_Quotient.pdf

[5] J. Pedro, J. Santos, and R. M. Morais, "Dynamic setup of multi-granular services over next-generation OTN/DWDM networks: Blocking versus add/drop port usage," in *Proc International Conf. on Transparent Optical Networks - ICTON*, pp. Tu.B1.5, Coventry, United Kingdom, July 2012.

[6] A. Saleh and J. Simmons, "Evolution toward the next-generation core optical network," *IEEE/OSA Journal of Lightwave Technology*, vol. 24, no. 9, pp. 3303–3321, September 2006.

[7] A. Eira, J. Pedro, and J. Pires, "Optimized design of multistage passive optical networks," *IEEE/OSA Journal of Optical Communications and Networking*, vol. 4, no. 5, pp. 402–411, May 2012.

CHAPTER 6

Multi-period planning

Usually the network deployment process span over multiple periods along a time horizon, due to the constraints on CapEx and the gradual growth of traffic. During the network operation time, changes in the equipment costs, technology available, and traffic may occur. These potential changes influence the performance of the implemented architectures. Thus, the development of optimization methods suitable for multi-period planning is mandatory in the deployment of multilayer optical transport networks.

In a multi-period planning, the operation time horizon of the network is taken into consideration. The network is dimensioned to support the client traffic requests up to the end of the planning horizon. At each period, new client services are preferably installed in already deployed resources. New equipment is deployed only in the case that these resources are not sufficient. Thus, deciding which client traffic should reuse installed equipment and which one should use new equipment (if needed) is an important optimization problem in a multi-period planning. Various multi-period planning approaches can be employed [1–5]. The major difference between the various approaches is the amount of forecasted information that is required. One of the most influencing piece of information is the client traffic requirements for all or a determined number of periods. However, nowadays, client traffic in transport networks is very uncertain [4, 6]. Thus, changes in the predictions used for network planning can lead to insufficient or over-provisioning of the network. In this chapter we focus on the incremental planning approach where dimensioning is performed successively and separately for each period, one at a time, without having any knowledge about the traffic of future periods. We present ILP models for multi-period planning using the three electrical layer architectures, namely muxponders-based, non-blocking EXC and partial non-blocking EXCs. Additionally, to take advantage of the flexibility enabled by EXC-based architectures, the benefits of implementing hitless re-grooming are also evaluated. Hitless re-grooming is defined has the ability to re-optimize the grooming configurations without traffic disruption.

The remainder of this chapter is organized in five sections. In Section 6.1 the incremental approach for multi-period planning and the hitless re-grooming concept are presented. After, Section 6.2 is devoted to the multi-period dimensioning model for muxponders-based architectures, and Section 6.3 to the models for non-blocking EXC and partial non-blocking EXCs architectures. In Section 6.4 the impact of the node architecture and traffic pattern in the number of line interfaces, CapEx, power consumption, and footprint requirements over multiple periods is assessed. Finally, in Section 6.5 the chapter is summarized.

6.1 Multi-period planning and hitless re-grooming

This section overview the major approaches for multi-period planning and introduces the hitless re-grooming concept. There are mainly four approaches to perform multi-period planning: all-periods planning, end-of-life planning, incremental planning, and begin-of-life with forecast planning [1]. In the all-periods planning, end-of-life planning, and begin-of-life with forecast planning, predictions of the client traffic is required for all (or some) periods whereas in the incremental planning only traffic information of the period under planning is needed. Figure 6.1 presents a schematic of the four approaches. Red lines mark the place where planning is performed.

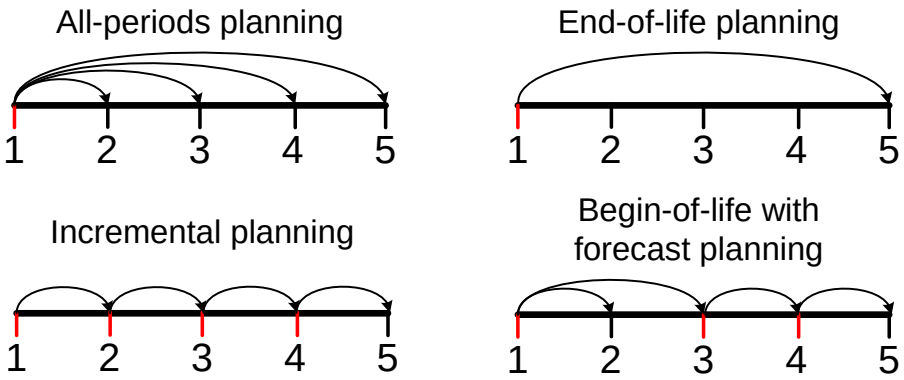

Figure 6.1: Approaches for multi-period planning. The all-periods, the end-of-life, and the begin-of-life with forecast planning approaches requires information regarding all or a determined number of periods. The incremental approach only requires information about the current period (adapted from [7]).

In the all-periods planning the optimization is performed for all periods at the same time, in one step. Thus, it demands the knowledge of the traffic for all periods under study. The end-of-life planning also requires traffic predictions for all periods under study, however the network is dimensioned to support the cumulative traffic existing in the last one. After, the network is deployed in order to converge to the last period solution. In terms of planning methodology, this approach is similar to the greenfield planning. These two approaches lead to an optimal overall solution, as they have complete knowledge about the traffic in all periods [1, 2]. However, they are also very sensitive to discrepancies between the forecasted traffic and the real one. In the incremental planning and in the begin-of-life with forecast planning

approaches, the network optimization is performed in all or some periods. In the incremental approach the planning is performed at every period. The inputs are the traffic of the period under planning and the current status of the network. Finally, the begin-of-life with forecast planning is a combination of the all-periods and the incremental planning. In this approach the periods with traffic forecasted are planned using the all-periods approach whereas future periods are planned using the incremental planning. The solutions obtained using these two approaches are optimal for the periods where the calculation is performed, however the global optimality is not guaranteed [1, 2].

In the following we focus on the incremental planning. Figure 6.2 presents a generic algorithm for multi-period incremental planning. In the first period a greenfield dimensioning is performed for the first set of client traffic. After, new sets of client traffic arises. Demands can be added, dropped or changed destination. The equipment supporting dropped demands is released. The added demands and the demands changing destination, are preferably supported by equipment already installed. If the resources are not enough to accommodate all the traffic, new equipment needs to be added. At this stage, two approaches can be employed in EXC-based architectures. The planning can allow (or not) the reconfiguration of established demands, i.e. enabled or disabled hitless re-grooming. In the muxponders-based architecture any reconfiguration requires the technician intervention on the site, thus any change in the grooming configuration implies traffic disruption or previous re-routing of established demands. Therefore, hitless re-grooming cannot be employed in this architecture.

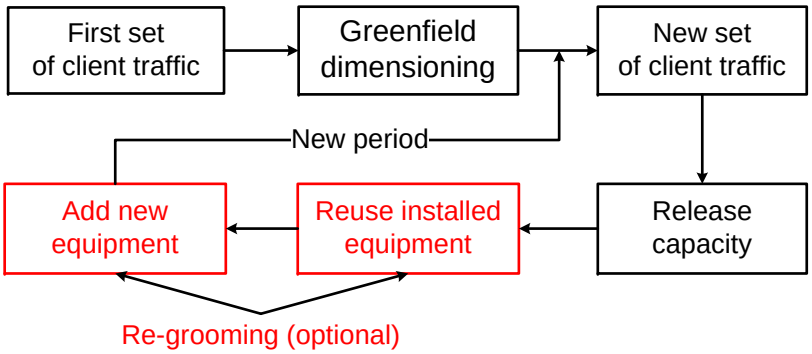

Figure 6.2: Flowchart of a generic algorithm for multi-period incremental planning. The first period dimensioning is the greenfield planning. After, demands are release and added in the next periods. Installed equipment are reused by the new demands. If more equipment is required it needs to be added. In the reuse/add equipment phase, hitless re-grooming can be employed in flexible architectures allowing the rearrangement of established demands without traffic disruption.

As pointed before, flexible electrical layer node architectures enable remote reconfiguration. Therefore, re-optimization of the grooming configurations can be performed whenever traffic changes. Moreover, as ODU switching and rearrangement can be realized in several milliseconds and with bit-loss-free, this re-optimization can be performed without traffic disruption [8–10]. Hitless re-grooming is then defined has the ability to re-optimize the grooming configurations without traffic interruption [8–10]. It is worth to note that in a non-blocking EXC architecture no constraints exist for the hitless re-grooming operation, whereas in a

partial non-blocking EXCs architecture hitless re-grooming is restricted to client and line signals installed in the same shelf (backplane).

Figure 6.3 presents an example of the potential benefits of enabling hitless re-grooming. The modules presented at the top are client modules whereas the modules presented at the bottom are line modules. Figure 6.3(a) presents the current status of a node. As can be seen, three client signals are groomed into the line signal presented in blue, two client signals are groomed into the line signal presented in red, and further two client signals are groomed into the line signal presented in yellow. Note that the client signal presented in green is switched between two line modules whereas all remaining client signals (blue, red, and yellow) are switched between client and line modules. The line signals presented in blue and red have the same destination node. In the next period, one client signal (in red) changed its destination node, see Figs. 6.3(b) and (c). This client was previously groomed into the red line signal, however in the next period it needs to be sent to the destination node of the yellow line signal. In the case that hitless re-grooming is disabled, see Fig. 6.3(b), the line module with the red line signal has to continue operating with only one client signal. However, if hitless re-grooming is enabled, see Fig. 6.3(c), that client signal can be electronically switched to the blue line signal (as they have the same destination node). In this case the line module with the red line signal can be disconnected, shutted down, or relocated to other node.

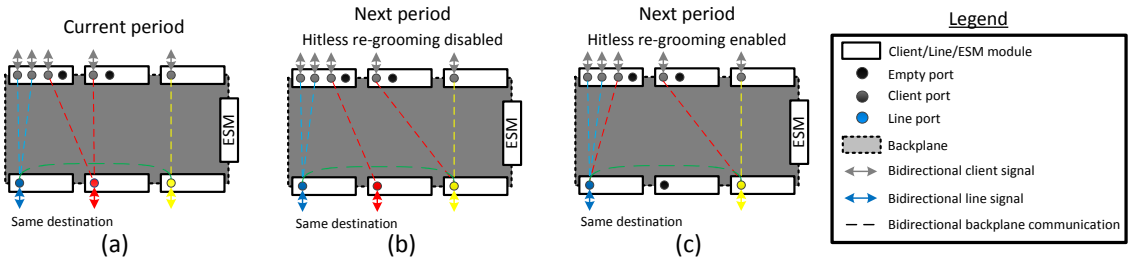

Figure 6.3: Hitless re-grooming concept example: (a) current status of the node, (b) node configuration in the next period not enabling hitless re-grooming, and (c) node configuration in the next period enabling hitless re-grooming. If hitless re-grooming is enabled re-optimization of the grooming configurations without traffic disruption can be performed, leading to potential modules savings.

In the following, the proposed ILP models for dimensioning the electrical layer of the nodes in multi-period scenarios are presented. For EXC-based architectures, extensions to perform hitless re-grooming are also derived. In a multi-period planning each module needs to be uniquely identified, thus in order to formulate the models the set of modules is introduced. The set of modules, a, will be denoted by $A_C = \{a\}$.

6.2 Muxponders-based architecture

This section presents the ILP models for the muxponders-based architecture. As in Chapter 4 we assume a maximum of two stage grooming and that for all considered c^* exists a cascade of muxponders able to perform: $c^* \rightarrow c \rightarrow l$. To formulate the ILP model two variables are used. The muxponders have input and output ports in the same module, there-

fore the variable $O_c^{c^*,\epsilon}(o,d,a)$ is the number of input ports with bit rate c^* for the demands between the nodes o and d in the muxponder module a generating an output signal with bit rate c in the grooming configuration ϵ. The variable $M_c^{\epsilon}(o,d,a)$ is a binary variable indicating whether the muxponder module a generating an output signal with bit rate c in the grooming configuration ϵ between the nodes o and d is used or not. In a multi-period planning, installed capacity can be already in the field. Thus, the number of ports already in use is an input of the model and is denoted by $\overline{O}_c^{c^*,\epsilon}(o,d,a)$. Note that in the first period $\overline{O}_c^{c^*,\epsilon}(o,d,a)$ is zero as it corresponds to a greenfield scenario. The ILP model calculating the cumulative number of modules in the first stage grooming for muxponders-based architecture is as follows

$$\textit{minimize} \quad \sum_{c\in C\setminus C^*}\sum_{\epsilon\in X^*}\sum_{(o,d)\in E_c}\sum_{a\in A_C} M_c^{\epsilon}(o,d,a) \tag{6.1}$$

subject to

$$t_{c^*}(o,d) \le \sum_{\epsilon\in X^*}\sum_{a\in A_C} O_c^{c^*,\epsilon}(o,d,a), \qquad \forall (o,d)\in E_c, \forall c^*\in C^* \tag{6.2}$$

$$\sum_{c^*\in C^*} c^*(\overline{O}_c^{c^*,\epsilon}(o,d,a) + O_c^{c^*,\epsilon}(o,d,a)) \le cM_c^{\epsilon}(o,d,a), \qquad \forall (o,d)\in E_c, \forall \epsilon\in X^*, \forall a\in A_C \tag{6.3}$$

$$\sum_{c^*\in C^*}\sum_{\epsilon\in X^*}\sum_{a\in A_C} (\overline{O}_c^{c^*,\epsilon}(o,d,a) + O_c^{c^*,\epsilon}(o,d,a)) \le \sum_{c\in C\setminus C^*}\sum_{\epsilon\in X^*}\sum_{a\in A_C} M_c^{\epsilon}(o,d,a), \qquad \forall (o,d)\in E_c \tag{6.4}$$

$$O_c^{c^*,\epsilon}(o,d,a) \le H_c^{c^*,\epsilon}, \qquad \forall (o,d)\in E_c, \forall \epsilon\in X^*, \forall a\in A_C \tag{6.5}$$

$$O_c^{c^*,\epsilon}(o,d,a) \in \mathbb{N}_0, \qquad \forall (o,d)\in E_c, \forall \epsilon\in X^*, \forall a\in A_C \tag{6.6}$$

$$M_c^{\epsilon}(o,d,a) \in \{0,1\}, \qquad \forall (o,d)\in E_c, \forall \epsilon\in X^*, \forall a\in A_C \tag{6.7}$$

Objective function (6.1) intends to minimize the total number of muxponder modules used in the first stage grooming. Constraint (6.2) guarantees that all client signals requiring a two stage grooming between the nodes o and d, $t_{c^*}(o,d)$, have an input port with the same bit rate in one muxponder module a generating an output signal with bit rate c in the grooming configuration ϵ, $O_c^{c^*,\epsilon}(o,d,a)$. Constraint (6.3) ensures that the bandwidth required by all input ports with bit rate c^* is smaller or equal than the bandwidth provided by the output port with bit rate c, in each muxponder module. Note that the established demands, $\overline{O}_c^{c^*,\epsilon}(o,d,a)$, also need to be taken into account. Moreover, constraint (6.4) ensures that the total bandwidth required for all client signals with bit rate c^* between the nodes o to d is smaller or equal to the bandwidth of all output signals with bit rate c in all muxponders with the same origin and destination. Constraint (6.5) states that a maximum of $H_c^{c^*,\epsilon}$ ports with bit rate c^* can be used in the muxponder module generating an output signal with bit rate c in the grooming configuration ϵ. Finally, constraint (6.6) define the variables $O_c^{c^*,\epsilon}(o,d,a)$ as non negative integer variables, and constraint (6.7) define the variables $M_c^{\epsilon}(o,d,a)$ as binary.

Each client port with bit rate c^* requires a short-reach transceiver with the same bit-rate. Thus, the total number of short-reach transceivers with bit rate c^* required in node o for muxponders-based architectures, $Tsv^{mb}_{c^*}(o)$ is calculated as

$$Tsv^{mb}_{c^*}(o) = \sum_{d\in V}\sum_{\epsilon\in X^*}\sum_{a\in A_C}(\overline{O}^{c^*,\epsilon}_c(o,d,a) + O^{c^*,\epsilon}_c(o,d,a)), \quad \forall c^* \in C^*, \forall o \in V. \tag{6.8}$$

The output signals generated in the first stage grooming are input signals of the muxponders used in the second stage, thus $t_c(o,d)$ needs to be updated to $t'_c(o,d)$ by

$$t'_c(o,d) = t_c(o,d) + \sum_{\epsilon\in X^*}\sum_{a\in A_C} M^{\epsilon}_c(o,d,a), \quad \forall c \in C \setminus C^*, \forall (o,d) \in E_c. \tag{6.9}$$

The muxponders used in the second stage (or in a single stage grooming) receive input signals with bit rate c and generate output line signals with bit rate l. The ILP for the second stage grooming is similar to the one used in the first stage grooming but replacing $O^{c^*,\epsilon}_c(o,d,a)$ by $O^{c,\epsilon}_l(o,d,a)$, and $M^{\epsilon}_c(o,d,a)$ by $M^{\epsilon}_l(o,d,a)$. The variables $O^{c,\epsilon}_l(o,d,a)$ are the number of input ports with bit rate c for the demands between the nodes o and d in the muxponder module a generating an output signal with bit rate l in the grooming configuration ϵ. The binary variables $M^{\epsilon}_l(o,d,a)$ indicate whether the muxponder module a generating an output signal with bit rate l in the grooming configuration ϵ between the nodes o and d is used or not. As in the first stage grooming ILP, the parameter $\overline{O}^{c,\epsilon}_l(o,d,a)$ holds the number of ports already being used. Therefore is zero in the first period. The ILP for the second stage grooming is as follows

$$\textit{minimize} \quad \sum_{l\in L}\sum_{\epsilon\in X}\sum_{(o,d)\in E_c}\sum_{a\in A_C} M^{\epsilon}_l(o,d,a) \tag{6.10}$$

subject to

$$t'_c(o,d) \le \sum_{\epsilon\in X}\sum_{a\in A_C} O^{c,\epsilon}_l(o,d,a), \qquad \forall (o,d) \in E_c, \forall c \in C \setminus C^* \tag{6.11}$$

$$\sum_{c\in C\setminus C^*} c(\overline{O}^{c,\epsilon}_l(o,d,a) + O^{c,\epsilon}_l(o,d,a)) \le l M^{\epsilon}_l(o,d,a), \qquad \forall (o,d) \in E_c, \forall \epsilon \in X, \forall a \in A_C \tag{6.12}$$

$$\sum_{c\in C\setminus C^*}\sum_{\epsilon\in X}\sum_{a\in A_C}(\overline{O}^{c,\epsilon}_l(o,d,a) + O^{c,\epsilon}_l(o,d,a)) \le \sum_{l\in L}\sum_{\epsilon\in X}\sum_{a\in A_C} M^{\epsilon}_l(o,d,a), \qquad \forall (o,d) \in E_c \tag{6.13}$$

$$O^{c,\epsilon}_l(o,d,a) \le H^{c,\epsilon}_l, \qquad \forall (o,d) \in E_c, \forall \epsilon \in X, \forall a \in A_C \tag{6.14}$$

$$O^{c,\epsilon}_l(o,d,a) \in \mathbb{N}_0, \qquad \forall (o,d) \in E_c, \forall \epsilon \in X, \forall a \in A_C \tag{6.15}$$

$$M^{\epsilon}_l(o,d,a) \in \{0,1\}, \qquad \forall (o,d) \in E_c, \forall \epsilon \in X, \forall a \in A_C \tag{6.16}$$

The output ports of the muxponders used in the first stage grooming, and the input ports of the muxponders used in the second stage grooming require short-reach transceivers with bit rate c. Therefore, the total number of transceivers with bit rate c in node o for muxponders-based architectures is calculated as

$$Tsv_c^{mb}(o) = \sum_{d\in V}\sum_{a\in A_C}\left(\sum_{\epsilon\in X^*} M_c^{\epsilon}(o,d,a) + \sum_{\epsilon\in X}(\overline{O}_l^{c,\epsilon}(o,d,a) + O_l^{c,\epsilon}(o,d,a))\right), \quad \forall c\in C\setminus C^*, \forall o\in V. \tag{6.17}$$

The output ports of the muxponders used in the second stage grooming generate a line signal, thus require long-reach transceivers with bit rate l. The total number of long-reach transceivers with bit rate l in node o for muxponders-based architectures is calculated by

$$Tsv_l^{mb}(o) = \sum_{d\in V}\sum_{a\in A_C}\sum_{\epsilon\in X} M_l^{\epsilon}(o,d,a), \quad \forall l\in L, \forall o\in V. \tag{6.18}$$

In muxponders-based architectures the modules can be connected into any shelf, see Section 4.1. The total number of slots at node o in muxponders-based architectures, $S_{tot}^{mb}(o)$, is achieved by

$$S_{tot}^{mb}(o) = \sum_{a\in A_C}\left(\sum_{\epsilon\in X^*} M_c^{\epsilon}(o,a)S_c^{\epsilon} + \sum_{\epsilon\in X} M_l^{\epsilon}(o,a)S_l^{\epsilon}\right), \quad \forall o\in V. \tag{6.19}$$

Therefore, the total number of shelves and of control modules is calculated using (4.16)

$$M_{sf}^{mb}(o) = M_{ctr}^{mb}(o) = \left\lceil \frac{S_{tot}^{mb}(o)}{S_{sf}^{mb} - S_{ctr}^{mb}} \right\rceil, \quad \forall o\in V. \tag{4.16}$$

At this stage, $\overline{O}_c^{c^*,\epsilon}(o,d,a)$ and $\overline{O}_l^{c,\epsilon}(o,d,a)$ are updated for the next period. The parameter $\overline{O}_c^{c^*,\epsilon}(o,d,a)$ is updated by

$$\overline{O}_c^{c^*,\epsilon}(o,d,a) = \overline{O}_c^{c^*,\epsilon}(o,d,a) + O_c^{c^*,\epsilon}(o,d,a), \forall (o,d)\in E_c, \forall \epsilon\in X^*, \forall a\in A_C, \tag{6.20}$$

and the parameter $\overline{O}_l^{c,\epsilon}(o,d,a)$ by

$$\overline{O}_l^{c,\epsilon}(o,d,a) = \overline{O}_l^{c,\epsilon}(o,d,a) + O_l^{c,\epsilon}(o,d,a), \forall (o,d)\in E_c, \forall \epsilon\in X, \forall a\in A_C. \tag{6.21}$$

6.3 Electrical cross connects based architectures

The EXC-based architectures can be remotely reconfigurable, thus hitless re-grooming can be employed. In the following the ILP models for non-blocking EXC and partial non-blocking

EXCs architectures, enabling and disabling re-grooming, are presented.

6.3.1 Non-blocking electrical cross connect

The non-blocking EXC architecture do not have any constraint in the interconnection between modules. Thus, to formulate the model four variables are required. The variables $O_c(o,d,a)$ and $O_l(o,d,a)$ are the number of ports with bit rate c (and l respectively) required for the demands between the nodes o and d located in module a. Note that each module can have one or more ports. The variables $M_c(o,a)$ and $M_l(o,a)$ are binary variables indicating whether the module a with bit rate c (and l respectively) is used in node o or not. Additionally, the number of ports already in use in previous periods is an input of the model. We will denote by $\overline{O}_c(o,d,a)$ and $\overline{O}_l(o,d,a)$ the number of ports with bit rate c (and l respectively) already being used by the demands between the nodes o and d located in module a. It is worth to note that in the first period $\overline{O}_c(o,d,a)$ and $\overline{O}_l(o,d,a)$ are zero. The ILP model calculates the cumulative number of modules and is as follows

$$minimize \quad \sum_{o\in V}\sum_{a\in A_C}\left(\sum_{c\in C}M_c(o,a)+\sum_{l\in L}M_l(o,a)\right) \tag{6.22}$$

subject to

$$t_c(o,d) \le \sum_{a\in A_C} O_c(o,d,a), \qquad \forall (o,d)\in E_c, \forall c\in C \tag{6.23}$$

$$c\sum_{c\in C}\sum_{a\in A_C}\left(\overline{O}_c(o,d,a)+O_c(o,d,a)\right) \le l\sum_{l\in L}\sum_{a\in A_C}\left(\overline{O}_l(o,d,a)+O_l(o,d,a)\right), \qquad \forall (o,d)\in E_c \tag{6.24}$$

$$M_c(o,a) \ge \frac{\sum_{d\in V}\left(\overline{O}_c(o,d,a)+O_c(o,d,a)\right)}{P_c}, \qquad \forall c\in C, \forall o\in V, \forall a\in A_C \tag{6.25}$$

$$M_l(o,a) \ge \frac{\sum_{d\in V}\left(\overline{O}_l(o,d,a)+O_l(o,d,a)\right)}{P_l}, \qquad \forall l\in L, \forall o\in V, \forall a\in A_C \tag{6.26}$$

$$O_c(o,d,a)\in \mathbb{N}_0, \qquad \forall c\in C, \forall (o,d)\in E_c, \forall a\in A_C \tag{6.27}$$

$$O_l(o,d,a)\in \mathbb{N}_0, \qquad \forall l\in L, \forall (o,d)\in E_c, \forall a\in A_C \tag{6.28}$$

$$M_c(o,a)\in \{0,1\}, \qquad \forall c\in C, \forall o\in V, \forall a\in A_C \tag{6.29}$$

$$M_l(o,a)\in \{0,1\}, \qquad \forall l\in L, \forall o\in V, \forall a\in A_C \tag{6.30}$$

Objective function (6.22) intends to minimize the total number of client and line modules in the network. Constraint (6.23) guarantees that the $t_c(o,d)$ client signals between the nodes o and d with bit rate c have a client port in one of the modules a, $O_c(o,d,a)$. Constraint (6.24) ensures that the total bandwidth required for all client signals, in all periods, $\overline{O}_c(o,d,a) + O_c(o,d,a)$, is smaller or equal than the total bandwidth provided by all line ports, $\overline{O}_l(o,d,a)+ O_l(o,d,a)$. Constraints (6.25) determines whether the client module a with bit rate c in node o, $M_c(o,a)$, is used or not. Note that each module with bit rate c has P_c available ports.

Constraint (6.26) is similar to constraint (6.25) however regarding line modules with bit rate l, $M_l(o,a)$, and assuming that the line module with bit rate l has P_l ports. Finally, constraints (6.27) and (6.28) define the variables $O_c(o,d,a)$ and $O_l(o,d,a)$ as non negative integer variables, and constraints (6.29) and (6.30) define the variables $M_c(o,a)$ and $M_l(o,a)$ as binary.

Client and line ports are equipped with short-reach and long-reach transceivers, respectively. The number of short reach transceivers in node o with bit rate c for non-blocking EXC architectures, $Tsv_c^{nbe}(o)$ is calculated as

$$Tsv_c^{nbe}(o) = \sum_{d\in V}\sum_{a\in A_C}\left(\overline{O}_c(o,d,a) + O_c(o,d,a)\right), \quad \forall c \in C, \forall o \in V, \tag{6.31}$$

and the number of long reach transceivers in node o with bit rate l for non-blocking EXC architectures, $Tsv_l^{nbe}(o)$ as

$$Tsv_l^{nbe}(o) = \sum_{d\in V}\sum_{a\in A_C}\left(\overline{O}_l(o,d,a) + O_l(o,d,a)\right), \quad \forall l \in L, \forall o \in V. \tag{6.32}$$

The total number of slots for client and line modules in node o for non-blocking EXC architectures, $S_{tot}^{nbe}(o)$, is then achieved by

$$S_{tot}^{nbe}(o) = \sum_{a\in A_C}\left(\sum_{c\in C} M_c(o,a)S_c + \sum_{l\in L} M_l(o,a)S_l\right), \quad \forall o \in V. \tag{6.33}$$

Bear in mind that only one shelf, one control module, and one ESM is required in this type of architecture.

At this stage, $\overline{O}_c(o,d,a)$ and $\overline{O}_l(o,d,a)$ are updated to use in the next period. Regarding $\overline{O}_c(o,d,a)$ is updated by

$$\overline{O}_c(o,d,a) = \overline{O}_c(o,d,a) + O_c(o,d,a), \quad \forall c \in C, \forall (o,d) \in E_c, \forall a \in A_C. \tag{6.34}$$

Considering the updating of $\overline{O}_l(o,d,a)$ two cases are considered. If hitless re-grooming is disabled, $\overline{O}_l(o,d,a)$ is updated in a similar way than $\overline{O}_c(o,d,a)$, thus guaranteeing that the previous grooming configurations are maintained. Thus, for disabled hitless re-grooming $\overline{O}_l(o,d,a)$ is updated as

$$\overline{O}_l(o,d,a) = \overline{O}_l(o,d,a) + O_l(o,d,a), \quad \forall l \in L, \forall (o,d) \in E_c, \forall a \in A_C. \tag{6.35}$$

In the scenarios that hitless re-grooming is enabled, $\overline{O}_l(o,d,a)$ is set as zero. In this way the grooming configurations can be changed. Thus, for enabled hitless re-grooming $\overline{O}_l(o,d,a)$ is updated as

$$\overline{O}_l(o,d,a) = 0, \quad \forall l \in L, \forall (o,d) \in E_c, \forall a \in A_C. \tag{6.36}$$

6.3.2 Partial non-blocking electrical cross connects

The partial non-blocking EXCs architecture introduce restrictions in the interconnection between modules. Particularly, only client and line modules connected to the same backplane can switch traffic. Four variables are also required in this case, however the shelf in which the modules are connected needs to be considered. The variables $O_c(o,d,a,s)$ and $O_l(o,d,a,s)$ are the number of ports with bit rate c (and l respectively) required for the demands between the nodes o and d located in module a and shelf s, and the variables $M_c(o,a,s)$ and $M_l(o,a,s)$ are binary variables indicating whether the module a with bit rate c (and l respectively) is used in node o and shelf s or not. As in the previous ILP, the parameters $\overline{O}_c(o,d,a,s)$ and $\overline{O}_l(o,d,a,s)$ hold the number of ports with bit rate c (and l respectively) already being used. Once again $\overline{O}_c(o,d,a,s)$ and $\overline{O}_l(o,d,a,s)$ are set as zero in the first period. The ILP model for partial non-blocking EXC architectures is as follows

$$min \quad \sum_{o\in V}\sum_{s\in S}\left(\sum_{a\in A_C}\left(\sum_{c\in C}M_c(o,a,s)+\sum_{l\in L}M_l(o,a,s)\right) + B(o,s)\right) \tag{6.37}$$

subject to

$$t_c(o,d) \le \sum_{a\in A_C}\sum_{s\in S}O_c(o,d,a,s), \qquad \forall (o,d)\in E_c, \forall c\in C \tag{6.38}$$

$$c\sum_{c\in C}\sum_{a\in A_C}\left(\overline{O}_c(o,d,a,s)+O_c(o,d,a,s)\right) \le l\sum_{l\in L}\sum_{a\in A_C}\left(\overline{O}_l(o,d,a,s)+O_l(o,d,a,s)\right), \qquad \forall (o,d)\in E_c, \forall s\in S \tag{6.39}$$

$$M_c(o,a,s) \ge \frac{\sum_{d\in V}\left(\overline{O}_c(o,d,a,s)+O_c(o,d,a,s)\right)}{P_c}, \qquad \forall c\in C, \forall o\in V, \forall a\in A_C, \forall s\in S \tag{6.40}$$

$$M_l(o,a,s) \ge \frac{\sum_{d\in V}\left(\overline{O}_l(o,d,a,s)+O_l(o,d,a,s)\right)}{P_l}, \qquad \forall l\in L, \forall o\in V, \forall a\in A_C, \forall s\in S \tag{6.41}$$

$$\sum_{c\in C}\sum_{a\in A_C}M_c(o,a,s)S_c+\sum_{l\in L}\sum_{a\in A_C}M_l(o,a,s)S_l \le S_{sf}^{pbe}B(o,s), \qquad \forall o\in V, \forall s\in S \tag{6.42}$$

$$O_c(o,d,a,s)\in\mathbb{N}_0, \qquad \forall c\in C, \forall (o,d)\in E_c, \forall a\in A_C, \forall s\in S \tag{6.43}$$

$$O_l(o,d,a,s)\in\mathbb{N}_0, \qquad \forall l\in L, \forall (o,d)\in E_c, \forall a\in A_C, \forall s\in S \tag{6.44}$$

$$M_c(o,a,s)\in\{0,1\}, \qquad \forall c\in C, \forall o\in V, \forall a\in A_C, \forall s\in S \tag{6.45}$$

$$M_l(o,a,s)\in\{0,1\}, \qquad \forall l\in L, \forall o\in V, \forall a\in A_C, \forall s\in S \tag{6.46}$$

$$B(o,s)\in\{0,1\}, \qquad \forall o\in V, \forall s\in S \tag{6.47}$$

Objective function (6.37) minimizes the total number of client modules, line modules, and shelves in the network. Constraint (6.38) ensures that all $t_c(o,d)$ client signals between the

nodes o and d have a client port with bit rate c in one module a located in one of the shelves s. Constraints (6.39), (6.40) and (6.41) are similar to constraints (6.24), (6.25) and (6.26), thus guaranteeing that exist enough bandwidth to accommodate all client traffic and that the number of client, $M_c(o,a,s)$, and line, $M_l(o,a,s)$, modules are sufficient to accommodate all the required ports. However, note that in this case the client ports and line ports switching traffic are located in the same shelf s. Constraint (6.42) guarantees that in each node o the number of slots required for client and line modules located in the same shelf, $B(o,s)$, does not exceeds its maximum number of slots, S_{sf}^{pbe}. Finally, constraints (6.43) and (6.44) define the variables $O_c(o,d,a,s)$ and $O_l(o,d,a,s)$ as non negative integer variables, and constraints (6.45), (6.46) and (6.47) define the variables $M_c(o,a,s)$, $M_l(o,a,s)$ and $B(o,s)$ as binary.

The number of short-reach transceivers with bit rate c in node o for partial non-blocking EXCs architectures is then calculated by

$$Tsv_c^{pbe}(o) = \sum_{d\in V}\sum_{a\in A_C}\sum_{s\in S}\left(\overline{O}_c(o,d,a,s) + O_c(o,d,a,s)\right), \quad \forall c \in C, \forall o \in V, \tag{6.48}$$

and the number of long-reach transceivers with bit rate l in node o for partial non-blocking EXCs architectures by

$$Tsv_l^{pbe}(o) = \sum_{d\in V}\sum_{a\in A_C}\sum_{s\in S}\left(\overline{O}_l(o,d,a,s) + O_l(o,d,a,s)\right), \quad \forall l \in L, \forall o \in V. \tag{6.49}$$

The total number of shelves, control modules, and ESMs are outputs of the ILP model and are calculated using (4.40),

$$M_{sf}^{pbe}(o) = M_{ctr}^{pbe}(o) = M_{esm}^{pbe}(o) = \sum_{s\in S} B(o,s), \quad \forall o \in V. \tag{4.40}$$

Once again, at the end of each period, $\overline{O}_c(o,d,a,s)$ and $\overline{O}_l(o,d,a,s)$ needs to be updated. The parameter $\overline{O}_c(o,d,a,s)$ is updated by

$$\overline{O}_c(o,d,a,s) = \overline{O}_c(o,d,a,s) + O_c(o,d,a,s), \quad \forall c \in C, \forall (o,d) \in E_c, \forall a \in A_C, \forall s \in S. \tag{6.50}$$

Considering the updating of $\overline{O}_l(o,d,a)$, it depends on whether hitless re-grooming is disabled or not. If hitless re-grooming is disabled $\overline{O}_l(o,d,a)$ is updated by

$$\overline{O}_l(o,d,a,s) = \overline{O}_l(o,d,a,s) + O_l(o,d,a,s), \quad \forall l \in L, \forall (o,d) \in E_c, \forall a \in A_C, \forall s \in S, \tag{6.51}$$

if hitless re-grooming is enabled, $\overline{O}_l(o,d,a,s)$ is set to zero, allowing the rearrangement of client signals within each shelf. Thus, for enabled hitless re-grooming

$$\overline{O}_l(o,d,a,s) = 0, \quad \forall l \in L, \forall (o,d) \in E_c, \forall a \in A_C, \forall s \in S. \tag{6.52}$$

6.4 Impact of node architecture

The results obtained using the models presented in Sections 6.2 and 6.3 are reported in this section. We analyze the cumulative number of line interfaces, the CapEx, the power consumption, and the footprint requirements of a node. As in Chapter 5, we assume a single source node exchanging traffic with a set of destination nodes, four client bit rates (1.25 Gbit/s, 2.5 Gbit/s, 10 Gbit/s, and 40 Gbit/s) and a single line bit rate of 100 Gbit/s. The traffic is distributed following an uniform distribution, using the same methodology presented in Section 5.1. The modules specifications are the ones presented in Table 5.1. Regarding non-blocking EXC architecture the 128 slots shelf is deployed whereas for partial non-blocking EXCs is the 16 slots shelf, see Table 5.1. Two different number of destination nodes (five and ten), and two traffic patterns (pattern 1 and pattern 4 presented in Table 5.2) are considered. The initial total traffic is of 200 Gbit/s, increasing 10% in each of the 20 periods considered, thus being of 1.2 Tbit/s in the last period. Additionally, and in order to evaluate the impact of traffic variability, three scenarios were used for each combination of destination nodes and traffic pattern. In the first scenario only added traffic exist. In the remaining two scenarios, apart of the added traffic, some of the established traffic is forced to change its destination. One considers that 20% of the traffic change its destination, and the other considers 40% of traffic changing destination. For each combination of number of destination nodes, traffic pattern, and traffic variability, 100 independent runs were performed.

The obtained average values for the number of line interfaces are presented in Figs. 6.4 and 6.5. The obtained results for the cumulative CapEx can be found in Figs. 6.6 and 6.7 whereas the results for cumulative power consumption are presented in Figs. 6.8 and 6.9. Finally, the results for the footprint requirements are shown in Figs. 6.10 and 6.11. Additionally, for the number of line interfaces, an analysis to the standard deviation obtained among the 100 simulations are also reported. The number of line interfaces is analyzed in more detail as it is the most influential parameter in the CapEx and OpEx (as observed in Section 5.3), and affects the cost of the ROADMs. In all cases, the results for muxponders-based architectures are presented as gray lines; for non-blocking EXC as black lines; for non-blocking EXC with hitless re-grooming as red lines; for partial non-blocking EXCs as blue lines; and for partial non-blocking EXCs with hitless re-grooming as light blue lines.

6.4.1 Number of line interfaces

Figure 6.4 presents the average values of the cumulative number of line interfaces in scenarios where the traffic is distributed according to pattern 1. The figures on the left (see Figs. 6.4(a), 6.4(c), and 6.4(e)) are related to 5 destination nodes and the figures on the right (see Figs. 6.4(b), 6.4(d), and 6.4(f)) to 10 destination nodes. Moreover, Figs. 6.4(a) and

6.4(b) consider only added traffic, Figs. 6.4(c) and 6.4(d) consider 20% of traffic changing destination, and Figs. 6.4(e) and 6.4(f) consider 40% of traffic changing destination.

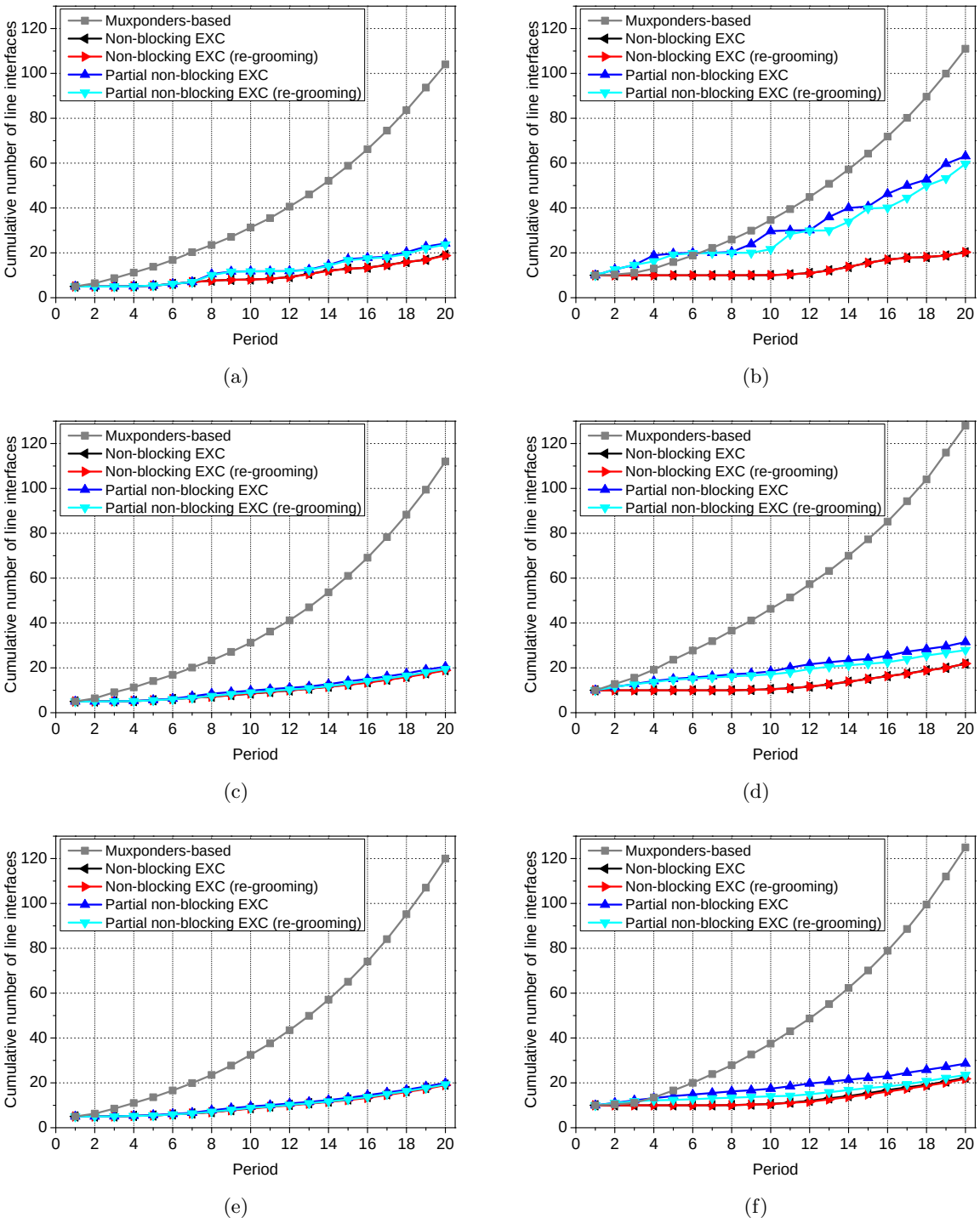

Figure 6.4: Cumulative number of line interfaces for 20 periods, pattern 1 and: (a) 5 destination nodes; (b) 10 destination nodes; (c) 5 destination nodes and 20% of traffic changing destination; (d) 10 destination nodes and 20% of traffic changing destination; (e) 5 destination nodes and 40% of traffic changing destination; and (f) 10 destination nodes and 40% of traffic changing destination.

As can be observed, enhancing node flexibility tends to imply a decrease in the number of

line interfaces required, under all scenarios. As expected, the full non-blocking EXC always requires less number of line interfaces, whereas in the opposite side is the muxponders-based architecture. The partial non-blocking EXCs architecture relies in between. Moreover, the results suggest that hitless re-grooming only enables savings for the partial non-blocking EXCs, and in particular scenarios. In non-blocking EXC there are no restrictions in the interconnection between client and line modules, thus the bandwidth is almost always well exploited and hitless re-grooming cannot bring significant benefits. Considering 5 destination nodes (see Figs. 6.4(a), 6.4(c), and 6.4(e)), it can be observed that the differences in number of line interfaces required between the non-blocking EXC and the partial non-blocking EXCs are not significant. Moreover, this gap decreases with the increase of traffic variability, requiring almost the same number of line interfaces, in all the periods, in the scenarios where traffic is forced to change its destination, see Figs. 6.4(c) and 6.4(e). Therefore for pattern 1 and 5 destination nodes, the savings provided by enabling hitless re-grooming are negligible. When the number of destination nodes is small, the partial non-blocking EXCs can behave as a non-blocking EXC because with an optimized planning all the client and line modules switching traffic can fit in the same shelf. Moreover, traffic variability gives more chances to re-optimize the available ports, as the amount of client signals that can be optimized at each period increases. With the increase on the number of destination nodes, the differences between the architectures performance widens. As can be observed in Figs. 6.4(b), 6.4(d), and 6.4(f), for 10 destination nodes, the partial non-blocking EXCs tend to require more line interfaces than the non-blocking EXC, in all periods and scenarios. Moreover, in the case that traffic is only added the amount of additional line interfaces is significant, see Fig. 6.4(b). For 10 destination nodes, the partial non-blocking EXCs architecture only requires almost the same number of line interfaces than the non-blocking EXC in the last period of the case where 40% of traffic is forced to change its destination, and enabling hitless re-grooming, see Fig. 6.4(f). With the increase of the number of destination nodes, the probability of existing enough slots in the same shelf for all client and line modules switching traffic decreases, impacting negatively the number of line interfaces required. However, for 10 destination nodes the savings provided by enabling hitless re-grooming increase. Although, these savings are not significant. A detailed analysis on the number of line interfaces percentage increase due to the decrease in the node flexibility will be presented later on.

To analyze the dependence between the node architecture flexibility and the distribution of the traffic among the destination nodes, Table 6.1 presents the standard deviation obtained in the 20^{th} period. We analyze the last period because the standard deviation tends to increase with the increase in the number of periods, thus the 20^{th} period corresponds to the worst case. As can be seen, the muxponders-based architecture is the one with the highest standard deviation, for all cases. The standard deviation presented by this type of architecture can be more than 5 times greater than of the EXC-based architectures. Additionally, partial non-blocking EXCs tend to have a higher standard deviation than non-blocking EXC. Moreover, it is worth to note that the standard deviation increases, in all the architectures, from 5 to 10 destination nodes. Hence, the number of line interfaces is more predictable and less

dependent on the traffic distribution and number of destination nodes as more flexibility the node offers. Regarding the influence of the re-grooming, it can be observed that for non-blocking EXC architectures, the hitless re-grooming tend to increase the standard deviation. However, the opposite happens in the partial non-blocking EXCs where hitless re-grooming tend to decrease the standard deviation. Regarding traffic variability, it has an irregular impact in the standard deviation. There are cases where traffic variability increases the standard deviation and other cases where it decreases (see Table 6.1).

Table 6.1: Standard deviation of the number of line interfaces in the 20^{th} period for pattern 1.

	Only added traffic		**20% changing destination**		**40% changing destination**	
	5 nodes	10 nodes	5 nodes	10 nodes	5 nodes	10 nodes
Muxponders-based	3.91	4.33	4.63	12.04	3.81	4.26
Non-blocking EXC	0.71	0.77	0.69	0.94	0.71	0.92
Non-blocking EXC (re-grooming)	0.73	0.90	0.70	0.99	0.63	0.94
Partial non-blocking EXCs	0.95	1.91	0.81	1.87	0.66	1.45
Partial non-blocking EXCs (re-grooming)	0.97	1.28	0.61	2.07	0.66	1.12

Figure 6.5 presents the average number of line interfaces for 5 and 10 destinations nodes with traffic distributed according to pattern 4. As in the previous case, the figures on the left (see Figs. 6.5(a), 6.5(c), and 6.5(e)) are related to 5 destination nodes and the figures on the right (see Figs. 6.5(b), 6.5(d), and 6.5(f)) to 10 destination nodes. Moreover, Figs. 6.5(a) and 6.5(b) consider only added traffic, Figs. 6.5(c) and 6.5(d) consider 20% of traffic changing destination, and Figs. 6.5(e) and 6.5(f) consider 40% of traffic changing destination.

As presented in Fig. 6.5, and in line with the results presented for pattern 1 in Fig. 6.4, the muxponders-based architecture is the one requiring more line interfaces, followed by the partial non-blocking EXCs architecture. Once again, and as expected, the non-blocking EXC architecture is the most efficient one. However, for pattern 4 the differences between the architectures performance are greater. Regarding the utilization of hitless re-grooming, the gains are greater than in pattern 1. In pattern 4, the bit rate of the client traffic is closer to the bit rate of the line signal. Thus, the number of client signals that need to be re-arranged in order to save a line interface is much smaller than when the majority of the client traffic bit rate presents very low granularity as in pattern 1. However, the savings provided by enabling hitless re-grooming are only visible in the partial non-blocking EXCs architecture. In partial non-blocking EXCs, some line interfaces have wasted bandwidth due to the lack of available client ports in their shelf. This is particularly relevant when the number of destination nodes is high or when the bit rate of the client traffic is close to the line bit-rate. In this case, hitless re-grooming enables an optimization of the relation between the client and line ports

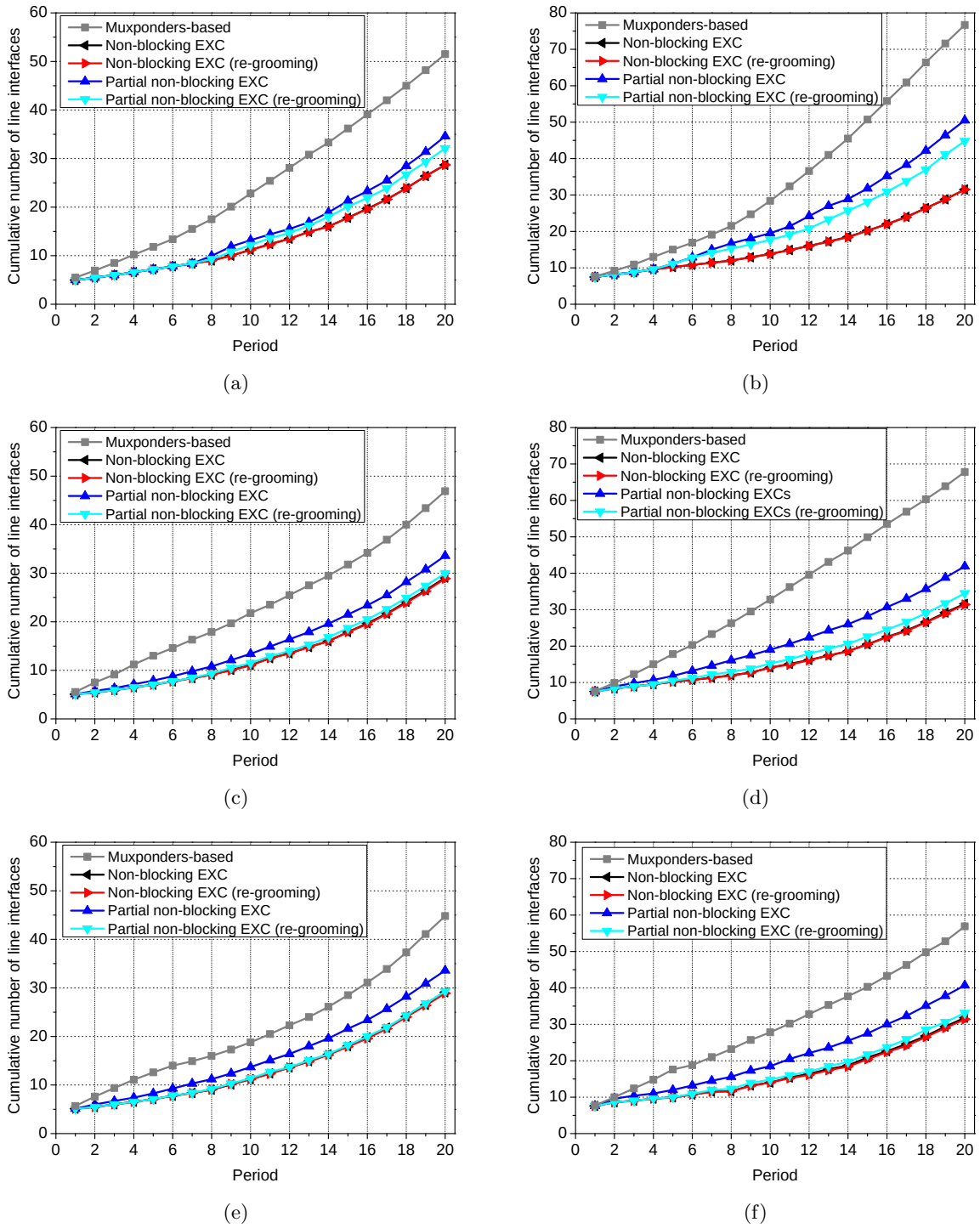

Figure 6.5: Cumulative number of line interfaces for 20 periods, pattern 4 and: (a) 5 destination nodes; (b) 10 destination nodes; (c) 5 destination nodes and 20% of traffic changing destination; (d) 10 destination nodes and 20% of traffic changing destination; (e) 5 destination nodes and 40% of traffic changing destination; and (f) 10 destination nodes and 40% of traffic changing destination.

in each shelf. In spite of the bigger differences between the partial non-blocking EXCs and the non-blocking EXC when compared to the pattern 1 results, the utilization of hitless re-grooming still enables partial non-blocking EXCs to attain almost the same performance as

that of a non-blocking EXC, when traffic variability is large (see Figs. 6.5(c), 6.5(d), 6.5(e) and 6.5(f)).

Table 6.2 presents the standard deviation obtained in the 20^{th} period when using traffic distributed according to pattern 4. The behavior is the same as observed in Table 6.1, i.e., the muxponders-based is the architecture with higher standard deviation, followed by the partial non-blocking EXCs. Moreover, the standard deviation increases from 5 to 10 destination nodes, in all the architectures. Comparing the results with the ones obtained for the pattern 1 (see Tables 6.2 and 6.1) it can be seen that the standard deviation tends to increase in the pattern 4. Traffic variability continues having a small impact in the standard deviation, especially in EXC-based architectures.

Table 6.2: Standard deviation of the number of line interfaces in the 20^{th} period for pattern 4.

	Only added traffic		**20% changing destination**		**40% changing destination**	
	5 nodes	10 nodes	5 nodes	10 nodes	5 nodes	10 nodes
Muxponders-based	4.27	7.24	2.70	8.27	1.64	3.79
Non-blocking EXC	0.68	0.98	0.72	0.87	0.66	1.12
Non-blocking EXC (re-grooming)	0.67	0.97	0.63	0.87	0.62	0.91
Partial non-blocking EXCs	1.30	3.62	1.36	1.46	1.54	1.64
Partial non-blocking EXCs (re-grooming)	1.16	2.26	0.78	1.37	0.71	1.17

In order to summarize the obtained results, Table 6.3 presents the percentage of line interface increase compared to the non-blocking EXC with hitless re-grooming, in the 20^{th} period. The increase in the number of line interfaces due to the lack of node flexibility tends to decrease from pattern 1 to pattern 4. As can be seen, there are only 3 exceptions out of 24 cases. The partial non-blocking EXCs architecture for 5 destination nodes, in both scenarios that traffic changes destination, and the non-blocking EXC architecture for 10 destination nodes and 20% of traffic changing destination. Comparing the results obtained for the different number destination nodes, it can be seen that the percentages raised from 5 to 10 destination nodes. The unique exceptions are the muxponders-based in pattern 1, and the non-blocking EXC architecture in pattern 1 and in scenarios where traffic is only added and 20% of the traffic is changing destination. These observations suggest that enhanced node flexibility produce more relative savings in scenarios where the majority of the client traffic is much smaller than the line bit rate and the number of destination nodes is high. Regarding the hitless re-grooming, it tends to present more relative savings in pattern 4 than in pattern 1. In the pattern 4 the majority of the client traffic is close to the line signal bit rate, therefore just a few demands need to be re-allocated in order to save a line signal. The opposite happens in pattern 1, where the majority of the client signals is of very low

granularity. In this type of pattern the line signal carries a huge number of small demands, therefore the amount of demands that needs to be re-optimized in order to save a line signal is much higher than in pattern 4.

Table 6.3: Excess of line interfaces in percentage after 20 periods compared to the non-blocking EXC with hitless re-grooming.

	Only added traffic		**20% changing destination**		**40% changing destination**	
	Pattern 1	Pattern 4	Pattern 1	Pattern 4	Pattern 1	Pattern 4
			5 destination nodes			
Muxponders-based	454.51 %	79.39 %	491.46 %	62.19 %	535.02 %	55.06 %
Non-blocking EXC	1.17 %	0.00 %	0.80 %	0.41 %	1.27 %	0.87 %
Partial non-blocking EXCs	28.34 %	20.61 %	8.64 %	16.03 %	4.69 %	16.31 %
Partial non-blocking EXCs (re-grooming)	25.74 %	11.80 %	3.61 %	3.52 %	1.58 %	1.32 %
			10 destination nodes			
Muxponders-based	447.86 %	143.93 %	485.09 %	115.62 %	474.75 %	81.27 %
Non-blocking EXC	0.00 %	0.00 %	0.00 %	0.48 %	2.30 %	1.24 %
Partial non-blocking EXCs	210.73 %	60.65 %	44.35 %	33.15 %	31.08 %	29.55 %
Partial non-blocking EXCs (re-grooming)	193.70 %	42.28 %	27.73 %	9.83 %	8.03 %	5.29 %

6.4.2 Capital expenditures

Figure 6.6 presents the average values of the cumulative CapEx in scenarios where the traffic is distributed according to pattern 1 whereas Fig. 6.7 presents the results in scenarios where traffic distributed according to pattern 4. In both cases, the figures on the left are related to 5 destination nodes and the figures on the right to 10 destination nodes. Moreover, Figs. (a) and (b) consider only added traffic, Figs. (c) and (d) consider 20% of traffic changing destination, and Figs. (e) and (f) consider 40% of traffic changing destination.

As can be seen in Figs. 6.6 and 6.7, and aligned with the results presented in Section 5.1.1, the muxponders-based architecture is the most cost efficient architecture in the firsts periods. In the opposite is the non-blocking EXC, being the partial non-blocking EXCs architecture in between. However, with the increase in the number of periods, the flexibility provided by the EXC-based architectures start bringing cost benefits in some scenarios. Considering the results obtained for pattern 1 (see Fig. 6.6), the non-blocking EXC architecture is the most cost efficient one, after 20 periods, for four out of the six analyzed scenarios. Moreover, in the remaining two scenarios, the non-blocking EXC is only outperformed by the partial non-blocking EXC architecture with hitless re-grooming (see Figs. 6.6(c) and 6.6(e)). Regarding the results for pattern 4 (see Fig. 6.7), it can be observed that, even with lack of flexibility, the

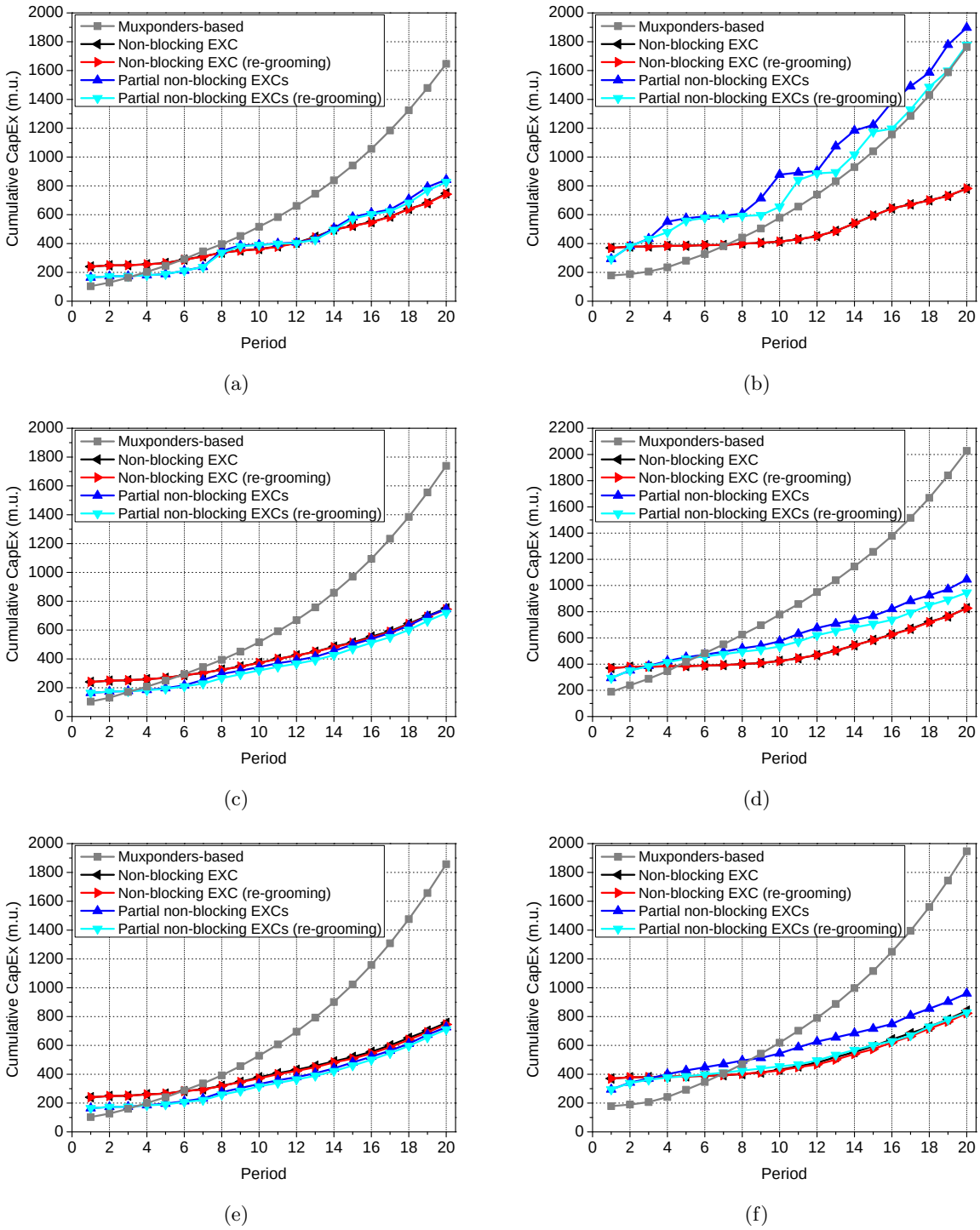

Figure 6.6: Cumulative CapEx for 20 periods, pattern 1 and: (a) 5 destination nodes; (b) 10 destination nodes; (c) 5 destination nodes and 20% of traffic changing destination; (d) 10 destination nodes and 20% of traffic changing destination; (e) 5 destination nodes and 40% of traffic changing destination; and (f) 10 destination nodes and 40% of traffic changing destination.

muxponders-based architecture is the less expensive one during the 20 periods for four out of the six scenarios. Moreover, for 10 destination nodes and 20% of traffic changing destination, the muxponders-based architecture is the most cost efficient one in the last period (see Fig.

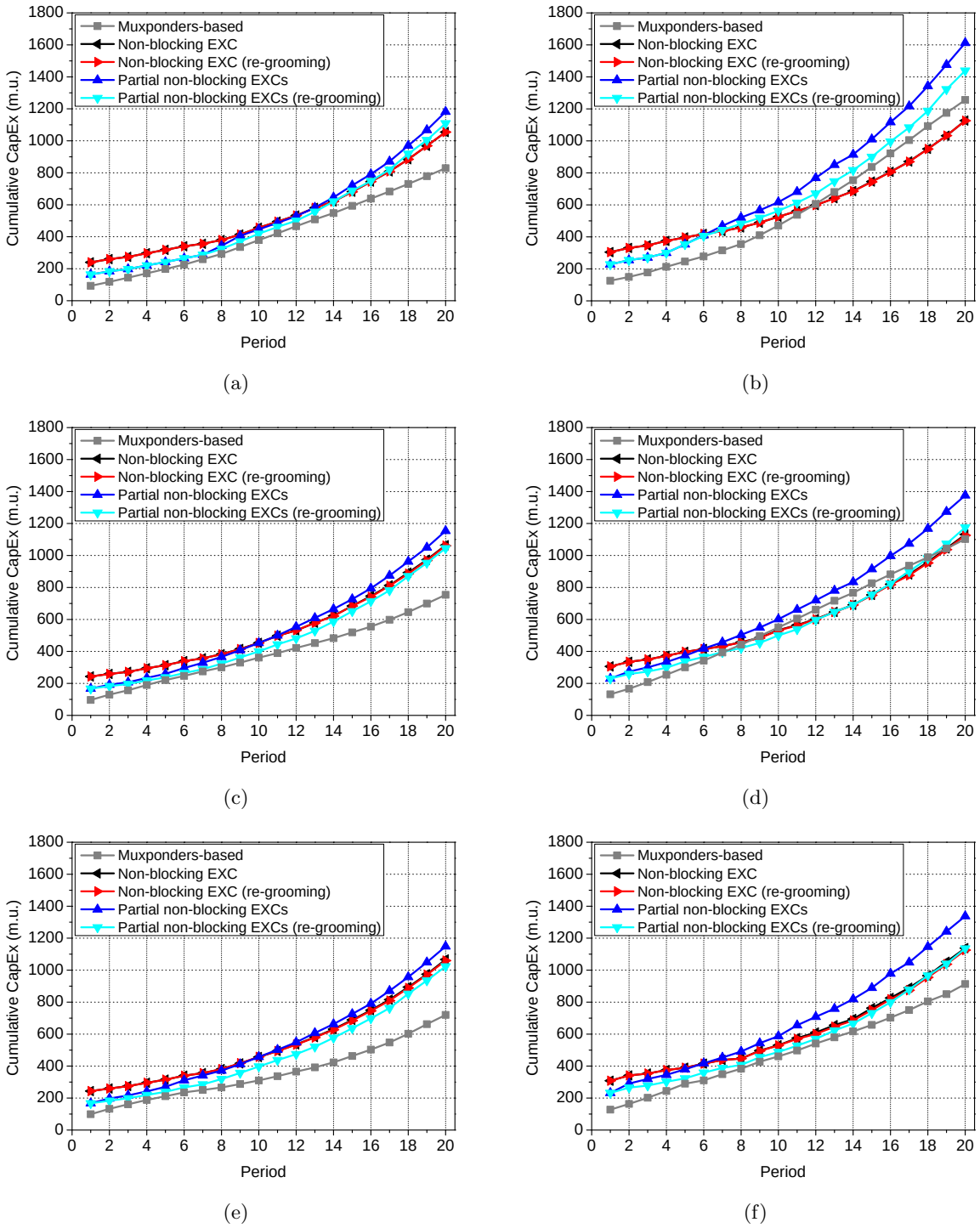

Figure 6.7: Cumulative CapEx for 20 periods, pattern 4 and: (a) 5 destination nodes; (b) 10 destination nodes; (c) 5 destination nodes and 20% of traffic changing destination; (d) 10 destination nodes and 20% of traffic changing destination; (e) 5 destination nodes and 40% of traffic changing destination; and (f) 10 destination nodes and 40% of traffic changing destination.

6.7(d)). This can be explained by the use of a single stage grooming for the majority of the traffic and the lower cost of the muxponder modules compared to the modules for EXC-based architectures. Regarding the most expensive architectures at the end of the 20 periods, it can

be seen that for pattern 1 the muxponders-based architecture turns into the most expensive architecture for five out of the six scenarios (see Fig. 6.6). In the remaining scenario, is the partial non-blocking EXCs the architecture with the higher cumulative CapEx (see Figs. 6.6(b)). Considering the pattern 4, the partial non-blocking EXC architecture is the most expensive one in all the scenarios. This is mainly explained by the cost with the various required shelves.

As observed in Section 6.4.1, traffic variability tends to improve the performance of the muxponders-based and partial non-blocking EXCs. The same behavior was observed regarding the CapEx. Table 6.4 summarizes the relative increase/decrease in percentage of CapEx when compared with the non-blocking EXC with hitless re-grooming in the last period. With the increase in traffic variability, the CapEx of the partial non-blocking EXCs suffers an huge decrease, especially for 10 destination nodes and pattern 1. However, in spite of the savings provided by the traffic variability being higher with 10 destination nodes, only for 5 destination nodes the CapEx of partial non-blocking EXCs outperforms the CapEx of the non-blocking EXC with hitless re-grooming, see Table 6.4. The muxponders-based architecture also decreases the CapEx with traffic variability, however this savings are more visible in pattern 4. In this case, even for 10 destination nodes the CapEx of the muxponders-based architecture is smaller than the CapEx of the non-blocking EXC with hitless re-grooming, see Table 6.4.

Table 6.4: Percentage of CapEx increase/decrease after 20 periods compared to the non-blocking EXC with hitless re-grooming.

	Only added traffic		**20% changing destination**		**40% changing destination**	
	Pattern 1	Pattern 4	Pattern 1	Pattern 4	Pattern 1	Pattern 4
			5 destination nodes			
Muxponders-based	121.87 %	-21.40 %	133.83 %	-28.94 %	149.18 %	-32.05 %
Non-blocking EXC	0.78 %	0.01 %	0.88 %	0.31 %	1.45 %	0.67 %
Partial non-blocking EXCs	13.58 %	12.05 %	0.23 %	8.75 %	-2.56 %	8.40 %
Partial non-blocking EXCs (re-grooming)	11.34 %	5.18 %	-3.42 %	-1.53 %	-4.64 %	-3.40 %
			10 destination nodes			
Muxponders-based	125.44 %	11.55 %	145.15 %	-2.07 %	136.62 %	-18.85 %
Non-blocking EXC	0.00 %	0.09 %	0.00 %	0.43 %	2.17 %	1.12 %
Partial non-blocking EXCs	142.57 %	43.19 %	26.55 %	22.15 %	16.78 %	18.90 %
Partial non-blocking EXCs (re-grooming)	127.28 %	27.80 %	14.35 %	4.38 %	0.69 %	0.89 %

6.4.3 Power consumption

Figure 6.8 presents the average values of the cumulative power consumption in scenarios where the traffic is distributed according to pattern 1 whereas Fig. 6.9 presents the results in scenarios where traffic distributed according to pattern 4. In both cases, the figures on the left are related to 5 destination nodes and the figures on the right to 10 destination nodes. Moreover, Figs. (a) and (b) consider only added traffic, Figs. (c) and (d) consider 20% of traffic changing destination, and Figs. (e) and (f) consider 40% of traffic changing destination.

As expected by the analysis performed in Section 5.1.2, the muxponders-based architecture is the most power efficient one in the first periods, followed by the partial non-blocking EXCs architecture. The non-blocking EXC is the architecture presenting higher power consumption. In order to behave as a non-blocking EXC, the shelf size and respective control modules need to be large enough to accommodate and support all the required modules, during all the periods. Thus, the higher power required by the larger shelves and respective control modules have a negative impact in the node power consumption at the early periods. With the increase of the number of periods the power consumption of the non-blocking EXC architecture starts being lower than of the partial non-blocking EXCs, evidencing the benefits of an initial higher investment in power consumption. However, in spite of the power consumption of non-blocking EXC being almost always smaller than of the partial non-blocking EXCs, it only outperforms the muxponders-based architecture in the pattern 1. In this pattern a two stage grooming is required for the majority of the traffic, thus increasing the power consumption of the muxponders-based architecture. When traffic is distributed according to pattern 4 (see Fig. 6.9), the muxponders-based architecture requires less modules, and consequently shelves and control modules. Therefore, under pattern 4, the muxponders-based architecture is the most power efficient architecture in the 20 periods considered and for all the analyzed scenarios. Regarding the hitless re-grooming, it only produces significant power consumption savings for the partial non-blocking EXCs architecture in pattern 4. Regarding the architectures with the highest power consumption at the last period, it can be observed that for pattern 1 the muxponders-based architecture is the one requiring more power for five out of the six analyzed scenarios. In the remaining scenario (see Fig. 6.8(b)) is the partial non-blocking EXCs the architecture with higher power consumption. Considering the pattern 4, it can be seen that the partial non-blocking EXCs is the architecture requiring more power under all the scenarios.

Table 6.5 presents the relative increase/decrease in power consumption when compared to the non-blocking EXC with hitless re-grooming, after 20 periods. As can be observed, traffic variability tends to decrease the power consumption of the partial non-blocking EXCs and muxponders-based architectures, under pattern 4. Moreover, the gains provided by the muxponders-based architecture in pattern 4 increase with the traffic variability. The reduction in power consumption observed in the partial non-blocking EXCs due to the traffic variability is not enough to outperform the non-blocking EXC, however it is significant for

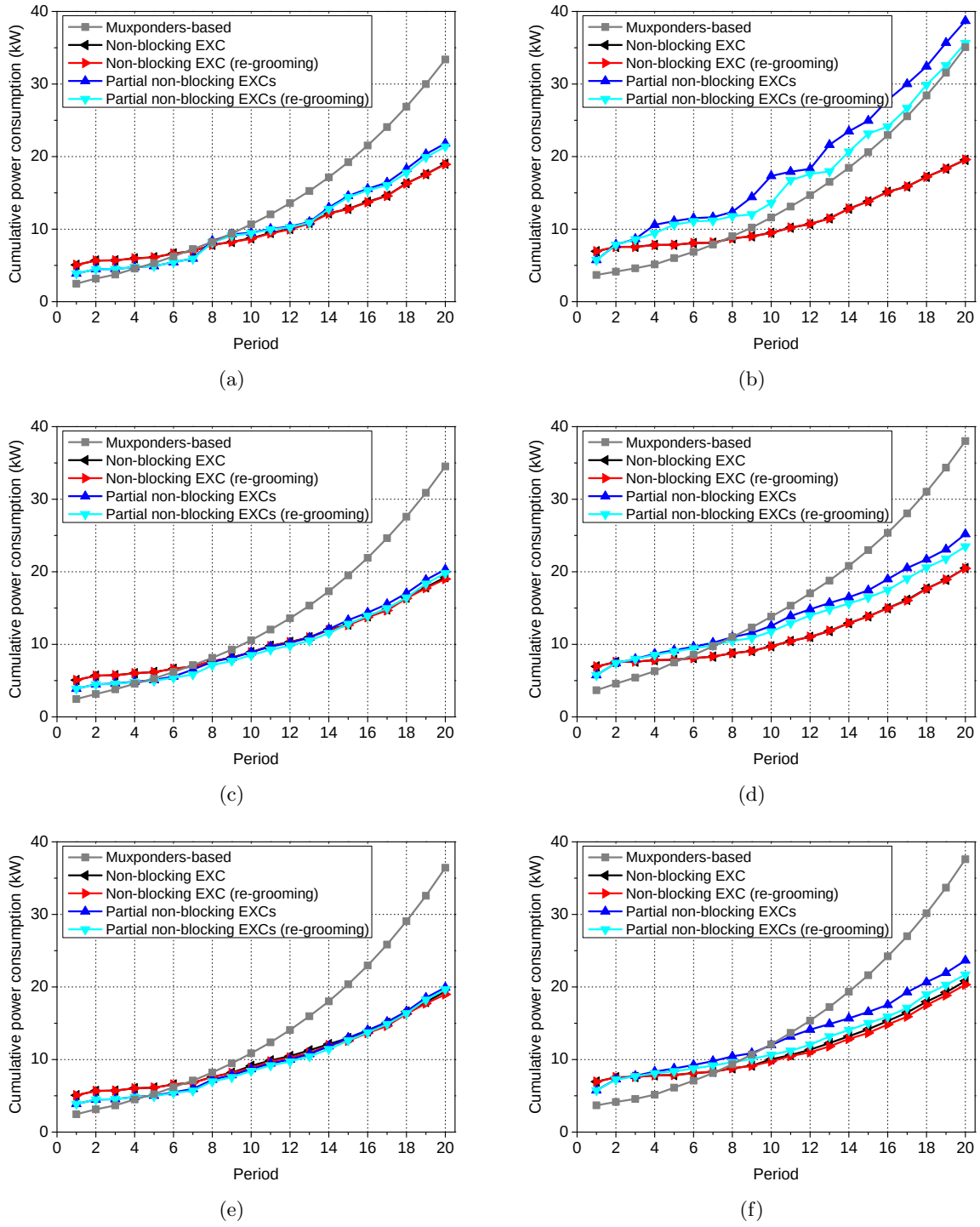

Figure 6.8: Cumulative power consumption for 20 periods, pattern 1 and: (a) 5 destination nodes; (b) 10 destination nodes; (c) 5 destination nodes and 20% of traffic changing destination; (d) 10 destination nodes and 20% of traffic changing destination; (e) 5 destination nodes and 40% of traffic changing destination; and (f) 10 destination nodes and 40% of traffic changing destination.

10 destination nodes. Nevertheless, for 5 destination nodes and pattern 1, the differences between the partial non-blocking EXCs and the non-blocking EXC architectures are below 10%.

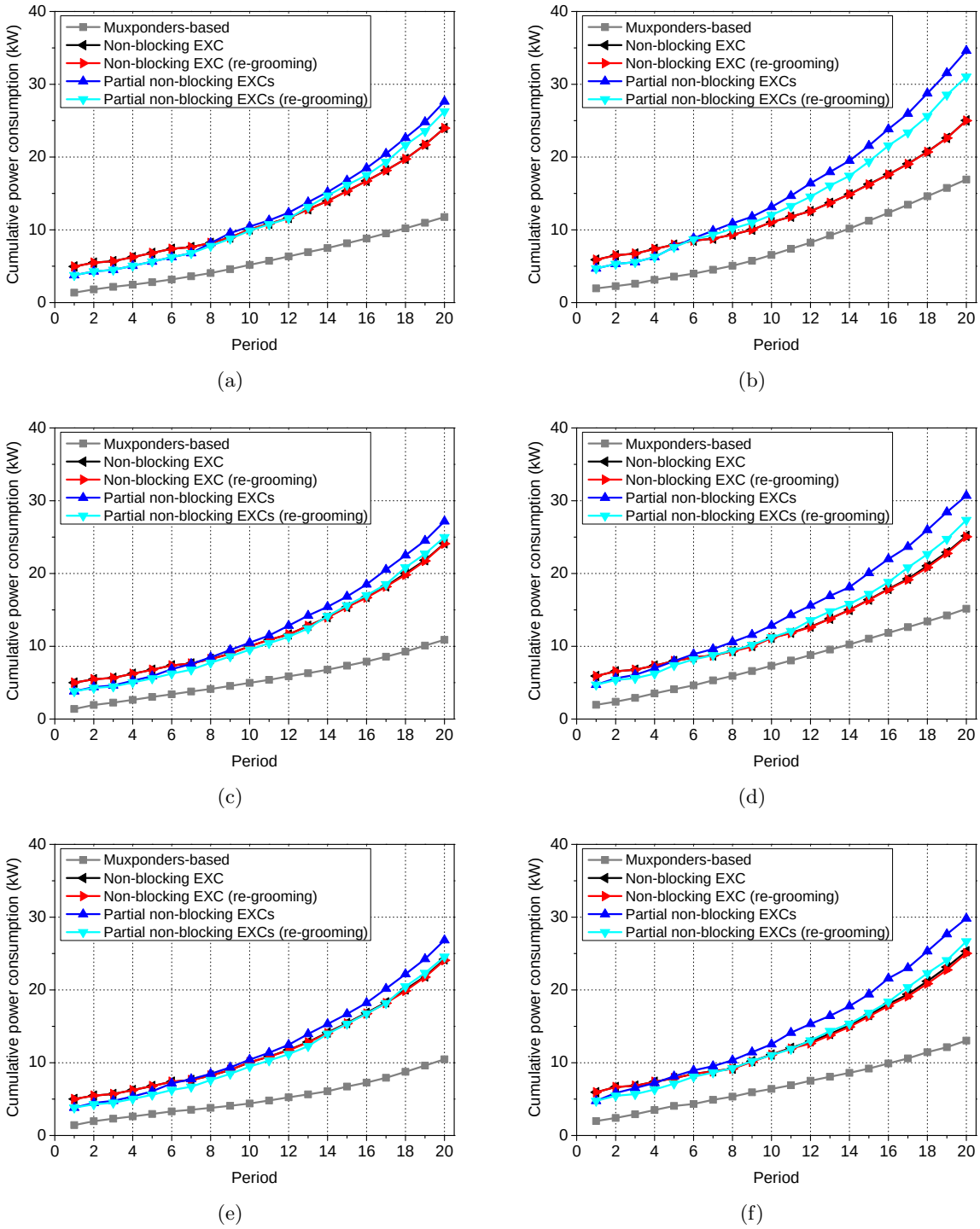

Figure 6.9: Cumulative power consumption for 20 periods, pattern 4 and: (a) 5 destination nodes; (b) 10 destination nodes; (c) 5 destination nodes and 20% of traffic changing destination; (d) 10 destination nodes and 20% of traffic changing destination; (e) 5 destination nodes and 40% of traffic changing destination; and (f) 10 destination nodes and 40% of traffic changing destination.

Table 6.5: Percentage of power consumption increase/decrease after 20 periods compared to the non-blocking EXC with hitless re-grooming.

	Only added traffic		**20% changing destination**		**40% changing destination**	
	Pattern 1	Pattern 4	Pattern 1	Pattern 4	Pattern 1	Pattern 4
			5 destination nodes			
Muxponders-based	76.33 %	-50.99 %	81.68 %	-54.81 %	91.98 %	-56.50 %
Non-blocking EXC	0.43 %	0.01 %	1.33 %	0.22 %	2.14 %	0.55 %
Partial non-blocking EXCs	15.22 %	15.26 %	6.93 %	12.77 %	4.96 %	11.50 %
Partial non-blocking EXCs (re-grooming)	12.91 %	9.50 %	4.23 %	3.68 %	3.67 %	2.05 %
			10 destination nodes			
Muxponders-based	79.11 %	-32.38 %	85.73 %	-39.49 %	85.10 %	-47.89 %
Non-blocking EXC	0.00 %	0.12 %	0.20 %	0.45 %	2.55 %	1.20 %
Partial non-blocking EXCs	97.65 %	38.43%	23.11 %	22.55 %	16.46 %	19.20 %
Partial non-blocking EXCs (re-grooming)	81.99 %	24.11 %	14.74 %	9.16 %	6.83 %	6.57 %

6.4.4 Footprint requirements

Figure 6.10 presents the average values of the cumulative footprint requirements in scenarios where the traffic is distributed according to pattern 1 whereas Fig. 6.11 presents the results in scenarios where traffic distributed according to pattern 4. In both cases, the figures on the left are related to 5 destination nodes and the figures on the right to 10 destination nodes. Moreover, Figs. (a) and (b) consider only added traffic, Figs. (c) and (d) consider 20% of traffic changing destination, and Figs. (e) and (f) consider 40% of traffic changing destination.

Contrariwise of what was observed for the cumulative CapEx and power consumption, no interceptions between the footprint requirements of the various architectures exist, among the 20 periods. The muxponders-based architecture tend to require more slots than EXC-based architectures, independently of the traffic pattern and number of destination nodes, see Figs. 6.10 and 6.11. Nevertheless, the differences are higher in pattern 1 and tend to increase with the increase of the number of destination nodes. Regarding EXC-based architectures, it can be seen that the non-blocking EXC architecture requires less slots than the partial non-blocking EXCs architecture. This difference widens from 5 to 10 destination nodes and tend to be higher under pattern 4. Considering the gains provided by enabling hitless re-grooming, they are smaller than the ones reported for the CapEx and power consumption. Moreover, they are only significative for 10 destination nodes and pattern 4.

Table 6.6 presents the relative increase in footprint requirements when compared to the non-blocking EXC with hitless re-grooming, after 20 periods. As observed, traffic variability

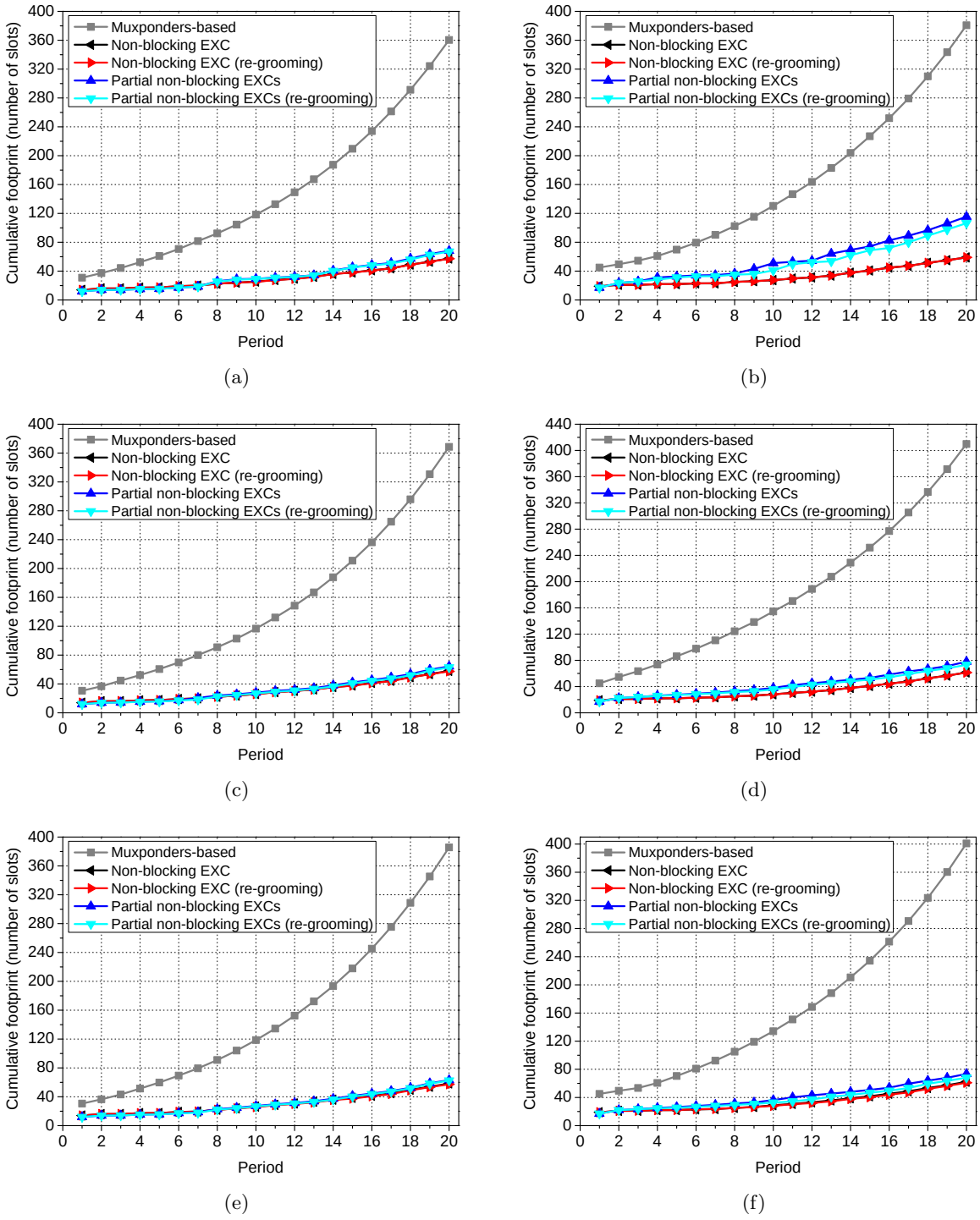

Figure 6.10: Cumulative footprint requirements for 20 periods, pattern 1 and: (a) 5 destination nodes; (b) 10 destination nodes; (c) 5 destination nodes and 20% of traffic changing destination; (d) 10 destination nodes and 20% of traffic changing destination; (e) 5 destination nodes and 40% of traffic changing destination; and (f) 10 destination nodes and 40% of traffic changing destination.

tends to decrease the footprint requirements, especially for partial non-blocking EXCs and 10 destination nodes. However, in this case the improvements in terms of footprint requirements are not enough to outperform the non-blocking EXC architecture in any scenario. Moreover,

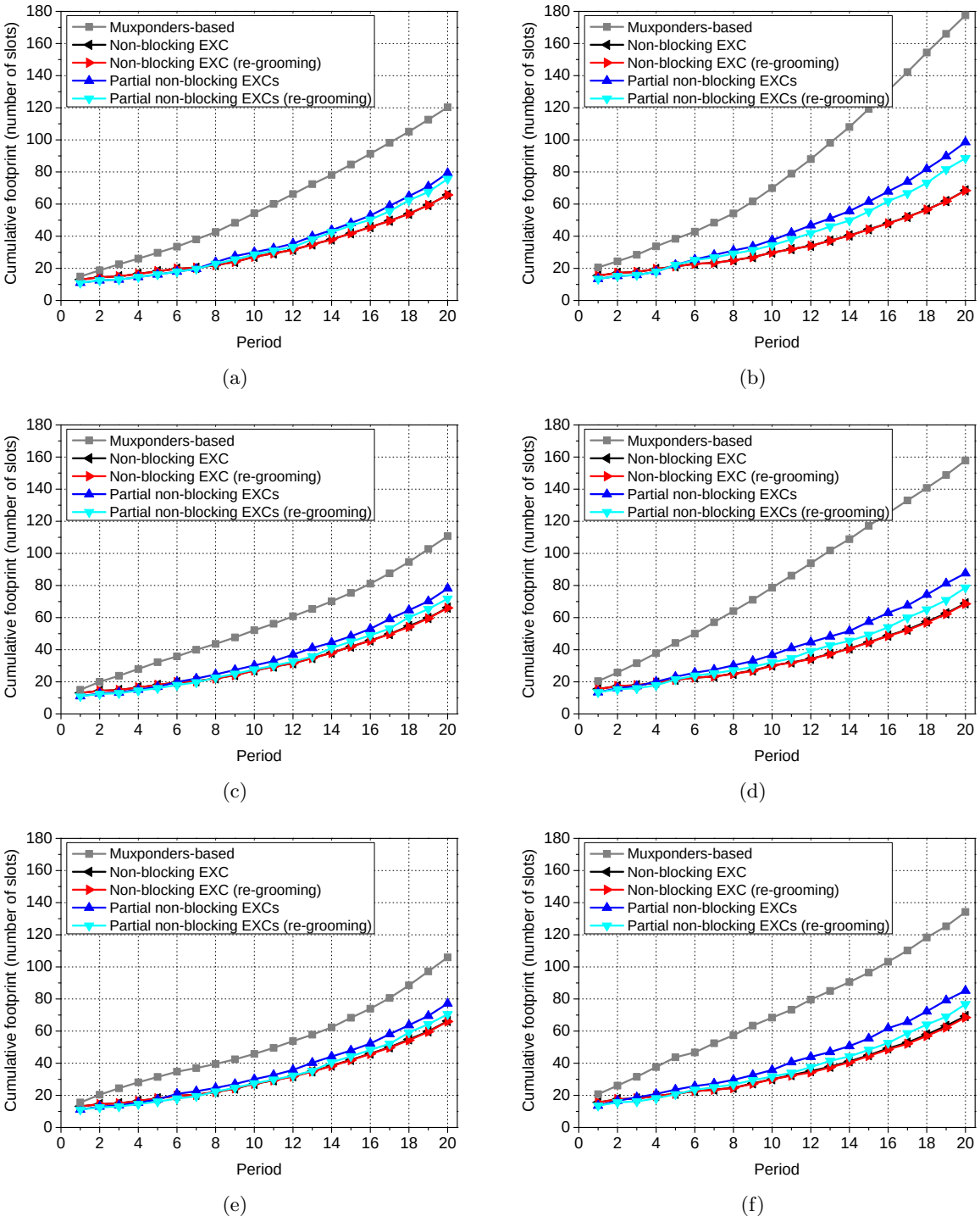

Figure 6.11: Cumulative footprint requirements for 20 periods, pattern 4 and: (a) 5 destination nodes; (b) 10 destination nodes; (c) 5 destination nodes and 20% of traffic changing destination; (d) 10 destination nodes and 20% of traffic changing destination; (e) 5 destination nodes and 40% of traffic changing destination; and (f) 10 destination nodes and 40% of traffic changing destination.

considering the partial non-blocking EXCs with hitless re-grooming, only for 5 destination nodes the increase in number of slots is smaller than 10%.

Table 6.6: Percentage of footprint requirements increase after 20 periods compared to the non-blocking EXC with hitless re-grooming.

	Only added traffic		**20% changing destination**		**40% changing destination**	
	Pattern 1	Pattern 4	Pattern 1	Pattern 4	Pattern 1	Pattern 4
			5 destination nodes			
Muxponders-based	530.27 %	83.05 %	541.88 %	67.66 %	573.18 %	60.53 %
Non-blocking EXC	0.44 %	0.02 %	1.18 %	0.20 %	1.94 %	0.52 %
Partial non-blocking EXCs	19.22 %	20.72 %	11.96 %	18.32 %	10.11 %	17.02 %
Partial non-blocking EXCs (re-grooming)	17.26 %	15.17 %	9.51 %	8.65 %	9.11 %	6.84 %
			10 destination nodes			
Muxponders-based	544.78 %	159.39 %	567.25 %	130.17 %	558.06 %	95.96 %
Non-blocking EXC	0.00 %	0.13 %	0.20 %	0.44 %	2.28 %	1.18 %
Partial non-blocking EXCs	95.58 %	43.95%	27.03 %	27.70 %	20.70 %	24.34 %
Partial non-blocking EXCs (re-grooming)	80.20 %	29.32 %	19.13 %	14.67 %	11.82 %	12.07 %

6.5 Chapter summary

In this chapter the various approaches for multi-period planning are briefly presented, and the differences in terms of required information and level of optimality highlighted. Moreover, the hitless re-grooming concept, that can be employed in flexible architectures, is explained. After, dimensioning models based on ILPs to use in multi-period planning are presented. The models consider the three electrical layer architectures namely, muxponders-based, non-blocking EXC, and partial non-blocking EXCs. Additionally, for EXC-based architectures, both disabled and enabled hitless re-grooming are considered. Using the developed models and considering different traffic patterns, number of destination nodes, and levels of traffic variability, an evaluation and comparison for the cumulative number of line interfaces, CapEx, power consumption and footprint requirements is performed. Results show that non-blocking EXC architectures tend to require less line interfaces than architectures with less flexibility. In the opposite is the muxponders-based architecture. Moreover, the line interfaces increase in muxponders-based architectures tend to be higher when the majority of the client traffic requires a two stage grooming. Regarding the gains provided by the hitless re-grooming, significant savings were only observed in the partial non-blocking EXCs. Moreover, the benefits of hitless re-grooming are higher when the majority of the client traffic bit rate is closer to the bit rate of the line signal. Additionally, this savings tend to increase with the increase in the traffic variability. Regarding the CapEx, power consumption and footprint requirements, results show that non-blocking EXC architectures tend to have higher CapEx and power consumption at the early periods. However, with the network evolution and traffic

increase, the flexibility provided by this type of architecture starts bringing significant cost benefits. In the contrary, the muxponders-based architecture offers a cost and power efficient solution in the firsts periods. However, the lack of flexibility increases the CapEx and power consumption considerably, in the forthcoming periods. Regarding the footprint requirements, non-blocking EXC always offers the most compact solution in terms of number of slots whereas the muxponders-based architecture is the one requiring more space. The partial non-blocking EXCs evolves in a more scalable way being usually in between of the two above mentioned architectures. However, hitless traffic re-grooming can assist in mitigating the impact of grooming limitations that arise when deploying the more scalable partial non-blocking EXCs.

References

[1] D. Schupke and C. Kronberger, "Multiperiod planning for optical networks," in *Proc International Telecommunications Network Strategy and Planning Symposium - NETWORKS*, pp. 1–6, September 2010.

[2] S. Strauss, A. Kirstadter, and D. Schupke, "Multi-period planning of WDM networks: Comparison of incremental and Eol approaches," in *Proc IEEE/IFIP International Conference in Central Asia on Internet*, pp. 1–7, September 2006.

[3] E. Palkopoulou, C. Meusburger, D. Schupke, L. Wosinska, and T. Bauschert, "Combining multi-period and multi-layer network planning: Ignored potential?" in *Proc European Conference and Exhibition on Optical Communication - ECOC*, pp. Th.10.F.2, Sept 2010.

[4] K. Guan and C. Guan, "Multi-period planning of WDM transport networks incorporating demand uncertainties," in *Proc Biennial Symposium on Communications*, pp. 135–139, June 2006.

[5] N. Geary, A. Antonopoulos, J. O'Really, and E. Drakopoulos, "Planning techniques for multi-period optical network designs," in *Proc London Communications Symposium*, September 2000.

[6] S. Yang and F. Kuipers, "Traffic uncertainty models in network planning," *IEEE Communications Magazine*, vol. 52, no. 2, pp. 172–177, February 2014.

[7] C. Meusburger, "Multiperiod planning for optical networks," in *Workshop der ITG-Fachgruppe 5.2.1*, 2009. [Online]. Available: http://www.comnets.uni-bremen.de/itg/itgfg521/aktuelles/fg-workshop-13112009/Multiperiod%20planning%20for%20optical%20Networks_ITG_Meusburger.pdf

[8] M. Fukutoku, T. Ohara, A. Kadohata, A. Hirano, T. Kawai, T. Komukai, M. Suzuki, S. Aisawa, T. Takahashi, M. Tomizawa, O. Ishida, and S. Matsuoka, "Optimized multi-layer optical network using in-service ODU / wavelength path re-grooming," in *Proc Optical Fiber Communication Conference and Exposition and the National Fiber Optic Engineers Conference - OFC/NFOEC*, pp. NMC5, March 2011.

[9] A. Kadohata, A. Hirano, M. Fukutoku, T. Ohara, Y. Sone, and O. Ishida, "Multi-layer greenfield re-grooming with wavelength defragmentation," *IEEE Communications Letters*, vol. 16, no. 4, pp. 530–532, April 2012.

[10] *ITU-T Recommendation G.7044/Y.1347, Hitless adjustment of ODUflex (GFP)*, International Telecommunication Union Std., 2011.

CHAPTER 7

Conclusions and future directions

In the framework of this PhD thesis, optimization models for the various planning stages of a multilayer transport network were developed. The thesis starts by proposing a genetic algorithm for the design of physical topologies with minimum CapEx for links. After, ILP models for the nodes dimensioning in both greenfield and multi-period scenarios are also developed. The models take into account the several hardware implementation constraints and limitations. Using the developed models, a methodology to perform detailed techno-economic analysis is proposed, focusing on the CapEx, power consumption and footprint requirements of a node. In the following, we overview the developed work and summarize the main conclusions obtained. Finally, in Section 7.2 some suggestions for future work are presented.

7.1 Conclusions

This thesis starts by overviewing the opaque, transparent and translucent transport modes, in Chapter 2. Moreover, the grooming schemes that can be used in each of the transport modes are also reported. Multilayer optical transport networks comprise a set of nodes connected by bidirectional links. Thus, the links and nodes architectures are explained in detail in Chapter 2. The links architecture is composed by one or more transmission systems which comprises the optical fiber and optical amplifiers. Nodes are complex systems assembled with multiple types of modules. Therefore, the building blocks used in a general node architecture are explained before the detailed presentation of the various modules, constraints, and limitations involved in the nodes dimensioning. Later, fixed and flexible architectures for the electrical and the optical layer of a node are discussed. Considering the architectures for the electrical layer, a fixed architecture based on muxponders, and a flexible architecture based on EXCs are presented in detail. Muxponders-based architectures require the tech-

nician visit to the site for reconfiguration whereas in flexible architectures reconfiguration can be performed by remote action. Regarding the optical layer, the building blocks used in the various ROADM architectures are explained, before the presentation of ROADMs with different levels of flexibility. Thus, ROADMs with fixed frequency, fixed direction, colorless, directionless and contentionless capabilities are described.

After the detailed study of the hardware constraints and limitations of the various considered architectures, optimization methods for planning multilayer networks are proposed. The first stage of the overall network planning process is the physical topological design. At this stage the links to be implemented are chosen. As transport networks are responsible to support massive amounts of data, the physical topology should guarantee the survivability of the client signals. Therefore, in Chapter 3 a genetic algorithm for the design of minimum CapEx survivable topologies is proposed. The chapter starts by presenting a dimensioning model for the links, and for the network topology.. After, and as the convergence of the genetic algorithm depends on the used genetic operators, an analysis to their impact on the quality of the obtained solutions is performed. To do that, an ILP model is also presented. The performance of two initial population generators, two selection methods, two crossover operators, and two population sizes are compared and benchmarked using the ILP model and a set of node locations of real-world transport networks. Computational results showed that initial populations generated using a method that preserves the main characteristics of real optical networks improves the quality of the obtained solutions. Regarding the selection method, results suggest that selection methods that give preference to the fittest individuals tend to improve the quality of the obtained solutions. Moreover, crossover operators that do not preserve large blocks of the genetic code increase the diversity of the population and the probability of finding better solutions. Hence, the quality of the obtained results and the saved processing time encourage the use of this kind of heuristic within the survivable topological design problem.

After the deployment of the network physical topology, the nodes are planned. Chapter 4 is dedicated to the presentation of the dimensioning model for nodes. The novel models can be used in greenfield scenarios and to calculate the number and type of modules required at each node, considering the hardware implementation constraints of the different architectures. The inputs of the models are the client traffic, the network topology, and the type of modules available. Regarding the electrical layer, the models are based on ILP formulations and intend to optimize the grooming of the client signals minimizing the number of modules involved. Different node architectures were considered with distinct levels of flexibility. The muxponders-based architecture introduces constraints in the client signals that can be connected to the same muxponder module. Moreover, not all mixture of client signals can be groomed as the grooming configuration is fixed by the module itself. On the opposite, EXC-based architectures enable the connection of a client signal into any module that can accept it, and all grooming configurations are allowed. However, as the switching of the electrical signals is done using backplane communications, only modules connected to the same backplane can interact. In this context, models for non-blocking EXC and for partial

non-blocking EXCs architectures are proposed. Regarding the optical layer, a set of equations are proposed to dimension a ROADM. Depending on the architecture, the ROADM can be fixed or have different degrees of flexibility. In a colorless architecture the wavelength assigned to any add/drop port can be changed remotely, and in a directionless ROADM any add/drop channel can be remotely redirected to any transmission system that converges to the node. Additionally, contentionless ROADM allows the use of multiple copies of the same wavelength in the same add/drop structure, as long as they follow different transmission systems. As a result, models for fixed frequency and fixed direction, colorless and fixed direction, fixed frequency and directionless, colorless and directionless, and colorless, directionless and contentionless ROADMs are developed.

Using the models presented in Chapter 4 for greenfield scenarios, and a consolidated database for the modules specifications, a techno-economic analysis is presented in Chapter 5. The analysis focuses in the CapEx, power consumption, and footprint requirements of the various architectures for the electrical and the optical layer. The proposed methodology assumes a single node, varying the factors that impact the node costs. For the electrical layer architectures, different traffic loads, client traffic patterns, and number of nodes to/from which traffic is exchanging are considered. Results show that the CapEx and the power consumption are, in most cases, smaller for the muxponders-based architectures. Regarding the footprint requirements, EXC-based architectures tend to be more efficient. However, the cost of muxponders-based architectures tend to be more dependent on the number of destination nodes than the cost of EXCs-based architectures. Regarding the optical layer architectures, different number of add/drop channels and of convergent fibers are considered. In this type of structure the most efficient architecture depends on a relation between the nodal degree and the number of add/drop channels. After, a sensitivity analysis of the modules was also performed. Results show that the line modules are the most influential parameter in the total network cost. Variations in the modules used in the ROADM part of the node have a residual impact. As a result of the detailed techno-economic study, an optimization method based on node architecture selection is proposed. The optimization method is based on statistical and simple rules, identifying the scenarios where a determined architecture brings cost benefits. At the end, the applicability of the proposed optimization method is demonstrated with a network. Results show that to optimize the network OpEx related to the power consumption and footprint requirements, an heterogeneous network should be deployed.

Finally, in Chapter 6 the multi-period planning problem is addressed. The various approaches for multi-period planning as well as the re-grooming concept are presented. Later, dimensioning models based on ILPs for the dimensioning of the muxponders-based, non-blocking EXC, and partial non-blocking EXCs architectures are proposed. Regarding the EXC-based architectures, the models consider both enable and disable hitless traffic re-grooming. At the end, a techno-economic analysis is performed assuming a single source node, different client traffic patterns, levels of traffic variability, and number of nodes to/from which traffic is exchanged. The analysis focused on the cumulative number of line interfaces,

CapEx, power consumption and footprint requirements. Results show that besides the expected decrease in cost when adopting more flexible architectures, these savings are greater when the client traffic bit rate has very low granularity, and the number of destination nodes is high. Moreover, traffic re-grooming can assist in mitigating the limitations that arise when deploying the more scalable partial non-blocking EXCs. In fact, when traffic variability is large, the utilization of re-grooming enables partial non-blocking EXCs to attain almost the same performance as that of a non-blocking EXC. This is particularly evident when the client traffic bit rate is close to the line bit rate.

7.2 Future directions

From the work developed during this PhD, the following topics are suggested as future work:

- The models developed in this thesis, in spite of being vendor independent, are restricted to circuit switching technologies. Therefore, a first step to continue this work is the extension of the models for packet switching technologies (e.g., MPLS-TP). In this way, detailed techno-economic comparisons between packet and circuit switches can be performed, leading to the identification of the traffic conditions where circuit or packet switching has advantages. Moreover, from the models for circuit and packet switching, the mixture of the two types of traffic can also be evaluated. For instance comparing the three alternatives presented in Fig. 2.8, namely parallel, layered, and hybrid.

- The developed models for the electrical layer, in spite of allowing a mixed line rate dimensioning, consider single bit rate transponders. Thus, one possible future direction is the extension of the models to support bandwidth variable transponders. Regarding the optical layer, the models assume fixed-grid transponders. When flexi-grid transponders are used the number of channels that can be added/dropped at a node depends on the respective spectral width of the optical channels. Hence, extending the optical layer models to support flexi-grid transponders is another suggestion to continue this work.

- The dimensioning models presented in this thesis rely on ILPs. Thus, scalability limitations may arise depending on the size of the problem and on the computational resources available. In this context, the development and benchmarking of heuristic algorithms to use in large networks is also a direction that can be pursued from this thesis. The benchmarking of the heuristics can be realized using the presented ILP models. After, the heuristics can be used to perform techno-economic analysis considering several networks with different topological characteristics.

- The last topic addressed in this thesis regards the multi-period planning using the incremental approach. In the incremental approach the dimensioning is performed without having any knowledge about the traffic of future periods. Hence, one possible

future work could consider other approaches such as the end-of-life and the begin-of-life with forecast planning approaches, and evaluate the impact that erroneous information can have. This type of study can be particularly interesting when using bandwidth and spectral variable transponders, and taking into account the OpEx savings with technicians, whenever reconfiguration is needed.